

Electronic Thesis and Dissertation Repository

11-16-2022 1:15 PM

The Synthesis, Lewis Acidity and Catalytic Activity of Bis(catecholato)germanes

Andrew T. Henry, *The University of Western Ontario*

Supervisor: Baines, Kim M., *The University of Western Ontario*

A thesis submitted in partial fulfillment of the requirements for the Doctor of Philosophy degree in Chemistry

© Andrew T. Henry 2022

Follow this and additional works at: <https://ir.lib.uwo.ca/etd>

 Part of the [Inorganic Chemistry Commons](#)

Recommended Citation

Henry, Andrew T., "The Synthesis, Lewis Acidity and Catalytic Activity of Bis(catecholato)germanes" (2022). *Electronic Thesis and Dissertation Repository*. 9001.
<https://ir.lib.uwo.ca/etd/9001>

This Dissertation/Thesis is brought to you for free and open access by Scholarship@Western. It has been accepted for inclusion in Electronic Thesis and Dissertation Repository by an authorized administrator of Scholarship@Western. For more information, please contact wlsadmin@uwo.ca.

Abstract

Main group Lewis acids have been shown to be viable alternatives to state-of-the-art transition metal catalysts. While extensive research into a variety of *p*-block Lewis acids have been reported, the field of germanium Lewis acid chemistry has been described as “almost non-existent”. A variety of bis(catecholato)germane derivatives have been synthesized. The Lewis acidity of these compounds was analyzed by the Gutmann-Beckett and fluoride ion affinity methods demonstrating the high Lewis acidity of these complexes. The bis(catecholato)germanes were utilized as Lewis acid catalysts for the hydrosilylation of aldehydes, the hydroboration of alkynes, Friedel-Crafts alkylation of alkenes, and the oligomerization of styrene derivatives. Notably, the use of donor additives resulted in tunable product selectivity in the oligomerization of α -methylstyrene comparable to the selectivity that can be achieved using transition metal catalysts. The mechanism of catalysis by bis(catecholato)germanes in the oligomerization of α -methylstyrene was examined using variable time normalization analysis, Hammett analysis, and density functional theory calculations of Gibbs free energies of key intermediates, revealing the species with only one donor solvent ligated to the germanium centre is the active catalyst species. Finally, the use of bis(catecholato)germanes as potential Lewis acid components in frustrated Lewis pairs was investigated. The reactivity of the bis(catecholato)germane complexes with various bulky bases and supporting DFT calculations revealed the formation of Lewis adducts. The reactivity of the Lewis pairs was explored; however, no small molecule activation or catalysis, typical reactivity of frustrated Lewis pairs, was observed.

While Lewis pairs derived from bis(catecholato)germanes do not exhibit any reactivity typical of frustrated Lewis pairs, weak donor complexes of bis(catecholato)germanes are highly Lewis acidic and capable of facilitating several reactions as a Lewis acid catalyst.

Previous work in the literature has shown the potential of a green, solvent free synthesis of the bis(catecholato)germanes and catalytic activity using water as a solvent,

demonstrating the principles of green chemistry. The green chemistry of bis(catecholato)germanes, in conjunction with their high catalytic activity in a variety of reactions and their tuneability to influence product selectivity, illustrate that bis(catecholato)germanes are exciting alternatives to transition metal catalysts and should be explored further.

Keywords

Main group, germanium, catechol ligand framework, Lewis acid, catalysis, mechanism of catalysis, frustrated Lewis pair, density functional theory.

Summary for Lay Audience

Certain chemical reactions can require a lot of energy to proceed. As such, ways to reduce the energy needed is important. One way to reduce energy needed is to use catalyst. Catalysts are compounds which make chemical reactions more efficient. They are also not consumed during the reaction. Catalysts are used in over 80% of industrial chemical processes. The current best catalysts feature expensive elements, such as platinum and palladium. These elements also have supply risks due to low earth abundance. Also, political issues affect obtaining these elements. Chemists have looked for other viable catalysts featuring cheaper and more accessible elements. The element germanium is more abundant and cheaper than platinum. However, catalysts using germanium have not been explored in depth. In fact, recent reviews have described germanium catalysts as “almost non-existent”. The goal of this thesis is to explore germanium-based catalysts.

A variety of germanium compounds were made. These compounds were successfully used as catalysts for several types of reactions. The efficiency of the germanium catalyst is comparable to other alternatives. Experiments to understand how the germanium catalysts function were performed. This work presents the first steps in the development of germanium Lewis acids.

Co-Authorship Statement

This thesis includes work from a previously published manuscript which is presented in Chapters 2, 3 and 4. The article was coauthored by A. H. Henry, T. P. L. Cosby, and K. M. Baines, *Dalton Trans.* **2021**, *50*, 15906-15913. ATH performed the synthesis, assessment of Lewis acidity, and computational work. TPLC performed the catalytic oligomerization of α -methylstyrene experiments supervised by ATH.

The hydroboration of alkynes presented in Chapter 3 was performed in collaboration with Dana Nanan.

Acknowledgments

First and foremost, the biggest of thanks to my supervisor, Dr. Kim Baines. I could not imagine finishing my degree with any other supervisor. You have provided me guidance in both my research and professional career. The knowledge and problem-solving skills you imparted on me has helped me overcome numerous obstacles in my research project. You encouraged me to branch out and learn a variety of skills to become a better researcher. While there were numerous times my confidence was at a low, you always reminded me that you were confident in my abilities and kept me pushing on. I am so honoured to be your last Ph.D. student and wish you the best of times in your retirement.

Secondly, I would like to thank the numerous group members I worked beside during the course of my thesis. Whether it was the fights over the thermostat, the ‘Rage Against the Machine’ ambience, the Sporcle quizzes and trivia, or the various celebrations and cakes were the perfect breaks, you were all a part of making my time in the lab special. I learned so much from our interactions together, whether you were my mentors or mentees in the lab.

Thanks to all the friends I’ve made at Western over my time here. I am fortunate enough to have met so many of you over my time here that I cannot name you all. Thank you to my undergrad friends who made learning chemistry fun to begin with. Shoutout to the boys. Even though few of you remain in London, we have always remained close through our time playing games together. You provided me a space where I can escape from whatever is on my mind. Thank you to the friends I met in grad school. You all made the campus such an inviting place and I always felt at home walking in the halls. Finally, thank you Maissa. You were always a rock for me and someone I could vent to and be my true self around.

Table of Contents

Abstract.....	ii
Summary for Lay Audience.....	iv
Co-Authorship Statement.....	v
Acknowledgments.....	vi
Table of Contents.....	vii
List of Tables.....	xii
List of Figures.....	xv
List of Schemes.....	xviii
List of Charts.....	xxiii
List of Appendices.....	xxiv
Table of Abbreviations.....	xxvi
Chapter 1.....	1
1 Introduction.....	1
1.1 Main Group Compounds as Potential Alternative to Transition Metal Catalysis.....	1
1.2 Main Group Complexes in Small Molecule Activation and Catalysis.....	4
1.3 Lewis Acid Catalysis.....	7
1.4 Frustrated Lewis Pairs.....	10
1.5 Germanium Lewis Acids.....	11
1.6 Bis(catecholato)silanes.....	13
1.7 Scope of the Thesis.....	15
References.....	17
Chapter 2.....	22
2 Synthesis and Lewis Acidity Assessment of Bis(catecholato)germanes.....	22

2.1	Introduction.....	22
2.1.1	Synthesis of Bis(catecholato)- Complexes with Group 14 Elements	22
2.1.2	Quantification of Lewis Acidity	26
2.1.3	Lewis Acidity of Bis(catecholato)silanes and -germanes.....	30
2.1.4	Project Goal: Bis(catecholato)germanes.....	32
2.2	Results and Discussion	33
2.2.1	Synthesis and Reactivity.....	33
2.2.2	Lewis Acidity Assessment – Gutmann Beckett.....	36
2.2.3	Lewis Acidity Assessment – FIA and GEI Calculations	43
2.3	Conclusions.....	46
2.4	Experimental	47
2.4.1	General Experimental	47
2.4.2	Synthesis of Bis(catecholato)germanes	47
2.4.3	Reactions of Bis(catecholato)germanes with Tetrabutylammonium Chloride.....	49
2.4.4	Reaction of Ge(dtbc) ₂ (THF) ₂ with Pyridine	50
2.4.5	Gutmann-Beckett Assessment of Lewis Acidity	50
2.4.6	Computational Details for FIA and GEI Calculations	51
2.4.7	X-Ray Crystallography Details.....	52
	References.....	54
	Chapter 3.....	57
3	The Lewis Acid Catalytic Applications of Bis(catecholato)germanes	57
3.1	Introduction.....	57
3.1.1	Lewis Acid Catalysis of Addition Reactions	57
3.1.2	Oligomerization of Alkenes	66
3.1.3	Group 14 Bis(catecholato)- Catalysts	67

3.1.4	Project Goal	70
3.2	Results and Discussion	71
3.2.1	Hydrosilylation of Aldehydes/Ketones.....	71
3.2.2	Hydroboration of Terminal Alkynes.....	77
3.2.3	Hydroamination and Friedel-Crafts Alkylation of Alkenes.....	83
3.2.4	Oligomerization Alkenes	87
3.3	Conclusion	94
3.4	Experimental.....	94
3.4.1	General Experimental	94
3.4.2	General Catalytic Procedures and Product Characterization	94
3.4.3	Hydrosilylation of Aldehydes	95
3.4.4	Oligomerization of Alkenes	96
3.4.5	Hydroboration of Alkynes	97
3.4.6	Friedel-Crafts Alkylation	98
References	100
Chapter 4	103
4	Mechanistic Study of Lewis Acid Catalysis with Bis(catecholato)germanes.....	103
4.1	Introduction.....	103
4.1.1	Methods for the Elucidation of Reaction Mechanisms.....	103
4.1.2	Mechanisms of Alkene Oligomerization	105
4.1.3	Mechanistic Studies of Bis(catecholato)silanes as Lewis Acid Catalysts.....	108
4.1.4	Project Goal	109
4.2	Results and Discussion	111
4.2.1	Experimental Studies	111
4.2.2	Computational Calculations.....	115

4.2.3	Proposed Mechanism for the Catalytic Oligomerization of α -methylstyrene by Bis(catecholato)germanes	119
4.3	Comparison to InBr_3 - and HI-Catalyzed Oligomerization of α -methylstyrene..	122
4.4	Conclusion	123
4.5	Experimental	124
4.5.1	General Experimental	124
4.5.2	Hammett Plot	124
4.5.3	Visual Kinetic Analysis	125
4.5.4	Computational Details	126
References	127
Chapter 5	129
5	Bis(catecholato)germanes as Potential Frustrated Lewis Pair Components	129
5.1	Introduction.....	129
5.1.1	The Design of Frustrated Lewis Pairs.....	129
5.1.2	Reactivity of Frustrated Lewis Pairs.....	130
5.1.3	Group 14 Frustrated Lewis Pairs	133
5.1.4	Project Goal	137
5.2	Results and Discussion	137
5.2.1	Synthesis of Lewis Acid-Base Adducts.....	138
5.2.2	Attempted Reactivity of FLPs	147
5.2.3	Computational Analysis of Lewis Adduct Formation	150
5.3	Conclusion	153
5.4	Experimental	154
5.4.1	General Experimental	154
5.4.2	Ligand Exchange Reactions from $\text{Ge}(\text{dtbc})_2(\text{py})_2$	154

5.4.3	Ligand Exchange Reactions from Bis(catecholato)germanes with weak donors.....	154
5.4.4	Reactivity studies with Bis(catecholato)germanes and Bulky Bases	155
5.4.5	Catalytic Activity of Ge(cat ^X) ₂ and Bulky Bases in the hydrosilylation of <i>p</i> -tolualdehyde	155
5.4.6	Computational Details	156
5.4.7	X-Ray Crystallography Details.....	156
	References.....	157
	Chapter 6.....	161
6	Conclusions and Future Work.....	161
6.1	Summary	161
6.2	Conclusion	164
6.3	Future Work	165
	References.....	168
	Appendices.....	169
	Curriculum Vitae	192

List of Tables

Table 2.1: The $^{31}\text{P}\{^1\text{H}\}$ chemical shifts and acceptor numbers of various Lewis acids (using hexanes as a reference).	28
Table 2.2: Calculated FIA values of common Lewis acids	29
Table 2.3: The $^{31}\text{P}\{^1\text{H}\}$ chemical shift and acceptor numbers from Gutmann-Beckett experiments with bis(catecholato)silanes. ⁵	31
Table 2.4: Calculated FIA values for the bis(catecholato)silanes.....	32
Table 2.5: Lewis Acidities of bis(catecholato)germanes and -silanes as determined by the Gutmann-Beckett method.	38
Table 2.6: Computational results for the FIA and GEI values of the bis(catecholato)germanes and the reported FIA values for the bis(catecholato)silanes for comparison.....	44
Table 2.7: Relative energies of $\text{Ge}(\text{cat}^{\text{Br}})_2$ derivatives.....	45
Table 3.1: Catalyst scope of various bis(catecholato)germane catalysts.....	71
Table 3.2: Optimization of the hydrosilylation of <i>para</i> -tolualdehyde with triethylsilane	73
Table 3.3: Aldehyde/Ketone Substrate Scope for Hydrosilylation using bis(catecholato)germane catalyst	74
Table 3.4 Silane substrate scope for the hydrosilylation of <i>para</i> -tolualdehyde with $\text{Ge}(\text{cat}^{\text{Cl}})_2(\text{ACN})_2$ as a catalyst.....	75
Table 3.5: The hydrosilylation of <i>para</i> -tolualdehyde with triethylsilane catalyzed by various main group Lewis acids	76

Table 3.6: Optimization of the conditions of the hydroboration of phenylacetylene using Ge(cat ^{Cl}) ₂ (ACN) ₂ as a catalyst.....	79
Table 3.7: Influence on substrate structure on the conversion of phenylacetylene to borylated alkenes.	80
Table 3.8: Examples of main group Lewis acid catalysts in the hydroboration of phenylacetylene with pinacolborane.....	82
Table 3.9: Hydroarylation of styrene and α -methylstyrene with diphenylamine	84
Table 3.10: Different bis(catecholato)germane catalysts in the Friedel-Crafts alkylation of styrene with diphenylamine.	86
Table 3.11: Substrate scope of various <i>para</i> -substituted styrene derivatives in the Friedel-Crafts alkylation of diphenylamine.....	87
Table 3.12: The effect of donor ligands and silane/borane additives on the dimerization of α -methylstyrene	89
Table 3.13: The effect of donor ligands and donor additives on the dimerization of α -methylstyrene in toluene- <i>d</i> ₈	91
Table 3.14: The effect of silane and borane additives on the dimerization of α -methylstyrene in CD ₂ Cl ₂	91
Table 3.15: Comparison of different catalysts in the dimerization of α -methylstyrene. ..	93
Table 4.1: Summary of key reactions on the catalytic oligomerization of α -methylstyrene.	111
Table 4.2 Calculation of Gibbs free energy of the association of ACN and THF to Ge(cat ^{Br}) ₂	117

Table 4.3: Calculated Gibbs free energies for the coordination of various substrates to $\text{Ge}(\text{cat}^{\text{Br}})_2(\text{ACN})$	119
Table 4.4: Concentrations used for the VTNA rate study	126
Table 5.1: Calculated Gibbs free energies of formation for Lewis acid-base adduct formation.....	137
Table 5.2: The change in $^3\text{P}\{^1\text{H}\}$ chemical shift of various phosphines when in solution with borane 5.10.....	147
Table 5.3: Energetics of ligand association of various Lewis bases with $\text{Ge}(\text{cat}^{\text{Br}})_2$	152
Table 5.4: Energetics of the association of different Lewis bases to $\text{Ge}(\text{cat}^{\text{Br}})_2(\text{ACN})$..	153

List of Figures

- Figure 2.1: a) The different coordination environments of bis(catecholato) complexes. b) An orbital picture illustrating the *sp* hybridization of the group 14 element relative to the octahedral geometry. c) The molecular orbitals involved in the 3-centre-4-electron bonding in $E(\text{cat})_2(\text{Donor})_2$ 24
- Figure 2.2: The reactions involved in the anchor point system for calculating FIA. 29
- Figure 2.3: Thermal ellipsoid plot of $\text{Ge}(3,5\text{-dtbc})_2(\text{THF})_2$ showing naming and numbering scheme. Ellipsoids are at the 50% probability level and hydrogen atoms were omitted for clarity. Selected bond lengths (Å) and angles (°): Ge1-O1 = 1.8247(13), Ge1-O2 = 1.8297(13), Ge1-O3 = 2.1126(14); O1-Ge1-O2 = 89.60(6), O1-Ge1-O3 = 90.69(6); O2-Ge1-O3 = 92.23(6). 34
- Figure 2.4: Thermal ellipsoid plot of $[\text{NBu}_4][\text{Ge}(\text{cat}^{\text{Br}})_2\text{Cl}]$ showing naming and numbering scheme. Ellipsoids are at the 50% probability level. NBu_4 cation and hydrogen atoms were omitted for clarity. Selected bond lengths (Å) and angles (°): Ge1-O1 = 1.8387(16), Ge1-O2 = 1.8529(16), Ge1-O3 = 1.8489(16), Ge1-O4 = 1.8369(16), Ge1-Cl1 = 2.1622(13); O1-Ge1-O4 = 150.29(8), O2-Ge1-O3 = 158.98(8), O1-Ge1-Cl1 = 106.68(6), O3-Ge1-Cl1 = 99.60(6). 36
- Figure 2.5: ^1H NMR (400 MHz in CD_2Cl_2) stacked spectra of $\text{Ge}(3,5\text{-dtbc})_2(\text{THF})_2$ and various equivalents of triethylphosphine oxide 39
- Figure 2.6: $^{31}\text{P}\{^1\text{H}\}$ VT-NMR spectrum of a solution containing 1 eq. $\text{Ge}(\text{dtbc})_2(\text{THF})_2$ and 3 eq. of OPEt_3 , at room temperature (top) and -80°C (bottom) (66.6 ppm=*trans*- $\text{Ge}(\text{dtbc})_2(\text{OPEt}_3)_2$; 53.5 ppm= OPEt_3) 39
- Figure 2.7: a) Thermal ellipsoid plot of $\text{Ge}(3,5\text{-dtbc})_2(\text{OPEt}_3)_2$ showing naming and numbering scheme. Ellipsoids are at the 50% probability level and hydrogen atoms were omitted for clarity. Selected bond lengths (Å) and angles (°): Ge1-O1 = 1.9863(8), Ge1-O2 = 1.8467(7), Ge1-O3 = 1.8484(8), P1-O1 = 1.5208(7); O1-Ge1-O2 = 89.75(3), O1-Ge1-O3 = 90.36(3); O2-Ge1-O3 = 88.61(3). 40

Figure 2.8: $^{31}\text{P}\{^1\text{H}\}$ NMR (162 MHz in CD_2Cl_2) stacked spectra of $\text{Ge}(\text{cat}^{\text{Cl}})_2(\text{THF})_2$ and various equivalents of triethylphosphine oxide	41
Figure 2.9: $^{31}\text{P}\{^1\text{H}\}$ NMR (162 MHz in CD_2Cl_2) stacked spectra of $\text{Ge}(\text{cat}^{\text{Br}})_2(\text{THF})_2$ and various equivalents of triethylphosphine oxide	42
Figure 2.10: ^1H NMR (400 MHz in CD_2Cl_2) stacked spectra of $\text{Ge}(\text{cat}^{\text{Br}})_2(\text{THF})_2$ and various equivalents of triethylphosphine oxide. Similar signals for the chlorinated derivative were observed and in agreement with the literature. ⁶	43
Figure 3.1: Dimer products 3.6 (red trace), 3.7 (green trace), and 3.8 (blue trace) formed in reactions with α -methylstyrene and $\text{Ge}(\text{cat}^{\text{Br}})_2(\text{ACN})_2$ over a period of 24 hours at 100°C	88
Figure 4.1: VTNA plots for the oligomerization of α -methylstyrene. The order of α -methylstyrene is 1.5	113
Figure 4.2: Hammett plot for the oligomerization of various <i>para</i> -substituted styrene derivatives. The points are averages of at least two runs.....	114
Figure 4.3: Dimers 3.6 (red trace), 3.7 (green trace), and 3.8 (blue trace) formed in reactions with α -methylstyrene and $\text{Ge}(\text{cat}^{\text{Br}})_2(\text{ACN})_2$ over a period of 24 hours at 100°C	115
Figure 4.4: Energetics of the coordination of styrene to $\text{Ge}(\text{cat}^{\text{Br}})_2(\text{ACN})_x$ ($x = 0-2$). ...	118
Figure 4.5: VTNA plot of α -methylstyrene oligomerization with a reactant order of 1.5 showing error bars.....	125
Figure 4.6: VTNA plots of α -methylstyrene oligomerization with reactant orders of 1.4 and 1.6	126

Figure 5.1: The basic premise behind frustrated Lewis pair chemistry	129
Figure 5.2: ^1H NMR spectra stack (600 MHz) of $\text{Ge}(\text{dtbc})_2(\text{py})_2$ and $\text{Ge}(\text{dtbc})_2(\text{lut})_2$ in CDCl_3	139
Figure 5.3: Thermal ellipsoid plot of $[\text{Ge}(3,5\text{-dtbc})_2\text{Cl}]^-$ showing naming and numbering scheme. Ellipsoids are at the 50% probability level and hydrogen atoms and cation were omitted for clarity. Selected bond lengths (\AA) and angles ($^\circ$): $\text{Ge1-O1} = 1.8322(12)$, $\text{Ge1-O2} = 1.8585(13)$, $\text{Ge1-O3} = 1.8416(12)$, $\text{Ge1-O4} = 1.8261(13)$, $\text{Ge1-Cl1} = 2.1755(7)$; $\text{O1-Ge1-O3} = 153.96(6)$, $\text{O1-Ge1-O4} = 87.37(6)$, $\text{O1-Ge-Cl1} = 101.95(5)$	141
Figure 5.4: ^1H NMR (400 MHz, C_6D_6) spectrum of $\text{Ge}(\text{dtbc})_2(\text{lut})$	141
Figure 5.5: Thermal ellipsoid plot of $\text{Ge}(3,5\text{-dtbc})_2\text{OH}_2\text{-lut}$, with a C_6D_6 solvent molecule showing naming and numbering scheme. Ellipsoids are at the 50% probability level and hydrogen atoms were omitted for clarity. Selected bond lengths (\AA) and angles ($^\circ$): $\text{Ge1-O1} = 1.788(8)$, $\text{Ge1-O2} = 1.811(7)$, $\text{Ge1-O3} = 1.854(6)$, $\text{Ge1-O4} = 1.871(7)$, $\text{Ge1-O5} = 1.825(7)$; $\text{O2-Ge1-O5} = 129.6(4)$, $\text{O3-Ge1-O4} = 170.1(4)$	143
Figure 5.6: a) Thermal ellipsoid plot of $[\text{Ge}(\text{cat}^{\text{Cl}})_2\text{Cl}_2]$ showing naming and numbering scheme. Ellipsoids are at the 50% probability level and the cations and hydrogen atoms were omitted for clarity. Selected bond lengths (\AA) and angles ($^\circ$): $\text{Ge1-O1} = 1.8683(12)$, $\text{Ge1-O2} = 1.8685(11)$, $\text{Ge1-Cl1} = 2.3419(9)$, $\text{O1-Ge1-O2} = 89.11(4)$, $\text{O1-Ge1-Cl1} = 89.15(4)$, $\text{O2-Ge1-Cl1} = 88.85(3)$. b) Thermal ellipsoid plot of $[\text{Ge}(\text{cat}^{\text{Br}})_2\text{-O-Ge}(\text{cat}^{\text{Br}})_2]^{2-}$ showing naming and numbering scheme. Ellipsoids are at the 50% probability level and hydrogen atoms and cation were omitted for clarity. Selected bond lengths (\AA) and angles ($^\circ$): $\text{Ge1-O1} = 1.833(2)$, $\text{Ge1-O2} = 1.888(2)$, $\text{Ge1-O3} = 1.882(2)$, $\text{Ge1-O4} = 1.824(2)$, $\text{Ge1-O9} = 1.750(2)$; $\text{O1-Ge1-O3} = 87.31(10)$, $\text{O2-Ge1-O3} = 167.49(10)$	146

List of Schemes

Scheme 1.1: An example of a typical catalytic cycle illustrating the oxidation state changes of the metal catalyst [M] from oxidative addition and reductive elimination reactions.	2
Scheme 1.2: Oxidation of cyclohexene by iron catalyst 1.1	3
Scheme 1.3: Activation of H ₂ by digermene 1.2 and activation of CO ₂ by diborene 1.3 . .	4
Scheme 1.4: Hydrogen and main group oxide activation by silylene 1.6 (Dipp = 2,6-diisopropylphenyl)	5
Scheme 1.5: Nitrogen activation achieved by borylenes (Dur = 2,3,5,6-tetramethylphenyl)	6
Scheme 1.6: Hydroboration of aldehydes achieved using germylene 1.8 and stannylene 1.9 catalysts.....	7
Scheme 1.7: a) Example of Lewis acid adduct formation. b) Example of Lewis acid activation of a carbonyl moiety.....	8
Scheme 1.8: AlCl ₃ catalyzed reactions: a) Hydrosilylation of an alkene b) Intramolecular Friedel-Crafts alkylation	8
Scheme 1.9: Hydrosilylation of styrene catalyzed by B(C ₆ F ₅) ₃	9
Scheme 1.10: The catalytic ring-forming C _{sp3} -H functionalization by phosphonium catalyst 1.10	9
Scheme 1.11: H ₂ activation by an FLP.	10
Scheme 1.12: Hydrogenation of imines achieved with a Sn/N FLP catalyst	11
Scheme 1.13: Reduction of CO ₂ with a borane with FLP catalyst 1.13	11

Scheme 1.14: C-N and C-H bond activation of triethylamine achieved by the germanium Lewis acid 1.14	12
Scheme 1.15: Reactivity of Ge/P FLPs.....	13
Scheme 1.16: Hydrosilylation of <i>para</i> -nitrobenzaldehyde catalyzed by Si(cat ^F) ₂	14
Scheme 2.1: <i>a</i>) Synthesis of Si(cat ^F) ₂ . <i>b</i>) Synthesis of Si(cat ^{Cl}) ₂ (ACN) ₂ and Si(cat ^{Br}) ₂ (ACN) ₂ . <i>c</i>) Synthesis of Si(cat ^{CF₃}) ₂ (sulfolane) ₂ . <i>d</i>) Synthesis of Ge(cat ^{Cl}) ₂ with water and acetonitrile donor ligands.	25
Scheme 2.2: <i>a</i>) Synthesis of bis(catecholato)germanes via two different routes. <i>b</i>) A proposed mechanism for the redox reaction between quinone and GeCl ₂ •diox (dioxane and quinone substituents were omitted for clarity).....	33
Scheme 2.3: Addition of NBu ₄ Cl and pyridine to bis(catecholato)germanes.	36
Scheme 3.1: Generalized addition reactions to a representative alkene.	57
Scheme 3.2: An example of polysiloxane crosslinking	58
Scheme 3.3: Hydrosilylation of a tetrasubstituted alkene using AlCl ₃ as a Lewis acid catalyst.	59
Scheme 3.4: Hydrosilylation of alkenes using B(C ₆ F ₅) ₃ as the catalyst.	59
Scheme 3.5: Silicon cation 3.1 facilitates the hydrosilylation of alkenes at low catalyst loadings.	59
Scheme 3.6: Hydroamination of norbornene with an electron-deficient aniline catalyzed by main group halides.	60

Scheme 3.7: Hydroamination of phenylacetylene with an electron-deficient aniline performed using main group halide Lewis acids.	61
Scheme 3.8: Intramolecular hydroamination using catalyst 3.2	62
Scheme 3.9: Hydroamination of alkynes using bulky amines catalyzed by $B(C_6F_5)_3$	62
Scheme 3.10: <i>a)</i> Hydroboration of an alkyne using fluorinated aryl borane catalysts. <i>b)</i> The equilibrium between the catalysts and the active catalytic species.	64
Scheme 3.11: Hydroboration of alkenes achieved using 3.5 as a Lewis acid catalyst.	64
Scheme 3.12: Friedel-Crafts alkylation using $Bi(OTf)_3$ as a Lewis acid catalyst.	65
Scheme 3.13: Intramolecular Friedel-Crafts reaction using $AlCl_3$ as the catalyst.....	66
Scheme 3.14: Dimerization of α -methylstyrene achieved using $InBr_3$	67
Scheme 3.15: Hydrosilylation of benzaldehyde derivatives using $Si(cat^F)_2$ as the catalyst.	67
Scheme 3.16: Hydrodefluorination using $Si(cat^{Cl})_2(ACN)_2$ as the catalyst yielding adamantane and polymethylfluorodisiloxane (PMFS)	68
Scheme 3.17: Examples of the reactions catalyzed by $Si(cat^{CF_3})_2(sulfolane)_2$	69
Scheme 3.18: Examples of the reactions using $Ge(cat^{Cl})_2(ACN)_2$ as the catalyst.....	70
Scheme 3.19: Friedel-crafts alkylation of anisole and styrene catalyzed by $Ge(cat^{Cl})_2(ACN)_2$	87
Scheme 4.1: Proposed mechanism for the dimerization of α -methylstyrene catalyzed by $InBr_3$	106

Scheme 4.2: Proposed mechanism for the oligomerization of α -methylstyrene catalyzed by HI gas with the use of methyl <i>para</i> -tolyl ketone as an additive.	108
Scheme 4.3: Calculated energetics of ACN dissociation from $\text{Si}(\text{cat}^{\text{Cl}})_2(\text{ACN})_2$	109
Scheme 4.4: The reaction conditions used for the VTNA rate study	112
Scheme 4.5: The reaction between styrene and <i>para</i> -substituted styrenes used to generate the Hammett plot.....	113
Scheme 4.6: Proposed mechanism for the oligomerization of α -methylstyrene in toluene	121
Scheme 4.7: Proposed formation of trimer 3.19 by trimerization and subsequent Friedel-Crafts alkylation.....	122
Scheme 4.8: Selected portion of the mechanism for the oligomerization of α -methylstyrene by bis(catecholato)germanes highlighting intermediates 4.8 , 4.9 , and 4.10	123
Scheme 5.1: Reversible activation of dihydrogen by FLP 1.11	131
Scheme 5.2: Activation of various main group oxides by $\text{B}(\text{C}_6\text{F}_5)_3$ and P^tBu_3	131
Scheme 5.3: An example of catalytic hydrogenation of an imine and alkene using $\text{B}(\text{C}_6\text{F}_5)_2\text{Mes}$ and DABCO. ¹⁰	132
Scheme 5.4: Catalytic hydrosilylation of imines achieved using FLP 5.2	133
Scheme 5.5: Activation of small molecules using geminal FLP's using group 14 Lewis acid centres.....	133
Scheme 5.6: Catalytic hydrogenation of an imine using a Sn/N FLP.	134

Scheme 5.7: Bis(catecholato)silanes in combination with bidentate Lewis bases as FLP's.	135
Scheme 5.8: Reactivity of $\text{Si}(\text{am}^{\text{F}}\text{ph}^{\text{F}})_2$ with various bulky bases.	136
Scheme 5.9: Reaction of $\text{Ge}(\text{dtbc})_2(\text{py})_2$ with excess 2,6-lutidine.....	138
Scheme 5.10: Reaction of $\text{Ge}(\text{dtbc})_2(\text{THF})_2$ with 2,6-lutidine.	142
Scheme 5.11: Addition of water to $\text{Ge}(\text{dtbc})_2(\text{lut})$	142
Scheme 5.12: Reaction of $\text{Ge}(\text{dtbc})_2(\text{THF})_2$ with tri- <i>tert</i> -butylphosphine.....	144
Scheme 5.13: The reactivity that will be attempted with the bis(catecholato)germane FLPs.	148
Scheme 5.14: The attempted hydrosilylation of <i>para</i> -tolualdehyde with bis(catecholato)germanes and bulky Lewis bases.	150
Scheme 6.1: Synthesis of bis(catecholato)germanes	161
Scheme 6.2: Dimerization of α -methylstyrene catalyzed by $\text{Ge}(\text{cat}^{\text{Cl}})_2(\text{ACN})_2$	162
Scheme 6.3: Proposed mechanism for the oligomerization of α -methylstyrene catalyzed by bis(catecholato)germanes.....	163
Scheme 6.4: The formation of Lewis adducts which inhibits FLP reactivity.....	164
Scheme 6.5: A Lewis acid catalyzed Diels-Alder reaction illustrating the Lewis acid coordination with methyl acrylate.	166

List of Charts

Chart 1.1: Bis(catecholato)silanes showing the naming convention which will be utilized throughout the thesis: $E(\text{cat}^X)_2(\text{donor})_2$	14
Chart 3.1: Pinacolborane (HBpin) and catecholborane (HBcat).	63
Chart 3.2: Aluminum Lewis acid catalysts	81
Chart 3.3: Ruthenium catalyst for dimerization of α -methylstyrene.	92
Chart 5.1: FLP's 1.11 , $P^t\text{Bu}_3$ and $B(\text{C}_6\text{F}_5)_3$, and 5.1	130
Chart 6.1: Proposed synthetic targets.....	165
Chart 6.2: Proposed FLP involving bis(catecholato)germanes and a bidentate Lewis base.	167

List of Appendices

Appendix A: ^1H NMR (CDCl_3 , 400 MHz) spectrum of $\text{Ge}(\text{dtbc})_2(\text{THF})_2$	169
Appendix B: $^{13}\text{C}\{^1\text{H}\}$ NMR (CDCl_3 , 101 MHz) spectrum of $\text{Ge}(\text{dtbc})_2(\text{THF})_2$	170
Appendix C: ^1H NMR (CDCl_3 , 400 MHz) spectrum of $\text{Ge}(\text{dtbc})_2(\text{ACN})_2$	170
Appendix D: ^1H NMR (CDCl_3 , 400 MHz) spectrum of $[\text{NBu}_4][\text{Ge}(\text{dtbc})_2\text{Cl}]$	171
Appendix E: ^1H NMR (CDCl_3 , 400 MHz) spectrum of $[\text{NBu}_4][\text{Ge}(\text{cat}^{\text{Cl}})_2\text{Cl}]$	171
Appendix F: ^1H NMR (CDCl_3 , 400 MHz) spectrum of $[\text{NBu}_4][\text{Ge}(\text{cat}^{\text{Br}})_2\text{Cl}]$	172
Appendix G: $^{31}\text{P}\{^1\text{H}\}$ NMR (CH_2Cl_2 , 162 MHz) stacked spectrum of the Gutmann-Beckett analysis performed with sub-stoichiometric amounts of triethylphosphine oxide on the halogenated bis(catecholato)germanes.	173
Appendix H: $^{31}\text{P}\{^1\text{H}\}$ NMR (162 MHz, CD_2Cl_2) stacked spectrum of the Gutmann-Beckett analysis performed with sub-stoichiometric amounts of triethylphosphine oxide on the 3,5-di- <i>tert</i> -butyl bis(catecholato)germanes. In each case, the signal is assigned to $\text{Ge}(3,5\text{-dtbc})_2(\text{OPEt}_3)$	174
Appendix I: $^{31}\text{P}\{^1\text{H}\}$ NMR (162 MHz in CD_2Cl_2) stacked spectra of $\text{Ge}(3,5\text{-dtbc})_2(\text{THF})_2$ and various equivalents of triethylphosphine oxide.....	175
Appendix J: $^{13}\text{C}\{^1\text{H}\}$ NMR (101 MHz in CD_2Cl_2) stacked spectra of $\text{Ge}(3,5\text{-dtbc})_2(\text{THF})_2$ and various equivalents of triethylphosphine oxide	176
Appendix K: ^1H NMR (400 MHz in CD_2Cl_2) stacked spectra of $\text{Ge}(\text{cat}^{\text{Cl}})_2(\text{THF})_2$ and various equivalents of triethylphosphine oxide	177
Appendix L: $^{13}\text{C}\{^1\text{H}\}$ NMR (C_6D_6 , 101 MHz) spectrum of $\text{Ge}(\text{dtbc})_2(\text{lut})$	178
Appendix M: ^1H NMR (C_6D_6 , 400 MHz) spectrum of $\text{Ge}(\text{dtbc})_2(\text{P}^t\text{Bu}_3)$	179

Appendix N: $^{31}\text{P}\{^1\text{H}\}$ NMR (C_6D_6 , 162 MHz) spectrum of $\text{Ge}(\text{dtbc})_2(\text{P}'\text{Bu}_3)$	179
Appendix O: ^1H NMR (C_6D_6 , 400 MHz) spectrum of $\text{Ge}(\text{cat}^{\text{Cl}})_2(\text{P}'\text{Bu}_3)$	180
Appendix P: $^{31}\text{P}\{^1\text{H}\}$ NMR (C_6D_6 , 162 MHz) spectrum of $\text{Ge}(\text{cat}^{\text{Cl}})_2(\text{P}'\text{Bu}_3)$	180
Appendix Q: ^1H NMR (C_6D_6 , 400 MHz) spectrum of $\text{Ge}(\text{cat}^{\text{Br}})_2(\text{P}'\text{Bu}_3)$	181
Appendix R: $^{31}\text{P}\{^1\text{H}\}$ NMR (C_6D_6 , 162 MHz) spectrum of $\text{Ge}(\text{cat}^{\text{Cl}})_2(\text{P}'\text{Bu}_3)$	181
Appendix S: Summary of Crystal Data for $\text{Ge}(\text{dtbc})_2(\text{THF})_2$, $[\text{NBu}_4][\text{Ge}(\text{cat}^{\text{Br}})_2\text{Cl}]$, and $\text{Ge}(\text{dtbc})_2(\text{OPEt}_3)_2$	182
Appendix T: Summary of Crystal Data for $[\text{H-lut}][\text{Ge}(\text{dtbc})_2\text{Cl}]$, $\text{Ge}(\text{dtbc})_2(\text{H}_2\text{O})\text{---lut}$, $2[\text{Cl-P}'\text{Bu}_3][\text{Ge}(\text{cat}^{\text{Cl}})_2\text{Cl}_2]$, $\text{Ge}(\text{cat}^{\text{Br}})_2\text{-O- Ge}(\text{cat}^{\text{Br}})_2$	184
Appendix U: The anchor point data used in the determination of FIA values	186
Appendix V: Calculated data for the determination of the FIA values of the bis(catecholato)germane complexes.	186
Appendix W: Calculated data for the determination of the GEI values of the bis(catecholato)germane complexes.	188
Appendix X: Calculated energetics of ligand dissociation and substrate activation with $\text{Ge}(\text{cat}^{\text{Br}})_2$	189
Appendix Y: Calculated energetics of ligand dissociation association of tested Lewis bases with $\text{Ge}(\text{cat}^{\text{Br}})_2$	191

Table of Abbreviations

9-BBN	9-Borabicyclo(3.3.1)nonane
ACN	Acetonitrile
AN	Acceptor Number
Ar	Aryl Group
Ar ^F	2,4,6-Trifluorophenyl
aug-cc- pVQZ	Augmented Correlation-Consistent Polarized Valence Quadruple Zeta
B3LYP	Becke 3-Parameter Lee-Yang-Parr
br	Broad Signal
Bu	Butyl
CAD	Canadian Dollars
[cat]	Catalyst
CCSD(T)	Couple Cluster Singles, Doubles, and Perturbative Triples
Cp*	1,2,3,4,5-Pentamethylcyclopentadiene
Cy	Cyclohexyl
d	Doublet
D3(BJ)	Becke-Johnson Damping
DCE	1,2-Dichloroethane

Def2- mSVP	Default2- Modified Single Valence Single Zeta Polarization
def2- TZVPP	Default2-Valence Triple Zeta with two sets of Polarization Functions
DFS	Double Focusing Sector
DFT	Density Functional Theory
diox	1,4-Dioxane
Dipp	2,6-Diisopropylphenyl
DLPNO	Domain-Based Local Pair Natural Orbital
DMF	Dimethylformamide
DN	Donor Number
dtbc	3,5-Di- <i>tert</i> -butylcatecholato
DABCO	1,4-diazabicyclo[2.2.2]octane
Dur	2,3,5,6-Tetramethylphenyl
EA	Elemental Analysis
EI	Electron Impact
eq	Equivalent(s)
ESI	Electrospray Ionization
Et	Ethyl
FIA	Fluoride Ion Affinity

FLP	Frustrated Lewis Pair
G	Gibbs Free Energy
GEI	Global Electrophilicity Index
{ ¹ H}	Proton Decoupled
h	Hour(s)
HBcat	Catecholborane
HBpin	Pinacolborane
HSAB	Hard Soft Acid Base
HOMO	Highest Occupied Molecular Orbital
ⁱ Pr	<i>Iso</i> -propyl
IR	Infrared
<i>I</i> Bu	1,3-di- <i>tert</i> -butyl-1,3-imidazol-2-ylidene
KIE	Kinetic Isotope Effect
LUMO	Lowest Unoccupied Molecular Orbital
lut	2,6-Lutidine
m	Multiplet
Me	Methyl
Mes	Mesityl
MS	Mass Spectrometry

m/z	Mass to Charge Ratio
NHC	N-Heterocyclic Carbene
NMR	Nuclear Magnetic Resonance
OTf	Triflate
PBEh-3c	Perdew-Burke-Ernzerhoff 3-fold corrected Hartree-Fock
Ph	Phenyl
PMHS	Polymethylhydrodisiloxane
PMFS	Polymethylfluorodisiloxane
pmp	1,2,2,6,6-Pentamethylpiperidine
py	Pyridine
py ^{<i>t</i>Bu₂}	di- <i>tert</i> -butylpyridine
q	Quartet
rt	Room Temperature
s	Singlet
t	Triplet
<i>t</i> Bu	<i>Tert</i> -butyl
THF	Tetrahydrofuran
TLC	Thin-Layer Chromatography
tmp	Tetramethylpiperidine

TMS	Trimethylsilyl
TOF	Turnover Frequency
TON	Turnover Number
VT-NMR	Variable Temperature Nuclear Magnetic Resonance
VTNA	Variable Time Normalization Analysis
k	Rate Constant
η	Chemical Hardness
σ	Substituent Constant
ρ	Reaction Constant
μ	Chemical Potential
ν	Reaction Rate
ω	Global Electrophilicity Index Value

Chapter 1

1 Introduction

1.1 Main Group Compounds as Potential Alternative to Transition Metal Catalysis

There is an ever-growing demand for more sustainable chemical processes, the methodologies used to convert raw materials into consumer and industrial products. Catalysts, compounds which lower the activation barrier of a chemical reaction without being consumed during the course of the reaction, are used in over 90% of industrial processes and are key in the development of sustainable chemical processes.¹ Catalysis is one of the 12 principles of green chemistry resulting in more energetically efficient chemical transformations and, depending on the reaction, can allow the use of atom economical feedstocks.²

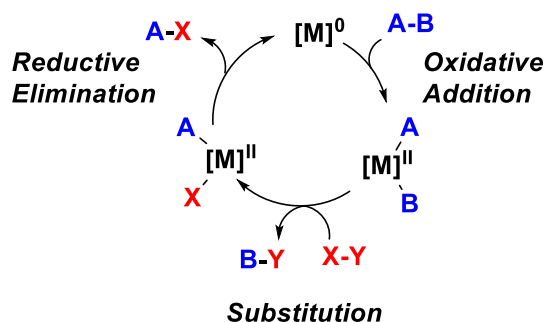
With the importance of catalysis in industry, it is critical to choose the most efficient catalyst for a reaction. There are many different metrics used to evaluate the effectiveness of a catalyst, including substrate conversion, turnover number (TON), turnover frequency (TOF) and product selectivity. Substrate conversion is the percentage of a substrate that is consumed during the reaction. Turnover, the ability for a catalyst to transform substrates into products, is quantified by turnover number (TON), the number of moles of substrate that a mole of catalyst can convert before becoming inactivated. Turnover frequency (TOF) is the turnover number divided by time and is a measure of how quickly the transformation takes place. Catalysts with high turnover numbers can be used to facilitate multiple substrate transformations without being deactivated by decomposition or side reactions which render the catalyst inactive.

$$(1) \quad \text{TON} = n_{\text{product}}/n_{\text{catalyst}}$$

$$(2) \quad \text{TOF} = \text{TON}/t$$

Product selectivity refers to the ability of a catalyst to selectively catalyze a reaction leading to a specific product. In addition to reaction metrics such as conversion, turnover numbers and product selectivity, other metrics such as price and toxicity of the catalyst are important considerations as well.

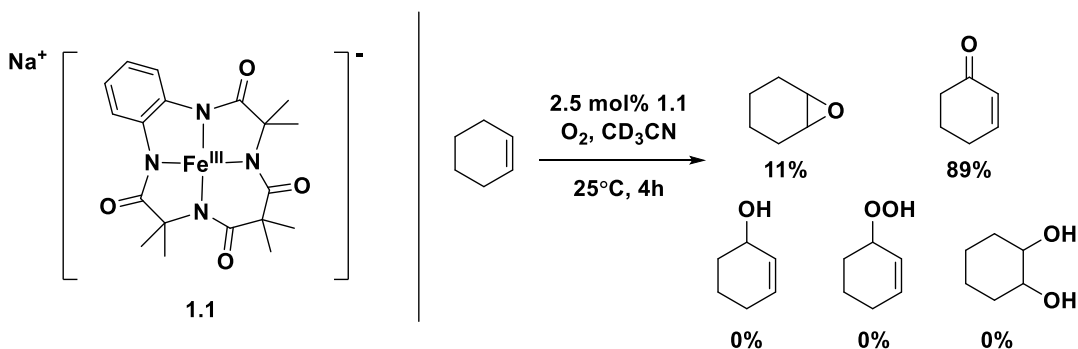
State-of-the-art catalysts are, primarily, based on second and third row transition metals, such as the noble metals, platinum and palladium.³ The second and third row transition metals exhibit high turnover and product selectivity due to their ability to reliably perform two-electron oxidation state changes, via oxidative addition and reductive elimination reactions (Scheme 1.1). While high turnover and selectivity make these second and third row transition metals preferable catalysts, the use of these elements are not without disadvantages. Second and third row transition metals are expensive, with elements such as platinum, palladium, and gold, costing between \$36,000 – \$53,000 CAD per kilogram.⁴ Some transition metals exhibit human toxicity, which can make their use in the pharmaceutical industry challenging. The residual metal in the final drug has to be as minimal, at the parts per million (ppm) or parts per billion (ppb) levels, making efficient removal of the metal necessary.⁵ Finally, the second and third row transition metals all exhibit supply risks, either due to low earth abundance or due to geopolitical or sustainability issues that affect the mining of the source metals.⁶ These disadvantages increase the demand for alternative catalysts.



Scheme 1.1: An example of a typical catalytic cycle illustrating the oxidation state changes of the metal catalyst [M] from oxidative addition and reductive elimination reactions.

Base metals, such as iron and copper, have been explored as alternatives to second and third row metal catalysts. The first-row transition metals are substantially cheaper and more earth abundant.^{4,6} However, the preference of base metals to undergo single electron oxidation state changes results in the formation of radical intermediates which is not observed with the two electron oxidation state changes common in noble metal catalysis. The presence of radical intermediates often leads to the formation of side products often not observed in two-electron processes. This presents an on-going challenge in the field of base metal catalysis. As a consequence, ligand design strategies are critical. A common strategy is utilizing redox-active ligands with base metals to mimic the two-electron oxidation state changes that the later transition metals exhibit.⁷ While redox-active ligands have the potential to address the disadvantages of one-electron oxidation state changes, the increased cost of these specialty ligands can pose a new disadvantage.

An example of a base metal-catalyzed one electron reaction is the oxidation of cyclohexene with molecular oxygen.⁸ O₂ is the ideal oxidant in terms of atom economy; however, the oxidation is often not selective giving a variety of different oxygenated products (Scheme 1.2).⁹ The iron catalyst **1.1** shows promise as reactions catalyzed by **1.1** only lead to the formation of only two products, the ketone and epoxide in 89% and 11% yield respectively. While, it is still not selective towards one product, the selectivity is an improvement on other catalytic systems.

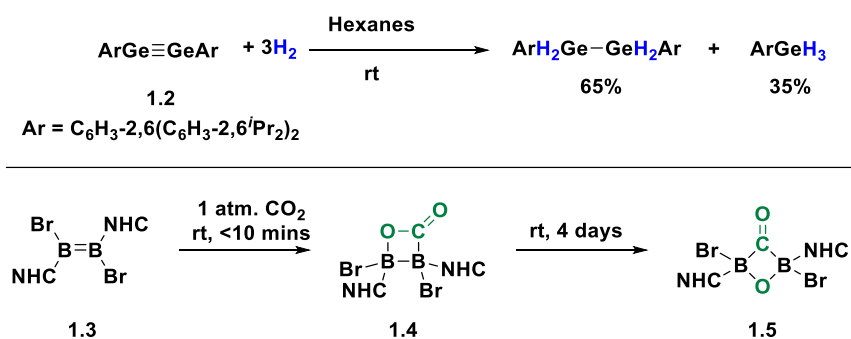


Scheme 1.2: Oxidation of cyclohexene by iron catalyst **1.1**

1.2 Main Group Complexes in Small Molecule Activation and Catalysis

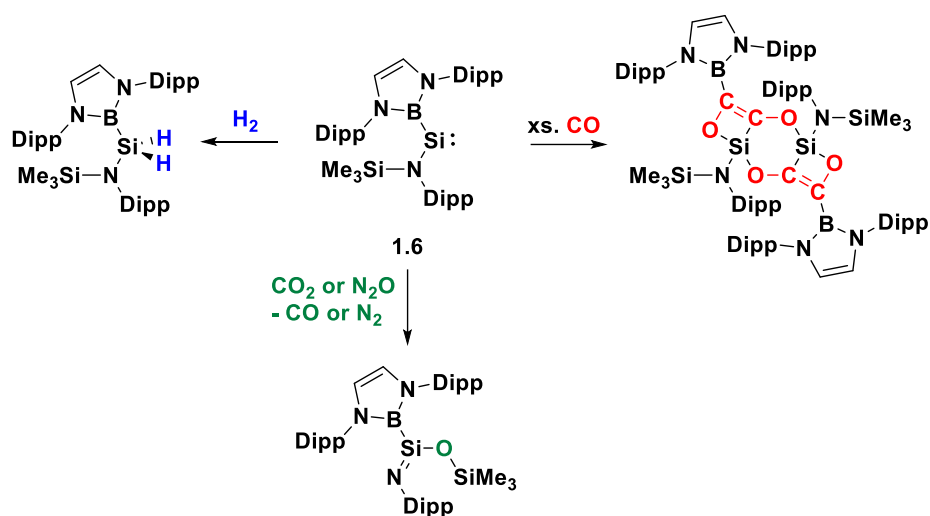
Another alternative to transition metal catalysts are catalysts based on main group elements.¹⁰ Depending on the element used, the main group element can be more earth abundant and less expensive than precious metals. While the chemistry of heavier *p*-block elements has naturally been compared to their first-row counterparts, more recently it has been recognized that heavier *p*-block compounds can mimic the catalytic activity of transition metals including the ability to activate small molecules and perform catalytic transformations.¹⁰

Main group compounds, particularly low-valent derivatives, have been shown to activate numerous small molecules including feedstocks such as H₂,¹¹ CO₂,¹² CO,¹³ NH₃,¹⁴ and O₂.¹⁵ The activation of small molecules is generally a precursor to the use of the reaction in catalysis. The use of unsaturated main group molecules is one class of low-valent compounds that have been studied in this regard. For example, digermynes **1.2**, the heavier group 14 analogue of an alkyne, undergoes addition of H₂ across the Ge-Ge triple bond under mild conditions (Scheme 1.3).¹¹ While the reaction results in a mixture of products, the ratio of products formed could be tuned by the amount of dihydrogen added. Another example is the activation of CO₂ achieved with diborene **1.3** with *N*-heterocyclic carbenes (NHC).¹⁶ In less than 10 minutes at room temperature, diborene **1.3** reacts with CO₂ in a [2+2] cycloaddition yielding the thermally unstable adduct **1.4**. **1.4** was successfully characterized by nuclear magnetic resonance (NMR) spectroscopy and X-ray crystallography. Rearrangement of **1.4** to **1.5** took place over the course of 4 days.



Scheme 1.3: Activation of H₂ by digermynes **1.2** and activation of CO₂ by diborene **1.3**.

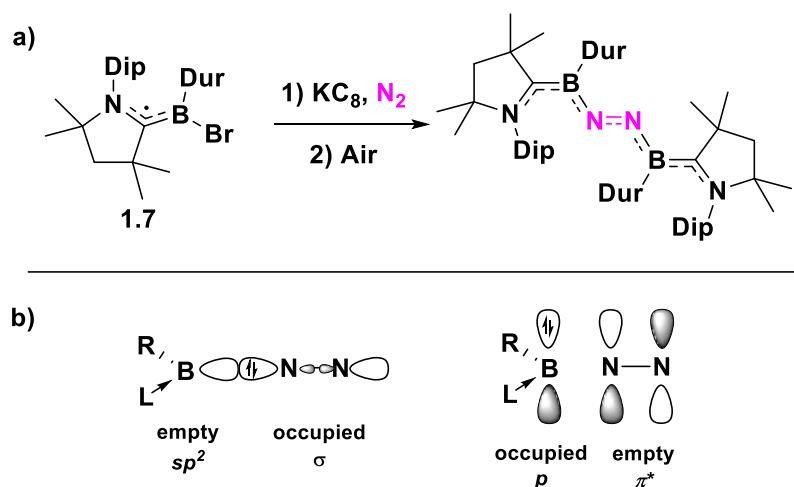
Another class of main group compounds typically used in small molecule activation is the tetrylenes, the heavier Group 14 analogues of carbenes. For example, the silicon analogues, silylenes, have been shown to activate a variety of small molecules. Hydrogen activation was achieved using silylene **1.6** under mild conditions yielding the addition of both hydrogen atoms to the low-valent silicon centre (Scheme 1.4).¹⁷ The same silylene was later reported to activate a variety of main group oxides.¹⁸ When reacted with excess carbon monoxide, a dimeric compound with four CO units was isolated. However, when **1.6** was reacted with CO₂ and N₂O, oxygen abstraction was observed with the formation of CO and N₂, respectively.



Scheme 1.4: Hydrogen and main group oxide activation by silylene **1.6** (Dipp = 2,6-diisopropylphenyl)

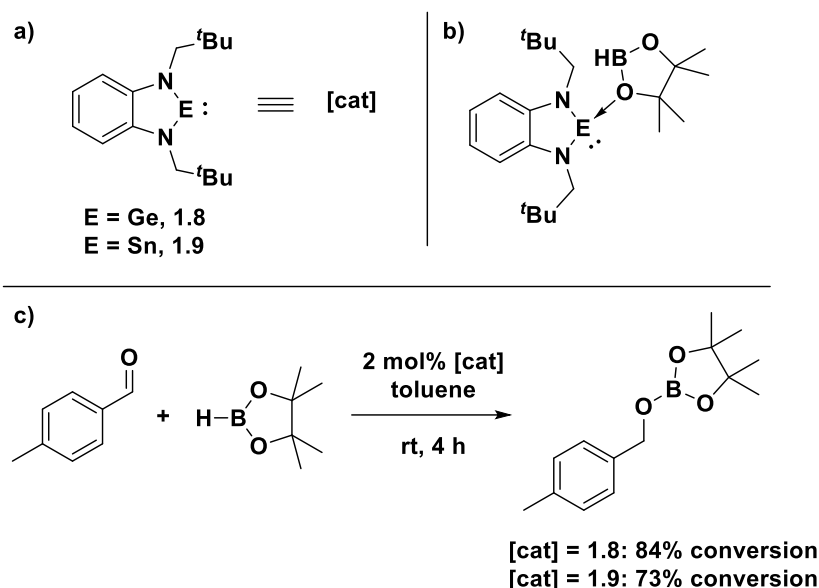
A major milestone was recently achieved in main group chemistry: the activation of N₂, which was achieved using a borylene.¹⁹ While the name borylene implies a similarity to tetrylenes, the electronic structure of borylenes can be very different. Carbenes and their congeners exist in either the singlet state, where two electrons occupy the non-bonding sp² orbital, or the triplet state, where one electron occupies the sp² orbital and one electron occupies the p orbital. In contrast, the singlet state is the favoured electronic configuration for the heavier tetrylenes. Borylene **1.7** has an empty sp²-orbital and a filled p-orbital allowing **1.7** to accept the lone pair from dinitrogen through its empty sp² orbital and back bond into the π* orbital of dinitrogen by donating the electron

density in the borylene p-orbital (Scheme 1.5). This reactivity mimics the reactivity achieved by transition metal-based nitrogen activation using *d*-orbitals.



Scheme 1.5: Nitrogen activation achieved by borylenes (Dur = 2,3,5,6-tetramethylphenyl)

While there are numerous reports of small molecule activation with main group compounds, the number of examples of their use in catalysis is sparse in comparison. One disadvantage to main group catalysts is while they can activate small molecules in a fashion similar to transition metals via oxidative addition and undergo subsequent reactivity with a substrate, reductive elimination of the product remains challenging. One of the few successful examples is that of N-heterocyclic germylene **1.8** and -stannylene **1.9** which have been shown to catalyze the hydroboration (Scheme 1.6) and cyanosilylation of aldehydes.²⁰ The mechanism of catalysis was calculated using density functional theory (DFT). N-heterocyclic tetrylenes act as electrophiles, receiving electrons from the N and O lone pairs on the trimethylsilyl cyanide and pinacolborane (HBpin) substrates, respectively, allowing the addition of the C-Si and B-H bonds across the carbonyl moiety (Scheme 1.6b).



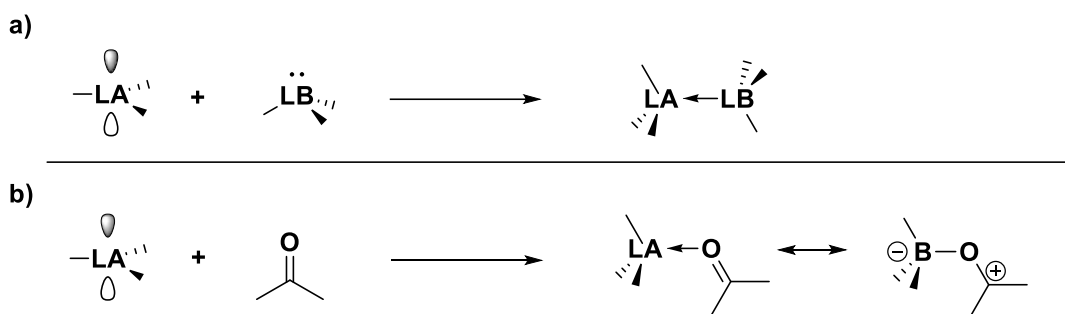
Scheme 1.6: Hydroboration of aldehydes achieved using germylene **1.8** and stannylene **1.9** catalysts

1.3 Lewis Acid Catalysis

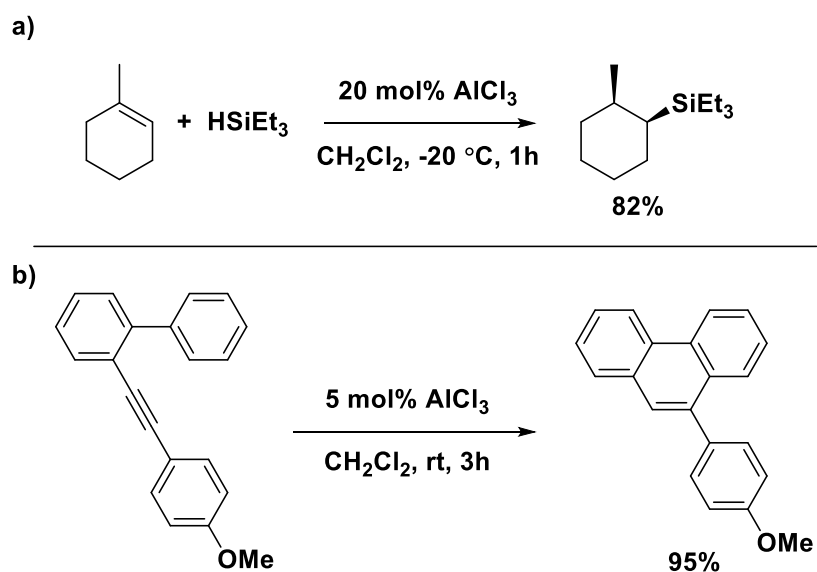
Lewis acids and bases are compounds which accept an electron pair (Lewis acids) or donate an electron pair (Lewis bases) and form a Lewis acid-base adduct (Scheme 1.7a). The bond that is formed is typically represented as a dative bond, which will be utilized throughout this thesis, denoting that heterolytic cleavage would occur at high temperatures. Typically, Lewis acid catalysts function by coordinating a substrate. As a consequence, the substrate becomes electrophilic. For example, in the presence of a Lewis acid, a carbonyl moiety donates a lone pair from the oxygen and the carbonyl carbon becomes more electrophilic (Scheme 1.7b).

Simple Lewis acids, such as the main group halides, have long been utilized in catalytic applications. AlCl_3 , a ubiquitous Lewis acid, has been used to catalyze many different reactions. For example, the hydrosilylation of alkenes is easily achieved under mild conditions using AlCl_3 as the catalyst (Scheme 1.8a).²¹ The reaction proceeds stereospecifically with the addition of the silane yielding the *anti*-product. A common application of Lewis acids is in Friedel-Craft alkylations. AlCl_3 is most often employed

with alkyl halides; however, it can also be used with alkenes and alkynes as substrates, such as in the intramolecular cyclization of arenes with alkynes (Scheme 1.8b).²²



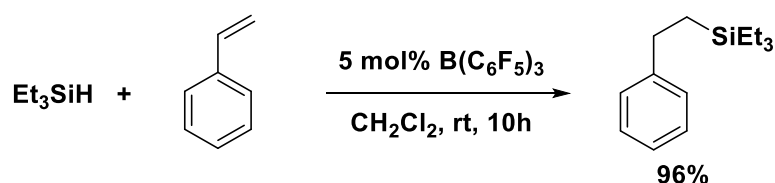
Scheme 1.7: a) Example of Lewis acid adduct formation. b) Example of Lewis acid activation of a carbonyl moiety.



Scheme 1.8: AlCl₃ catalyzed reactions: a) Hydrosilylation of an alkene b) Intramolecular Friedel-Crafts alkylation

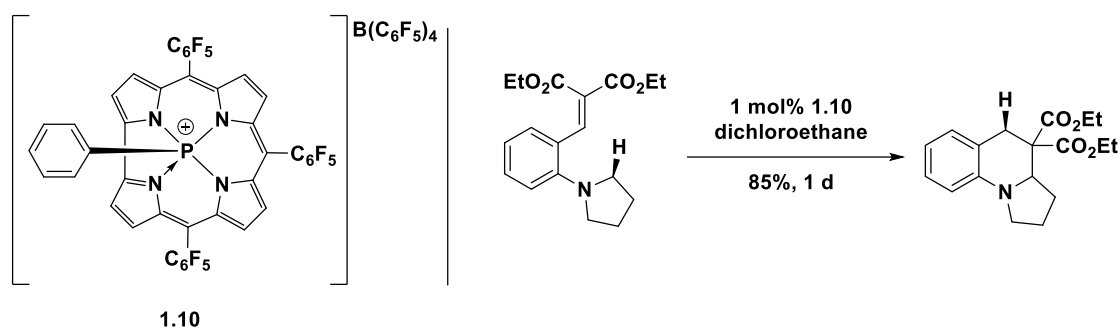
The ability of simple main group Lewis acids halides to act as catalysts led to the development of more complex ligand systems for main group Lewis acids. For example, halogenated alkyl/aryl substituents on the main group elements are a common ligand used to achieve higher selectivity and/or greater conversions. One of the most extensively explored second generation main group Lewis acid catalysts is B(C₆F₅)₃. The highly

Lewis acidic borane has been used to catalyze a multitude of reactions.²³ For example, the hydrosilylation of alkenes is easily achieved under mild conditions in dichloromethane (Scheme 1.9).²⁴ Notably, while traditional Lewis acids catalyze hydrosilylation by coordination of the unsaturated substrate (alkene, alkyne, aldehyde, etc.), $B(C_6F_5)_3$ activates the Si-H bond of the silane, making the $H-B(C_6F_5)_3^-$ borate and the corresponding SiR_3^+ cation. The hydrosilylation proceeds without the concurrent polymerization of styrene, a common side reaction observed with Lewis acid catalysts.



Scheme 1.9: Hydrosilylation of styrene catalyzed by $B(C_6F_5)_3$

Another example of advanced ligand design is the application of multidentate ligands that constrict the geometry of the Lewis acidic centre. For example, the tetragonal phosphonium salt **1.10** with a planar corrole ligand exhibits high Lewis acidity and water tolerance (Scheme 1.10).²⁵ **1.10** was shown to catalyze the challenging ring-forming C_{sp^3} -H functionalization reaction (Scheme 1.10) as well as the exhaustive deoxygenation of D-glucose to hexane and hexene isomers.

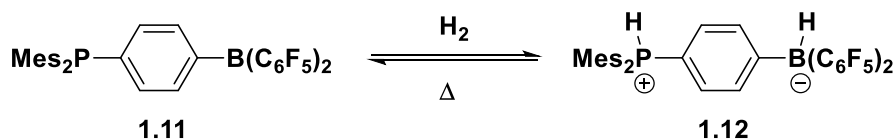


Scheme 1.10: The catalytic ring-forming C_{sp^3} -H functionalization by phosphonium catalyst **1.10**.

1.4 Frustrated Lewis Pairs

The field of Lewis acid/base catalysis underwent a paradigm shift with the discovery of frustrated Lewis pairs (FLPs).²⁶ A Lewis acid-base adduct is enthalpically favoured when a Lewis acid and Lewis base are in solution. However, in FLPs, Lewis acid-base adduct formation is unfavourable; different strategies can be used to alter the equilibrium constant for adduct formation and favour the free Lewis acid and base. The primary strategy utilized is to add sufficient steric bulk around the Lewis acid and the Lewis base disfavoring the formation of the Lewis adduct. Other methods employed take advantage of geometric constraints to prevent Lewis adduct formation.

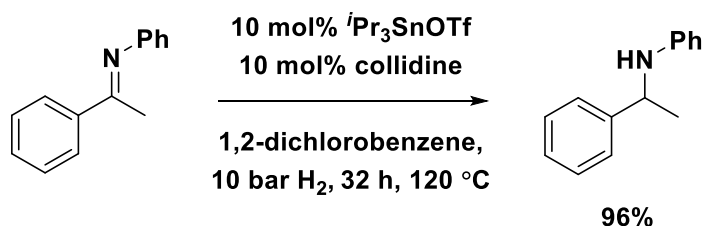
In 2006, Doug Stephan and coworkers discovered that the phenylene bridged bulky borane and phosphine **1.11** in the presence of hydrogen gas activated the hydrogen-hydrogen bond yielding the zwitterion **1.12** (Scheme 1.11).²⁷ The pentafluorophenyl and mesityl (Mes) substituents on the boron and phosphorus centres, respectively, enhance the Lewis acidity and basicity of the boron and phosphorus centre, respectively whereas the steric bulk disfavours Lewis acid-base adduct formation. Through cooperative action, **1.11** can activate dihydrogen. Notably, heating the zwitterion **1.12** to temperatures over 100 °C resulted in the reversible dissociation of hydrogen gas and the regeneration of FLP **1.11**. The ability of frustrated Lewis pairs to activate small molecules has been explored with various substrates, with the activation of CO₂, CO, N₂O, NO, SO₂, olefins, alkynes, and cyclopropanes being reported.^{26g-j}



Scheme 1.11: H₂ activation by an FLP.

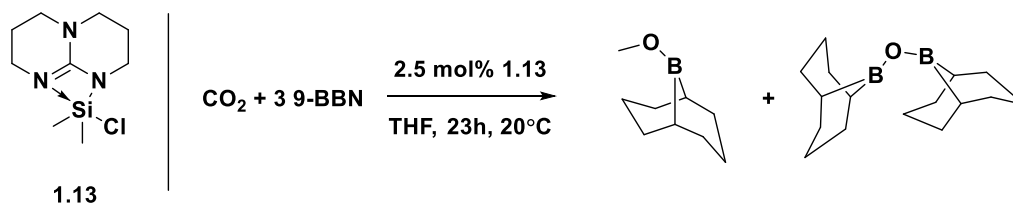
The reversible activation and release of dihydrogen gas was an early observation that led to frustrated Lewis pairs being developed as metal-free hydrogenation catalysts.^{26f,28} Numerous hydrogenation substrates have been studied including imines, nitriles, olefins, alkynes, anilines, enones, enamines, and silyl enol ethers.^{26f} FLPs have

also been shown to catalyze other reactions such as hydroamination, C-H bond borylation and intramolecular cyclization.^{26f} For example, the hydrogenation of imines was achieved using $i\text{Pr}_3\text{SnOTf}$ as the Lewis acid and collidine as the Lewis base, forming a frustrated Lewis pair *in situ* (Scheme 1.12).²⁹



Scheme 1.12: Hydrogenation of imines achieved with a Sn/N FLP catalyst

While the research on frustrated Lewis pairs has focused on hydrogenation reactions of organic substrates, attempts to catalyze the hydrogenation of CO_2 , a C_1 building block, have been unsuccessful; however, the stoichiometric hydrogenation of CO_2 has been achieved.³⁰ An alternative pathway for the reduction of CO_2 , the FLP catalyzed hydroboration of carbon dioxide with 9-Borabicyclo(3.3.1)nonane (9-BBN) has been reported with the Si/N FLP **1.13** (Scheme 1.13).³¹ The reaction proceeds via hydroboration reduction to the protected methanol derivative under mild conditions.

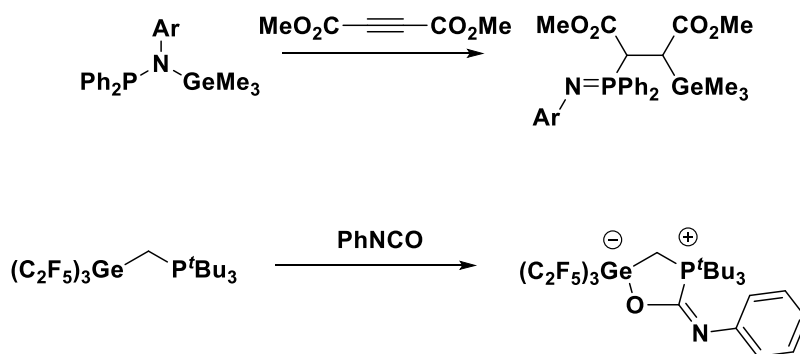


Scheme 1.13: Reduction of CO_2 with a borane with FLP catalyst **1.13**

1.5 Germanium Lewis Acids

While the field of *p*-block Lewis acid chemistry has focused on exploring the chemistry of boron, aluminum and silicon-centred complexes, the field of germanium-based Lewis acid chemistry is only emerging. In a recent review on main group Lewis acid chemistry, the authors describe “The field of germanium Lewis acids is almost not

Germanium has also been incorporated as the Lewis acid component of a frustrated Lewis pair.³⁷ While there are no examples of intermolecular FLPs using a germanium Lewis acid component, the reactivity of an intramolecular geminal frustrated Lewis pair was explored. The geminal FLP provides a geometrical constraint disfavoring the formation of a 3-membered ring Lewis acid-base adduct. A variety of different geminal Ge-P FLP's have been synthesized and have been shown to activate small molecules such as alkynes, isocyanates, HCl, and NO (Scheme 1.15). While successful in achieving stoichiometric small molecule activation, the use of germanium FLPs as catalysts, as well as in dihydrogen activation, has yet to be reported.



Scheme 1.15: Reactivity of Ge/P FLPs

1.6 Bis(catecholato)silanes

Recently, the bis(catecholato)- scaffold has been used to synthesize a variety of group 14 Lewis acid catalysts. For the purpose of this thesis, bis(catecholato)- complexes will be abbreviated as $E(\text{cat}^X)_2(\text{donor})_2$, where E is the central element, cat^X describes the substituents on the catechol ring, and donor describes the ligated donors in hypercoordinate complexes. Electron-withdrawing substituents on the catechol ring, such as fluorine,³⁸ chlorine,³⁹ bromine,⁴⁰ and fluoromethyl,⁴¹ increases the Lewis acidity of the group 14 centre (Chart 1.1). The perhalogenated derivatives, $\text{Si}(\text{cat}^F)_2$, $\text{Si}(\text{cat}^{\text{Cl}})_2(\text{ACN})_2$, and $\text{Si}(\text{cat}^{\text{CF}_3})_2(\text{ACN})_2$, are easily synthesized in one step in acetonitrile (ACN) using SiCl_4 or HSiCl_3 and the corresponding perhalogenated catechol. The fluoromethyl derivative, $\text{Si}(\text{cat}^{\text{CF}_3})_2(\text{sulfolane})_2$, on the other hand, required multiple steps to be synthesized.

Except for the perfluorinated derivative, the bis(catecholato)silanes all contain weakly bound donor solvent molecules such as acetonitrile and sulfolane.

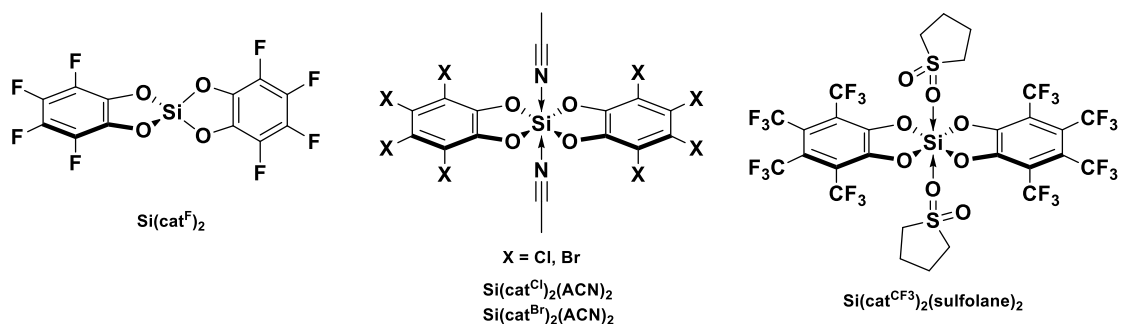
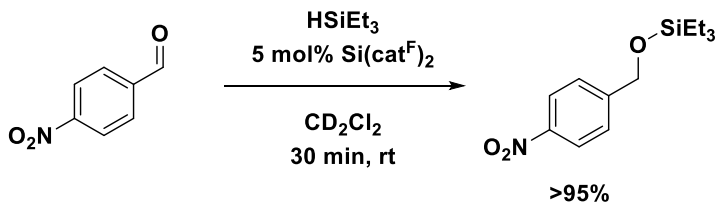


Chart 1.1: Bis(catecholato)silanes showing the naming convention which will be utilized throughout the thesis: $E(\text{cat}^X)_2(\text{donor})_2$.

The bis(catecholato)silane complexes have been shown to catalyze a variety of reactions, such as hydrosilylation,³⁸ hydrodefluorination,³⁹ and intramolecular carbonyl-olefin metathesis.⁴¹ The hydrosilylation of benzaldehyde derivatives catalyzed by $\text{Si}(\text{cat}^F)_2$ takes place in under an hour at room temperature illustrating the high catalytic activity of these species (Scheme 1.16).³⁸ Mechanistic studies revealed that catalysis takes place via coordination of the aldehyde to the silane and not by coordination of the silane as was observed in the hydrosilylation of benzaldehyde derivative using $\text{B}(\text{C}_6\text{F}_5)_3$ as the catalyst. The hydrosilylation of aldehydes using $\text{Si}(\text{cat}^F)_2$ as the catalyst tolerates the use of bulky silanes which are unreactive with the bulky borane catalyst. However, in consideration of the scope of aldehydes, electron-donating benzaldehyde derivatives were not tolerated and gave substantially lower conversions compared to the electron-withdrawing derivatives, a limitation not observed when using $\text{B}(\text{C}_6\text{F}_5)_3$.



Scheme 1.16: Hydrosilylation of *para*-nitrobenzaldehyde catalyzed by $\text{Si}(\text{cat}^F)_2$.

1.7 Scope of the Thesis

Bis(catecholato)silanes have been studied as Lewis acids extensively,³⁸⁻⁴¹ and it has been demonstrated that the Lewis acidity of the silane centre can be enhanced by altering the catecholato substituents. Several catalytic applications, and in the case of $\text{Si}(\text{cat}^{\text{F}})_2$, a mechanistic study have been reported. Research into the reactivity of bis(catecholato)germanes is limited.⁴² While a recent report showed that bis(catecholato)germanes are highly Lewis acidic and catalyze hydrosilylation, Friedel-Crafts alkylation, and intramolecular carbonyl-olefin metathesis reactions, the report is limited to two derivatives of bis(catecholato)germanes and the scope and mechanism of catalysis is limited.⁴²

The potential of bis(catecholato)germanes as Lewis acid catalysts remains under explored. Precedence for a green, sustainable synthesis of bis(catecholato)germanes has been shown with the solvent-free mechanochemical synthesis of $\text{Ge}(\text{dtbc})_2(\text{py})_2$, where dtbc is 3,5-di-*tert*-butylcatecholato and py is pyridine.⁴³ Furthermore, the preliminary work on the perchlorocatecholato derivatives demonstrated that not only are the bis(catecholato)germanes water-tolerable, but the water ligated derivative, $\text{Ge}(\text{cat}^{\text{Cl}})_2(\text{H}_2\text{O})_x$, can be used as a Lewis acid catalyst which provides an avenue for water to be used as a solvent instead of organic solvents. With such promise for the bis(catecholato)germanes, the goal of this thesis is to expand the field of bis(catecholato)germane chemistry by synthesizing multiple bis(catecholato)germane derivatives and assessing their Lewis acidity, exploring the scope of catalytic reactivity, analyzing the mechanism by which bis(catecholato)germanes act as catalysts, and to explore the application of bis(catecholato)germanes as frustrated Lewis pairs.

In chapter 2, the synthesis of a variety of bis(catecholato)germanes from commercially available materials, in one step, via two different synthetic routes will be presented. The Lewis acidity of the bis(catecholato)germanes will be assessed using the Gutmann-Beckett, Fluoride Ion Affinity (FIA) and Global Electrophilicity Index (GEI) methods.

In chapter 3 the catalytic ability of the bis(catecholato)germanes will be assessed in various reactions including the hydrosilylation of benzaldehyde derivatives, dimerization of aryl alkenes, hydroboration of aryl alkynes, and Friedel-Crafts alkylation reactions. The influence of the catecholato substituents and the donor ligands of the bis(catecholato)germanes and the influence of donor additives on catalytic performance and product selectivity will be examined.

In chapter 4, the mechanism of alkene oligomerization catalysis will be elucidated using Density functional theory (DFT) calculations, a Hammett plot and rate law experiments. A mechanism for the catalytic oligomerization of α -methylstyrene by bis(catecholato)germanes is proposed.

In chapter 5 the reactivity of the Lewis acidic bis(catecholato)germanes with a variety of bulky bases will be examined. The potential FLPs will be examined in both small molecule activations and selected catalytic reactions. DFT will be used to understand the reactivity trends.

References

1. Toniato, A.; Vaucher, A. C.; Laino, T. *Catalysis Today* **2021**, *387*, 140-142.
2. Anastas, P. T.; Warner, J. C. *Green Chemistry: Theory and Practice*, Oxford University Press: New York, **1998**, 30.
3. Ludwig, J. R.; Schindler, C. S. *Chem* **2017**, *2*, 313-316.
4. http://www.leonland.de/elements_by_price/list?ccy=CAD&unit=kg (accessed July 16, 2022) *Chemical Elements by Price*
5. Egorova, K. S.; Ananikov, V. P. *Organometallics* **2017**, *36*, 4071–4090.
6. American Chemical Society <https://www.acs.org/content/acs/en/greenchemistry/research-innovation/endangered-elements.html> (accessed Aug. 3, 2022) *Endangered Elements*
7. Luca, O. R.; Crabtree, R. H. *Chem. Soc. Rev.* **2013**, *42*, 1440-1459.
8. Sankaralingam, M.; Lee, Y. M.; Nam, W.; Fukuzumi, S. *Inorg. Chem.* **2017**, *56*, 5096–5104.
9. a) Cao, Y.; Yu, H.; Peng, F.; Wang, H. *ACS Catal.* **2014**, *4*, 1617-1625; b) Zou, G.; Jing, D.; Zhong, W.; Zhao, F.; Mao, L.; Xu, Q.; Xiao, J.; Yin, D. *RSC Adv.* **2016**, *6*, 3729-3734.
10. a) Power, P. P. *Nature* **2010**, *463*, 171–177; b) Weetman, C.; Inoue, S. *ChemCatChem* **2018**, *10*, 4213–4228; c) Wilkins, L. C.; Melen, R. L. *Coord. Chem. Rev.* **2016**, *324*, 123-139; d) Weetman, C. *Chem. Eur. J.* **2021**, *27*, 1941-1954.
11. Spikes, G. H.; Fettinger, J. C.; Power, P. P. *J. Am. Chem. Soc.* **2005**, *127*, 12232–12233.

12. Mömning, C. M.; Otten, E.; Kehr, G.; Fröhlich, R.; Grimme, S.; Stephan, D. W.; Erker, G.; *Angew. Chem. Int. Ed.* **2009**, *48*, 6643–6646.
13. Dahcheh, F.; Martin, D.; Stephan, D. W.; Bertrand, G. *Angew. Chem. Int. Ed.* **2014**, *53*, 13159–13163.
14. Zhu, Z.; Wang, X.; Peng, Y.; Lei, H.; Fettinger, J. C.; Rivard, E.; Power, P. P. *Angew. Chem. Int. Ed.* **2009**, *48*, 2031–2034.
15. Wendel, D.; Szilvási, T.; Henschel, D.; Altmann, P. J.; Jandl, C.; Inoue, S.; Rieger, B. *Angew. Chem. Int. Ed.* **2018**, *57*, 14575–14579.
16. Stoy, A.; Böhnke, J.; Jiménez-Halla, J. O. C.; Dewhurst, R. D.; Thiess, T.; Braunschweig, H. *Angew. Chem. Int. Ed.* **2018**, *57*, 5947–5951.
17. Protchenko, A. V.; Birjkumar, K. H.; Dange, D.; Schwarz, A. D.; Vidovic, D.; Jones, C.; Kaltsoyannis, N. Mountford, P.; Aldridge, S. *J. Am. Chem. Soc.* **2012**, *134*, 6500–6503.
18. Protchenko, A. V.; Vasko, P.; Do, D. C. H.; Hicks, J.; Fuentes, M. Á.; Jones, C.; Aldridge, S. *Angew. Chem. Int. Ed.* **2019**, *58*, 1808–1812.
19. a) Légaré, M. A.; Bélanger-Chabot, G.; Dewhurst, R. D.; Welz, E.; Krummenacher, I.; Engels, B.; Braunschweig, H. *Science* **2018**, *359*, 896–900; b) Zhang, H.; Yuan, R.; Wu, W.; Mo, Y. *Chem. Eur. J.* **2020**, *26*, 2619–2625.
20. Dasgupta, R.; Das, S.; Hiwase, S.; Pati, S. K.; Khan, S. *Organometallics* **2019**, *38*, 1429–1435.
21. Song, Y. S.; Yoo, B. R.; Lee, G. H.; Jung, I. N. *Organometallics* **1999**, *18*, 3109–3115.
22. Li, Y.; Wang, Y.; Xu, D.; Jin, R.; Gu, G.; Guo, H. *Synlett* **2017**, *28*, 2159–2162.

23. a) Parks, D. J.; Piers, W. E. *J. Am. Chem. Soc.* **1996**, *118*, 9440–9441; b) Parks, D. J.; Blackwell, J. M.; Piers, W. E. *J. Org. Chem.* **2000**, *65*, 3090–3098; c) Hermeke, J.; Mewald, M.; Oestreich, M. *J. Am. Chem. Soc.* **2013**, *135*, 17537–17546.
24. Rubin, M.; Schwier, T.; Gevorgyan, V. *J. Org. Chem.* **2002**, *67*, 1936–1940.
25. Gilhula, J. C.; Radosevich, A. T. *Chem. Sci.* **2019**, *10*, 7177–7182.
26. a) Lam, J.; Szkop, K. M.; Mosafieri, E.; Stephan, D. W. *Chem. Soc. Rev.* **2019**, *48*, 3592–3612; b) Stephan, D. W. *J. Am. Chem. Soc.* **2021**, *143*, 20002–20014; c) Stephan, D. W. *Org. Biomol. Chem.* **2008**, *6*, 1535–1539; d) Fontaine, F. G.; Stephan, D. W. *Phil. Trans. R. Soc. A.* **2017**, *375*, 201770004; e) Li, N.; Zhang, W. X. *Chin. J. Chem.* **2020**, *38*, 1360–1370; f) Stephan, D. W. *Chem* **2020**, *6*, 1520-1526; g) Stephan, D. W. *J. Am. Chem. Soc.* **2015**, *137*, 10018–10032; h) Stephan, D. W.; Erker, G. *Chem. Sci.* **2014**, *5*, 2625-2641; i) Pal, R.; Ghara, M.; Chattaraj, P. K. *Catalysts* **2022**, *12*, 201; j) Jupp, A. R.; Stephan, D. W. *Trends Chem.* **2019**, *1*, 35-48.
27. Welch, G. C.; San Juan, R. R.; Masuda, J. D.; Stephan, D. W. *Science*, **2006**, *314*, 1124–1126.
28. Scott, D. J.; Fuchter, M. J.; Ashley, A. E. *Chem. Soc. Rev.* **2017**, *46*, 5689-5700.
29. Scott, D. J.; Phillips, N. A.; Sapsford, J. S.; Deacy, A. C.; Fuchter, M. J.; Ashley, A. E. *Angew. Chem. Int. Ed.* **2016**, *55*, 14738-14742.
30. Ashley A. E.; O’Hare D. *FLP-Mediated Activations and Reductions of CO₂ and CO*. In: Erker G., Stephan D. *Frustrated Lewis Pairs II: Topics in Current Chemistry*, Springer-Berlin: Heidelberg, **2012**, Vol 334, pp 191-217.
31. von Wolff, N.; Lefèvre, G.; Berthet, J. C.; Thuéry, P.; Cantat, T. *ACS Catal.* **2016**, *6*, 4526–4535.
32. Greb, L. *Chem. Eur. J.* **2018**, *24*, 17881–17896.

33. Sarker, P.; Das, S.; Pati, S. K. *Chem. Asian. J.* **2022**, *17*, e202200148.
34. a) Holmquist, C. R.; Roskamp, E. J. *J. Org. Chem.* **1989**, *54*, 3258-3260; b) Kanazawa, A.; Kanaoka, S.; Aoshima, S. *Macromolecules* **2009**, *42*, 3965-3972; c) Thiele, U. K. *Intern. J. Polymeric Mater.* **2001**, *50*, 387-394.
35. a) Acocella, M. R.; De Rosa, M.; Massa, A.; Palombi, L.; Villano, R.; Scettri, A. *Tetrahedron* **2005**, *61*, 4091-4097; b) Denmark, S. E.; Stavenger, R. A.; Wong, K. T. *J. Org. Chem.* **1998**, *63*, 918-919; c) Kotani, S.; Yoshiwara, Y.; Ogasawara, M.; Sugiura, M.; Nakajima, M. *Angew. Chem. Int. Ed.* **2018**, *57*, 15877-15881; d) Patil, M. L.; Borate, H. B.; Ponde, D. E.; Bhawal, B. M.; Deshpande, V. H. *Tetrahedron Lett.* **1999**, *40*, 4437-4438; e) Johnson, J. R.; May, G. E. *Org. Synth.* **1938**, *18*, 1-2; f) Thurston, D. E.; Murty, V. S.; Langley, D. R.; Jones, G. B. *Synthesis* **1990**, *1*, 81-84.
36. Jing, H.; Ge, H.; Li, C.; Jin, Y.; Wang, Z.; Du, C.; Fu, X.; Fang, H. *Organometallics* **2019**, *38*, 2412-2416.
37. a) Kinder, T. A.; Pior, R.; Blomeyer, S.; Neumann, B.; Stammeler, H. G.; Mitzel, N. *Chem. Eur. J.* **2019**, *25*, 5899-5903; b) Yu, Y.; Li, J.; Liu, W.; Ye, Q.; Zhu, H. *Dalton Trans.* **2016**, *45*, 6259-6268.
38. Liberman-Martin, A. L.; Bergman, R. G.; Tilley, T. D. *J. Am. Chem. Soc.* **2015**, *137*, 5328-5331.
39. Maskey, R.; Schädler, M.; Legler, C.; Greb, L. *Angew. Chem. Int. Ed.* **2018**, *57*, 1717-1720.
40. Hartmann, D.; Schädler, M.; Greb, L. *Chem. Sci.* **2019**, *10*, 7379-7388.
41. Thaddäus, T.; Roth, D.; Greb, L. *Chem. Eur. J.*, **2021**, *27*, 10422-10427.
42. Roth, D.; Wadepohl, H.; Greb, L. *Angew. Chem. Int. Ed.* **2020**, *59*, 20930-20934.

43. Glavinović, M.; Krause, M.; Yang, L.; McLeod, J. A.; Liu, L.; Baines, K. M.; Friščić T.; Lumb, J. P. *Sci. Adv.*, **2017**, *3*, e1700149.

Chapter 2

2 Synthesis and Lewis Acidity Assessment of Bis(catecholato)germanes

2.1 Introduction

2.1.1 Synthesis of Bis(catecholato)- Complexes with Group 14 Elements

An emerging scaffold for the design of Lewis acidic neutral group 14 catalysts, is the catecholato framework. The bidentate catecholato ligands feature four sites for substitution at the 3, 4, 5 and 6 positions of each aromatic ring providing the means to tune the electronic environment about the Group 14 centre. The bis(catecholato)-substituted tetrelanes exhibit two different coordination environments at the Group 14 element: a tetrahedral, tetracoordinate arrangement of ligands at the Group 14 centre, $E(\text{cat})_2$ (where E = group 14 element, and cat = catechol), or an octahedral, hexacoordinate structure, $E(\text{cat})_2(\text{donor})_2$, where two donor ligands (Lewis bases) are also bound to the Lewis acidic centre (Figure 2.1). The hybridization of the central group 14 element in the hexacoordinate species is sp , allowing for 3-centre-4 electron bonding between the oxygens of the catechol and the p -orbital from the group 14 element. The empty sp hybrid orbitals are then available to bind Lewis bases.

The synthesis of bis(catecholato)silanes and -germanes generally follows two different approaches: a substitution reaction between a E(IV) halide and the catechol, or a redox reaction between germanium dichloride and an *ortho*-quinone. The first synthesis of a bis(catecholato)silane used a substitution reaction of silicon tetrachloride and the parent catechol and was believed to yield bis(catecholato)silane;¹ however, it was later determined that the product likely had an oligomeric structure. To prevent oligomerization, the use of donor solvents is necessary.² The reaction of either SiCl_4 or GeCl_4 and catechol in refluxing pyridine (py) results in the formation of $\text{Si}(\text{cat})_2(\text{py})$ and $\text{Ge}(\text{cat})_2(\text{py})_2$, respectively (where cat = catecholato). $\text{Si}(\text{cat})_2(\text{NEt}_3)$ and $\text{Ge}(\text{cat})_2(\text{NEt}_3)_2$ can be formed in a similar manner by the addition of the corresponding group 14 halide to catechol and triethylamine. Bis(perfluorocatecholato)silane, $\text{Si}(\text{cat}^{\text{F}})_2$, was synthesized

using SiCl_4 and tetrafluorocatechol in acetonitrile (ACN) at $0\text{ }^\circ\text{C}$.³ After warming to room temperature overnight, an insoluble white powder was obtained in 53% yield (Scheme 2.1a). Greb and coworkers reported the synthesis of $\text{Si}(\text{cat}^{\text{Cl}})_2(\text{ACN})_2$ by the addition of HSiCl_3 to tetrachlorocatechol in ACN at $-20\text{ }^\circ\text{C}$. After stirring for 20 minutes at room temperature, the perchlorinated derivative was obtained as an insoluble white precipitate (Scheme 2.1b).⁴ Greb and coworkers extended their research synthesizing and characterizing the perbrominated analogue, $\text{Si}(\text{cat}^{\text{Br}})_2(\text{ACN})_2$, by adding HSiCl_3 to tetrabromocatechol in ACN at room temperature and then stirring at $40\text{ }^\circ\text{C}$ for 12 hours to give $\text{Si}(\text{cat}^{\text{Br}})_2(\text{ACN})_2$ as a white powder (Scheme 2.1b).⁵ The series of bis(catecholato)silanes was extended further when $\text{Si}(\text{cat}^{\text{CF}_3})_2(\text{sulfolane})_2$, featuring the strongly electron-withdrawing CF_3 substituents on the catechol ring, was synthesized, using a more elaborate substitution synthesis, (Scheme 2.1c). Employing a similar strategy to the other halogenated bis(catecholato)silanes, HSiCl_3 was added to a solution of tetrakis(trifluoromethyl)guaiacol in acetonitrile; however, instead of the desired bis(per(trifluoromethyl)catecholato)silane with two bound acetonitrile donors, the formation of a chlorosilicate with a protonated acetonitrile counterion was observed. To prevent solvent protonation, the addition of HSiCl_3 was performed in a mixture of sulfolane and benzene (97:3) to yield the desired $\text{Si}(\text{cat}^{\text{CF}_3})_2(\text{sulfolane})_2$ in a 90% yield. Only one halogenated bis(catecholato)germane derivative has been reported: the synthesis of bis(perchlorocatecholato)germane, $\text{Ge}(\text{cat}^{\text{Cl}})_2(\text{ACN})_2$.⁶ Notably, the synthesis differed from that of the reported bis(catecholato)silanes in that the acetonitrile derivative was not synthesized in one step. The addition of tetrachlorocatechol to germanium dioxide in water yielded $\text{Ge}(\text{cat}^{\text{Cl}})_2(\text{H}_2\text{O})_n$ ($n = 4$ or 6) in high yield. The water derivative was then placed in a mixture of acetonitrile and dichloromethane in the presence of 3 \AA molecular sieves, which facilitated the displacement and adsorption of water and the formation of the acetonitrile ligated $\text{Ge}(\text{cat}^{\text{Cl}})_2(\text{ACN})_2$. The reaction of GeO_2 with 3,5-di-*tert*-butylcatechol in refluxing pyridine for three days yielded $\text{Ge}(3,5\text{-dtbc})_2(\text{py})_2$.⁷

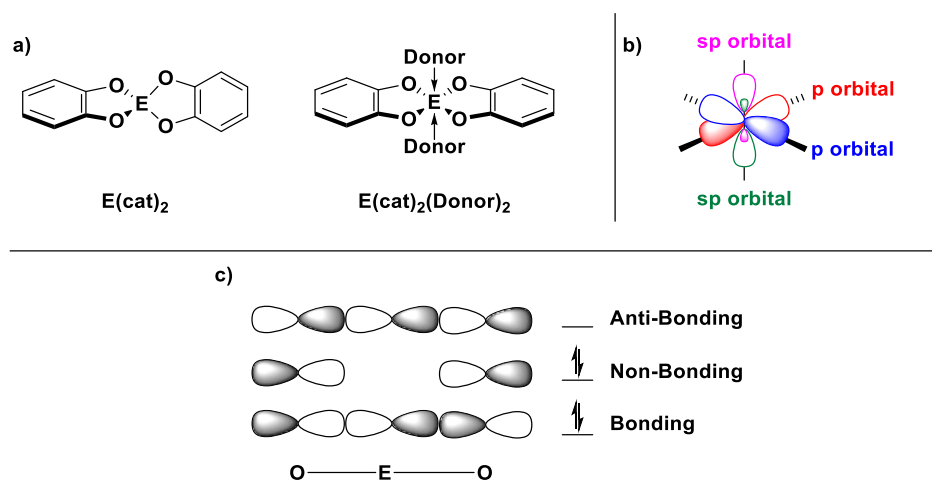
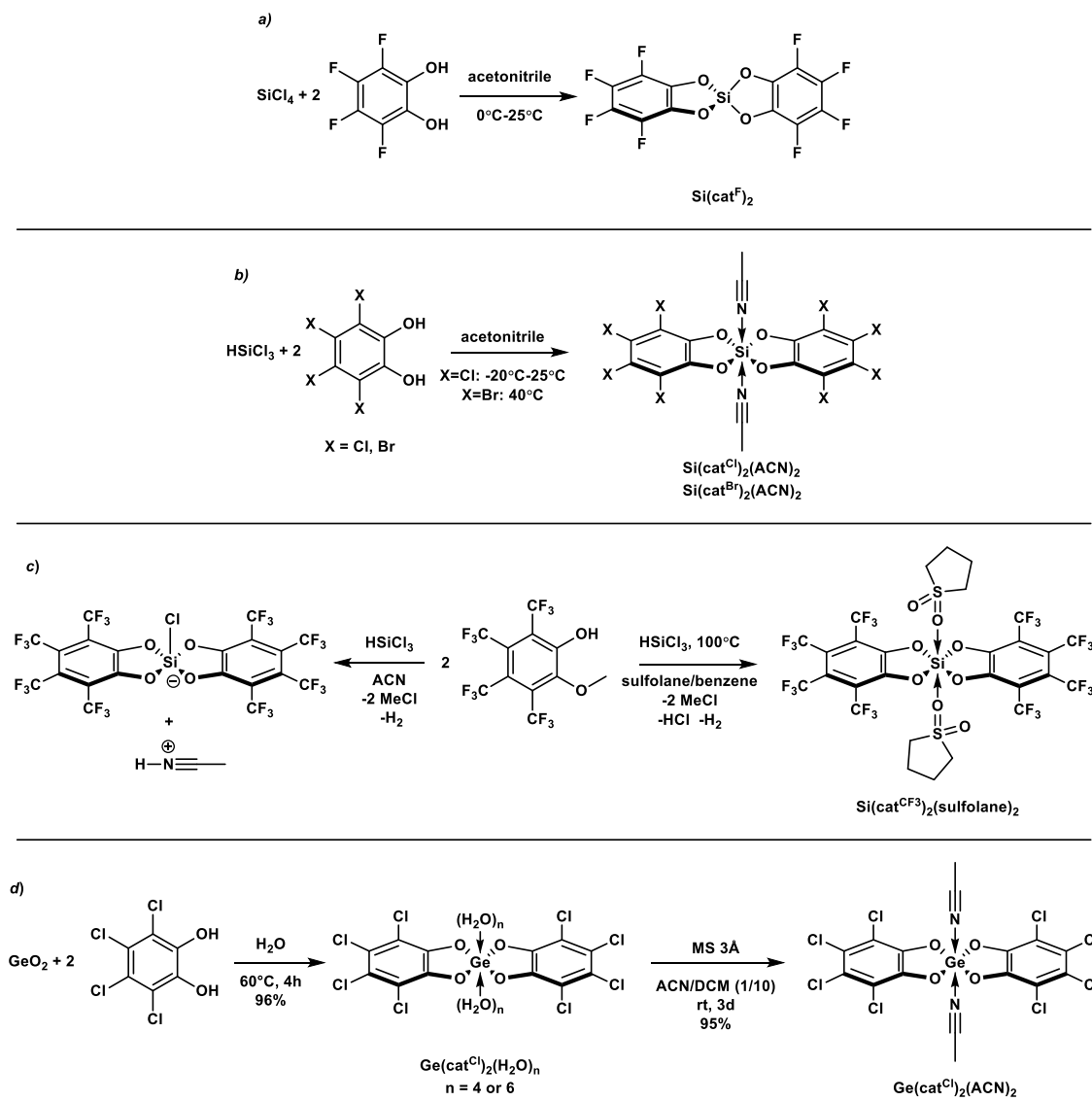


Figure 2.1: a) The different coordination environments of bis(catecholato) complexes. b) An orbital picture illustrating the *sp* hybridization of the group 14 element relative to the octahedral geometry. c) The molecular orbitals involved in the 3-centre-4-electron bonding in $E(\text{cat})_2(\text{Donor})_2$.

While the substitution reaction of group 14 halides with catechol has proven to be a successful method for the synthesis of bis(catecholato)silanes and -germanes, the redox reaction of *ortho*-quinones with $\text{GeCl}_2 \cdot \text{dioxane}$ or germanium powder is also a viable route. Addition of 3,6-di-*tert*-butyl-*ortho*-quinone (3,6-dtbq) to $\text{GeCl}_2 \cdot \text{dioxane}$ in tetrahydrofuran (THF) or diethyl ether (Et_2O) yielded an equivalent of GeCl_4 and the desired $\text{Ge}(3,6\text{-dtbc})_2(\text{THF})_2$ or $\text{Ge}(3,6\text{-dtbc})_2(\text{Et}_2\text{O})_2$, respectively.⁸ $\text{Ge}(\text{dtbc})_2(\text{py})_2$ can also be synthesized, using green chemistry protocols, mechanochemically in a ball mill with minimal solvent and using germanium powder and 3,5-di-*tert*-butylquinone in a redox reaction.⁷

The ability to exchange donor ligands on bis(catecholato)germanes and -silanes has been demonstrated. The pyridine ligands of $\text{Ge}(\text{cat})_2(\text{pyridine})_2$ can be displaced by heating the compound in dimethylformamide (DMF), yielding $\text{Ge}(\text{cat})_2(\text{DMF})_2$. Furthermore, the pyridine can be displaced by stirring $\text{Ge}(\text{cat})_2(\text{py})_2$ in an excess of triethylamine, a stronger donor, at room temperature.



Scheme 2.1: a) Synthesis of $\text{Si}(\text{cat}^{\text{F}})_2$. b) Synthesis of $\text{Si}(\text{cat}^{\text{Cl}})_2(\text{ACN})_2$ and $\text{Si}(\text{cat}^{\text{Br}})_2(\text{ACN})_2$. c) Synthesis of $\text{Si}(\text{cat}^{\text{CF}_3})_2(\text{sulfolane})_2$. d) Synthesis of $\text{Ge}(\text{cat}^{\text{Cl}})_2$ with water and acetonitrile donor ligands.

The spectroscopic characterization of bis(catecholato)silanes and -germanes can be a challenge. While the parent and alkyl-substituted catechol derivatives can be characterized easily by ^1H and ^{13}C NMR spectroscopy as well as X-ray diffraction, the insolubility of the halogenated bis(catecholato)silane and germane derivatives prevents solution-based characterization techniques from being effective. The characterization of $\text{Si}(\text{cat}^{\text{F}})_2$ and $\text{Si}(\text{cat}^{\text{Cl}})_2(\text{ACN})_2$ will be used as examples to illustrate. For $\text{Si}(\text{cat}^{\text{F}})_2$, a

combination of ^{19}F NMR spectroscopy, elemental analysis (EA), and reactivity studies were used to identify the species. For $\text{Si}(\text{cat}^{\text{Cl}})_2(\text{ACN})_2$, characterization by electron impact (EI) mass spectrometry revealed a signal corresponding to $[\text{Si}(\text{cat}^{\text{Cl}})_2]^+$. Elemental analysis of the product revealed the presence of two equivalents of acetonitrile and IR spectroscopy revealed a slight shift in the wavenumber of the signal assigned to the C-N stretching vibration suggesting the acetonitrile is bound to the silicon centre and that the compound is $\text{Si}(\text{cat}^{\text{Cl}})_2(\text{ACN})_2$.

To provide further evidence for the formation of the halogenated bis(catecholato) species, reactions to give soluble complexes facilitates characterization. Specifically, $\text{Si}(\text{cat}^{\text{F}})_2$ was reacted with tris(dimethylamino)sulfonium difluorotrimethylsilicate, to give the soluble penta-coordinated anion, $[\text{Si}(\text{cat}^{\text{F}})_2\text{F}]^-$, and was reacted with N,N'-diisopropylbenzamide, which coordinated through the oxygen atom of the amide group to the silicon centre. Both reactions gave crystals suitable for X-ray crystallography providing further evidence for the bis(catecholato)silane structure. Reactions of $\text{Si}(\text{cat}^{\text{Cl}})_2(\text{ACN})_2$ with 1 eq. of $\text{KF}/[18]\text{crown-6}$ and 2 eq. of tris(dimethylamino)sulfonium difluorotrimethylsilicate yielded the desired $\text{Si}(\text{cat}^{\text{Cl}})_2\text{F}^-$ and $\text{Si}(\text{cat}^{\text{Cl}})_2\text{F}_2^{2-}$ anions, respectively, the identity of which were confirmed by X-ray crystallography.

2.1.2 Quantification of Lewis Acidity

Even though the concept of Lewis acidity has been around since the 1920's, the methods for the quantification of Lewis acid strength are still under active development.⁹ Unlike Brønsted acidity, which has a universal scale for assessing the strength of an acid (pKa), Lewis acidity does not have a universal scale because the strength of a given Lewis acid is highly dependent on the nature of the Lewis base. Specifically, Lewis bases have different steric and electronic properties which can favor binding to one Lewis acid over another. As such, it is common to employ a variety of methods to assess the Lewis acidity of a given species.

While there is no universal method for assessing Lewis acidity, there are several methods that are commonly employed. Lewis acidity can be determined both

experimentally or computationally. Experimental methods, such as the Gutmann-Beckett¹⁰ and the Childs' method¹¹ use NMR spectroscopy to assess the Lewis acidity. The Gutmann-Beckett method utilizes the $^{31}\text{P}\{^1\text{H}\}$ NMR shift of coordinated triethylphosphine oxide, while the Childs' method uses the ^1H NMR shift of the proton on the β -carbon of coordinated crotonaldehyde. Pyridine- d_5 ¹² and fluorobenzonitrile¹³ have also been used as NMR probes in Lewis acidity assessments, although to a lesser extent. The Baumgartner and Caputo groups have utilized a dithienophosphole oxide as a probe to assess Lewis acidity of a species by evaluating changes in the fluorescence spectra between the uncomplexed and complexed Lewis acid.¹⁴ Computationally, Fluoride Ion Affinity (FIA) calculations, where the enthalpy of the reaction of a Lewis acid with a fluoride anion is calculated, are commonly used to assess Lewis acidity.¹⁵ Similarly, the analogous hydride,¹⁶ chloride,¹⁷ methide,¹⁸ water,¹⁹ and ammonia²⁰ affinities are also used to assess the Lewis acidity of a compound.¹⁸ The Global Electrophilicity Index (GEI) is a computational method in which the highest occupied molecular orbitals (HOMO) and the lowest unoccupied molecular orbitals (LUMO) energies of a Lewis acid are used to assess its Lewis acid strength.²¹ The Gutmann-Beckett, FIA, and GEI methods were used to assess the Lewis acidity of bis(catecholato)silanes and -germanes, and thus, are discussed in detail.

The Gutmann-Beckett method is simple to perform.¹⁰ Typically, 1, 0.5 or 0.33 equivalents of triethylphosphine oxide is added to a solution of a Lewis acid and the $^{31}\text{P}\{^1\text{H}\}$ NMR spectrum of the solution is recorded. The strength of the Lewis acid is inferred by the downfield shift in the $^{31}\text{P}\{^1\text{H}\}$ NMR signal of the triethylphosphine oxide upon coordination to the Lewis acid compared to that of free triethylphosphine oxide (41.0 ppm in hexanes). The chemical shift can then be converted into an acceptor number (AN) by the following formula:

$$(1) \quad \text{AN} = 2.21(\delta^{31}\text{P}\{^1\text{H}\} - 41.0)$$

By converting the chemical shift to acceptor number, it places the Lewis acid on a scale where SbCl_5 has an acceptor number of 100 and hexanes has an acceptor number of 0

(Table 2.1). Some examples of common Lewis acids are given in Table 2.1, Entries 2-7 and show ANs between 70-105.

FIA is determined by taking the negative value of the enthalpy change upon binding a fluoride ion to a Lewis acid.¹⁵ FIA values can be calculated computationally or determined experimentally. To calculate FIA values, an anchor point reaction must be utilized as calculating the direct reaction of a Lewis acid with a naked fluoride ion is unreliable at lower levels of theory. While several anchor point systems have been developed, the most commonly used is the trimethylsilyl (TMS) system (Figure 2.2).²² Examples of common Lewis acids and their FIA values are presented in Table 2.2 (Entries 1-7) and show a range of FIA values between 323-505 kJ/mol.

Table 2.1: The $^{31}\text{P}\{^1\text{H}\}$ chemical shifts and acceptor numbers of various Lewis acids (using hexanes as a reference).

Entry	Lewis Acid	$^{31}\text{P}\{^1\text{H}\}$ Chemical Shift (ppm)	Acceptor Number
1	Hexanes ^{10b}	41.0	0
2	TiCl ₄ ²³	72.7	70
3	B(C ₆ F ₅) ₃ ²³	78.1	82
4	AlCl ₃ ²³	80.3	87
5	BF ₃ •Et ₂ O ²⁴	80.9	88.5
6	SbCl ₅ ^{10b}	86.1	100
7	BCl ₃ ²⁴	88.7	105.7

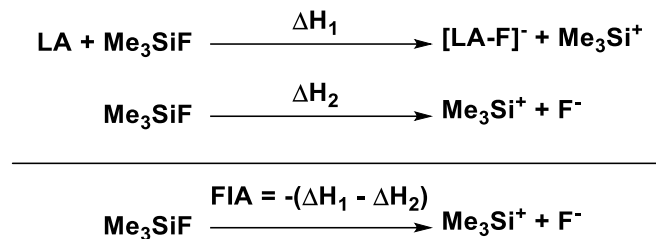


Figure 2.2: The reactions involved in the anchor point system for calculating FIA.

The determination of FIA's experimentally is challenging. FIA values are obtained using ion cyclotron resonance spectroscopy or through Born-Fajans-Haber cycles both of which are far more elaborate methods than other methods of experimental Lewis acidity assessments, with the former requiring specialized instrumentation and the latter being challenging to measure.²⁵ However, qualitative relative FIA tests are much simpler, in which one Lewis acid (LA_a) and a fluoride adduct of a second Lewis acid [LA_b-F]⁻ are mixed in solution. The FIA of LA_a can be determined to be greater than the LA_b if the fluoride is transferred between the Lewis acids, forming [LA_a-F]⁻ and LA_b. Conversely, if no change is observed, then LA_a is weaker than the second.

Table 2.2: Calculated FIA values of common Lewis acids²⁶

Entry	Lewis Acid	FIA (kJ/mol)	Entry	Lewis Acid	FIA (kJ/mol)
1	SiCl ₄ ^a	328	5	BF ₃ ^a	346
2	GeCl ₄ ^a	323	6	SbCl ₅ ^a	438
3	B(C ₆ F ₅) ₃ ^b	448	7	BCl ₃ ^a	404
4	AlCl ₃ ^a	505			

a) Energy calculated at the DLPNO-CCSD(T)/aug-cc-pVQZ level of theory. *b)* Energy calculated at the DLPNO-CCSD(T)/cc-pVQZ level of theory.

The Global Electrophilicity Index (GEI) is the only method for the assessment of Lewis acidity that is independent of the Lewis base. The GEI method utilizes the

calculated energies of the HOMO and LUMO calculations of a Lewis acid to determine chemical potential (μ) and chemical hardness (η) by the following formulas:²¹

$$(2) \quad \mu = \frac{1}{2}(E_{\text{HOMO}} + E_{\text{LUMO}})$$

$$(3) \quad \eta = (E_{\text{LUMO}} - E_{\text{HOMO}})$$

The chemical potential and chemical hardness values can be further converted to a GEI value, ω :

$$(3) \quad \omega = \mu^2/2\eta = \chi^2/2\eta$$

While the GEI method is easy to perform and is computationally inexpensive, it only takes into account the inherent electronic properties of a Lewis acid and does not include critical factors such as the steric bulk of the Lewis acid and Hard Soft Acid Base (HSAB) factors. Thus, GEI values are not reliable for a comparison of the strengths of Lewis acids which differ greatly in structure and electronic characteristics. For example, a comparison of the GEI values of BF_3 and $\text{B}(\text{C}_6\text{F}_5)_3$ would not be reliable as the steric bulk of the pentafluoroaryl substituents is not considered. However, GEI can be used to quickly determine the Lewis acidity of a series of compounds which are very similar, in nature such as a comparison of the halides within a group of the periodic table (BF_3 , AlF_3 , GaF_3 , etc.) or a comparison of the Lewis acidity of compounds with the same Lewis acidic centre, but different halide substituents (BF_3 , BCl_3 , BBr_3 , etc.).

2.1.3 Lewis Acidity of Bis(catecholato)silanes and -germanes

Previous reports have shown that bis(catecholato)silanes and -germanes with electron-withdrawing substituents on the catechol ring are highly Lewis acidic.³⁻⁵ Gutmann-Beckett $^{31}\text{P}\{^1\text{H}\}$ chemical shifts and acceptor numbers, from the reaction of bis(catecholato)silanes with one equivalent of triethylphosphine oxide, are presented in Table 2.3. Notably, bis(catecholato)silanes with halogenated catechol ligands (Table 2.3, Entries 3-5) have higher acceptor numbers than that of a derivative with alkyl substituents, $\text{Si}(\text{dtbc})_2$, or the parent derivative $\text{Si}(\text{cat})_2$ (Table 2.3, Entries 1-2). The

Lewis acidities of the halogenated bis(catecholato)silanes follow the trend of $F < Cl < Br$, which is attributed to the greater size of the halogen which disfavours π -donation from the lone pairs due to a greater mismatch in orbital size with the aromatic carbon p-orbitals rather than the relative electronegativities and inductive effect of the halogen substituents. While the coordination of one equivalent of triethylphosphine oxide is typically used to determine acceptor numbers, the addition of two equivalents of triethylphosphine oxide to $Si(cat^{Cl})_2(ACN)_2$ led to the formation of $Si(cat^{Cl})_2(OPEt_3)_2$ species. Attempts to assess the Lewis acidity of the germanium-based $Ge(cat^{Cl})_2(ACN)_2$ using the Gutmann-Beckett method were unsuccessful due to the preferential formation of the hexacoordinate species over the pentacoordinate neutral germanium species.⁶ The formation of both the *cis*- and *trans*- $Ge(cat^{Cl})_2(OPEt_3)_2$ was observed in the $^{31}P\{^1H\}$ NMR spectrum. Although a direct comparison of the Lewis acidity with other Lewis acids which only coordinate one equivalent of triethylphosphine oxide could not be made, the higher $^{31}P\{^1H\}$ NMR shift of the *cis*- and *trans*- $Ge(cat^{Cl})_2(OPEt_3)_2$ species, 75.1 and 70.1 ppm respectively, compared to the silicon derivative $Si(cat^{Cl})_2(OPEt_3)_2$, at 73.1 ppm,⁴ implies a greater Lewis acidity for the germanium species.

Table 2.3: The $^{31}P\{^1H\}$ chemical shift and acceptor numbers from Gutmann-Beckett experiments with bis(catecholato)silanes.⁵

Entry	$Si(cat^X)_2-OPEt_3$	$\delta^{31}P\{^1H\}$ NMR (ppm)	Acceptor Number
1	$Si(dtbc)_2$	81.6	90
2	$Si(cat)_2$	83.2	93
3	$Si(cat^F)_2$	86.6	101
4	$Si(cat^{Cl})_2$	87.2	102
5	$Si(cat^{Br})_2$	87.3	102

To further assess the Lewis acidity of the bis(catecholato)- group 14 species, fluoride ion affinity (FIA) calculations were performed.³⁻⁶ The results are presented in

Table 2.4. The FIA values of the bis(catecholato)silanes are in agreement with the experimental results from the Gutmann-Beckett analysis; however, the FIA of $\text{Ge}(\text{cat}^{\text{Cl}})_2$, 504 kJ/mol (Table 2.4 Entry 5), is lower than that of $\text{Si}(\text{cat}^{\text{Cl}})_2$, 507 kJ/mol (Table 2.4 Entry 3) and does not correlate to the greater $^{31}\text{P}\{^1\text{H}\}$ NMR shift observed for the bis-ligated $\text{Ge}(\text{cat}^{\text{Cl}})_2(\text{OPEt}_3)_2$ compared to the $\text{Si}(\text{cat}^{\text{Cl}})_2(\text{OPEt}_3)_2$ species. $\text{Si}(\text{cat}^{\text{Cl}})_2$, $\text{Si}(\text{cat}^{\text{Br}})_2$, and $\text{Ge}(\text{cat}^{\text{Cl}})_2$ are designated as Lewis superacids, a Lewis acid which has a FIA greater than that of SbF_5 . This was further confirmed in reactivity studies of the silicon derivatives by reacting $[\text{cation}][\text{SbF}_6]$ with $\text{Si}(\text{cat}^{\text{Cl}})_2(\text{ACN})_2$ and $\text{Si}(\text{cat}^{\text{Br}})_2(\text{ACN})_2$ which led to the formation of $\text{Si}(\text{cat}^{\text{X}})_2\text{F}$.

Table 2.4: Calculated FIA values for the bis(catecholato)silanes.

Entry	Compound	FIA (kJ/mol) ^a
1	$\text{Si}(\text{cat})_2$	391
2	$\text{Si}(\text{cat}^{\text{F}})_2$	490
3	$\text{Si}(\text{cat}^{\text{Cl}})_2$	507
4	$\text{Si}(\text{cat}^{\text{Br}})_2$	538
5	$\text{Ge}(\text{cat}^{\text{Cl}})_2$	504

^a) Calculated at DLPNO-CCSD(T)/aug-cc-pVQZ//PW6B95-D3(BJ)/def2-TZVPP level of theory

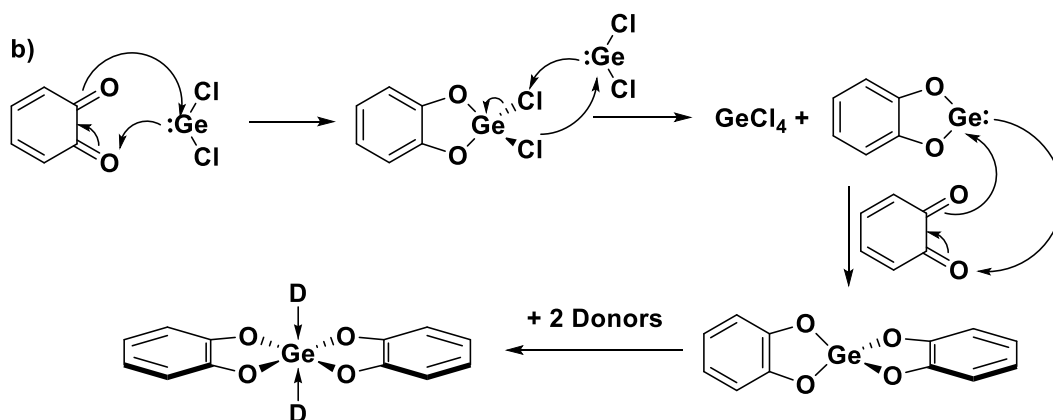
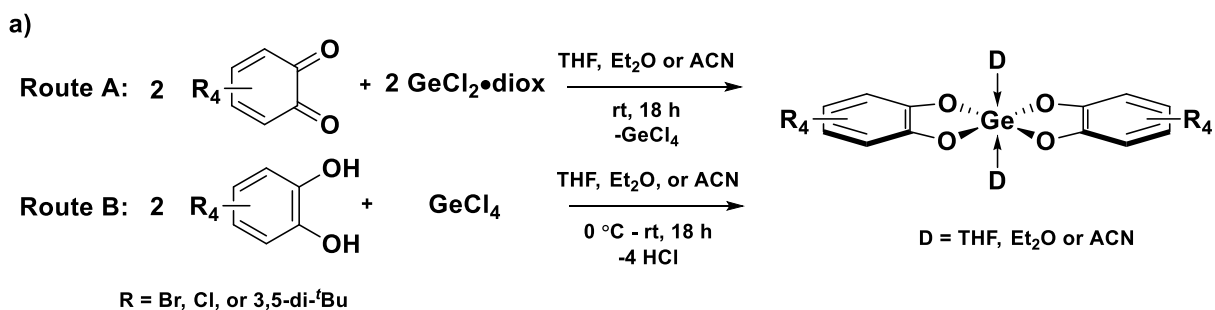
2.1.4 Project Goal: Bis(catecholato)germanes

Given that bis(catecholato)silanes with electron-withdrawing substituents on the catechol ring are strong silicon Lewis acids, there are only a limited number of investigations of germanium-based Lewis acids, and the softer nature of germanium compared to silicon, I decided to explore the synthesis of various bis(catecholato)germanes and assess their Lewis acidity using fluoride ion affinity and global electrophilicity index calculations, as well as the Gutmann-Beckett method. The results herein will be compared to the synthesis of bis(perchlorocatecholato)germane derivatives with water and acetonitrile donor ligands and the silicon derivatives and the Lewis acidity of the bis(catecholato)germanes will be compared to their silicon congeners and other common main group Lewis acids.

2.2 Results and Discussion

2.2.1 Synthesis and Reactivity

The syntheses of the bis(catecholato)germane derivatives were achieved using two different routes: the addition of a substituted quinone to $\text{GeCl}_2 \cdot \text{dioxane}$ (Route **A**) or the addition of a substituted catechol to GeCl_4 (Route **B**) (Scheme 2.2). The choice of reaction pathway was made on the basis of the availability and cost of the starting catechol/quinone.



Scheme 2.2: a) Synthesis of bis(catecholato)germanes via two different routes. b) A proposed mechanism for the redox reaction between quinone and $\text{GeCl}_2 \cdot \text{dioxane}$ (dioxane and quinone substituents were omitted for clarity).

The synthesis of the 3,5-di-*tert*-butyl-substituted derivatives was achieved using route **A**. Addition of 3,5-di-*tert*-butylquinone to $\text{GeCl}_2 \cdot \text{dioxane}$ in either THF or ACN yielded $\text{Ge}(3,5\text{-dtbc})_2(\text{THF})_2$ or $\text{Ge}(3,5\text{-dtbc})_2(\text{ACN})_2$ as white solids in 87% or 74%

yield, respectively. Attempts to synthesize these compounds by route **B** resulted in substantially lower yields. The complexes were characterized by ^1H and ^{13}C NMR spectroscopy, infrared (IR) spectroscopy, electron-impact mass spectrometry (EI-MS), and, in the case of $\text{Ge}(3,5\text{-dtbc})_2(\text{THF})_2$, X-ray crystallography (Figure 2.3). The germanium-catecholato oxygen bond distances of $\text{Ge}(3,5\text{-dtbc})_2(\text{THF})_2$ (Ge1-O1 : 1.8247(13) and Ge1-O2 : 1.8297(13) Å) are comparable to those of $\text{Ge}(3,6\text{-dtbc})_2(\text{THF})_2$ (1.819(1) Å) and $\text{Ge}(3,6\text{-dtbc})_2(\text{Et}_2\text{O})_2$ (1.8186(7) and 1.8256(7) Å),⁸ and are shorter than the corresponding bond distances in $\text{Ge}(3,5\text{-dtbc})_2(\text{pyridine})_2$ (1.847(1) and 1.849(1) Å) which features pyridine donor ligands.⁷

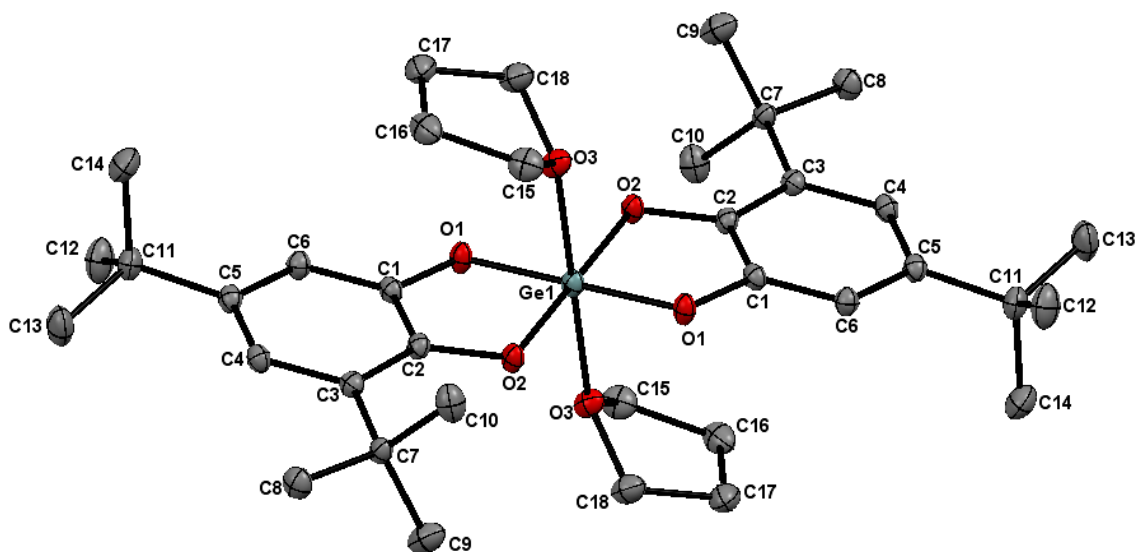
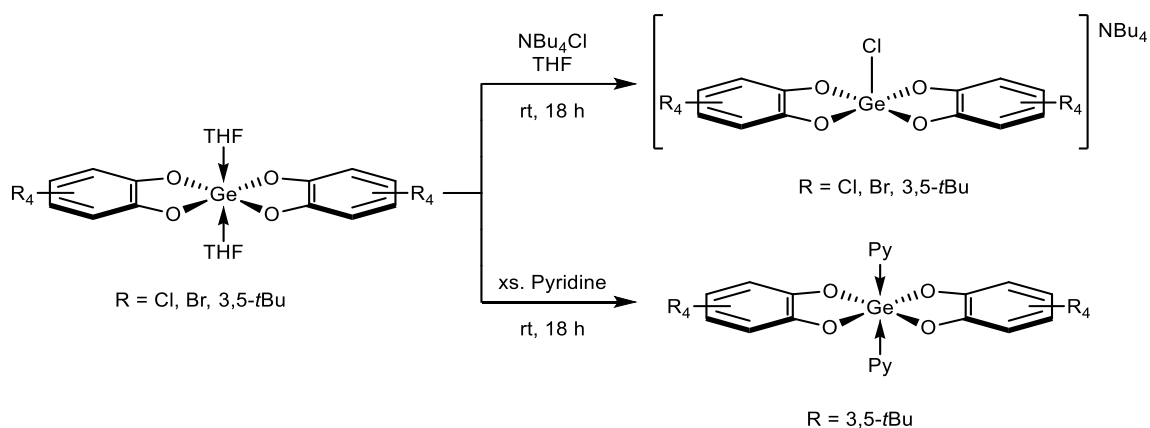


Figure 2.3: Thermal ellipsoid plot of $\text{Ge}(3,5\text{-dtbc})_2(\text{THF})_2$ showing naming and numbering scheme. Ellipsoids are at the 50% probability level and hydrogen atoms were omitted for clarity. Selected bond lengths (Å) and angles ($^\circ$): Ge1-O1 = 1.8247(13), Ge1-O2 = 1.8297(13), Ge1-O3 = 2.1126(14); O1-Ge1-O2 = 89.60(6), O1-Ge1-O3 = 90.69(6); O2-Ge1-O3 = 92.23(6).

With the successful synthesis of the donor-complexed $\text{Ge}(3,5\text{-dtbc})_2$ derivatives, the same strategy (Route **A**) was applied to synthesize the bis(perchlorocatecholato)germanes: $\text{Ge}(\text{cat}^{\text{Cl}})_2(\text{THF})_2$, $\text{Ge}(\text{cat}^{\text{Cl}})_2(\text{Et}_2\text{O})_2$ and

$\text{Ge}(\text{cat}^{\text{Cl}})_2(\text{ACN})_2$ in 48%, 87% and 88% yields, respectively. Notably, the yield of $\text{Ge}(\text{cat}^{\text{Cl}})_2(\text{ACN})_2$ is comparable to that derived from GeO_2 (91% overall yield)⁶ and provides an alternative one-step synthesis for $\text{Ge}(\text{cat}^{\text{Cl}})_2(\text{ACN})_2$ from commercially available materials. Furthermore, using tetrachlorocatechol and GeCl_4 , the chlorinated complexes can also be synthesized via route **B**, albeit in a lower yield. Using the commercially available tetrabromocatechol, $\text{Ge}(\text{cat}^{\text{Br}})_2(\text{THF})_2$ (46%), $\text{Ge}(\text{cat}^{\text{Br}})_2(\text{Et}_2\text{O})_2$ (11%) and $\text{Ge}(\text{cat}^{\text{Br}})_2(\text{ACN})_2$ (15%) were obtained via route **B**. While the $\text{Ge}(3,5\text{-dtbc})_2$ derivatives are readily soluble in most organic solvents and could be characterized by NMR spectroscopy, the halogenated derivatives are scarcely soluble. Due to the insolubility of these compounds and the lack of convenient NMR nuclei, characterization was limited to EI-MS for the halogenated derivatives.

To further confirm the formation of the bis(catecholato)germanes, the THF derivatives were reacted with NBu_4Cl to form the corresponding chlorogermanates that were easily identified by electrospray ionization mass spectrometry (ESI-MS) (Scheme 2.3). In the case of $[\text{NBu}_4][\text{Ge}(\text{cat}^{\text{Br}})_2\text{Cl}]$ single crystals suitable for X-ray crystallography were grown. The molecular structure shows a pentacoordinated germanium centre (Figure 2.4). Comparing this structure to that of the hexacoordinated $[\text{NBu}_4]_2[\text{Ge}(\text{cat}^{\text{Cl}})_2\text{Cl}_2]$ reported by Greb *et al.*, it is found that the Ge-O bond distances are similar in length and the Ge-Cl distance of $[\text{Ge}(\text{cat}^{\text{Br}})_2\text{Cl}]^-$, 2.1622(13) Å, is slightly shorter than those in $[\text{Ge}(\text{cat}^{\text{Cl}})_2\text{Cl}_2]^{2-}$, 2.353(2) Å.⁶ $\text{Ge}(3,5\text{-dtbc})_2(\text{THF})_2$ was also reacted with excess pyridine to give the known $\text{Ge}(3,5\text{-dtbc})_2(\text{pyridine})_2$,⁷ as observed by ¹H NMR spectroscopy. The observed reactivity implies the weak donor ligands, THF and ACN, are sufficiently labile to be displaced by a chloride anion or a strong donor, such as pyridine.



Scheme 2.3: Addition of NBu_4Cl and pyridine to bis(catecholato)germanes.

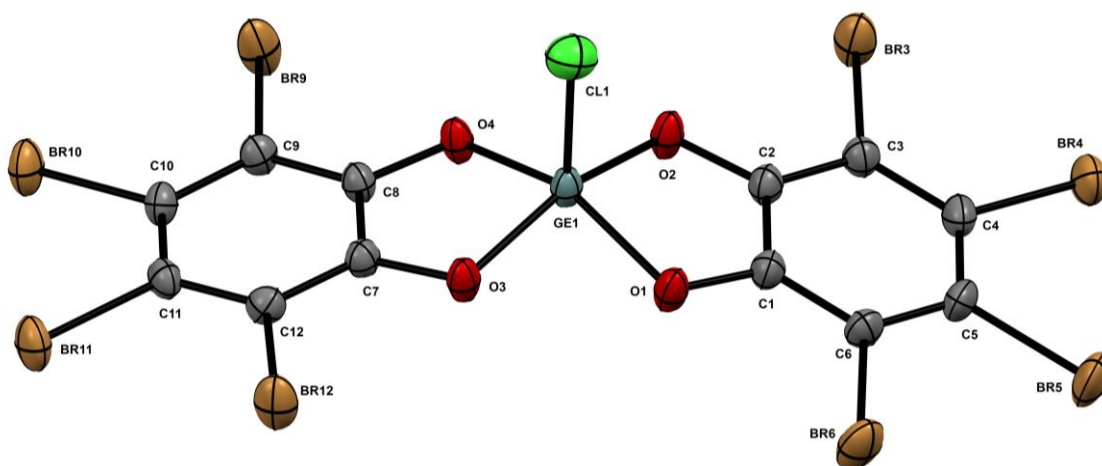


Figure 2.4: Thermal ellipsoid plot of $[\text{NBu}_4][\text{Ge}(\text{cat}^{\text{Br}})_2\text{Cl}]$ showing naming and numbering scheme. Ellipsoids are at the 50% probability level. NBu_4 cation and hydrogen atoms were omitted for clarity. Selected bond lengths (\AA) and angles ($^\circ$): $\text{Ge1-O1} = 1.8387(16)$, $\text{Ge1-O2} = 1.8529(16)$, $\text{Ge1-O3} = 1.8489(16)$, $\text{Ge1-O4} = 1.8369(16)$, $\text{Ge1-Cl1} = 2.1622(13)$; $\text{O1-Ge1-O4} = 150.29(8)$, $\text{O2-Ge1-O3} = 158.98(8)$, $\text{O1-Ge1-Cl1} = 106.68(6)$, $\text{O3-Ge1-Cl1} = 99.60(6)$.

2.2.2 Lewis Acidity Assessment – Gutmann Beckett

To assess the Lewis acidity of the bis(catecholato)germanes, the Gutmann-Beckett method was employed.¹⁰ Sub-stoichiometric amounts of triethylphosphine oxide was added to a suspension (or solution for the dtbc derivative) of both the THF and the

ACN derivatives of each bis(catecholato)germane in CH_2Cl_2 (1 mg/mL) and a $^{31}\text{P}\{^1\text{H}\}$ NMR spectrum of the mixture was recorded. The sub-stoichiometric amounts of triethylphosphine oxide and the dilute concentration gave rise to chemical shifts in the 82-88 ppm range, similar to the $^{31}\text{P}\{^1\text{H}\}$ chemical shifts of the mono- OPEt_3 adducts of the analogous bis(catecholato)silanes (Table 2.5).⁵ An increase in acceptor number of 6 and 9 was observed for both the $\text{Ge}(\text{cat}^{\text{Cl}})_2$ and $\text{Ge}(\text{cat}^{\text{Br}})_2$ derivatives (Table 2.5, Entries 2-3) when the acetonitrile-bound complexes are utilized for the experiments compared to the THF-bound complexes suggesting that the donor has an influence on the Lewis acidity of the halogenated complexes but not the $\text{Ge}(\text{dtbc})_2$ derivatives. These observations are consistent with the formation of a hexacoordinated $\text{Ge}(\text{cat}^{\text{X}})_2(\text{OPEt}_3)(\text{Donor})$ complex where one of the solvent donors remains ligated upon the addition of triethylphosphine oxide rather than the formation of a pentacoordinate $\text{Ge}(\text{cat}^{\text{X}})_2(\text{OPEt}_3)$ complex. To confirm that the results of these sub-stoichiometric experiments were consistent with the formation of a mono- OPEt_3 adduct, the soluble $\text{Ge}(3,5\text{-dtbc})_2(\text{THF})_2$ was reacted with exactly one equivalent of OPEt_3 in CD_2Cl_2 in a concentrated solution (0.048 M). In the resulting $^{31}\text{P}\{^1\text{H}\}$ NMR spectrum, only one signal at 82.2 ppm was observed which was assigned to $\text{Ge}(\text{dtbc})_2(\text{OPEt}_3)$ consistent with the chemical shifts observed in the sub-stoichiometric experiments. The dissociation of the THF ligands of $\text{Ge}(\text{dtbc})_2(\text{THF})_2$ upon reaction with triethylphosphine oxide was confirmed in the ^1H NMR spectrum of $\text{Ge}(\text{dtbc})_2(\text{OPEt}_3)$, which showed a shift in the ^1H NMR signals assigned to the THF moiety compared to $\text{Ge}(\text{dtbc})_2(\text{THF})_2$. Furthermore, the chemical shifts of the THF in the $\text{Ge}(\text{dtbc})_2(\text{THF})_2 + \text{OPEt}_3$ solution, match those of free THF and integrate to the value expected for two molecules. The observed dissociation of THF is consistent with the conclusion that the donor ligands for $\text{Ge}(\text{dtbc})_2(\text{donor})_2$ derivatives do not influence the Lewis acidity of the bis(catecholato)germane core.

Table 2.5: Lewis Acidities of bis(catecholato)germanes and -silanes as determined by the Gutmann-Beckett method.

Entry	Product	³¹ P{ ¹ H} Chemical Shift (ppm) {Acceptor Number} [M = Ge]		³¹ P{ ¹ H} Chemical Shift (ppm) {Acceptor Number} [M = Si] ⁵
		Donor = THF ^a	Donor = ACN ^b	
1	M(3,5-dtbc) ₂ (OPEt ₃)	82.6 {92}	82.8 {92}	81.6 {90} ^c
2	M(cat ^{Cl}) ₂ (OPEt ₃)•donor	84.0 {95}	88.2 {104}	87.2 {102} ^{b,d}
3	M(cat ^{Br}) ₂ (OPEt ₃)•donor	85.7 {99}	88.4 {105}	87.3 {102} ^{b,d}

a) Starting from Ge(cat^X)₂(THF)₂; *b)* starting from M(cat^X)₂(ACN)₂; *c)* starting from Si(3,5-dtbc)₂; *d)* Ligated donor was not observed in the silicon derivatives.

The reaction of Ge(3,5-dtbc)₂(THF)₂ with two equivalents of triethylphosphine oxide was also explored and revealed only a single signal at 61.9 ppm in the ³¹P{¹H} NMR spectrum (Figure 2.5). No diastereotopic PCH₂ signals, characteristic of a *cis*-isomer, were observed in the ¹H NMR spectrum, and thus, the structure of the product was assigned to the *trans*-isomer. The increased steric bulk around the catechol ring of Ge(3,5-dtbc)₂ evidently prevents the formation of the *cis*-isomer. Interestingly, the addition of three equivalents of triethylphosphine oxide to Ge(3,5-dtbc)₂(THF)₂ resulted in a broad signal at 58.8 ppm in the ³¹P{¹H} NMR spectrum. To understand the spectrum, variable temperature NMR (VT-NMR) experiments, from 25 °C to -80 °C, were performed on the mixture (Figure 2.6). As the solution was cooled, the signal at 58.8 ppm broadened and then disappeared into the baseline of the spectrum. Two ³¹P{¹H} NMR singlets at 66.6 and 53.5 ppm appeared at -80 °C which, on the basis of chemical shift, were assigned to *trans*-Ge(dtbc)₂(OPEt₃)₂ and free triethylphosphine oxide, respectively. The results of the VT-NMR experiments suggest a dynamic process between the di-OPEt₃ adduct of the germane and free triethylphosphine oxide. A solution of Ge(3,5-dtbc)₂(THF)₂ (1 eq.) and triethylphosphine oxide (3 eq.), dissolved in CH₂Cl₂ and layered with cyclohexane, yielded crystals of *trans*-Ge(dtbc)₂(OPEt₃)₂ suitable for X-ray

crystallography (Figure 2.7). The bond lengths and angles are comparable to that of *trans*-Ge(cat^{Cl})₂(OPEt₃)₂ reported by Greb *et al.*⁶

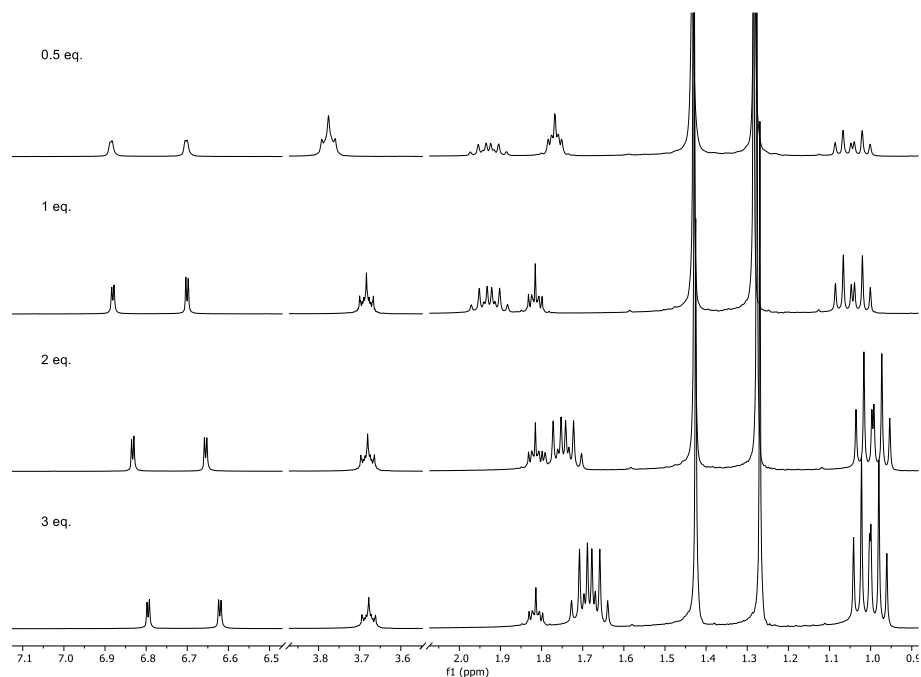


Figure 2.5: ¹H NMR (400 MHz in CD₂Cl₂) stacked spectra of Ge(3,5-dtbc)₂(THF)₂ and various equivalents of triethylphosphine oxide

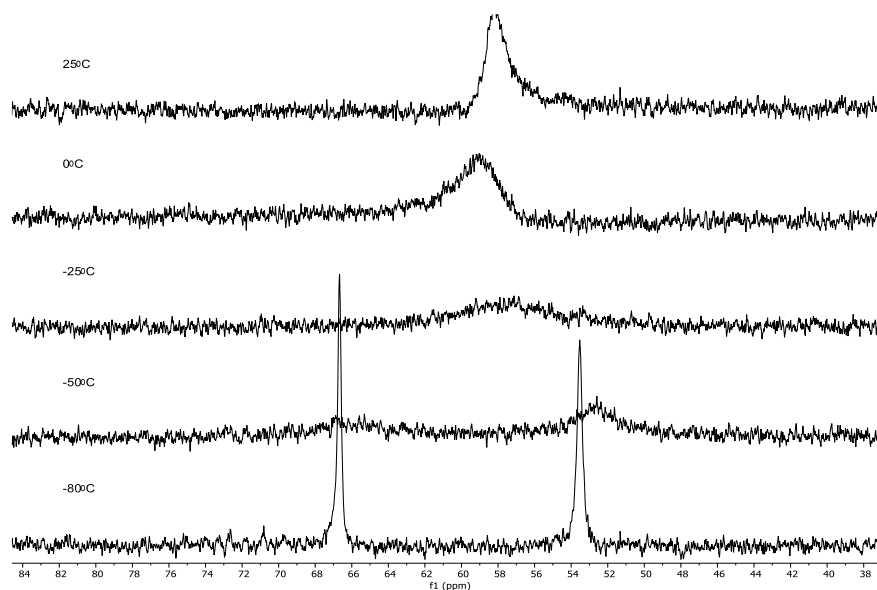


Figure 2.6: ³¹P{¹H} VT-NMR spectrum of a solution containing 1 eq. Ge(dtbc)₂(THF)₂ and 3 eq. of OPET₃, at room temperature (top) and -80 °C (bottom) (66.6 ppm=*trans*-Ge(dtbc)₂(OPET₃)₂; 53.5 ppm= OPET₃)

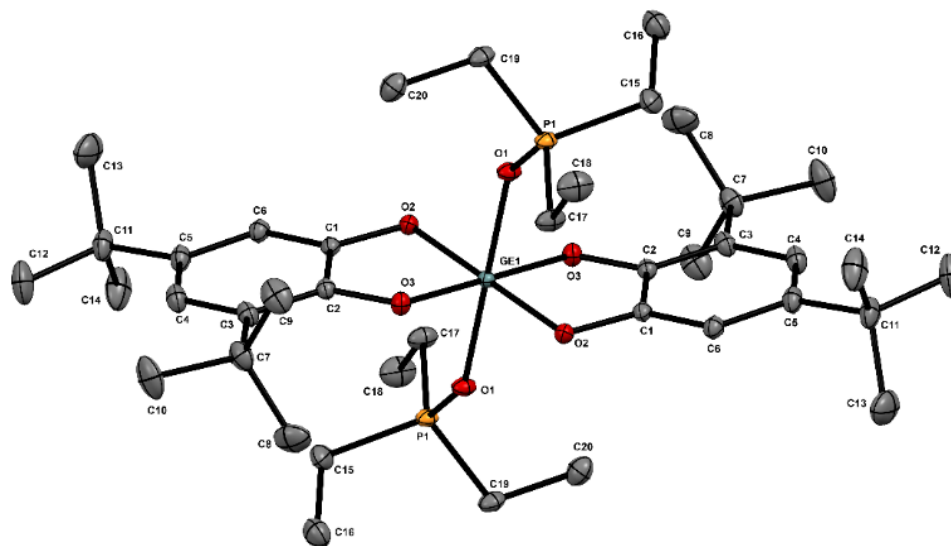


Figure 2.7: a) Thermal ellipsoid plot of $\text{Ge}(3,5\text{-dtbc})_2(\text{OPEt}_3)_2$ showing naming and numbering scheme. Ellipsoids are at the 50% probability level and hydrogen atoms were omitted for clarity. Selected bond lengths (\AA) and angles ($^\circ$): $\text{Ge1-O1} = 1.9863(8)$, $\text{Ge1-O2} = 1.8467(7)$, $\text{Ge1-O3} = 1.8484(8)$, $\text{P1-O1} = 1.5208(7)$; $\text{O1-Ge1-O2} = 89.75(3)$, $\text{O1-Ge1-O3} = 90.36(3)$; $\text{O2-Ge1-O3} = 88.61(3)$.

The reactivity of the halogenated bis(catecholato)germanes with triethylphosphine oxide in concentrated solution illustrated reactivity which differs compared to that of the $\text{Ge}(3,5\text{-dtbc})_2$ derivative. Notably, at 20 mg/mL, the halogenated bis(catecholato)germanes did not dissolve completely, and thus, without a diagnostic ^1H NMR signal for the halogenated derivatives, the ratio of OPEt_3 to germane in solution cannot be accurately determined. Adding 0.5 or one equivalent of triethylphosphine oxide to a suspension of either $\text{Ge}(\text{cat}^{\text{Cl}})_2(\text{THF})_2$ or $\text{Ge}(\text{cat}^{\text{Br}})_2(\text{THF})_2$ in CD_2Cl_2 (20 mg/mL) resulted in the appearance of three signals in the $^{31}\text{P}\{^1\text{H}\}$ NMR spectrum, two of which were assigned to the *cis* and *trans* di- OPEt_3 adducts (the di- OPEt_3 adducts are observed in the range of 70-76 ppm in the $^{31}\text{P}\{^1\text{H}\}$ NMR spectra, Figure 2.8 and Figure 2.9, respectively). The observation of both the *cis* and the *trans* di- OPEt_3 adducts of the germanes is consistent with the results reported by Greb *et al.*⁶ This is further confirmed in the ^1H NMR spectrum, for both the chloro and bromo derivatives, where diastereotopic ^1H signals at 2.0-2.5 ppm for the *cis*- $\text{Ge}(\text{cat}^{\text{X}})_2(\text{OPEt}_3)_2$ are observed (Figure 2.10). The remaining broad $^{31}\text{P}\{^1\text{H}\}$ signal, observed at 78.4 ppm or 77.9 ppm for the chloro- and

bromo-derivatives respectively, was assigned to $\text{Ge}(\text{cat}^{\text{X}})_2(\text{OPEt}_3)(\text{THF})$ on the basis of the greater $^{31}\text{P}\{^1\text{H}\}$ NMR shift compared to the di- OPEt_3 adducts. The downfield shift, compared to the di- OPEt_3 adducts, is attributed to the weaker THF donor causing an increase in Lewis acidity of the Ge core. Notably, the chemical shift of this signal is upfield of that recorded under dilute conditions (see Table 2.5) and the signal is broad, indicative of dynamic exchange of the donor ligands between $\text{Ge}(\text{cat}^{\text{X}})_2(\text{OPEt}_3)(\text{THF})$ and $\text{Ge}(\text{cat}^{\text{X}})_2(\text{OPEt}_3)_2$. Reaction of the halogenated bis(catecholato)germanes with 2 or 3 equivalents of triethylphosphine oxide resulted in the disappearance of the signal assigned to $\text{Ge}(\text{cat}^{\text{X}})_2(\text{OPEt}_3)(\text{THF})$, an increase in the sharpness of the $^{31}\text{P}\{^1\text{H}\}$ NMR signal assigned to the *trans* di- OPEt_3 adduct of the germane and the appearance of a signal assigned to free triethylphosphine oxide (Figure 2.8 and Figure 2.9).

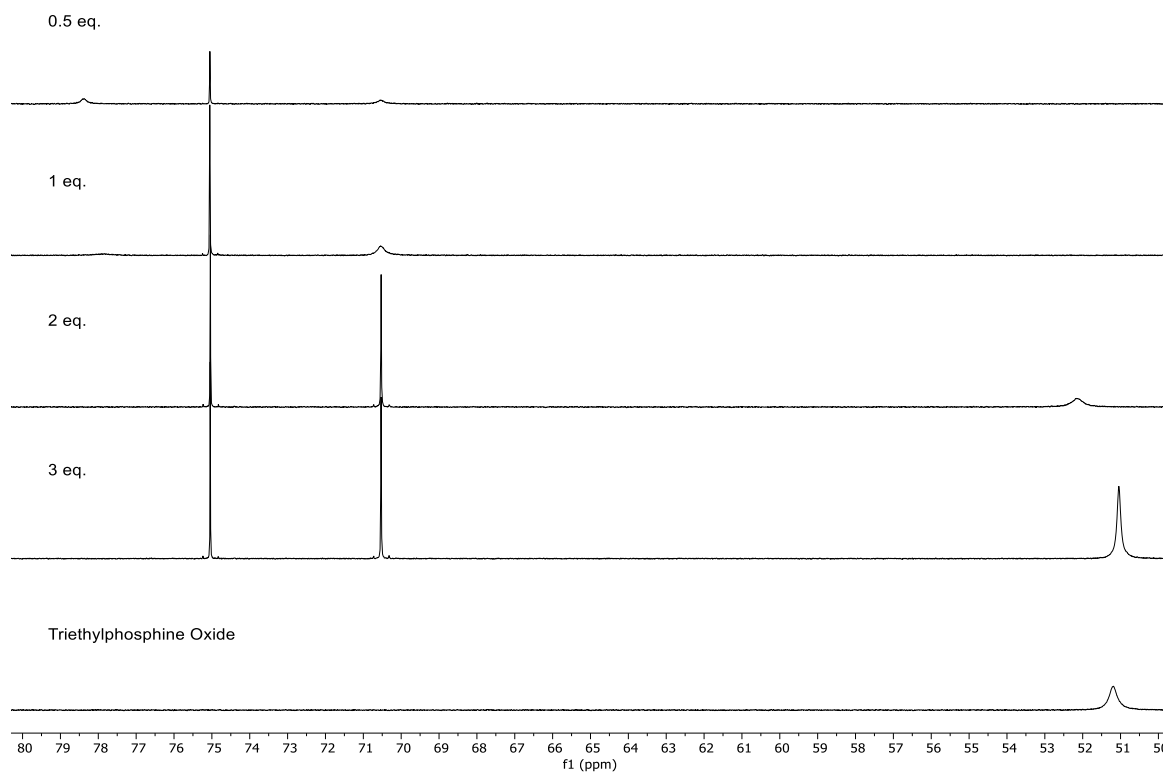


Figure 2.8: $^{31}\text{P}\{^1\text{H}\}$ NMR (162 MHz in CD_2Cl_2) stacked spectra of $\text{Ge}(\text{cat}^{\text{Cl}})_2(\text{THF})_2$ and various equivalents of triethylphosphine oxide

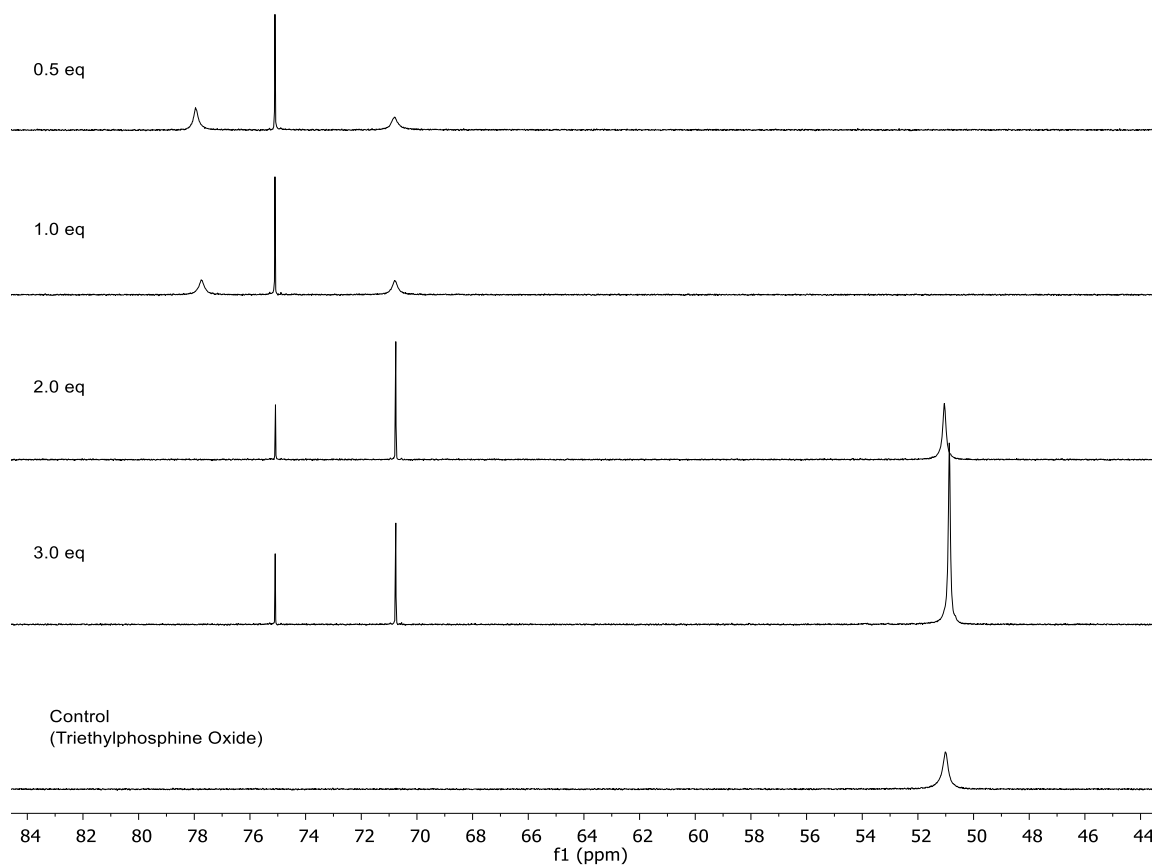


Figure 2.9: $^{31}\text{P}\{^1\text{H}\}$ NMR (162 MHz in CD_2Cl_2) stacked spectra of $\text{Ge}(\text{cat}^{\text{Br}})_2(\text{THF})_2$ and various equivalents of triethylphosphine oxide

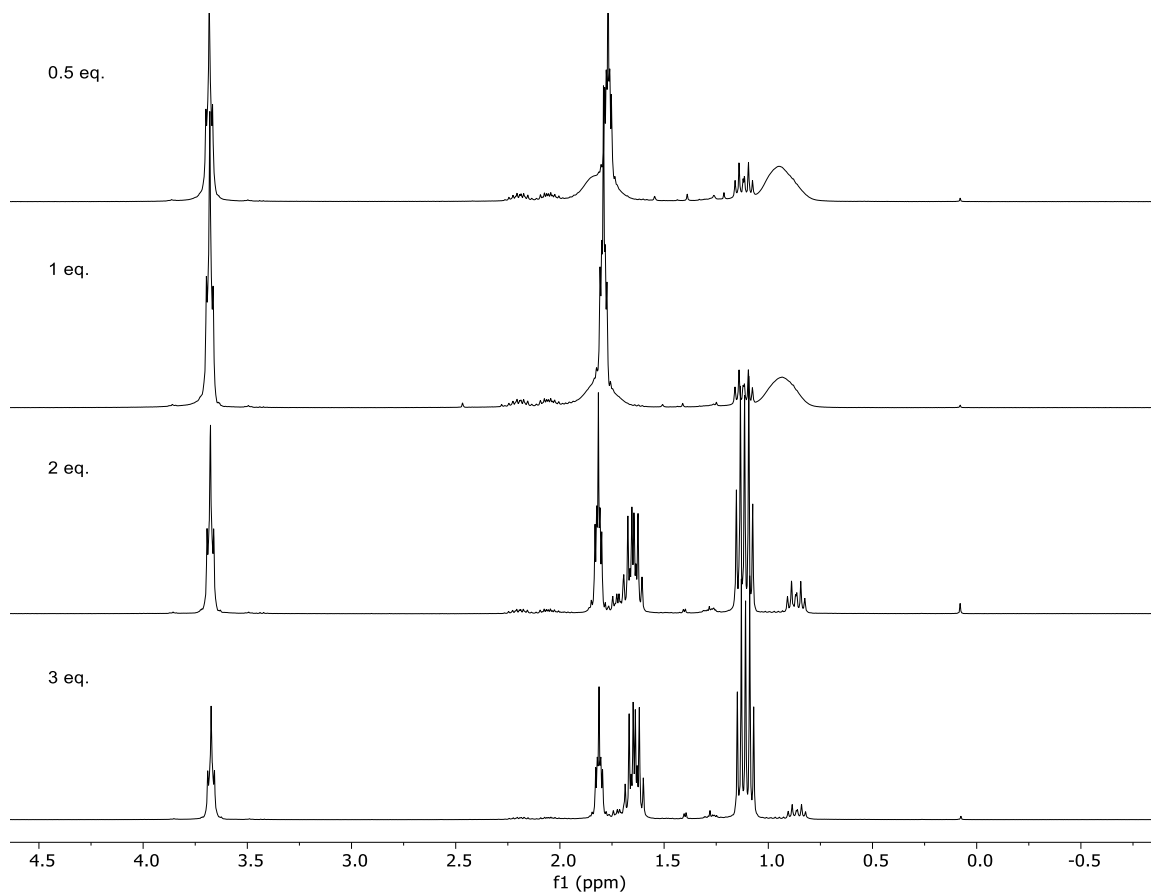


Figure 2.10: ^1H NMR (400 MHz in CD_2Cl_2) stacked spectra of $\text{Ge}(\text{cat}^{\text{Br}})_2(\text{THF})_2$ and various equivalents of triethylphosphine oxide. Similar signals for the chlorinated derivative were observed and in agreement with the literature.⁶

2.2.3 Lewis Acidity Assessment – FIA and GEI Calculations

To further assess the Lewis acidity of the bis(catecholato)germanes, fluoride ion affinity (FIA)¹⁵ and global electrophilicity index (GEI)²¹ calculations were performed using ORCA version 4.2.0 at the B3LYP D3(BJ)/def2-TZVPP//PBEh-3c/def2-mSVP level of theory.²⁷ The results, as well as the FIA values of the analogous silicon derivatives,⁵ are shown in Table 2.6. The FIA calculations demonstrate that the Lewis acidity of the donor-less bis(catecholato)germanes is comparable to that of the bis(catecholato)silanes and that the Lewis acidity of the parent catechol derivative and that of the *tert*-butyl-substituted derivative (Table 2.6, Entries 1-2) is less than that of the halogenated derivatives (Table 2.6, Entries 3-5). Notably, the range of the FIA values of

the halogenated bis(catecholato)germanes is much narrower (11 kJ/mol) compared to the halogenated bis(catecholato)silanes (48 kJ/mol) suggesting that the choice of halogen substituents on the bis(catecholato)germanes influences the strength of the Lewis acid less than in the silane derivatives (Table 2.6, Entries 3-5). The FIA values for $\text{Ge}(\text{cat}^{\text{Cl}})_2$ (508 kJ/mol) and $\text{Ge}(\text{cat}^{\text{Br}})_2$ (513 kJ/mol) are greater than the FIA value calculated for SbF_5 (507 kJ/mol) designating these germane derivatives as Lewis superacids (Table 2.6, Entries 4-5).

Table 2.6: Computational results for the FIA and GEI values of the bis(catecholato)germanes and the reported FIA values for the bis(catecholato)silanes for comparison.

Entry	Compound	FIA (kJ/mol) ^a [M = Ge]	FIA (kJ/mol) ^b [M = Si] ⁵	GEI (eV) ^a [M = Ge]
1	M(3,5-dtbc) ₂	433	-	1.20
2	M(cat) ₂	416	391	1.06
3	M(cat ^F) ₂	502	490	2.10
4	M(cat ^{Cl}) ₂	508	507	1.92
5	M(cat ^{Br}) ₂	513	538	2.01
6	M(3,5-dtbc) ₂ (ACN)	429	-	1.45
7	M(cat) ₂ (ACN)	420	-	1.48
8	M(cat ^F) ₂ (ACN)	484	-	2.16
9	M(cat ^{Cl}) ₂ (ACN)	492	-	2.17
10	M(cat ^{Br}) ₂ (ACN)	500	-	2.20
11	M(cat ^{Br}) ₂ (Et ₂ O)	498	-	1.69
12	M(cat ^{Br}) ₂ (THF)	494	-	1.68

^a) = B3LYP D3(BJ)/def2-TZVPP//PBEh-3c/def2-mSVP; ^b) = DLPNO-CCSD(T)/aug-cc-pVQZ//PW6B95-D3/def2-TZVPP. FIA of SbF_5^a = 507 kJ/mol; FIA of SbF_5^b = 501 kJ/mol; FIA of $\text{Ge}(\text{cat}^{\text{Cl}})_2^b$ = 504 kJ/mol⁶

To understand the influence of the donor ligands on the stability of the complexed bis(catecholato)germanes, the relative energies of the mono-ligated and donor-less

bis(perbromocatecholato)germanes were compared to the bis-ligated complex (Table 2.7). The removal of both the first and second donor ligand, where the donor is THF or ACN, is both endothermic and endergonic, in contrast with the results reported for the bis(catecholato)silane, $\text{Si}(\text{cat}^{\text{Cl}})_2(\text{ACN})_2$, where dissociation of both donors was overall exergonic.⁴ The calculations of the bis(catecholato)germanes suggest that complete dissociation of both donor ligands is unlikely for these complexes. As such, the FIA values for the mono-ACN ligated series of bis(catecholato)germanes and, in the case of the bromo-derivative, the FIA values for the mono-THF and mono- Et_2O complexes were also computed (Table 2.6). Notably, the FIA values of the mono-ligated bis(catecholato)germanes (Table 2.6, Entries 6-12) were 4-16 kJ/mol lower than their donor-free counterparts (Table 2.6, Entries 1-5), with the largest differences observed for the halogenated derivatives. Furthermore, the stronger the donor ability of the ligand ($\text{ACN} < \text{Et}_2\text{O} < \text{THF}$), the lower the FIA value, and consequently, the complex is a weaker Lewis acid.

Table 2.7: Relative energies of $\text{Ge}(\text{cat}^{\text{Br}})_2$ derivatives.

Entry	Complex	Relative Enthalpy ^a (kJ/mol)	Relative Gibbs Free Energy ^a (kJ/mol)
1	$\text{Ge}(\text{cat}^{\text{Br}})_2(\text{ACN})_2$	0	0
2	$\text{Ge}(\text{cat}^{\text{Br}})_2(\text{ACN}) + \text{ACN}$	93.81	29.57
3	$\text{Ge}(\text{cat}^{\text{Br}})_2 + 2\text{ACN}$	165.98	33.98

^a) = BP86 D3(BJ)/def2-SVP//PBEh-3c/def2-mSVP

The calculation of the global electrophilicity index (GEI) values of the bis(catecholato)germanes was also performed (Table 2.6).²¹ The GEI values of the bis(catecholato)germanes correlate well to the FIA values except for the donor-free $\text{Ge}(\text{cat}^{\text{F}})_2$ complex which has a higher GEI value compared to the chloro- and bromo-derivatives.

The results from the three different methods of Lewis acidity assessment demonstrate that the Lewis acidity of the halogenated derivatives of the bis(catecholato)germanes is greater than that of the ^tBu-substituted and parent catechol

derivatives. Using both the FIA and the Gutmann-Beckett methods, a consistent trend in the Lewis acidity of the halogenated bis(catecholato)germanes was observed ($\text{Br} > \text{Cl} > \text{F}$). Interestingly, the GEI values of the donor-free complexes do not follow the same trend with $\text{Ge}(\text{cat}^{\text{F}})_2$ having the highest GEI value. However, the GEI values of the mono-ligated derivatives are consistent with the FIA and Gutmann-Beckett trends. Notably, the range of FIA values among the halogenated bis(catecholato)germanes is narrower than their silane counterparts, suggesting that the choice of halogenated bis(catecholato)germane to employ as a Lewis acid catalyst will not greatly affect the reactivity. Instead, the choice of germanium Lewis acid can be governed by ease of synthesis and the cost of the starting materials required to make the bis(catecholato)germane. Furthermore, the results of the Lewis acidity assessments suggest that the catalytic activity may be easily tuned for a given reaction by altering the donor ligand.

Compared to commonly used main group Lewis acids such as BF_3 (AN = 88.5, FIA = 346 kJ/mol), AlCl_3 (AN = 87, FIA = 505 kJ/mol), and $\text{B}(\text{C}_6\text{F}_5)_3$ (AN = 82, FIA = 448 kJ/mol), the halogenated bis(catecholato)germanes are more Lewis acidic with acceptor numbers of 104-105 for the acetonitrile derivatives, and FIA values of 502-513 kJ/mol for the donorless derivatives. Even the FIA values of the bound ACN derivatives of the halogenated bis(catecholato)germanes, 484-500 kJ/mol, are more Lewis acidic than both BF_3 and $\text{B}(\text{C}_6\text{F}_5)_3$. The less Lewis acidic $\text{Ge}(\text{dtbc})_2$ derivative has a higher AN (AN = 92) than BF_3 , AlCl_3 and $\text{B}(\text{C}_6\text{F}_5)_3$. However, the FIA values of the $\text{Ge}(\text{dtbc})_2$ derivative (donorless = 433 kJ/mol, ACN = 429 kJ/mol), are higher than that of BF_3 , slightly lower than $\text{B}(\text{C}_6\text{F}_5)_3$, and significantly lower than AlCl_3 . Nevertheless, the comparisons between the bis(catecholato)germanes and BF_3 , AlCl_3 , and $\text{B}(\text{C}_6\text{F}_5)_3$, illustrate the high Lewis acidity afforded by the bis(catecholato)- scaffold.

2.3 Conclusions

Herein, the synthesis of various bis(catecholato)germanes with weak donor ligands are reported. The Lewis acidity of the bis(catecholato)germanes was assessed experimentally by the Gutmann-Beckett method, as well as computationally by calculating the FIA and GEI values. Our results confirm that the Lewis acidity of the

germane derivatives is comparable to that of the previously reported bis(catecholato)silanes, and as such, are promising catalysts for organic transformations.

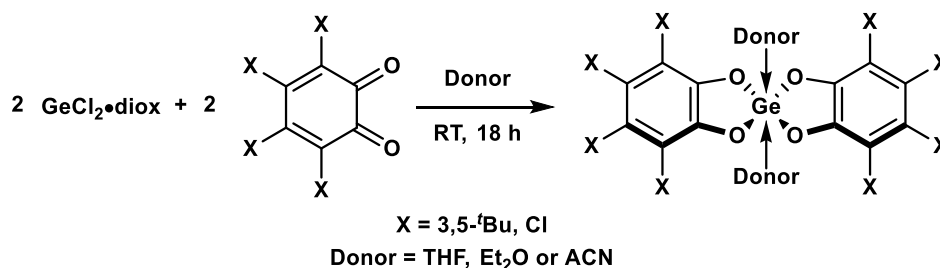
2.4 Experimental

2.4.1 General Experimental

All reactions were conducted under a nitrogen atmosphere using an MBraun Labmaster 130 glovebox. Solvents and reagents were purified by standard methods. $\text{GeCl}_2 \cdot \text{diox}$ (Gelest), tetrabromocatechol (Sigma-Aldrich), tetrachlorocatechol (Sigma-Aldrich), *ortho*-tetrachloroquinone (Fisher), and 3,5-di-*tert*-butylquinone (Fisher) were obtained from commercial sources. NMR data were obtained on a 600 MHz INOVA, 400 MHz INOVA or a 400 MHz Bruker Avance III NMR spectrometer. The standards used were as follows: residual CHCl_3 (7.26 ppm), CH_2Cl_2 (5.32 ppm), toluene- d_7 (2.09 ppm) relative to TMS for ^1H NMR spectra; CDCl_3 (77.16 ppm) for ^{13}C NMR spectra; J values are reported in Hertz. ESI mass spectra were recorded on a Bruker microTOF II mass spectrometer with an electrospray interface in negative ion mode while EI mass spectra were recorded on a Thermo Scientific DFS (Double Focusing Sector) mass spectrometer (reported in mass-to-charge units, m/z). Elemental analyses were performed by the University of Western Ontario – Analytical Services using an Elementar Vario Isotope Cube CHNS Analyzer.

2.4.2 Synthesis of Bis(catecholato)germanes

2.4.2.1 Route A: Synthesis from $\text{GeCl}_2 \cdot \text{diox}$ and Quinone



A solution of quinone (2.50 mmol) dissolved in THF, Et_2O or ACN (3 mL) was added dropwise to a clear solution of $\text{GeCl}_2 \cdot \text{diox}$ (0.58g, 2.50 mmol) dissolved in the same solvent (3 mL). For the di-*tert*-butyl derivatives, the solution became pale

yellow during the course of the addition. After 18 h of stirring, the crude reaction mixture was dried *in vacuo*. The resulting white solid was triturated in hexanes and then dried. For the chlorinated derivatives, the reaction mixture turned orange and a pale peach solid precipitated from solution. The reaction mixture was allowed to stir overnight. The precipitate was separated by centrifugation and then dried *in vacuo*. The mother liquor was placed in the freezer overnight which resulted in the precipitation of more solid which was subsequently isolated by centrifugation and dried *in vacuo*.

$\text{Ge}(\text{dtbc})_2(\text{THF})_2$:²⁸ Yield = 87%; ^1H NMR (CDCl_3 , 400 MHz): δ 6.88 (br, 2 H), 6.75 (br, 2 H), 3.91-3.84 (m, 8 H), 1.96-1.89 (m, 8 H), 1.44 (br s, 18 H), 1.29 (s, 18 H); ^{13}C NMR (CDCl_3 , 100.61 MHz): δ 142.9, 141.9, 141.2, 135.5, 115.6, 110.3, 68.3, 35.0, 34.4, 31.7, 29.7, 25.7; EI-MS m/z 514.2123 (calcd for $\text{C}_{28}\text{H}_{40}^{74}\text{GeO}_4$, m/z 514.2139) (M-2THF).

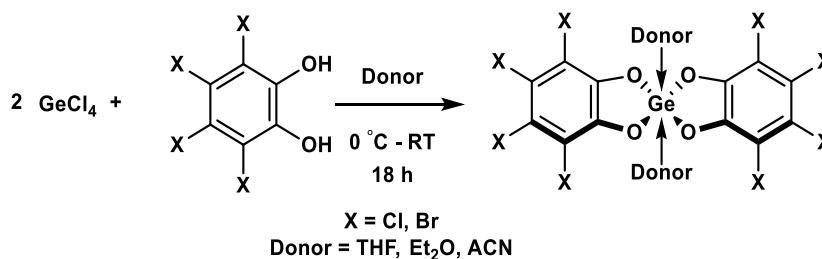
$\text{Ge}(\text{dtbc})_2(\text{ACN})_2$: Yield = 74%; ^1H NMR (CDCl_3 , 400 MHz): Product was too insoluble to obtain clean NMR data; EI-MS m/z 514.26 (calcd for $\text{C}_{28}\text{H}_{40}^{74}\text{GeO}_4$, m/z 514.2138) (M-2ACN).

$\text{Ge}(\text{cat}^{\text{Cl}})_2(\text{THF})_2$: Yield = 48%; EI-MS: m/z 557.6651 (calcd for $\text{C}_{12}^{35}\text{Cl}_8^{70}\text{GeO}_4$, m/z 557.6548) (M-2THF).

$\text{Ge}(\text{cat}^{\text{Cl}})_2(\text{Et}_2\text{O})_2$: Yield = 87%; EI-MS: m/z 557.6538 (calcd for $\text{C}_{12}^{35}\text{Cl}_8^{70}\text{GeO}_4$, m/z 557.6548) (M-2Et₂O).

$\text{Ge}(\text{cat}^{\text{Cl}})_2(\text{ACN})_2$:⁶ Yield = 88%. EA: calcd for $\text{C}_{16}\text{H}_6\text{Cl}_8\text{GeO}_4\text{N}_2$: 29.73% C, 0.94% H; found 29.70% C, %H was below the method reporting limit.

2.4.2.2 Route B: Synthesis from GeCl_4 and Catechol



A clear solution of GeCl_4 (0.1 g, 0.47 mmol) in THF, Et_2O or ACN (3 mL) was added dropwise to a suspension of either tetrachlorocatechol or tetrabromocatechol (0.94 mmol) in THF, Et_2O or ACN (3 mL) cooled to 0 °C (For the ACN derivative, 2 mL of DCM was also added to improve solubility of the catechol). After 30 minutes, the formation of white precipitate was observed, and the reaction mixture was warmed to room temperature and allowed to stir overnight. The precipitate was separated by centrifugation, triturated with DCM, and then dried *in vacuo*.

$\text{Ge}(\text{cat}^{\text{Br}})_2(\text{THF})_2$: Yield = 46%; EI-MS: m/z 919.25 (calcd for $\text{C}_{12}^{79}\text{Br}_3^{81}\text{Br}_5^{74}\text{GeO}_4$, m/z 919.2414) (M-2THF); EA: calcd for $\text{C}_{20}\text{H}_{16}\text{Br}_8\text{GeO}_6$: 22.57% C, 1.52% H; found 22.89 %C, %H was below the method reporting limit.

$\text{Ge}(\text{cat}^{\text{Br}})_2(\text{Et}_2\text{O})_2$: Yield = 11%; EI-MS: m/z 919.26 (calcd for $\text{C}_{12}^{79}\text{Br}_3^{81}\text{Br}_5^{74}\text{GeO}_4$, m/z 919.2414) (M-2 Et_2O).

$\text{Ge}(\text{cat}^{\text{Br}})_2(\text{ACN})_2$: Yield = 15%; EI-MS: m/z 919.25 (calcd for $\text{C}_{12}^{79}\text{Br}_3^{81}\text{Br}_5^{74}\text{GeO}_4$, m/z 919.2414) (M-2ACN); EA: calcd for $\text{C}_{14}\text{H}_3\text{Br}_8\text{GeO}_4\text{N}$ (M-ACN): 17.50% C, 0.31% H; found 17.51% C, %H was below the method detection limit.

2.4.3 Reactions of Bis(catecholato)germanes with Tetrabutylammonium Chloride

To a solution/suspension of the bis(catecholato)germane derivative (0.032 mmol) in THF (2 mL) was added a solution NBu_4Cl (0.009 g; 0.032 mmol) in THF (2 mL) dropwise and the reaction mixture was allowed to stir overnight. The resulting clear solution was dried *in vacuo* to yield the resulting bis(catecholato)germanium chloride salt.

$[\text{NBu}_4][\text{Ge}(\text{dtbc})_2\text{Cl}]$: Yield = 89%; ^1H NMR (CDCl_3 , 400 MHz): δ 6.77 (br, 2 H), 6.63 (br, 2 H), 2.92 (m, 8 H), 1.43 (s, 18 H), [1.22-1.37 (br), 1.25 (s), 34 H total] 0.87 (t, 12 H); ^{13}C NMR (CDCl_3 , 100.61 MHz): δ 147.66, 144.28, 138.83, 132.43, 112.14, 106.98, 58.37, 34.80, 34.48, 32.07, 29.81, 23.88, 19.60, 13.75. ESI-MS (negative ion) 549.1537 m/z (calcd for $\text{C}_{28}\text{H}_{40}^{35}\text{ClO}_4^{70}\text{Ge}$, $[\text{Ge}(\text{dtbc})_2\text{Cl}]^-$ m/z 549.1806).

[NBu₄][Ge(cat^{Cl})₂Cl]: Yield = >100%¹; ¹H NMR (CDCl₃, 400 MHz): δ 3.22 (br, 8 H), 1.66 (br, 8 H), 1.39 (br, 8 H) 0.95 (br t, 12 H); ESI-MS (negative ion) 592.6246 *m/z* (calcd for C₁₂O₄³⁵Cl₉⁷⁰Ge, (Ge(cat^{Cl})₂Cl⁻) *m/z* 592.6236).

[NBu₄][Ge(cat^{Br})₂Cl]: Yield = 73%¹; ¹H NMR (CDCl₃, 400 MHz): δ 3.26 (br, 8 H), 1.66 (br, 8 H), 1.34 (br, 8 H) 0.92 (t, 12 H); ESI-MS (negative ion) 954.2129 *m/z* (calcd for C₁₂O₄Br₈³⁵Cl₉⁷⁰Ge, (Ge(cat^{Br})₂Cl⁻) *m/z* 954.2089).

2.4.4 Reaction of Ge(dtbc)₂(THF)₂ with Pyridine

Pyridine (2 eq.) was added to a solution of Ge(dtbc)₂(THF)₂ dissolved in DCM. The reaction was allowed to stir overnight before the solution was dried *in vacuo*. The resulting solid was re-dissolved in CDCl₃ to record the ¹H NMR spectrum. The chemical shifts observed match those of the reported Ge(dtbc)₂(py)₂.⁷

2.4.5 Gutmann-Beckett Assessment of Lewis Acidity

To a suspension of bis(catecholato)germane in DCM (1 mg/mL) was added 1/3 equivalent of triethylphosphine oxide and the mixture was left to stir overnight. An aliquot of the reaction mixture was taken and a ³¹P{¹H} NMR spectrum was recorded

One equivalent of bis(catecholato)germane•2(THF) (20 mg/mL) and 0.5, 1, 2, and 3 eq. of triethylphosphine oxide were placed in CD₂Cl₂ (0.5 mL) in an NMR tube. A ³¹P{¹H} NMR spectrum of the mixture was immediately recorded. Signals assigned to the two equivalents of free THF, which originated from the starting bis(catecholato)germane, are omitted from the NMR assignments. Free triethylphosphine oxide was also observed upon addition of 2 or 3 equivalents (51 ppm).

Ge(3,5-dtbc)₂(OPEt₃): ³¹P{¹H} NMR (CH₂Cl₂, 162 MHz): δ 82.4; ¹H NMR (CDCl₃, 400 MHz): δ 6.88 (d, *J* = 2.3 Hz, 2 H), 6.70 (d, *J* = 2.3 Hz, 2 H) 1.93 (dq, *J* = 12.1 Hz, 7.7 Hz, 6 H), 1.43 (s, 18 H), 1.28 (s, 18 H), 1.04 (dt, *J* = 17.9 Hz, 7.7 Hz, 9 H); ¹³C

¹ THF is still evident (0.5 – 1 eq.) in the ¹H NMR spectra even after drying *in vacuo*: [NBu₄][Ge(cat^{Cl})₂Cl]: 0.6 eq of THF still remain; [NBu₄][Ge(cat^{Br})₂Cl]: 0.5 eq of THF still remain;

NMR (CDCl₃, 100.61 MHz)²: δ 147.7, 143.4, 141.2, 133.4, 113.0, 107.9, 35.1, 34.9, 32.1, 30.0, 18.2, 17.5, 5.4, 5.3; ESI-MS m/z 648.3 (calcd for C₃₄H₅₅⁷⁰GeO₅P: 648.2999).
 Ge(3,5-dtbc)₂(OPEt₃)₂: ³¹P{¹H} NMR (CH₂Cl₂, 162 MHz): δ 66.6 (-80 °C) ; ¹H NMR (CDCl₃, 400 MHz): δ 6.84 (d, J = 2.3 Hz, 2 H), 6.66 (d, J = 2.3 Hz, 2 H), 1.75 (dq, J = 12.2 Hz, 7.7 Hz, 12 H), 1.43 (s, 18 H), 1.28 (s, 18 H), 0.99 (dt, J = 17.5 Hz, 7.7 Hz, 18 H); ¹³C NMR (CDCl₃, 100.61 MHz)²: δ 148.1, 144.0, 140.5, 133.0, 112.5, 107.9, 35.1, 34.9, 32.1, 30.1, 19.0, 18.4, 5.7, 5.6; ESI-MS m/z 781.4 (calcd for C₄₀H₇₀⁷⁰GeO₆P₂ 782.3859).

trans-Ge(cat^{Cl})₂(OPEt₃)₂: ³¹P{¹H} NMR (CH₂Cl₂, 162 MHz): δ 70.5; ¹H NMR (CDCl₃, 400 MHz): δ 1.65 (dq, J = 11.7 Hz, 7.7 Hz, 12 H), 0.87 (dt, J = 17.8 Hz, 7.7 Hz, 18 H).

cis-Ge(cat^{Cl})₂(OPEt₃)₂: ³¹P{¹H} NMR (CH₂Cl₂, 162 MHz): δ 75.0; ¹H NMR (CDCl₃, 400 MHz): δ 1.96-2.10 and 2.10-2.24 (each m, 12 H total), 1.13 (dt, J = 16.3 Hz, 7.7 Hz, 18 H).

trans-Ge(cat^{Br})₂(OPEt₃)₂: ³¹P{¹H} NMR (CH₂Cl₂, 162 MHz): δ 75.1; ¹H NMR (CDCl₃, 400 MHz): δ 1.65 (dq, J = 11.7 Hz, 7.8 Hz, 12 H), 0.87 (dt, J = 17.9 Hz, 7.7 Hz, 18 H).

cis-Ge(cat^{Br})₂(OPEt₃)₂: ³¹P{¹H} NMR (CH₂Cl₂, 162 MHz): δ 75.8; ¹H NMR (CDCl₃, 400 MHz): δ 1.98-2.12 and 2.12-2.26 (each m, 12 H total), 1.11 (dt, J = 15.7 Hz, 7.7 Hz, 18 H).

2.4.6 Computational Details for FIA and GEI Calculations

All calculations (except G3/G4) have been performed with ORCA 4.1.2 and ORCA 4.2. Geometry optimizations were performed with PBEh-3c/def2-mSVP as implemented in ORCA, using grid5 settings. All calculated geometries have been confirmed as energetic minima on the potential energy surface by analytical calculation of harmonic frequencies at the PBEh-3c level. In case of negative frequencies >10 cm⁻¹, the geometries were reoptimized with grid6, TightOPT and VeryTightSCF settings. For

² Signals for the quaternary carbons were not observed

the fluoride ion affinities, the optimized geometries were then used to calculate the single point energies at B3LYP D3(BJ)/def2-TZVPP level of theory using the RIJCOSX approximation and def2/J as the auxiliary basis set. For the reaction coordinate calculations, the optimized geometries were used to calculate the thermodynamic values at BP86 D3(BJ)/def2-SVP level of theory using the RIJCOSX approximation and def2/J as the auxiliary basis set.

2.4.7 X-Ray Crystallography Details

The samples were mounted on a Mitegen polyimide micromount with a small amount of Paratone N oil. All X-ray measurements were made on a Bruker Kappa Axis Apex2 diffractometer at a temperature of 110 K. The unit cell dimensions were determined from a symmetry-constrained fit of 9916 reflections with $5.46^\circ < 2\theta < 63.72^\circ$. The data collection strategy was a number of ω and ϕ scans which collected data up to 67.682° (2θ). The frame integration was performed using SAINT.²⁹ The resulting raw data were scaled and absorption corrected using a multi-scan averaging of symmetry equivalent data using SADABS.³⁰

The structures were solved by using a dual space methodology using the SHELXT program.³¹ All non-hydrogen atoms were obtained from the initial solution. The hydrogen atoms were introduced at idealized positions and were allowed to ride on the parent atom. The structural models were fit to the data using full matrix least-squares based on F^2 . The calculated structure factors included corrections for anomalous dispersion from the usual tabulation. The structures were refined using the SHELXL program from the SHELX suite of crystallographic software.³² Graphic plots were produced using the Mercury program suite.³³

Late in the refinement of the $\text{Ge}(\text{dtbc})_2(\text{THF})_2$ crystal, there was a large peak ($2.68 e^-/\text{\AA}^3$) approximately 1.54\AA from C6. It was possible to refine this peak as a partially occupied (20%) carbon. However, it is not clear that this is truly peak of chemical significance. The difference maps did not show additional peaks corresponding to a *t*-butyl group, and the NMR and MS data indicate that the structure of this compound is

consistent with our proposed structure. In addition, the NMR data does not show evidence for the presence of a second compound.

References

1. a) Zuckerman, J. J. *J. Chem. Soc.*, **1962**, 165, 873–876. b) Allcock, H. R.; Nugent, T. A.; Smeltz, L. A. *Synth. React. Inorg. Met. Org. Chem.* **1972**, 2, 97–104.
2. Yoder, C. M. S.; Zuckerman, J. J. *Inorganic Chemistry* **1967**, 6, 163-164.
3. Liberman-Martin, A. L.; Bergman, R. G.; Tilley, T. D. *J. Am. Chem. Soc.* **2015**, 137, 5328-5331.
4. Maskey, R.; Schädler, M.; Legler, C.; Greb, L. *Angew. Chem. Int. Ed.* **2018**, 57, 1717-1720.
5. Hartmann, D.; Schädler, M.; Greb, L. *Chem. Sci.* **2019**, 10, 7379-7388.
6. Roth, D.; Wadepohl, H.; Greb, L. *Angew. Chem. Int. Ed.* **2020**, 59, 20930-20934.
7. Glavinović, M.; Krause, M.; Yang, L.; McLeod, J. A.; Liu, L.; Baines, K. M.; Friščić, T.; Lumb, J. P. *Sci. Adv.* **2017**, 3, e1700149-1-e1700149-8.
8. Lado, A. V.; Piskunov, A. V.; Zhdanovich, I. V.; Fukin, G. K.; Baranov, E. V. *Russ. J. Coord. Chem.* **2008**, 34, 251-255.
9. Gaffen, J. *Chem* **2019**, 5, 1355-1356.
10. a) Gutmann, V. *Coord. Chem. Rev.* **1976**, 18, 225-255; b) Mayer, U.; Gutmann, V.; Gerger, W. *Monatsh. Chem.* **1975**, 106, 1235-1257.
11. Childs, R. F.; Mulholland, D. L.; Nixon, A. *Can. J. Chem.* **1982**, 60, 801-808.
12. Hilt, G.; Nödling, A. *Eur. J. Org. Chem.* **2011**, 7071-7075.
13. Künzler, S.; Rathjen, S.; Merk, A.; Schmidtman, M.; Müller, T. *Chem. Eur. J.* **2019**, 25, 15123-15130.

14. Gaffen, J. R.; Bentley, J. N.; Torres, L. C.; Chu, C.; Baumgartner, T.; Caputo, C. B. *Chem.* **2019**, *5*, 1567-1583.
15. Mallouk, T. E.; Rosenthal, G. L.; Mueller, G.; Brusasco, R.; Bartlett, N. *Inorg. Chem.* **1984**, *23*, 3167-3173.
16. Vianello, R.; Maksić, Z. B. *Inorg. Chem.* **2005**, *44*, 1095-1102.
17. Poutsma, J. C.; Schroeder, O. E.; Squires, R. R. *Chem. Phys. Lett.* **2004**, *389*, 433-437.
18. Timoshkin, A. Y.; Frenking, G. *Organometallics* **2008**, *27*, 371-380.
19. Erdmann, P.; Greb, L. *ChemPhysChem* **2021**, *22*, 935-943.
20. Timoshkin, A. Y.; Suvorov, A. V.; Bettinger, H. F.; Schaefer, H. F. *J. Am. Chem. Soc.* **1999**, *121*, 5687-5699.
21. a) Jupp, A. R.; Johnstone, T. C.; Stephan, D. W. *Dalton Trans.* **2018**, *47*, 7029-7035; b) Jupp, A. R.; Johnstone, T. C.; Stephan, D. W. *Inorg. Chem.* **2018**, *57*, 14764-14771.
22. Bohrer, H.; Trapp, N.; Himmel, D.; Schleep, M.; Krossing, I. *Dalton Trans.* **2015**, *44*, 7489-7499.
23. Beckett, M. A.; Brassington, D. S.; Coles, S. J.; Hursthouse, M. B. *Inorg. Chem. Comm.* **2000**, *3*, 530-533.
24. Beckett, M. A.; Strickland, G. C.; Holland, J. R.; Varma, K. S. *Polymer* **1996**, *37*, 4629-4631.
25. a) Haartz, J. C.; McDaniel, D. H. *J. Am. Chem. Soc.* **1973**, *95*, 8562– 8565. b) Altshuller, A. P. *J. Am. Chem. Soc.* **1955**, *77*, 6187 – 6188.
26. Erdmann, P.; Leitner, J.; Schwarz, J.; Greb, L. *ChemPhysChem* **2020**, *21*, 987-994.

27. a) Becke, A. D. *J. Chem. Phys.* **1993**, *98*, 5648-5652; b) Grimme, S.; Antony, J.; Ehrlich, S.; Krieg, H. *J. Chem. Phys.* **2010**, *132*, 154104; c) Grimme, S.; Ehrlich, S.; Goerigk, L. *J. Comput. Chem.* **2011**, *32*, 1456-1465; d) Johnson, E. R.; Becke, A. D. *J. Chem. Phys.* **2005**, *123*, 024101; e) Becke, A. D.; Johnson, E. R. *J. Chem. Phys.* **2005**, *122*, 154101; f) Schafer, A.; Huber, C.; Ahlrichs, R. *J. Chem. Phys.* **1994**, *100*, 5829-5835; g) Grimme, S.; Brandenburg, J. G.; Bannwarth, C.; Hansen, A. *J. Chem. Phys.* **2015**, *143*, 054107; h) Cavasin, A. T.; Hillisch, A.; Uellendahl, F.; Schneckener, S.; Göller, A. H. *J. Chem. Inf. Model.* **2018**, *58*, 1005–1020.
28. The synthesis of $\text{Ge}(\text{dtbc})_2(\text{THF})_2$ was previously reported; however, no characterization data were given: Nikolaevskaya, E. N.; Saverina, E. A.; Starikova, A. A.; Farhati, A.; Kiskin, M. A.; Syroeshkin, M. A.; Egorov, M. P.; Jouikov, V. V. *Dalton Trans.* **2018**, *47*, 17127-17133.
29. Bruker-AXS, SAINT version 2013.8, 2013, Bruker-AXS, Madison, WI 53711, USA.
30. Bruker-AXS, SADABS version 2012.1, 2012, Bruker-AXS, Madison, WI 53711, USA.
31. Sheldrick, G. M. *Acta Cryst* **2015**, *A71*, 3-8.
32. Sheldrick, G. M. *Acta Cryst* **2015**, *C71*, 3-8.
33. Macrae, C. F.; Bruno, I. J.; Chisholm, J. A.; Edington, P. R.; McCabe, P.; Pidcock, P.; Rodriguez-Monge, L.; Taylor, R.; van de Streek, J.; Wood, P. A. *J. Appl. Cryst.* **2008**, *41*, 466-470.

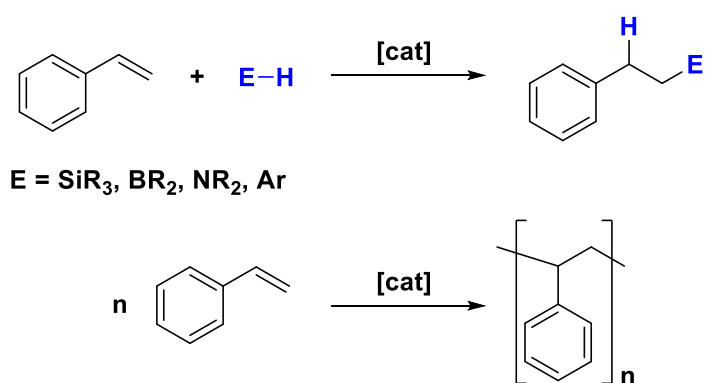
Chapter 3

3 The Lewis Acid Catalytic Applications of Bis(catecholato)germanes

3.1 Introduction

3.1.1 Lewis Acid Catalysis of Addition Reactions

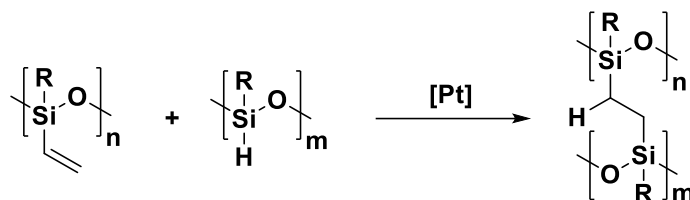
The reliance of industrial processes on catalysis presents an ever-growing need for efficient, cheap catalysts, as alternatives to second and third row transition metal-based catalysts, which are ubiquitous in state-of-the-art catalysis. As such, catalysts based on cheap and, often, non-toxic main group elements show much promise as alternatives to transition metal catalysts. Main group complexes often exhibit Lewis acidic behaviour, the ability to accept electron density from substrates, making them excellent candidates to act as Lewis acid catalysts. Addition reactions across molecules containing units of unsaturation, such as carbonyl, alkenyl, and alkynyl moieties and the oligomerization of alkenes are reactions which are typically catalyzed by Brønsted or Lewis acid catalysts (Scheme 3.1). The reactivity of bis(catecholato)germane complexes as Lewis acid catalysts in the hydrosilylation, hydroboration, hydroamination, and Friedel-Crafts alkylation of alkenes, and the oligomerization of alkenes will be explored in this chapter.



Scheme 3.1: Generalized addition reactions to a representative alkene.

3.1.1.1 Hydrosilylation

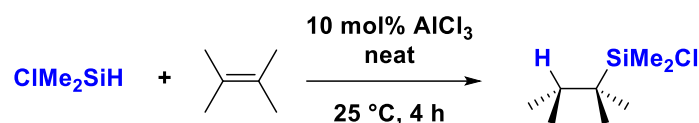
Hydrosilylation, the addition of a Si-H bond across a unit of unsaturation, is a well-known methodology for the formation of organosilicon compounds. The polysiloxane industry relies heavily on the hydrosilylation reaction. Polysiloxanes are important polymers as they are relatively inert and have favourable electrical and thermal properties attributed to the high Si-O bond strength and the flexibility of the O-Si-O linkage. A method to increase the rigidity of polysiloxanes, that is to convert polysiloxane oils into rubber, is to crosslink the polysiloxane chains, typically, by the reaction of a polysiloxane which features Si-H bonds with another polysiloxane which features a pendant alkene unit (Scheme 3.2). The hydrosilylation is catalyzed by a platinum-based catalyst, typically Speier's (H_2PtCl_6) or Karstedt's ($\text{Pt}_2(\text{HC}=\text{CHSiMe}_2\text{-O-SiMe}_2\text{CH}=\text{CH}_2)_3$) catalysts.¹



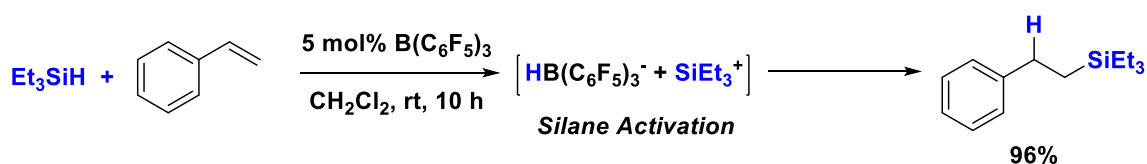
Scheme 3.2: An example of polysiloxane crosslinking

Hydrosilylation reactions can also be catalyzed by simple Lewis acids such as AlCl_3 . A variety of tetrasubstituted olefins were reacted with dialkylchlorosilanes under mild conditions (Scheme 3.3).² The resulting products were isolated by distillation in moderate yields (50-93%). The mechanism is proposed to involve the coordination of the alkene π -bond to the Lewis acid catalyst. Halogenated arylboranes, for example, $\text{B}(\text{C}_6\text{F}_5)_3$, have also been shown to be effective Lewis acid catalysts for the hydrosilylation of alkenes. $\text{B}(\text{C}_6\text{F}_5)_3$ catalyzes the hydrosilylation of various alkenes at 5 mol% catalyst loading under ambient conditions in 10-12 hours resulting in high conversions for most substrates (>90%) (Scheme 3.4).³ While traditional Lewis acid catalysts typically proceed through an alkene activation mechanism, the fluorinated arylborane activates the H-Si bond. As such, the bulky triisopropylsilane was not tolerated using the borane catalyst. An example of a Group 14 catalyst that catalyzes the

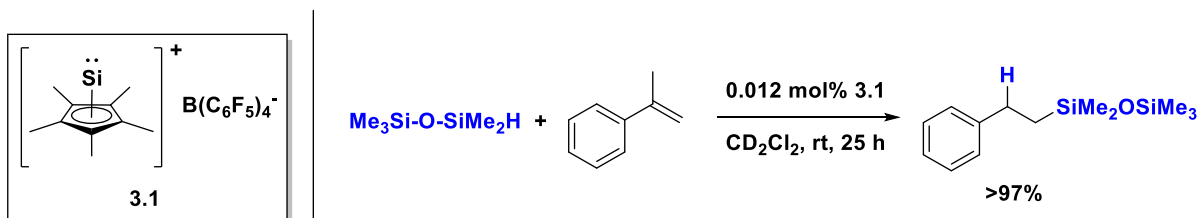
hydrosilylation reaction is illustrated with the silicon(II) cation **3.1**.⁴ The silyliumylidene cation **3.1** catalyzes the hydrosilylation of α -methylstyrene using pentamethyldisiloxane quantitatively under mild conditions with only a 0.012 mol% catalyst loading (Scheme 3.5). Catalyst loadings of this magnitude are rare for main group catalysts and are comparable to the high performance of state-of-the-art transition metal-based catalysts. The silyliumylidene cation **3.1** catalyzes the reaction of a wide scope of silanes and siloxanes. The proposed mechanism features Si-H bond activation, similar to the mechanism of activation of $B(C_6F_5)_3$. These main group catalysts, however, are not without their disadvantages. $AlCl_3$, while a commonly used Lewis acid catalyst, is reactive and hydrolyzes easily. $B(C_6F_5)_3$ is a sterically bulky Lewis acid that does not efficiently catalyze reactions involving bulky substrates. **3.1** is a highly efficient catalyst in hydrosilylation but requires a multi-step synthesis and is air- and moisture-sensitive.



Scheme 3.3: Hydrosilylation of a tetrasubstituted alkene using $AlCl_3$ as a Lewis acid catalyst.



Scheme 3.4: Hydrosilylation of alkenes using $B(C_6F_5)_3$ as the catalyst.

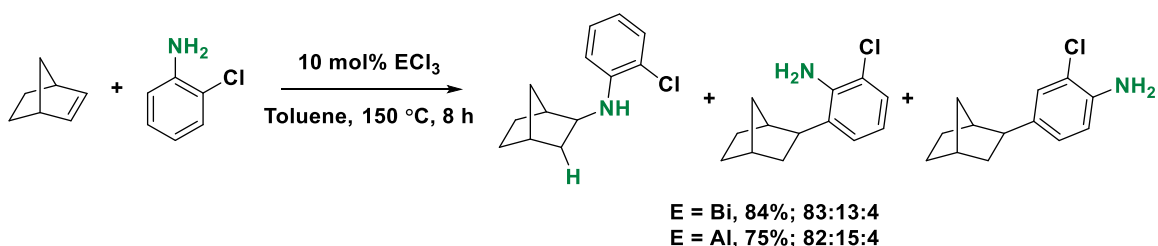


Scheme 3.5: Silicon cation **3.1** facilitates the hydrosilylation of alkenes at low catalyst loadings.

3.1.1.2 Hydroamination

The functionalization of amines is critical for the pharmaceutical and agricultural industries. In fact, three of the top ten pharmaceuticals that generate the highest revenue in the pharmaceutical industry contain functionalized amines.⁵ Hydroamination reactions are typically catalyzed by transition metals, as well as the alkali and alkali earth metals. In the search for alternative catalysts, main group catalysts as Lewis bases, Brønsted acids, and radicals have been explored extensively.⁶ However, the use of main group Lewis acid catalysts for hydroamination are less explored.

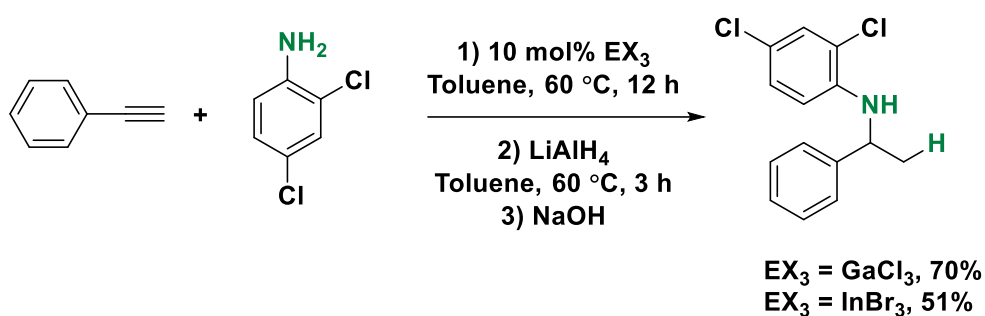
Many of the initial reports of Lewis acid catalyzed hydroaminations utilized simple Lewis acids. For example, AlCl_3 and BiCl_3 catalyze the hydroamination of norbornene using electron-deficient anilines (Scheme 3.6).⁷ Notably, BiCl_3 had higher yields in comparison to AlCl_3 , and selectivity for the hydroamination product, over the Friedel-Crafts alkylated products, was high for both catalysts. An amine activation mechanism was proposed, in which the Lewis acid coordinates to the amine enhancing the acidity of the amine proton to facilitate protonation of norbornene. The resulting carbocation of norbornene then reacts with another equivalent of amine to yield the desired product.



Scheme 3.6: Hydroamination of norbornene with an electron-deficient aniline catalyzed by main group halides.

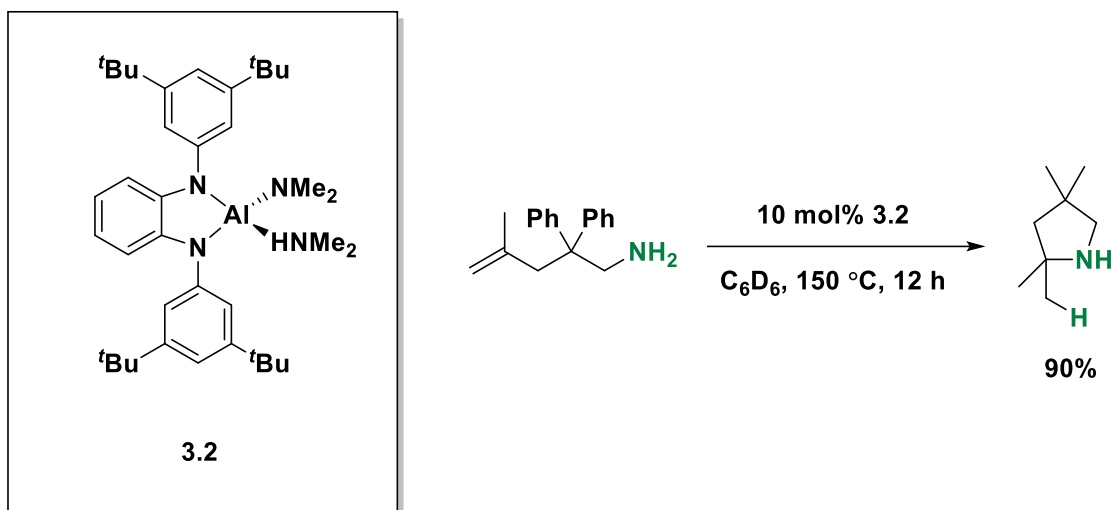
Gallium and indium halides have also been explored as Lewis acid catalysts in hydroamination reactions.⁸ GaCl_3 and InBr_3 were applied as catalysts for the hydroamination of alkynes (Scheme 3.7). Using an electron-deficient aniline and phenylacetylene, the corresponding amine was obtained after reduction of the initially

formed imine using LiAlH_4 . Notably, amines with strongly electron-withdrawing groups or electron donating groups have the highest conversions. Interestingly, the same reaction was not catalyzed by BiCl_3 or AlCl_3 that were efficient catalysts in the hydroamination of alkenes. DFT calculations supported the experimental observations and are consistent with an alkyne activation mechanism, where the Lewis acid coordinates to the alkyne allowing for nucleophilic attack of the amine. The electron-withdrawing groups on the anilines hamper the ability of the amine to coordinate to the Lewis acid preferentially over the alkyne.



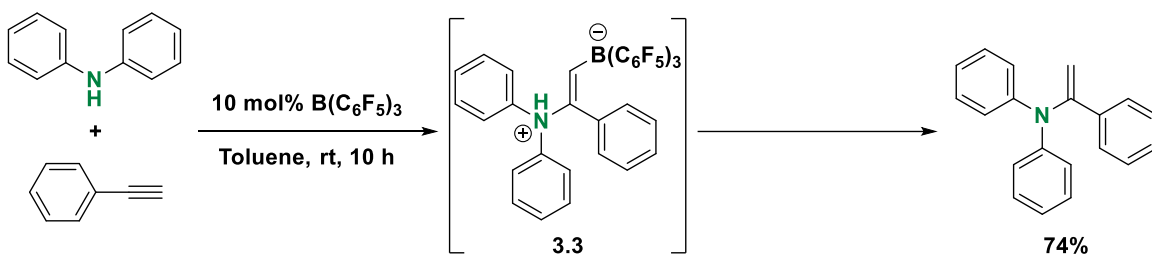
Scheme 3.7: Hydroamination of phenylacetylene with an electron-deficient aniline performed using main group halide Lewis acids.

Outside the use of halide substituents on the main group Lewis acid, only a few studies using more elaborate ligand frameworks have been reported. The aluminum-based Lewis acid **3.2** (Scheme 3.8), was shown to catalyze intramolecular hydroaminations; however, the substrate scope was limited, catalyst loadings were high and the synthesis of the catalyst was elaborate.⁹



Scheme 3.8: Intramolecular hydroamination using catalyst **3.2**

The fluorinated arylborane, $B(C_6F_5)_3$, which is an effective catalyst for hydrosilylation, has also been investigated as a hydroamination catalyst (Scheme 3.9).¹⁰ Unlike the simple halide-substituted Lewis acids, which react well with primary amines, $B(C_6F_5)_3$ requires a bulky secondary amine for significant conversion. The authors propose that the added bulk of the secondary amine prevents amine coordination to the boron centre disfavoring Lewis acid-base adduct formation. The borane coordinates the alkyne which prompts the addition of the Lewis basic amine forming zwitterion **3.3**. The acidic ammonium proton then migrates to the carbon adjacent to the boron and then release of the Lewis acid catalyst occurs.



Scheme 3.9: Hydroamination of alkynes using bulky amines catalyzed by $B(C_6F_5)_3$.

3.1.1.3 Hydroboration

Hydroboration, the addition of H-B bond across a unit of unsaturation, is often compared to hydrosilylation due to both being hydrofunctionalization reactions. However, whereas hydrosilylation can afford the desired commercial product directly or to prepare synthetic intermediates, hydroboration is typically only done to prepare synthetic intermediates. The organoborane intermediates are often converted directly to a variety of fine chemicals such as perfumes and pharmaceuticals without isolation.

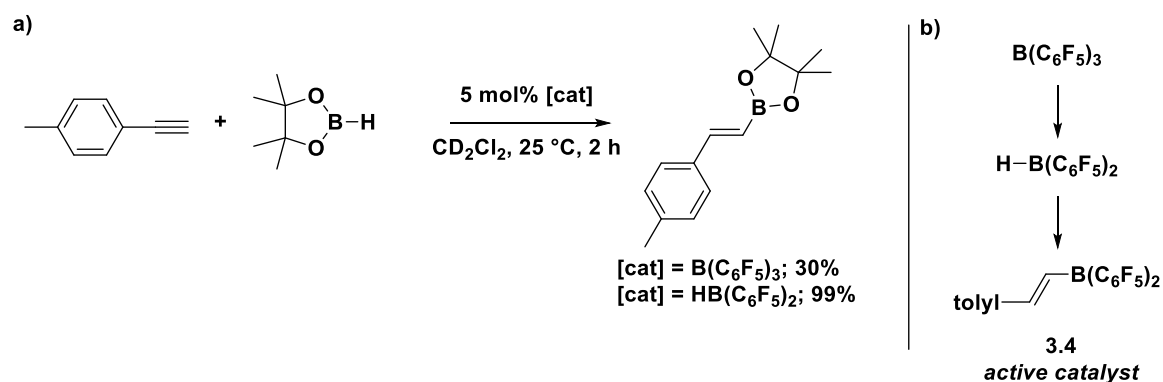
The use of catalysts in hydroboration is only required for the less reactive boranes. Borane reagents, such as BH_3 and 9-borabicyclo[3.3.1]nonane (9-BBN) do not require a catalyst and undergo hydroboration reactions exothermically. However, both the borane reagents and the resulting organoboranes are air-sensitive, and, in the case of BH_3 , can undergo hydroboration reaction with the remaining B-H bonds. Dialkoxy- and diaryloxyboranes, such as pinacolborane (HBpin) and catecholborane (HBcat), and the resulting hydroboration adducts derived from them have improved stability even allowing purification and separation by chromatography (Chart 3.1). However, the hydroboration reactions using these boranes are either very slow, even at high temperatures, or do not proceed at all unless a catalyst is used.



Chart 3.1: Pinacolborane (HBpin) and catecholborane (HBcat).

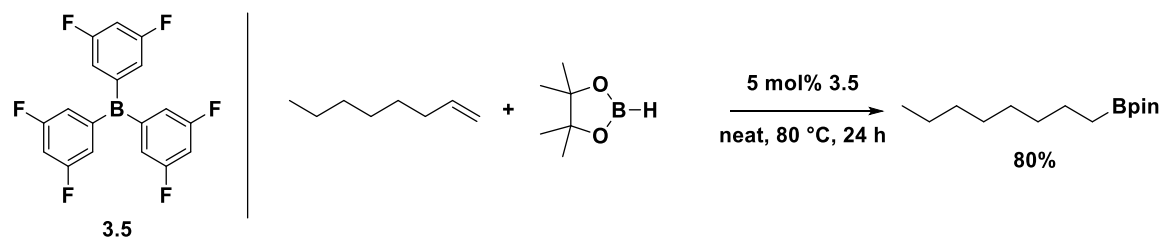
$\text{B}(\text{C}_6\text{F}_5)_3$ can be used to catalyze the hydroboration of alkynes using pinacolborane as the hydroboration substrate.¹¹ For example, the hydroboration of *para*-tolylacetylene proceeds quantitatively using 5 mol% of $\text{B}(\text{C}_6\text{F}_5)_3$ in dichloromethane (DCM) under ambient conditions in 15 hours (Scheme 3.10a). $\text{B}(\text{C}_6\text{F}_5)_3$ acts as a precatalyst, forming $\text{HB}(\text{C}_6\text{F}_5)_2$ in solution. When $\text{HB}(\text{C}_6\text{F}_5)_2$ was used as the catalyst, the same reaction proceeds in only 2 hours. It is proposed that the B-H bond of $\text{HB}(\text{C}_6\text{F}_5)_2$ adds across the alkyne bond of one equivalent of alkyne, generating **3.4**, the active

catalytic species (Scheme 3.10b), which then coordinates a second equivalent of alkyne which undergoes hydroboration and product release.



Scheme 3.10: a) Hydroboration of an alkyne using fluorinated aryl borane catalysts. b) The equilibrium between the catalysts and the active catalytic species.

Another fluorinated borane, tris[3,5-bis(trifluoromethyl)phenyl]borane, **3.5**, can also be used to catalyze the hydroboration of alkenes using pinacolborane.¹² For example **3.5** can catalyze the hydroboration of 1-octene using pinacolborane in an 80% yield (Scheme 3.11). Notably, substantial regioselectivity for the anti-Markovnikov product was observed. Numerous aryl- and alkyl-substituted alkenes were tolerated by **3.5**.

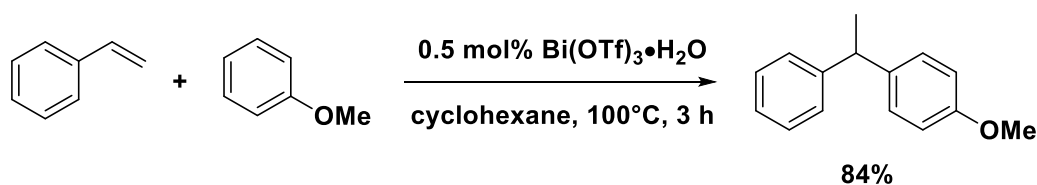


Scheme 3.11: Hydroboration of alkenes achieved using **3.5** as a Lewis acid catalyst.

3.1.1.4 Friedel-Crafts Alkylation using Alkenes

Since the 1800's, Friedel-Crafts alkylations are a key method for the alkylation of arenes. Typically, the reaction is performed using an aromatic compound and an alkyl halide in the presence of a Lewis acid. While Friedel-Crafts alkylations can be achieved using simple Lewis acid halides, such as AlCl_3 , $\text{BF}_3 \cdot \text{OEt}_2$, or SnCl_4 , the Lewis acid is typically used in stoichiometric amounts and results the formation of an equivalent of a salt. Another, more environmentally-friendly, approach is to utilize an alkene instead of a toxic alkyl halide. The reaction effectively adds an aryl C-H bond across a carbon-carbon double bond atom and eliminates the formation of side products. The Friedel-Crafts alkylation of alkenes typically utilizes a Brønsted acid catalyst.

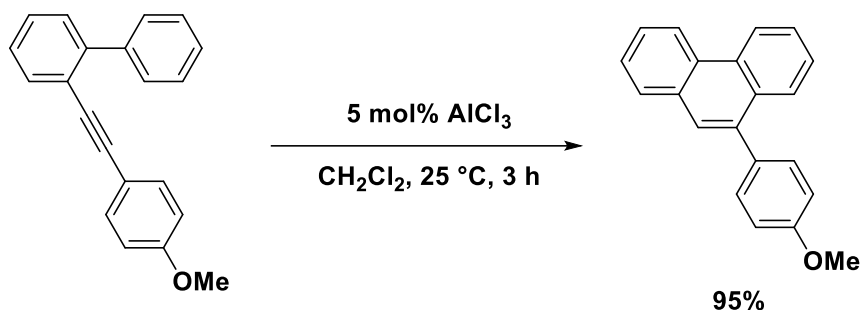
While main group Lewis acids have been utilized in Friedel-Crafts alkylations for decades, the use of main group Lewis acids in conjunction with alkenes was not observed until 2006 when $\text{Bi}(\text{OTf})_3$ was shown to catalyze the hydroarylation of anisole using styrene in high yields (Scheme 3.12).¹³ While the reaction requires high temperatures, the catalyst loading was only 0.5 mol%. A variety of different arenes and alkenes were tested, and the reaction favours the formation of the *para*-substituted product; however, minor amounts of the *ortho*-substituted product and, when styrene is utilized as the alkene, dimers of styrene were observed.



Scheme 3.12: Friedel-Crafts alkylation using $\text{Bi}(\text{OTf})_3$ as a Lewis acid catalyst.

The hydroarylation of alkynes can also be achieved using AlCl_3 as the Lewis acid catalyst (Scheme 3.13).¹⁴ The intramolecular hydroarylation of 2-[(4-methoxyphenyl)ethynyl]-1,1'-biphenyl was achieved under ambient conditions in only 3 hours using 5 mol% of AlCl_3 . These conditions are substantially milder than those used with $\text{Bi}(\text{OTf})_3$ as the catalyst. While the substrate scope included various derivatives of 2-

[(4-phenyl)ethynyl]-1,1'-biphenyl compounds, no example of intermolecular hydroarylation, as was achieved using $\text{Bi}(\text{OTf})_3$ as a catalyst, was reported in this work.

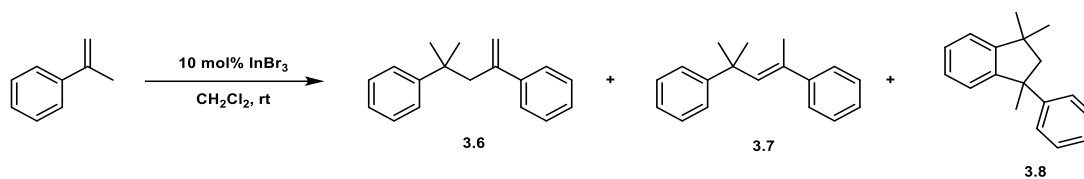


Scheme 3.13: Intramolecular Friedel-Crafts reaction using AlCl_3 as the catalyst.

3.1.2 Oligomerization of Alkenes

Plastics, synthesized by the polymerization of alkenes, have unique mechanical, chemical and electronic properties depending on the monomer used and the method by which it was formed. Several different compounds can be used to initiate polymerization including radical, cationic, and anionic initiators. Lewis acids can also be used to initiate cationic polymerization reactions. Sometimes, a Lewis base, such as water, is used as a co-initiator to stabilize the cationic species formed during the reaction.

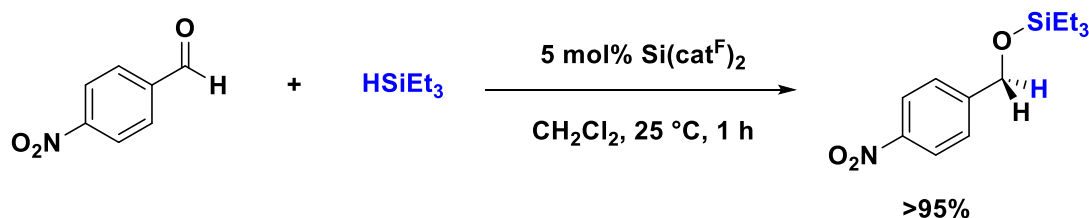
While main group Lewis acids are used as co-catalysts with transition metal Lewis acids, for example in Ziegler-Natta catalysis, the use of main group Lewis acids as catalysts to polymerize alkenes is less studied. However, their use in oligomerization reactions is known. For example, InBr_3 catalyzes the dimerization of α -methylstyrene derivatives to three different dimers **3.6**, **3.7**, and **3.8** (Scheme 3.14).¹⁵ By altering the reaction time, dimers **3.6** or **3.8** can be isolated in high yields after column chromatography. For example, after 2h, **3.6** is isolated in 90% yield, whereas after 4h, **3.8** is isolated in yield of 88%. The dimerization of substituted styrenes can also be achieved using 5 mol% of BiCl_3 .¹⁶ For example, the dimerization of α -methylstyrene was achieved at elevated temperatures yielding the cyclic dimer **3.8** selectively in 73% yield.



Scheme 3.14: Dimerization of α -methylstyrene achieved using InBr_3 .

3.1.3 Group 14 Bis(catecholato)- Catalysts

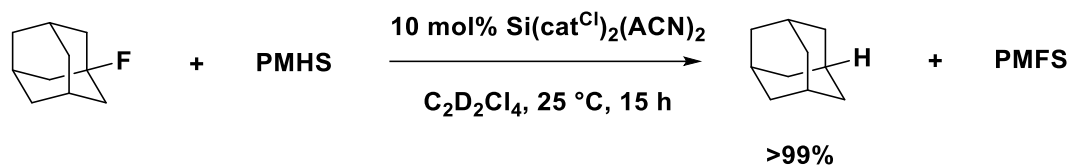
Group 14 bis(catecholato)silanes and -germanes exhibit high Lewis acidity which makes them prime candidates as catalysts. Tilley and coworkers reported the hydrosilylation of benzaldehyde derivatives using $\text{Si}(\text{cat}^{\text{F}})_2$ as the catalyst (Scheme 3.15).¹⁷ Using triethylsilane, $\text{Si}(\text{cat}^{\text{F}})_2$ quantitatively catalyzes the hydrosilylation of benzaldehydes with *para*-substituted electron-withdrawing substituents under mild conditions in an hour. Examination of the scope of benzaldehydes showed that electron-withdrawing substituents are required to achieve conversion values of greater than 70%. The silane substrate scope illustrated that sterically bulky silanes are tolerated, a feat not possible using $\text{B}(\text{C}_6\text{F}_5)_3$ as a catalyst. No evidence for complexation between stoichiometric amounts of triethylsilane and $\text{Si}(\text{cat}^{\text{F}})_2$ was observed by ^1H NMR spectroscopy which, in combination with reliance on the use of electron deficient-aldehydes, was consistent with the hydrosilylation occurring via aldehyde coordination and not a Si-H bond activation mechanism.



Scheme 3.15: Hydrosilylation of benzaldehyde derivatives using $\text{Si}(\text{cat}^{\text{F}})_2$ as the catalyst.

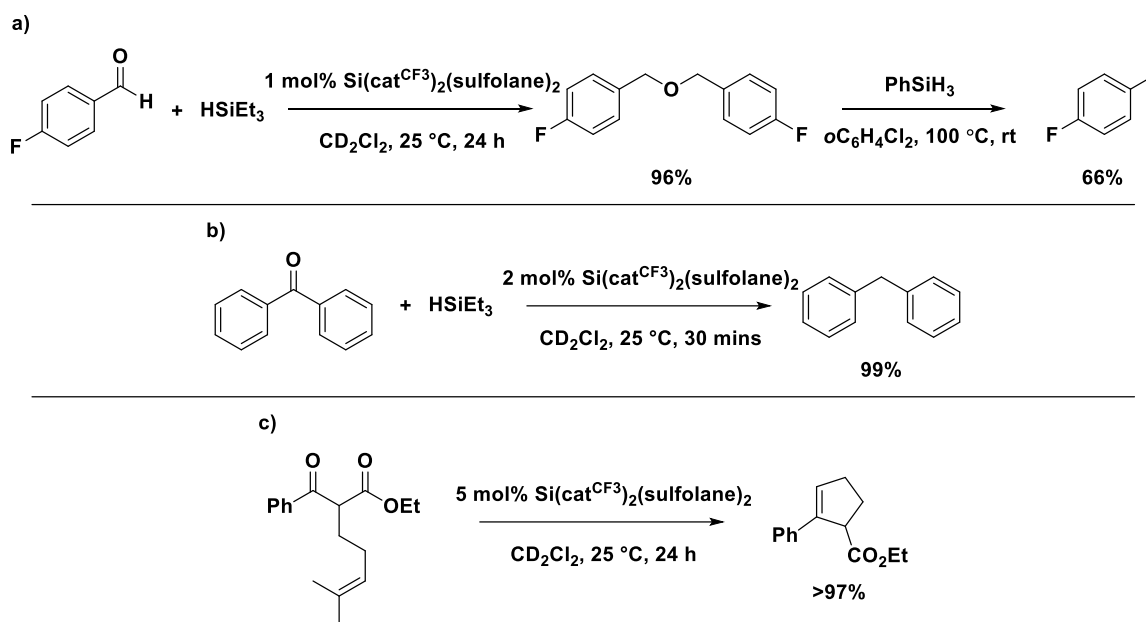
Greb and coworkers have synthesized and assessed the Lewis acidities of a variety of bis(catecholato)silanes and -germanes. The high fluoride ion affinity of $\text{Si}(\text{cat}^{\text{Cl}})_2(\text{ACN})_2$ inspired Greb and coworkers to explore the catalytic hydrodefluorination of 1-adamantyl fluoride with polymethylhydrodisiloxane (PMHS)

which proceeded cleanly and quantitatively with 10 mol% of $\text{Si}(\text{cat}^{\text{Cl}})_2(\text{ACN})_2$ (Scheme 3.16). $\text{Si}(\text{cat}^{\text{Br}})_2(\text{ACN})_2$, with a Lewis acidity greater than the chloride derivative, was not tested for catalytic activity.



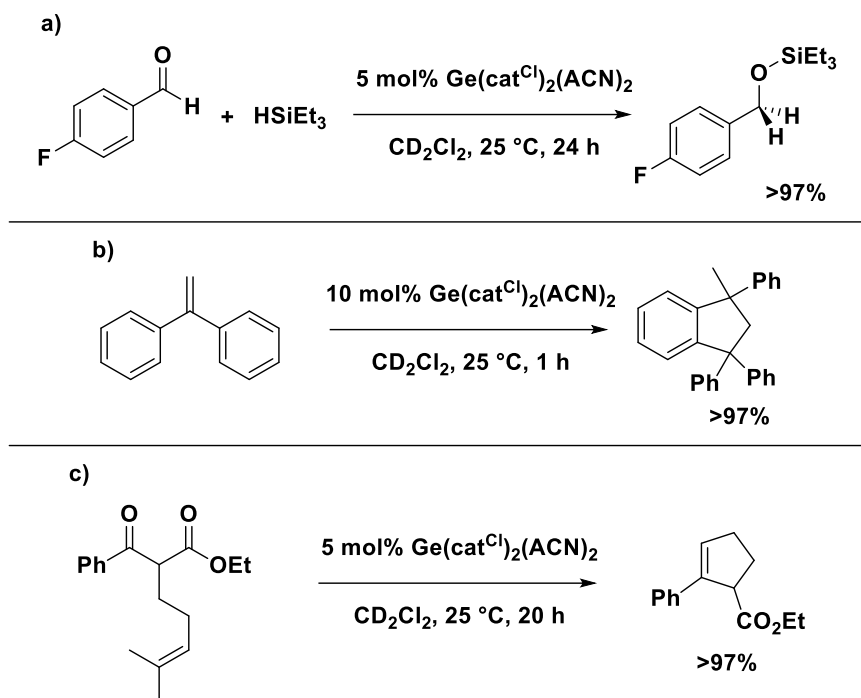
Scheme 3.16: Hydrodefluorination using $\text{Si}(\text{cat}^{\text{Cl}})_2(\text{ACN})_2$ as the catalyst yielding adamantane and polymethylfluorodisiloxane (PMFS)

$\text{Si}(\text{cat}^{\text{CF}_3})_2(\text{sulfolane})_2$ exhibits higher Lewis acidity than the analogous perhalogenated derivatives. $\text{Si}(\text{cat}^{\text{CF}_3})_2(\text{sulfolane})_2$ showed different catalytic reactivity than the simple halogenated congeners.¹⁸ For example, the hydrosilylation of aldehydes with triethylsilane catalyzed by $\text{Si}(\text{cat}^{\text{CF}_3})_2(\text{sulfolane})_2$ did not yield the same product as the $\text{Si}(\text{cat}^{\text{F}})_2$ catalyst. Rather than silyl ether formation, ether formation was observed (Scheme 3.17a). Subsequent deoxygenation was performed using phenylsilane. Catalytic deoxygenation of ketones and phosphine oxides was also carried out using $\text{Si}(\text{cat}^{\text{CF}_3})_2(\text{sulfolane})_2$ as a catalyst (Scheme 3.17b). The final reaction probed was a catalytic intramolecular carbonyl-olefin metathesis (Scheme 3.17c).



Scheme 3.17: Examples of the reactions catalyzed by $\text{Si}(\text{cat}^{\text{CF}_3})_2(\text{sulfolane})_2$

The catalytic activity of the bis(catecholato)germanes, $\text{Ge}(\text{cat}^{\text{Cl}})_2(\text{ACN})_2$ and $\text{Ge}(\text{cat}^{\text{Cl}})_2(\text{H}_2\text{O})_n$ (where $n = 4$ or 6), was also briefly explored.¹⁹ The hydrosilylation of aldehydes was achieved using $\text{Ge}(\text{cat}^{\text{Cl}})_2(\text{ACN})_2$ although the time required was significantly longer than that required when using $\text{Si}(\text{cat}^{\text{F}})_2$ as the catalyst (Scheme 3.18a). $\text{Ge}(\text{cat}^{\text{Cl}})_2(\text{ACN})_2$ also catalyzed the hydrodefluorination of 1-adamantyl fluoride similar to its silicon counterpart. The Friedel-Crafts alkylation of diphenylethylene was also accomplished using $\text{Ge}(\text{cat}^{\text{Cl}})_2(\text{ACN})_2$ as a catalyst (Scheme 3.18b). Using a hydrogen surrogate, such as 1,4-cyclohexadiene, the transfer hydrogenation of diphenylethylene can also be achieved. Intramolecular carbonyl-olefin metathesis can also be achieved with $\text{Ge}(\text{cat}^{\text{Cl}})_2(\text{ACN})_2$ (Scheme 3.18c).



Scheme 3.18: Examples of the reactions using $\text{Ge}(\text{cat}^{\text{Cl}})_2(\text{ACN})_2$ as the catalyst.

3.1.4 Project Goal

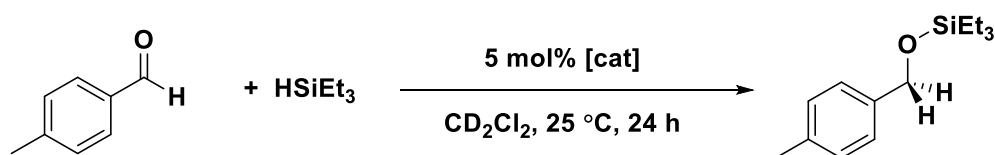
While the bis(catecholato)silanes and germanes have been shown to catalyze a variety of different reactions, studies into the mechanism of how the bis(catecholato)-species operate still remains to be explored. The study of the catalytic activity of $\text{Si}(\text{cat}^{\text{F}})_2$ was only preliminary as a moderate substrate scope of benzaldehydes and silanes for hydrosilylation was examined, and only a few experiments aimed at elucidating which species is activated along the reaction pathway were performed. The reports on the catalytic activity of $\text{Si}(\text{cat}^{\text{Cl}})_2(\text{ACN})_2$, $\text{Si}(\text{cat}^{\text{CF}_3})_2(\text{sulfolane})_2$, and $\text{Ge}(\text{cat}^{\text{Cl}})_2(\text{ACN})_2$ were limited to small substrate scopes and little insight into the mechanism of catalysis was provided. As such, the goal of this project is to explore the use of bis(catecholato)germanes as catalysts in depth, utilizing a series of bis(catecholato)germane derivatives as catalysts for hydrosilylation, hydroboration, hydroamination, Friedel-Crafts alkylation, and alkene oligomerization reactions. Reaction optimization and substrate scope will be explored in this chapter and mechanistic studies are presented in Chapter 4.

3.2 Results and Discussion

3.2.1 Hydrosilylation of Aldehydes/Ketones

With the successful hydrosilylation of benzaldehyde derivatives by $\text{Si}(\text{cat}^{\text{F}})_2$, this reaction was chosen to be explored first in the use of bis(catecholato)germanes as Lewis acid catalysts. Starting with the conditions utilized by Tilley *et al.* for $\text{Si}(\text{cat}^{\text{F}})_2$ to allow for a direct comparison of performance, a test of the different bis(catecholato)germanes were performed to determine the most effective catalyst under these reaction conditions (Table 3.1).

Table 3.1: Catalyst scope of various bis(catecholato)germane catalysts.



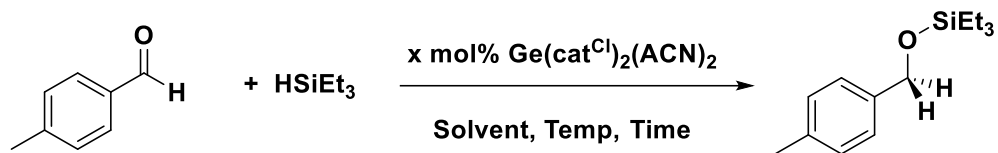
Entry	Catalyst	Conversion (%) ^a
1	$\text{Ge}(\text{cat}^{\text{Br}})_2(\text{THF})_2$	62
2	$\text{Ge}(\text{cat}^{\text{Br}})_2(\text{ACN})_2$	26
3	$\text{Ge}(\text{cat}^{\text{Cl}})_2(\text{THF})_2$	70
4	$\text{Ge}(\text{cat}^{\text{Cl}})_2(\text{ACN})_2$	84
5	$\text{Ge}(\text{dtbc})_2(\text{THF})_2$	<5
6	$\text{Ge}(\text{dtbc})_2(\text{ACN})_2$	<5

a) Conversion values were determined by the difference in ^1H NMR integration value of the aldehydic hydrogen relative to mesitylene, 1/9 eq., as an internal standard. Conversion values were the average of two runs. 0.01 mmol of catalyst used in 0.5 mL of solvent.

In the case of the halogenated derivatives (Table 3.1, Entries 1-4), moderate conversions were observed for all except $\text{Ge}(\text{cat}^{\text{Br}})_2(\text{ACN})_2$ (Table 3.1, Entry 2). Interestingly, this catalyst has the highest Lewis acidity as determined by FIA values of the bis(catecholato)germanes. The increased Lewis acidity of $\text{Ge}(\text{cat}^{\text{Br}})_2(\text{ACN})_2$ may

hamper catalytic activity by making release of the product from the catalyst more difficult. Of the other catalysts, $\text{Ge}(\text{cat}^{\text{Cl}})_2(\text{ACN})_2$ performed the best achieving 84% conversion after 24 hours (Table 3.1, Entry 4). The less Lewis acidic and more sterically bulky 3,5-di-tert-butylcatecholato derivatives resulted in little to no catalysis (Table 3.1, Entries 5,6).

To explore the conditions necessary for catalysis the hydrosilylation of *para*-tolualdehyde, which features two cleanly separated aromatic signals and a diagnostic methyl signal in the ^1H NMR spectrum, was selected as the test substrate. The silane agent selected was triethylsilane as it is the most utilized silane in hydrosilylation literature (Table 3.2). The conditions used in Table 3.2, Entry 1 are similar to those employed by Tilley and coworkers in the hydrosilylation of *para*-nitrobenzaldehyde with $\text{Si}(\text{cat}^{\text{F}})_2$. Increasing the catalyst loading to 10 mol% (Table 3.2, Entry 2) resulted in a slight decrease in conversion, while lowering the catalyst loading to 1 mol% (Table 3.2, Entry 3) resulted in a more significant decrease in conversion. The insolubility of the catalyst lead to some solid catalyst remaining undissolved in the reaction vessel, even at 1 mol%. As such, it is unsurprising that the increase from 5 to 10 mol% in catalyst loading doesn't lead to a significant increase in conversion. When the solvent was altered (Table 3.2, Entries 4-7), it was observed that non-polar solvents (toluene- d_8 , CDCl_3 , and C_6D_6) as well as donor solvents ($\text{ACN}-d_3$) halt any catalytic activity, even at elevated temperatures (Table 3.2, Entry 10). Decreasing the concentration of the reagents (Table 3.2, Entry 8) by doubling the amount of solvent resulted in a slight decrease in conversion. After 8 hours (Table 3.2, Entry 9), 66% conversion was observed suggesting most of the reaction is completed in the first 8 hours. After examination of a variety of reaction conditions, those listed in Table 3.2, Entry 1 were the most optimal and were used in further reactions.

Table 3.2: Optimization of the hydrosilylation of *para*-tolualdehyde with triethylsilane

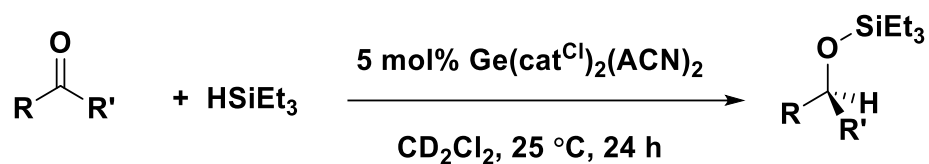
Entry	Catalyst Loading (mol%)	Solvent	Substrate Concentration	Time (h)	Temperature (°C)	Conversion (%) ^a
1	5	CD ₂ Cl ₂	0.4 M	24	rt	84
2	10	CD ₂ Cl ₂	0.4 M	24	rt	76
3	1	CD ₂ Cl ₂	0.4 M	24	rt	62
4	5	Toluene- <i>d</i> ₈	0.4 M	24	rt	<5
5	5	ACN- <i>d</i> ₃	0.4 M	24	rt	<5
6	5	CDCl ₃	0.4 M	24	rt	40
7	5	C ₆ D ₆	0.4 M	24	rt	<5
8	5	CD ₂ Cl ₂	0.2 M	24	rt	72
9	5	CD ₂ Cl ₂	0.4 M	8	rt	66
10	5	Toluene- <i>d</i> ₈	0.4 M	24	100	<5

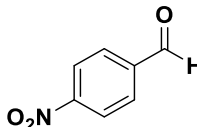
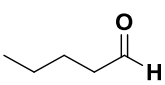
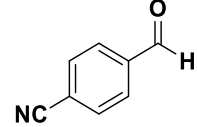
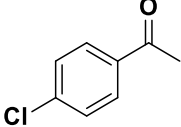
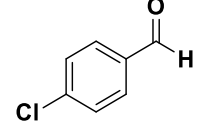
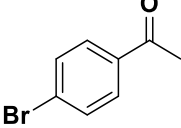
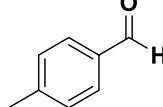
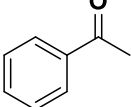
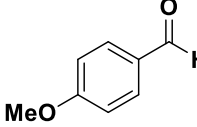
a) Conversion values were determined by the difference in ¹H NMR integration of the aldehyde proton relative to mesitylene, 1/9 eq., as an internal standard. Conversion values were the average of two runs. Entry 1 is similar conditions to that studied by Tilley with Si(cat^F)₂. Further shading in the table shows deviations in conditions from the conditions in Entry 1.

The hydrosilylation of a variety of carbonyl compounds with triethylsilane was examined (Table 3.3). Ge(cat^{Cl})₂(ACN)₂ was chosen as the catalyst since it exhibited the best catalytic performance with *para*-tolualdehyde. *Para*-substituted benzaldehydes with electron-withdrawing substituents were converted quantitatively (Table 3.3, Entries 1-3). When substituted with the electron-donating methoxy group, conversion was minimal (Table 3.3, Entries 4-5). This observation, that electron-withdrawing substituents on

benzaldehydes yield greater conversions, is similar to that reported by Tilley for the $\text{Si}(\text{cat}^{\text{F}})_2$ catalyst.¹⁷ The alkyl-substituted aldehyde was hydrosilylated quantitatively (Table 3.3, Entry 6); however, attempts to hydrosilylate aromatic ketones were unsuccessful (Table 3.3, Entries 7-9).

Table 3.3: Aldehyde/Ketone Substrate Scope for Hydrosilylation using bis(catecholato)germane catalyst



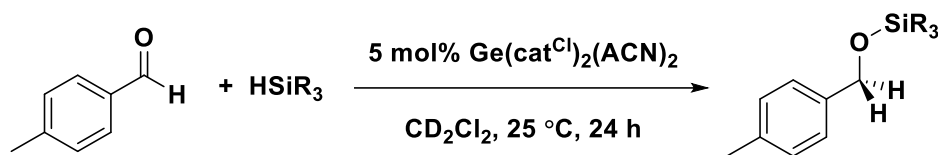
Entry	Substrate	Conversion (%) ^a	Entry	Substrate	Conversion (%) ^a
1		>95	6		>95
2		>95	7		<5
3		>95	8		<5
4		84	9		<5%
5		8			

^a) Conversion values were determined by the difference in ¹H NMR integration of the aldehydic proton or methyl ketone proton relative to mesitylene, 1/9 eq., as an internal standard. Conversion values were the average of two runs. 0.01 mmol of catalyst used in 0.5 mL.

A variety of different silanes were examined in the reaction of *para*-tolualdehyde using $\text{Ge}(\text{cat}^{\text{Cl}})_2(\text{ACN})_2$ as a catalyst. The conversion achieved using triethylsilane compared to triisopropylsilane, (Table 3.4, Entries 1-2) lead to a noticeable decrease and

is attributed to the increase in steric bulk of the substituents. Utilizing tris(trimethylsilyl)silane (Table 3.4, Entry 3), the conversion to the silyl ether dropped further to 20%. Other silanes (Table 3.4, Entries 4-5) without bulky substituents resulted in moderate conversions of 79% and 60%. Based on these experiments, triethylsilane was found to be the most efficient silane.

Table 3.4 Silane substrate scope for the hydrosilylation of *para*-tolualdehyde with $\text{Ge}(\text{cat}^{\text{Cl}})_2(\text{ACN})_2$ as a catalyst.



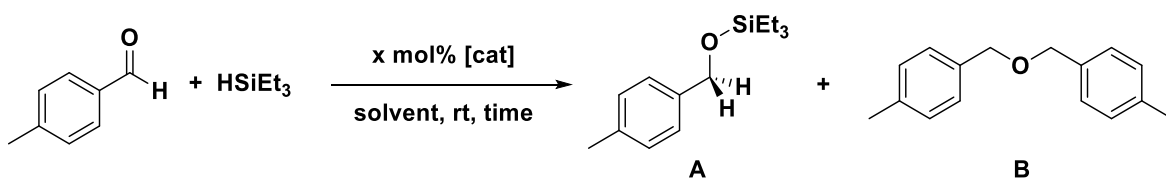
Entry	Substrate	Conversion (%) ^a	Entry	Substrate	Conversion (%) ^a
1	HSiEt_3	84	4		79
2	$\text{HSi}(\text{iPr})_3$	42	5		60
3	$\text{HSi}(\text{SiMe}_3)_3$	<5			

^a) Conversion values were determined by the difference in ^1H NMR integration of the aldehyde proton relative to mesitylene, 1/9 eq., as an internal standard. Conversion values were the average of two runs. 0.01 mmol of catalyst used in 0.5 mL.

While the trends in reactivity were similar between the bis(catecholato)germanes and $\text{Si}(\text{cat}^{\text{F}})_2$ as catalysts, the overall catalytic efficiency of $\text{Si}(\text{cat}^{\text{F}})_2$ was much better.¹⁷ $\text{Si}(\text{cat}^{\text{F}})_2$ facilitates the hydrosilylation of a variety of electron-deficient benzaldehyde derivatives, including the *para*- NO_2 , -CN, and -Cl substituted benzaldehydes tested with $\text{Ge}(\text{cat}^{\text{Cl}})_2(\text{ACN})_2$ (Table 3.3, Entries 1-3). While both $\text{Si}(\text{cat}^{\text{F}})_2$ and $\text{Ge}(\text{cat}^{\text{Cl}})_2(\text{ACN})_2$ achieve >90% conversions with these substrates, $\text{Si}(\text{cat}^{\text{F}})_2$ requires only 30-60 minutes. To compare catalyst efficiency with other main group catalysts, *para*-tolualdehyde was chosen as the substrate (Table 3.5). Using $\text{Ge}(\text{cat}^{\text{Cl}})_2(\text{ACN})_2$ as a catalyst requires multiple hours to reach a conversion of 84% with *para*-tolualdehyde (Table 3.5, Entry 1).

The highly Lewis acidic $\text{Si}(\text{cat}^{\text{CF}_3})_2(\text{sulfolane})_2$, when used as a catalyst with *para*-tolualdehyde and triethylsilane, did not afford the silyl ether as the product.¹⁸ Instead, after 24 hours at room temperature, the symmetric di-(4-methylbenzyl)ether was formed with a conversion of 97% (Table 3.5, Entry 2). Comparing to other main group Lewis acids, using $\text{B}(\text{C}_6\text{F}_5)_3$ as a catalyst, the hydrosilylation of *para*-tolualdehyde was achieved with 87% conversion (Table 3.5, Entry 3).²⁰ Using group 13 triflates as Lewis acid catalysts, the hydrosilylation of *para*-tolualdehyde proceeds to the symmetric di-(4-methylbenzyl)ether in varying conversions (Table 3.5, Entries 4-6). The bis(catecholato)germanes give similar results in comparison to $\text{B}(\text{C}_6\text{F}_5)_3$ and, unlike $\text{Si}(\text{cat}^{\text{CF}_3})_2(\text{sulfolane})_2$ and the group 13 triflates, selectively form the silyl ether over the dibenzyl ether.

Table 3.5: The hydrosilylation of *para*-tolualdehyde with triethylsilane catalyzed by various main group Lewis acids



Entry	Catalyst	Catalyst Loading (mol%)	Solvent	Time (h)	Product	Conversion (%)
1	$\text{Ge}(\text{cat}^{\text{Cl}})_2(\text{ACN})_2$	5	CD_2Cl_2	24	A	84%
2	$\text{Si}(\text{cat}^{\text{CF}_3})_2(\text{sulfolane})_2$	1	CD_2Cl_2	24	B	97%
3	$\text{B}(\text{C}_6\text{F}_5)_3$	2	Toluene- <i>d</i> ₈	“Overnight”	A	87%
4	$\text{Bi}(\text{OTf})_3$	4	neat	“Overnight”	B	53%
5	$\text{Al}(\text{OTf})_3$	4	neat	“Overnight”	B	100%
6	$\text{Ga}(\text{OTf})_3$	4	neat	“Overnight”	B	88%

3.2.2 Hydroboration of Terminal Alkynes

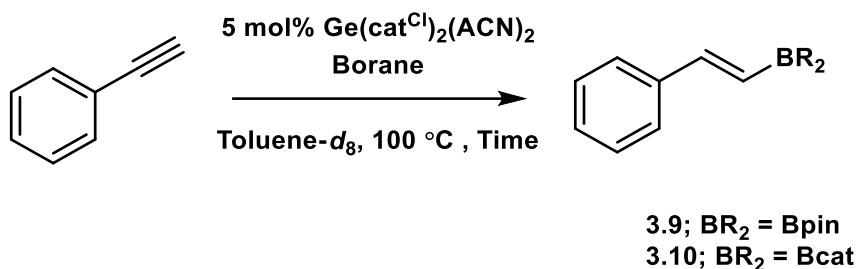
While attempts to hydroborate α -methylstyrene resulted in oligomerization, the reaction of phenylacetylene and 1.2 eq. pinacolborane with 10 mol% of $\text{Ge}(\text{cat}^{\text{Cl}})_2(\text{ACN})_2$ in toluene- d_8 at 100 °C for 24 hours yielded the anti-Markovnikov *E*-borylalkene **3.9** selectively (Table 3.6). This was evident by the disappearance of the ^1H NMR signal at 2.70 ppm attributed to the terminal alkynyl hydrogen of phenylacetylene and the appearance of ^1H NMR signals at 7.60 and 6.32 ppm, attributed to the vinylic hydrogens of **3.9**. The ^{11}B NMR spectral data were also consistent with this interpretation with the disappearance of the signal attributed to pinacolborane at 28.44 ppm and the appearance of the signal attributed to the borylalkene at 30.79 ppm.

Using 1.2 equivalents of pinacolborane with 10 mol% of $\text{Ge}(\text{cat}^{\text{Cl}})_2(\text{ACN})_2$ resulted in a yield of 40% of **3.9** after 24 hours (Table 3.6, Entry 1). If the reaction was allowed to proceed for 48 hours or 72 hours, the conversion increased slightly to 47% and 54%, respectively. Changing the catalyst loading from 10 mol% to 5 mol% showed a minimal difference in the extent of conversion; however, dropping the catalyst loading to 2 mol% resulted in the conversion at 24 hours to be halved (Table 3.6, Entries 1-3). Notably, if the reaction was performed in the absence of catalyst, a conversion of 6% was observed after 24 hours showing that, while this reaction does not need a catalyst to proceed, but a catalyst substantially increases the efficiency of the reaction (Table 3.6, Entry 4). Increasing the number of equivalents of pinacolborane to 2.0, relative to phenylacetylene, resulted in substantially greater conversion for hydroboration, both in the presence and absence of a catalyst (Table 3.6, Entries 5,6). With catecholborane as the borane, greater conversion to **3.10** was achieved when 10 mol% of catalyst was used, when both 1.2 and 2.0 equivalents of catecholborane were used (Table 3.6, Entries 7,9) in comparison to the conversion to **3.9** achieved with pinacolborane. However, the uncatalyzed reaction outperforms the reaction with the catalyst (Table 3.6, Entries 8,10 compared to Entries 7,9). When the reaction of pinacolborane with phenylacetylene in the presence of $\text{Ge}(\text{cat}^{\text{Cl}})_2(\text{ACN})_2$ was monitored by ^{11}B NMR spectroscopy, (Table 3.6, Entry 1) the formation of substantial quantities of pinB-O-Bpin and HO-Bpin was observed as broad singlets at 22.32 ppm and 21.78 ppm, respectively. With the borane

being converted into both **3.9** and the by-products, pinB-O-Bpin and HO-Bpin, the borane is consumed at a faster rate than phenylacetylene. This can lead to either minimal or no borane left in solution to hydroborate phenylacetylene. This observation explains why an increase in the number of equivalents of pinacolborane increases the conversion of phenylacetylene to the alkene as more borane is available to react with phenylacetylene (Table 3.6, Entries 1,5). The hydrolysis of the borane is also observed with catecholborane. As such, the bis(catecholato)germane catalyst, by hydrolysis, decreases the concentration of borane for hydroboration in solution, which explains how the catalyst is inhibiting the hydroboration reaction with catecholborane and phenylacetylene (Table 3.6, Entries 7-10).

To analyze electronic effects on the reaction, the *para*-substituent on the phenyl ring of the phenylacetylene was altered (Table 3.7). Compared to the parent phenylacetylene (Table 3.7, Entries 1,5), the use of the electron-donating methoxy group increased conversions while the use of the electron-withdrawing CF₃ group decreased conversions (Table 3.7, Entries 2,6,3,7). Interestingly, the use of a *tert*-butyl substituent resulted in a substantial decrease in conversion, 40% to 6% for pinacolborane compared to the parent phenylacetylene (Table 3.7, Entry 4). While the use of a *tert*-butyl substituent with catecholborane had a moderate conversion of 68%, the conversion was less than the uncatalyzed reaction (93%). The more electron-rich alkynes can better stabilize the postulated carbocation formed upon coordination to the bis(catecholato)germane making substrate coordination more favourable leading to higher conversions compared to electron-deficient alkynes.

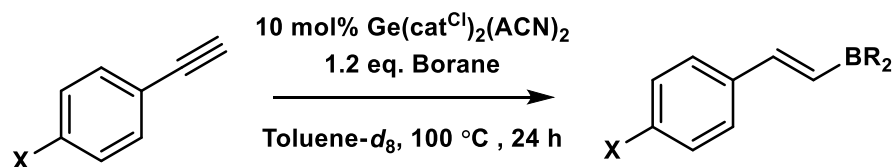
Table 3.6: Optimization of the conditions of the hydroboration of phenylacetylene using $\text{Ge}(\text{cat}^{\text{Cl}})_2(\text{ACN})_2$ as a catalyst.



Entry	Borane	Borane Eq.	Catalyst Loading (mol%)	Conversion (%) ^a		
				24 h	48 h	72 h
1	HBpin	1.2	10	40	47	54
2	HBpin	1.2	5	39	48	52
3	HBpin	1.2	2	15	29	38
4	HBpin	1.2	0	6	17	22
5	HBpin	2.0	10	60	74	86
6	HBpin	2.0	0	19	29	45
7	HBcat	1.2	10	46	50	55
8	HBcat	1.2	0	71	89	91
9	HBcat	2.0	10	93	98	100
10	HBcat	2.0	0	100	100	100

a) Conversion values were determined by the difference in ¹H NMR integration of the acetylene proton relative to mesitylene, 1/9 eq., as an internal standard. Conversion values were the average of two runs. 0.01 mmol of catalyst used in 0.5 mL of solvent.

Table 3.7: Influence on substrate structure on the conversion of phenylacetylene to borylated alkenes.



HBpin			HBcat		
Entry	X =	Conversion (%) ^a	Entry	X =	Conversion (%) ^a
1	H	40	5	H	46
2	OMe	46	6	OMe	93
3	CF ₃	26	7	CF ₃	17
4	^t Bu	6	8	^t Bu	68

a) Conversion values were determined by the difference in ¹H NMR integration of the acetylene proton relative to mesitylene, 1/9 eq., relative to the phenylacetylene derivative, as an internal standard. Conversion values were the average of two runs. 0.02 mmol of catalyst used in 0.5 mL.

While this report presents the first hydroboration of alkynes achieved with bis(catecholato)silanes or -germanes, a variety of other main group Lewis acids have been applied as catalysts for this reaction. B(C₆F₅)₃ has been utilized in the hydroboration of alkynes.¹¹ Notably, while B(C₆F₅)₃ catalyzes the reaction between phenylacetylene and pinacolborane, the active catalyst HB(C₆F₅)₂ can be used directly to achieve higher yields in a fraction of the time (Table 3.8, Entry 2). Similar to the bis(catecholato)germanes, B(C₆F₅)₃ does not catalyze the hydroboration of alkenes. Tris(2,4,6-trifluorophenyl)borane, BAr^F₃, is not only able to catalyze the reaction between pinacolborane and a variety of different alkenes, but also able to catalyze the reaction with phenylacetylene with similar conversions as observed using HB(C₆F₅)₂, however, at a higher temperature (Table 3.8, Entry 3).¹² In addition to boranes, a variety of different aluminum based catalysts, 3.11²¹, 3.12²², 3.13²³, and 3.14²⁴ have been shown to catalyze

the hydroboration of phenylacetylene (Chart 3.2 and Table 3.8, Entries 4-7). Notably, the aluminum catalysts require longer times or harsher conditions compared to the use of $\text{HB}(\text{C}_6\text{F}_5)_2$ as a catalyst. Compared to $\text{Ge}(\text{cat}^{\text{Cl}})_2(\text{ACN})_2$, however, 3.11-3.14 outperform both in the conversion achieved and the conditions used. Main group triflates have also been shown to catalyze the hydroboration of alkynes with the use of NaHBET_3 as an additive. Both $\text{Bi}(\text{OTf})_3$ and $\text{In}(\text{OTf})_3$ are employed using similar conditions to the reactions which utilize $\text{Ge}(\text{cat}^{\text{Cl}})_2(\text{ACN})_2$ as the catalyst; however, lower conversions were obtained (Table 3.8, Entries 8,9).²⁵ Overall, while $\text{Ge}(\text{cat}^{\text{Cl}})_2(\text{ACN})_2$ is not as efficient as a hydroboration catalyst compared to the boranes and alanes, the one-step synthesis from commercially available materials makes the synthesis of $\text{Ge}(\text{cat}^{\text{Cl}})_2(\text{ACN})_2$ easier than the more complex ligands in 3.11, 3.13, and 3.14. $\text{Ge}(\text{cat}^{\text{Cl}})_2(\text{ACN})_2$ is more efficient as a catalyst for the hydroboration of alkynes compared to the use of both bismuth and indium triflate.

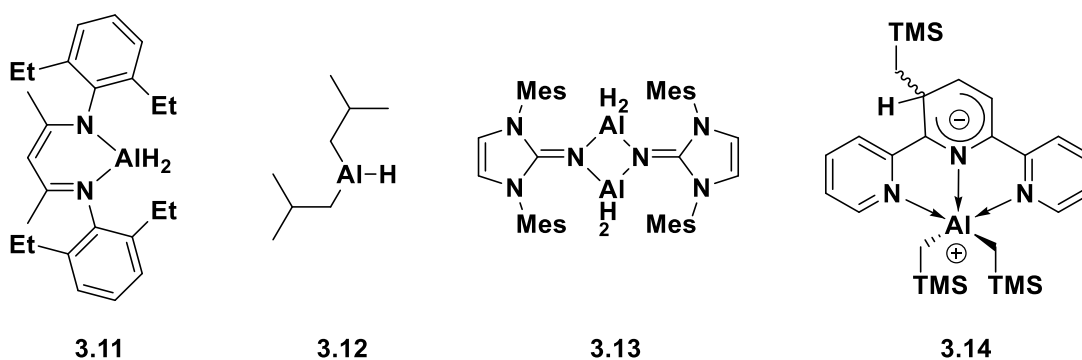
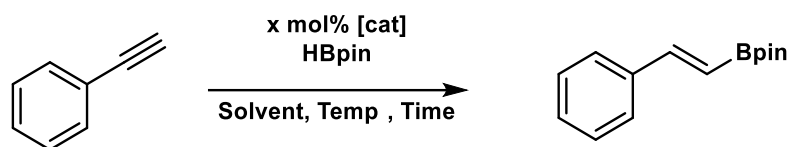


Chart 3.2: Aluminum Lewis acid catalysts

Table 3.8: Examples of main group Lewis acid catalysts in the hydroboration of phenylacetylene with pinacolborane.



Entry	Catalyst	Borane Eq.	Additive ^a	Solvent	Temp. (°C)	Time (h)	Conversion (%)
1	Ge(cat ^{Cl}) ₂ (ACN) ₂ (5 mol%)	1.2	-	Toluene- <i>d</i> ₈	100	24	40
2	HB(C ₆ F ₅) ₂ (5 mol%) ¹¹	1.2	-	CD ₂ Cl ₂	rt	5	90
3	BAr ^F ₃ (3 mol%) ¹²	1	-	Neat	50	15	85 ^b
4	3.11 (3 mol%) ²¹	1 ^c	-	CDCl ₃	30	12	73
5	3.12 (10 mol%) ²²	1.2	-	Toluene- <i>d</i> ₈	110	2	73
6	3.13 (4 mol%) ²³	1	-	C ₆ D ₆	80	28	58
7	3.14 (0.1 mol%) ²⁴	1.2	A	Toluene- <i>d</i> ₈	80	16	85
8	Bi(OTf) ₃ (5 mol%) ²⁵	1.2	B	Toluene- <i>d</i> ₈	100	24	11
9	In(OTf) ₃ (5 mol%) ²⁵	1.2	B	Toluene- <i>d</i> ₈	100	24	36

a) Additives: A = 1 mol% NaO^tBu; B = 5 mol% NaBHET₃ b) Deuterated Ph-C≡C-D was used for this experiment. c) 1.2 equivalents of phenylacetylene were used.

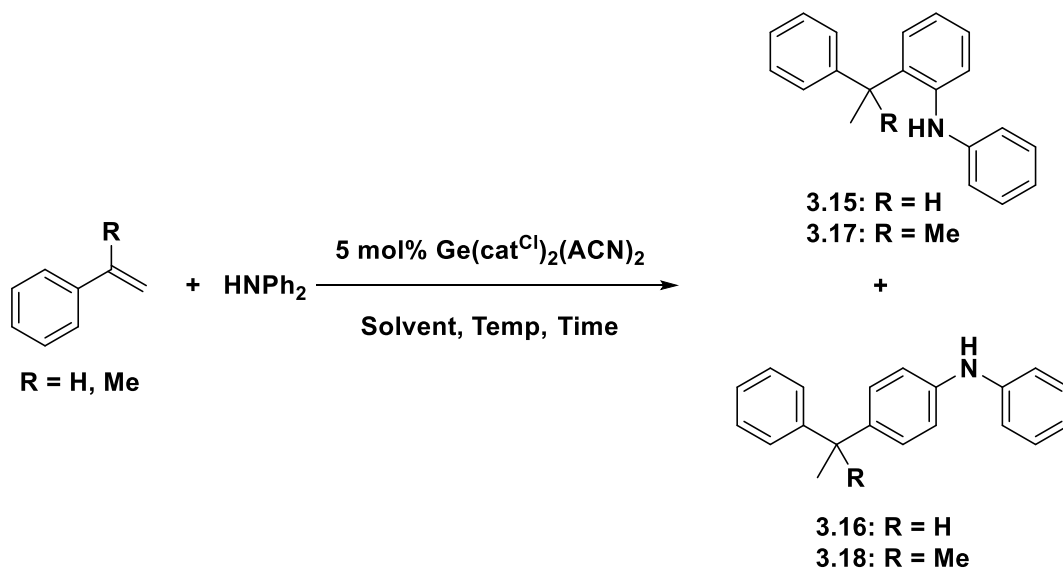
3.2.3 Hydroamination and Friedel-Crafts Alkylation of Alkenes

The hydroamination of alkenes was also examined as a reaction to test the effectiveness of bis(catecholato)germanes as catalysts in this reaction. $\text{Ge}(\text{cat}^{\text{Cl}})_2(\text{ACN})_2$ was selected as the catalyst because of its superior performance in the hydrosilylation of aldehydes and the oligomerization of alkenes. Electron-deficient anilines, such as 2,4,6-trichloroaniline, are typically chosen as amines due to their reduced Lewis basicity.⁸ Using $\text{Ge}(\text{cat}^{\text{Cl}})_2(\text{ACN})_2$ as a catalyst, 2,4,6-trichloroaniline was reacted with the reactive alkenes, norbornene, styrene, and α -methylstyrene. No reaction was observed when norbornene was used as the alkene. While substantial conversion of styrene and α -methylstyrene was observed, 93% and 76% respectively, no hydroamination products were isolated. Instead, dimerization of α -methylstyrene to give **3.6** and **3.7**, and the oligomerization of styrene was observed. Furthermore, no reaction took place between styrene and diethylamine.

Switching the amine from the electron-deficient 2,4,6-trichloroaniline to the bulky diphenylamine, based on a report on $\text{B}(\text{C}_6\text{F}_5)_3$ -catalyzed hydroaminations,¹⁰ the conversion of styrene to two different products was observed by ^1H NMR spectroscopy (Table 3.9, Entry 2). Separation of the products by preparative thin-layer chromatography (TLC) revealed that hydroarylation of the *ortho* and *para* positions of diphenylamine occurred, yielding **3.15** and **3.16**. **3.15** and **3.16** were identified by comparison of the ^1H chemical shifts to the literature values.²⁶ Similar to styrene, the reaction of α -methylstyrene also yielded the hydroarylation products at the *ortho* and *para* positions of diphenylamine (Table 3.9, Entry 6) yielding **3.17** and **3.18**. Allowing the reaction to proceed for 3 days lead to conversions of 80% and 72% for styrene and α -methylstyrene, respectively (Table 3.9, Entries 3,7). Reaction times of 6 days lead to a minimal increase in conversion (Table 3.9, Entries 4,8). Reaction in toluene- d_8 at room temperature resulted in no conversion of styrene, and a 3% conversion of α -methylstyrene to dimerization products suggesting elevated temperatures are needed for any substantial reaction to occur (Table 3.9, Entries 1,5). The reaction of α -methylstyrene and HNPh_2

can also be performed in C_6D_6 at a slightly lower temperature with slightly lower conversions in comparison to those achieved in toluene- d_8 (Table 3.9, Entries 6 and 9).

Table 3.9: Hydroarylation of styrene and α -methylstyrene with diphenylamine



Entry	Alkene	Solvent	Temp (°C)	Time (h)	Conversion (%) ^a (ortho:para)
1	Styrene	Toluene- d_8	rt	24 h	0
2	Styrene	Toluene- d_8	100	24 h	45 (56:44)
3	Styrene	Toluene- d_8	100	72 h	80 (56:44)
4	Styrene	Toluene- d_8	100	144 h	88 (57:43)
5	α -methylstyrene	Toluene- d_8	rt	24 h	3 ^a
6	α -methylstyrene	Toluene- d_8	100	24 h	31 (18:82)
7	α -methylstyrene	Toluene- d_8	100	72 h	72 (42:58)
8	α -methylstyrene	Toluene- d_8	100	144 h	79 (43:57)
9	α -methylstyrene	C_6D_6	80	24 h	27

a) Conversion values were determined by the difference in 1H NMR integration of a vinylic hydrogen relative to mesitylene, 1/9 eq., as an internal standard. Conversion values were the average of two runs. b) formation of dimer **3.6** was observed instead of Friedel-Crafts alkylation.

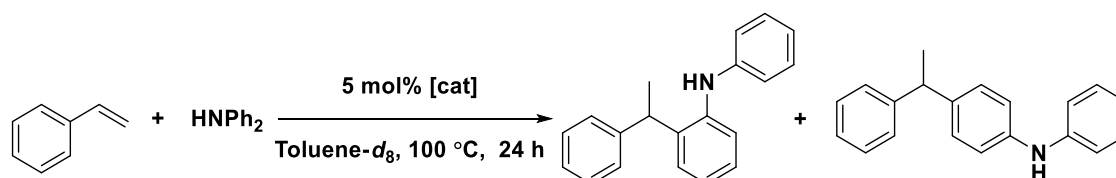
The performance of different bis(catecholato)germane catalysts was tested using styrene and diphenylamine (Table 3.10). Comparing the results obtained using the best catalyst for aldehyde hydrosilylation and alkene oligomerization, $\text{Ge}(\text{cat}^{\text{Cl}})_2(\text{ACN})_2$ (Table 3.10, Entry 1), with those obtained using the chlorinated derivatives with THF and Et_2O donors (Table 3.10, Entries 2,3), revealed that the derivative with the weaker donor, ACN, is the better catalyst. While THF is a stronger donor than diethyl ether, the catalyst with THF donors outperformed the ether derivative. Switching the catechol to the perbrominated derivative resulted in substantially less conversion for the THF derivative, and no conversion for the ACN derivative (Table 3.10, Entries 4,5). Surprisingly, when $\text{Ge}(\text{dtbc})_2(\text{THF})_2$ was used as a catalyst, 26% conversion was observed (Table 3.10, Entry 6). This less Lewis acidic and sterically bulky Lewis acid may disfavour coordination of the bulky amine allowing the reaction to proceed whereas the more Lewis acidic perbrominated derivatives may be poisoned by amine coordination.

To examine substituent effects on the alkene substrate, different *para*-substituted styrenes were utilized (Table 3.11). The use of electron-withdrawing substituents (Table 3.11, Entries 1-3) resulted in substantially lower conversions compared to the parent styrene (Table 3.11, Entry 4), while the use of electron-donating substituents resulted in near quantitative conversion (Table 3.11, Entries 5-6). Similar to the substrate scope of alkynes in hydroboration using the germane catalysts, electron-rich styrenes can better stabilize the postulated carbocationic intermediate which explains the higher conversions.

To provide a comparison to the catalytic performance of other main group Lewis acids which catalyze the same reaction, anisole was used as a substrate. For $\text{Ge}(\text{cat}^{\text{Cl}})_2(\text{ACN})_2$, styrene was reacted with anisole (1:1 ratio) to give quantitative conversion after only 2 hours at 100 °C (Scheme 3.19). Notably, a selectivity of 84:16 was obtained in favour of the *para*-isomer. Other main group Lewis acids that catalyze the same reaction include BiCl_3 ,²⁷ $\text{Bi}(\text{OTf})_3$,²⁸ and InCl_3 .²⁹ Ten mol% of BiCl_3 quantitatively converts anisole to an 80:20 ratio of the *para*- and *ortho*-substituted products after 10 hours at 100 °C. However, to obtain substantial conversion, a 10:1 molar ratio of anisole to styrene was needed; dropping the molar ratio of anisole and styrene to 5:1 resulted in a drop to 59%. $\text{Bi}(\text{OTf})_3$ catalyzes the reaction at 55 °C for 1

hour in DCM to give a 95% yield of products with a ratio of 80:20 of the *para*- and *ortho*-substituted products, respectively. The Bi(OTf)₃-catalyzed reactions used a 3:1 ratio of anisole to styrene. Five mol% of InCl₃ also catalyzes the reaction, with a molar ratio of 1.1:1 of anisole to styrene, in 2 hours at 80 °C resulting in a yield of 81% and a ratio of 87:23. Compared to the bismuth and indium catalysts, Ge(cat^{Cl})₂(ACN)₂ yielded quantitative conversion over a shorter period of time without the need for an excess of anisole.

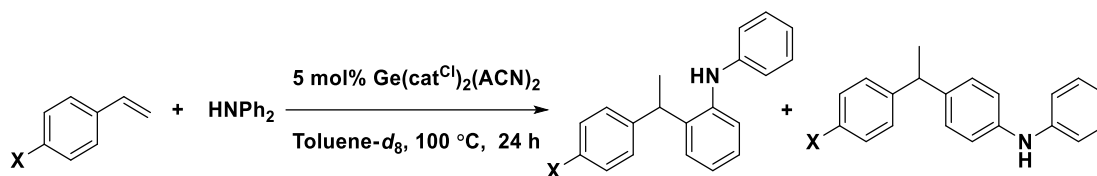
Table 3.10: Different bis(catecholato)germane catalysts in the Friedel-Crafts alkylation of styrene with diphenylamine.



Entry	Catalyst	Conversion (%) ^a (<i>ortho:para</i>)
1	Ge(cat ^{Cl}) ₂ (ACN) ₂	45 (53:47)
2	Ge(cat ^{Cl}) ₂ (THF) ₂	37 (62:38)
3	Ge(cat ^{Cl}) ₂ (Et ₂ O) ₂	20 (48:52)
4	Ge(cat ^{Br}) ₂ (ACN) ₂	0
5	Ge(cat ^{Br}) ₂ (THF) ₂	11 (60:40)
6	Ge(dtbc) ₂ (THF) ₂	26 (67:33)

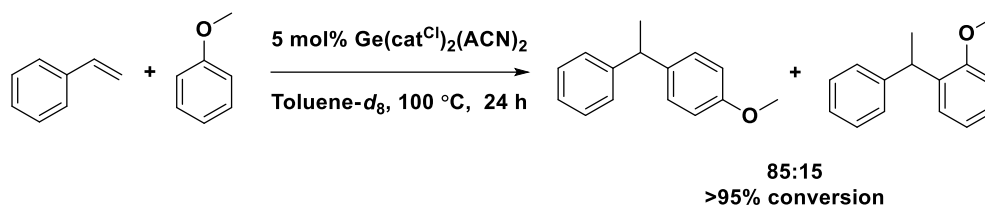
^a) Conversion values were determined by the difference in ¹H NMR integration of a vinylic proton relative to mesitylene, 1/9 eq., as an internal standard. Conversion values were the average of two runs.

Table 3.11: Substrate scope of various *para*-substituted styrene derivatives in the Friedel-Crafts alkylation of diphenylamine.



Entry	X =	Conversion (%) ^a (<i>ortho:para</i>)
1	CF ₃	<5
2	F	30 (57:43)
3	Br	<5
4	Me	>95 (55:45)
5	H	45 (53:47)
6	OMe	>95 (55:45)

a) Conversion values were determined by the difference in ¹H NMR integration of a vinylic proton relative to mesitylene, 1/9 eq., relative to the alkene, as an internal standard. Conversion values were the average of two runs.



Scheme 3.19: Friedel-Crafts alkylation of anisole and styrene catalyzed by $\text{Ge(cat}^{\text{Cl}})_2(\text{ACN})_2$.

3.2.4 Oligomerization Alkenes

To further assess the catalytic activity of bis(catecholato)germanes, the oligomerization of arylalkenes was probed. When styrene was added to a suspension of $5 \text{ mol\% Ge(cat}^{\text{Br}})_2(\text{THF})_2$ at $100 \text{ }^\circ\text{C}$ in $\text{tol-}d_8$ for 24 hours, the formation of polystyrene was observed as indicated by the appearance of broad

signals in the ^1H NMR spectrum of the reaction mixture. Integrating these signals against mesitylene as an internal standard showed a conversion of 21%.

With the bulkier α -methylstyrene under the same reaction conditions, high conversion to three dimerization products, **3.6**, **3.7**, and **3.8** was observed (Table 3.12, Entry 1). Using different donor ligands on the bis(catecholato)germane framework, the selectivity of the dimers could be tuned. While the catalysts with THF and ethyl ether donor ligands formed a mixture of the three dimers (Table 3.12, Entries 1,2,4,6), using $\text{Ge}(\text{cat}^{\text{Br}})_2(\text{ACN})_2$ (Table 3.12, Entry 3) or the perchlorocatecholato derivative, (Table 3.12, Entry 5) the selective formation of the cyclic dimer **3.8** was observed. Monitoring the reaction by ^1H NMR spectroscopy, using $\text{Ge}(\text{cat}^{\text{Br}})_2(\text{ACN})_2$ as the catalyst, confirmed that the formation of **3.6** occurs first and is consumed to make either **3.7** or **3.8** (Figure 3.1). Dimer **3.7** can also be converted into dimer **3.8** which is the thermodynamic sink of the reaction.

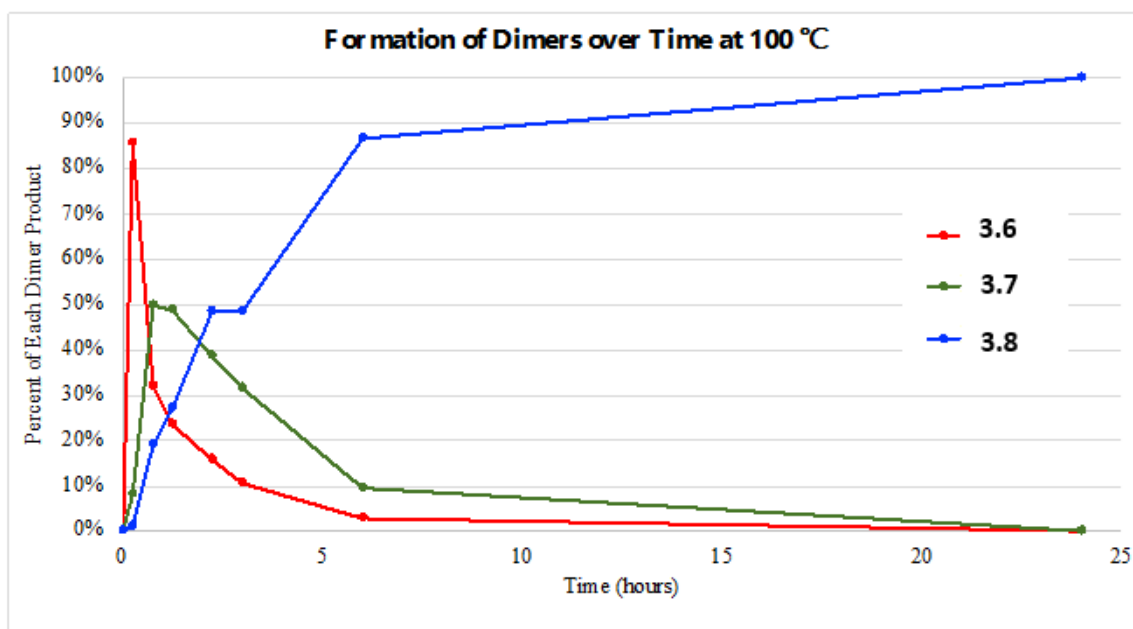
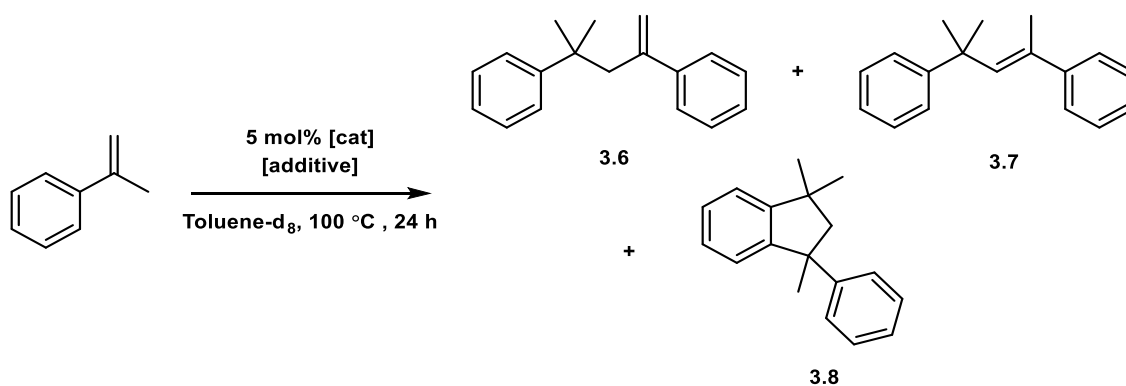


Figure 3.1: Dimer products **3.6** (red trace), **3.7** (green trace), and **3.8** (blue trace) formed in reactions with α -methylstyrene and $\text{Ge}(\text{cat}^{\text{Br}})_2(\text{ACN})_2$ over a period of 24 hours at 100°C .

Table 3.12: The effect of donor ligands and silane/borane additives on the dimerization of α -methylstyrene



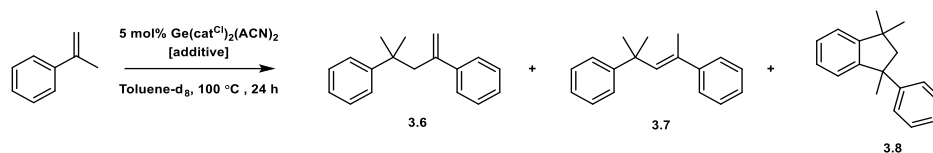
Entry	Catalyst	Additive	Conversion ^a (%)	Ratio of Products 3.6:3.7:3.8
1	Ge(cat ^{Br}) ₂ (THF) ₂	-	92	34:38:20
2	Ge(cat ^{Br}) ₂ (Et ₂ O) ₂	-	98	8:18:72
3	Ge(cat ^{Br}) ₂ (ACN) ₂	-	99	0:0:99
4	Ge(cat ^{Cl}) ₂ (THF) ₂	-	94	17:25:8
5	Ge(cat ^{Cl}) ₂ (ACN) ₂	-	99	0:0:99
6	Ge(dtbc) ₂ (THF) ₂	-	18	3:1:0
7	Ge(cat ^{Br}) ₂ (THF) ₂	1 eq. HSiEt ₃	14	14:0:0
8	Ge(cat ^{Br}) ₂ (Et ₂ O) ₂	1 eq. HSiEt ₃	67	65:2:0
9	Ge(cat ^{Br}) ₂ (ACN) ₂	1 eq. HSiEt ₃	16	16:0:0
10	Ge(cat ^{Cl}) ₂ (THF) ₂	1 eq. HSiEt ₃	4	4:0:0
11	Ge(cat ^{Cl}) ₂ (ACN) ₂	1 eq. HSiEt ₃	16	12:0:0
12	Ge(dtbc) ₂ (THF) ₂	1 eq. HSiEt ₃	2	0:0:0
13	Ge(cat ^{Cl}) ₂ (ACN) ₂	1 eq. HBcat	85	38:10:4
14	Ge(cat ^{Cl}) ₂ (ACN) ₂	1 eq. HBpin	85	50:20:4

^a) Conversion values were determined by the difference in ¹H NMR integration of a vinylic proton relative to mesitylene, 1/9 eq., as an internal standard. Conversion values were the average of two runs.

The addition of one equivalent of triethylsilane to the reaction resulted in a notable decrease in the conversion of α -methylstyrene to products when halogenated bis(catecholato)germanes were utilized as catalysts (Table 3.12, Entries 7-11). However, despite the low conversion, selective formation of dimer **3.6** was observed. The use of one equivalent of triethylsilane with $\text{Ge}(\text{dtbc})_2(\text{THF})_2$ resulted in no conversion (Table 3.12, Entry 12). When using 5 mol% of $\text{Ge}(\text{cat}^{\text{Br}})_2(\text{Et}_2\text{O})_2$ in the presence of 1 eq. of HSiEt_3 , the formation of dimer **3.6** was observed with a moderate conversion of 67% and only a minor amount of dimer **3.7** formed (2%) (Table 3.12, Entry 8). While the role of the silane in the reaction is currently unknown, it prompted the exploration of the effect of other additives on the selectivity of the reaction, specifically, the use of boranes (Table 3.12, Entries 13-14) and the use of donor additives, Et_2O and hexamethyldisiloxane (Table 3.13, Entries 1-4). Using an equivalent of pinacolborane or catecholborane resulted in higher conversion values compared to when triethylsilane was used; however, a mixture of the three dimers were, once again, formed. When utilizing one or half an equivalent of hexamethyldisiloxane as the additive, a mixture of dimers was observed with dimer **3.8** as the major product (Table 3.13, Entries 3-4). However, using one or half an equivalent of ethyl ether as the additive, the dimerization of α -methylstyrene proceeded at room temperature with high conversions and high selectivity for dimer **3.6**, demonstrating that the conversion and selectivity can be tuned by altering the additive and its concentration (Table 3.13, Entries 1-2).

Performing the oligomerization reaction with 5 mol% $\text{Ge}(\text{cat}^{\text{Cl}})_2(\text{ACN})_2$ in CD_2Cl_2 at room temperature, instead of in toluene- d_8 at elevated temperatures, resulted in the formation of a mixture of dimer **3.8** and trimer **3.19** in almost equal amounts (Table 3.14, Entry 1). The use of borane and silane additives resulted in a change of selectivity favouring the linear dimers **3.6** and **3.7**; however, in the case of triethylsilane as an additive, conversions were substantially lower than without an additive (Table 3.14, Entries 2-4). While the reactions in DCM also lead to formation of trimer **3.19**, the reactions performed in toluene resulted in better selectivity for single products.

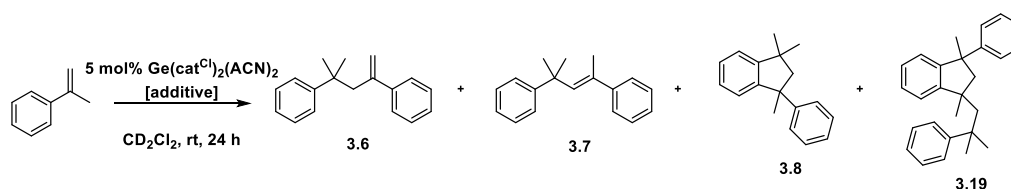
Table 3.13: The effect of donor ligands and donor additives on the dimerization of α -methylstyrene in toluene- d_8 .



Entry	Additive	Conversion ^a (%)	Ratio of Products (3.6:3.7:3.8)
1	1 eq. Et_2O^b	82	81:1:0
2	0.5 eq. Et_2O^b	96	91:3:2
3	1 eq. $\text{Me}_3\text{Si-O-SiMe}_3$	98	18:36:48
4	0.5 eq. $\text{Me}_3\text{Si-O-SiMe}_3$	99	13:20:70

a) Conversion values were determined by the difference in ^1H NMR integration of a vinylic proton relative to mesitylene, 1/9 eq., as an internal standard. Conversion values were the average of two runs. *b)* performed at room temperature.

Table 3.14: The effect of silane and borane additives on the dimerization of α -methylstyrene in CD_2Cl_2 .



Entry	Additive	Conversion ^a (%)	Ratio of Products (3.6:3.7:3.8:3.19)
1	-	99	0:0:43:56
2	1 eq. HSiEt_3	23	19:0:0:0
3	1 eq. HBpin	96	76:4:5:11
4	1 eq. HBcat	98	60:5:7:9

a) Conversion values were determined by the difference in ^1H NMR integration of a vinylic proton relative to mesitylene, 1/9 eq., as an internal standard. Conversion values were the average of two runs. *b)* performed at room temperature.

Comparing to other main group catalysts, the selective formation of either dimer **3.6** or **3.8** in the oligomerization of α -methylstyrene has been achieved using InBr_3 as the catalyst by altering the reaction time (Table 3.15, Entries 5,6).¹⁵ However, given the ratio of the products was reported after purification and separation by column chromatography, the selectivity of the dimers in the crude reaction mixture is not known. BiCl_3 has also been used as a catalyst for the dimerization of α -methylstyrene and selectively yields dimer **3.8** in 73% yield (Table 3.15, Entry 7).¹⁶ Selectivity in the dimerization of α -methylstyrene has also been achieved using different ionic liquids in a variety of solvents or by using acid catalysis under homogeneous or heterogeneous conditions (Table 3.15, Entry 8).³⁰ Comparing $\text{Ge}(\text{cat}^{\text{Cl}})_2(\text{ACN})_2$ to the other Lewis acids, $\text{Ge}(\text{cat}^{\text{Cl}})_2(\text{ACN})_2$ has comparable conversions to BiCl_3 under similar conditions but the germane system has the advantage of being able to tune product selectivity. InBr_3 was able to achieve high conversions and product selectivity under milder conditions but the selectivity reported was after product separation which may not reflect the actual ratio in the crude reaction mixture.¹⁵ Nevertheless, the ability to tune the reaction using a main group catalyst framework with donor additives is unprecedented. The performance of the bis(catecholato)germanes (Table 3.15, Entries 1-4) is comparable to that of a ruthenium-based transition metal catalyst system, **3.20** (Chart 3.3 and Table 3.15, Entries 9,10). With comparable performance and product selectivity via donor additives, the bis(catecholato)germanes showcase the ability of main group alternative catalysts in the oligomerization of α -methylstyrene.

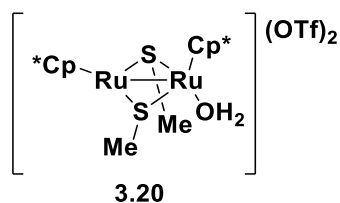
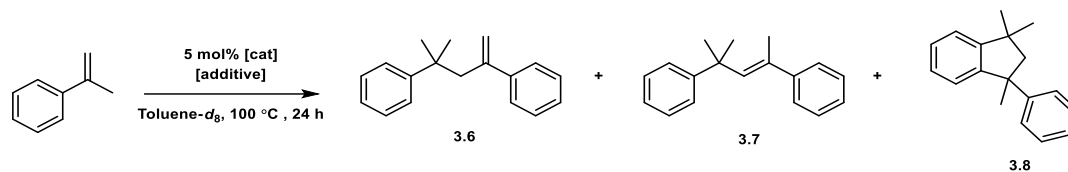


Chart 3.3: Ruthenium catalyst for dimerization of α -methylstyrene.

Table 3.15: Comparison of different catalysts in the dimerization of α -methylstyrene.

Entry	Catalyst	Additive	Solvent	Time (h)	Temp. (°C)	Conversion (%)	Ratio of Products 3.6:3.7:3.8
1	Ge(cat ^{Cl}) ₂ (ACN) ₂ (5 mol%)	-	Toluene- <i>d</i> ₈	0.5	100	95	87:8:0
2	Ge(cat ^{Cl}) ₂ (ACN) ₂ (5 mol%)	-	Toluene- <i>d</i> ₈	24	100	99	0:0:99
3	Ge(cat ^{Cl}) ₂ (ACN) ₂ (5 mol%)	1 eq. Et ₂ O ^a	Toluene- <i>d</i> ₈	24	100	82	81:1:0
4	Ge(cat ^{Cl}) ₂ (ACN) ₂ (5 mol%)	0.5 eq. Et ₂ O ^a	Toluene- <i>d</i> ₈	24	100	96	91:3:2
5	InBr ₃ (10 mol%)	-	DCM	2	0	90 ^b	90:0:0
6	InBr ₃ (10 mol%)	-	DCM	4	rt	88 ^b	0:0:88
7	BiCl ₃ (5 mol%)	-	<i>n</i> -octane	24	110	73	0:0:73
8	HI gas (20 mol%)	-	neat	24	rt	61	0:0:61
9	3.20 (1 mol%)	-	DCE ^c	20	60	68	51:17:0
10	3.20 (1 mol%)	2 mol% cinnamic chloride	DCE ^c	20	60	82	0:0:82

a) Reaction performed in room temperature; *b*) Isolated yields after column chromatography; *c*) DCE = 1,2-dichloroethane

3.3 Conclusion

Herein, a variety of bis(catecholato)germanes were shown to be excellent Lewis acid catalysts. The hydrosilylation of aldehydes, oligomerization of arylalkenes, hydroboration of phenylacetylene, and the Friedel-Crafts alkylation of diphenylamine were catalyzed by bis(catecholato)germanes and demonstrate the versatility of the catalyst system. $\text{Ge}(\text{cat}^{\text{Cl}})_2(\text{ACN})_2$ was found to be the most efficient catalyst among the germanium-based catalysts tested. It has high Lewis acidity afforded by the halogenated catecholato substituents and the weakly donating acetonitrile ligand and can be synthesized in high yield compared to the bromo-derivative. While $\text{Ge}(\text{cat}^{\text{Br}})_2(\text{ACN})_2$ has higher Lewis acidity, as shown in Chapter 2, the higher Lewis acidity of $\text{Ge}(\text{cat}^{\text{Br}})_2(\text{ACN})_2$ appears to have a negative impact on catalysis. The use of donor additives in the dimerization of α -methylstyrene resulted in selective control for the formation of one of two different products.

3.4 Experimental

3.4.1 General Experimental

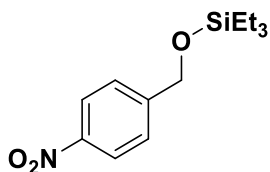
All reactions were conducted under a nitrogen atmosphere using an MBraun Labmaster 130 glovebox. Solvents and reagents were purified by standard methods.¹⁹ NMR data were obtained on a 600 MHz INOVA, 400 MHz INOVA or a 400 MHz Bruker Avance III NMR spectrometer. The standards used were as follows: residual CHCl_3 (7.26 ppm), CH_2Cl_2 (5.32 ppm), toluene- d_7 (2.09 ppm) relative to TMS for ^1H NMR spectra; CDCl_3 (77.16 ppm) for ^{13}C NMR spectra; J values are reported in Hertz.

3.4.2 General Catalytic Procedures and Product Characterization

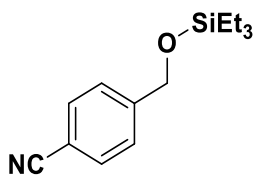
A mixture containing the substrates (0.2 mmol of substrate at 1 eq.), catalyst (0.010 mmol for 10 mol%), mesitylene (0.022 mmol) as an internal standard, and, when specified, an additive (0.2 mmol for additives at 1 eq.), in 0.5 mL deuterated solvent (CD_2Cl_2 , $\text{tol}-d_8$) were allowed to react for 24 hours in NMR tubes sealed with parafilm and electrical tape. Control experiments without catalyst were performed in parallel. Conversion of

substrates to products was determined by integration against mesitylene (C₉H₁₂) as an internal standard.

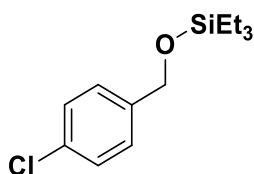
3.4.3 Hydrosilylation of Aldehydes



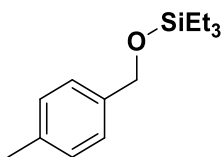
¹H NMR (600 MHz, CD₂Cl₂) 8.17 (d, *J* = 8.7 Hz, 2H), 7.52 (d, *J* = 8.7 Hz, 2H), 4.73 (s, 2H), 0.95 (t, *J* = 7.9 Hz, 9H), 0.54 (q, *J* = 7.9 Hz, 6H).¹⁷



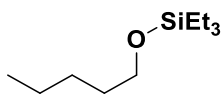
¹H NMR (600 MHz, CD₂Cl₂) δ 7.67 (d, *J* = 8.3 Hz, 2H), 7.50 (d, *J* = 8.0 Hz, 2H), 4.66 (s, 2H), 0.95 (t, *J* = 8.0 Hz, 9H), 0.55 (q, *J* = 8.0 Hz, 6H).¹⁷



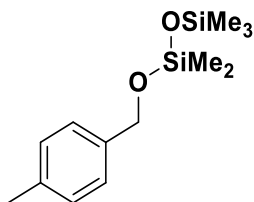
¹H NMR (600 MHz, CD₂Cl₂) δ 7.50 (d, *J* = 8.4 Hz, 2H), 7.25 (d, *J* = 8.4 Hz, 2H), 4.50 (s, 2H), 0.96 (t, *J* = 7.9 Hz, 9H), 0.56 (q, *J* = 8.0 Hz, 6H).¹⁷



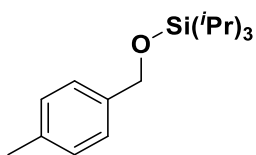
¹H NMR (400 MHz, CD₂Cl₂) δ 7.26 (d, *J* = 7.8 Hz, 2H), 7.18 (d, *J* = 7.7 Hz, 2H), 4.51 (s, 2H), 2.36 (s, 3H), 0.98 (t, *J* = 7.9 Hz, 9H), 0.57 (q, *J* = 7.9 Hz, 6H).¹⁹



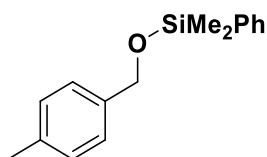
¹H NMR (600 MHz, CD₂Cl₂) δ 3.39 (t, *J* = 6.8 Hz, 2H), 1.55 (t, *J* = 7.1 Hz, 2H), 1.40 – 1.28 (m, 4H), 0.96 (t, *J* = 7.9 Hz, 9H), 0.91 (t, *J* = 7.0 Hz, 3H), 0.55 (q, *J* = 7.9 Hz, 6H).³¹



¹H NMR (600 MHz CD₂Cl₂) δ 7.27 (d, *J* = 7.5 Hz, 2H), 7.19 (d, *J* = 7.7 Hz, 2H), 4.52 (s, 2H), 2.37 (s, 3H), 0.14 (d, *J* = 3.4 Hz, 9H), 0.12 – 0.10 (m, 6H).³²

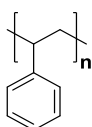


¹H NMR (600 MHz, CD₂Cl₂) δ 7.29 (d, *J* = 8.0 Hz, 2H), 7.22 (d, *J* = 7.6 Hz, 2H), 4.84 (s, 2H), 2.37 (s, 3H), 1.16 (s, 21H).

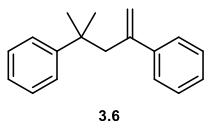


¹H NMR (600 MHz, CD₂Cl₂) δ 7.67-7.40 (5H), 7.31 (d, *J* = 7.6 Hz, 2H), 7.18 (d, *J* = 8.0 Hz, 2H), 4.55 (s, 2H), 2.40 (s, 3H), 0.68 (s, 3H).³¹

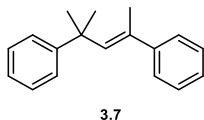
3.4.4 Oligomerization of Alkenes



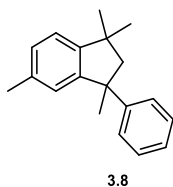
¹H NMR (400 MHz, CD₂Cl₂): δ 7.20-7.00 (br s, 3H), 6.65-6.45 (br s, 2H), 1.84 (br s, 1H), 1.47 (br s, 2H).³³



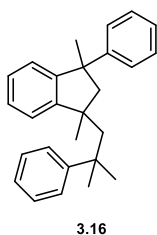
¹H NMR (400 MHz, Toluene-*d*₈): δ 7.00-7.30 (m, 10H), 5.10 (s, 1H), 4.74 (s, 1H), 2.71 (s, 2H), 1.15 (s, 6H).¹⁵



¹H NMR (400 MHz, Toluene-*d*₈): δ 7.00-7.30 (m, 10H), 6.09 (s, 1H), 1.53 (s, 3H).³⁰

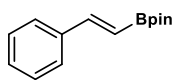


¹H NMR (400 MHz, Toluene-*d*₈): δ 7.00-7.30 (m, 9H), 2.33 (d, 1H), 2.05 (d, 1H), 1.58 (s, 3H), 1.24 (s, 3H), 1.00 (s, 3H).¹⁵

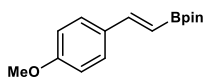


¹H NMR (600 MHz, Toluene-*d*₈): δ 7.20 – 7.50 (m, 15 H), 2.59 (d, *J* = 15 Hz, 1 H), 2.20 (d, *J* = 14 Hz, 1H), 1.90 (d, *J* = 15 Hz, 1H), 1.72 (d, *J* = 14 Hz, 1H), 1.60 (s, 3H), 1.28 (s, 3H), 1.15 (s, 3H), 0.96 (s, 3H).³⁴

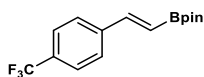
3.4.5 Hydroboration of Alkynes



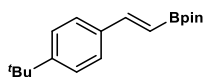
^1H NMR (400 MHz, Toluene- d_8): δ 7.60 (d, $J = 18.5$ Hz, 1 H), 7.27 (d, 2 H), 7.09 – 7.01 (m, 3 H), 6.32 (d, $J = 18.5$ Hz, 1 H), 1.12 (s, 12 H). ^{11}B NMR (128 MHz, Toluene- d_8): 30.79 (d).³⁵



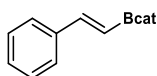
^1H NMR (400 MHz, Toluene- d_8): δ 7.60 (d, $J = 18.2$ Hz, 1 H), 7.23 (d, 2 H), 6.60 (m, 2 H), 6.20 (d, $J = 18.3$ Hz, 1 H), 3.28 (s, 3H), 1.14 (s, 12 H).³⁴



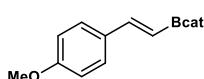
^1H NMR (400 MHz, Toluene- d_8): δ 7.46 (d, $J = 18.4$ Hz, 1 H), 7.20 (d, $J = 8.1$ Hz, 2 H), 7.03 (d, $J = 8.1$ Hz, 2 H), 6.28 (d, $J = 18.4$ Hz, 1 H), 1.12 (s, 12 H) ^{11}B NMR (128 MHz, Toluene- d_8): 30.05 (d).³⁴



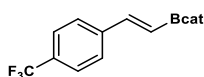
^1H NMR (400 MHz, Toluene- d_8): δ 7.65 (d, $J = 18.5$ Hz, 1 H), 7.29 (d, 2 H), 6.60 (d, 2 H), 6.20 (d, $J = 18.5$ Hz, 1 H), 1.20 (s, 9 H), 1.14 (s, 12 H).³⁴



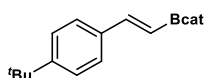
^1H NMR (400 MHz, Toluene- d_8): δ 7.72 (d, $J = 18.5$ Hz, 1 H), 7.27 – 7.24 (m, 2 H), 7.07 – 7.04 (m, 4 H), 6.84 – 6.81 (m, 2H), 6.38 (d, $J = 18.5$ Hz, 1 H). ^{11}B NMR (128 MHz, Toluene- d_8): 31.91 (d).³⁶



^1H NMR (400 MHz, Toluene- d_8): δ 7.75 (d, $J = 18.5$ Hz, 1 H), 7.23 (d, 2 H), 7.08 – 7.06 (d, 2 H), 6.85 – 6.82 (m, 2 H), 6.63 (m, 2H), 6.28 (d, $J = 18.5$ Hz, 1 H). ^{11}B NMR (128 MHz, Toluene- d_8): 32.16 (d).³⁷

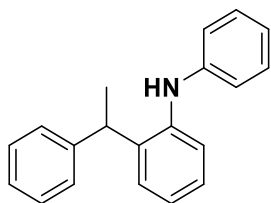


^1H NMR (400 MHz, Toluene- d_8): δ 7.52 (d, $J = 18.8$ Hz, 1 H), 7.25 (m, 2 H), 7.07 – 7.02 (m, 4 H), 6.84 (d, 2 H), 6.28 (d, $J = 18.8$ Hz, 1 H). ^{11}B NMR (128 MHz, Toluene- d_8): 31.93 (d).

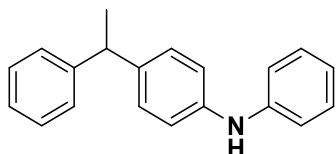


^1H NMR (400 MHz, Toluene- d_8) δ 7.80 (d, $J = 18.4$ Hz, 1H), 7.30 (d, $J = 8.2$ Hz, 2H), 7.18 (d, $J = 8.4$ Hz, 2H), 7.09 – 7.04 (m, 2H), 6.84–6.82 (m, 2H), 6.43 (d, $J = 18.4$ Hz, 1H), 1.19 (s, 9H). ^{11}B NMR (128 MHz, Toluene- d_8): 28.74 (d).

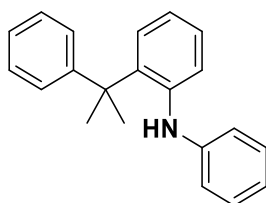
3.4.6 Friedel-Crafts Alkylation



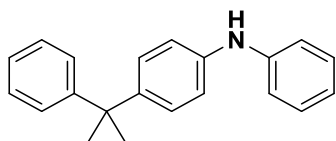
$^1\text{H NMR}$ (400 MHz, Toluene- d_8) δ 7.16 – 7.11 (m, 2H), 7.10 – 7.03 (m, 4H), 6.83 – 6.78 (m, 8H), 4.94 (s, 1H), 3.92 (q, $J = 7.2$ Hz, 1H), 1.50 (d, $J = 7.2$ Hz, 3H).^{26a}



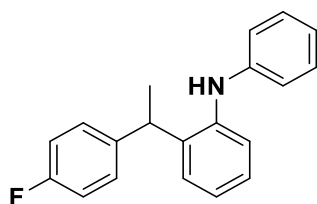
$^1\text{H NMR}$ (400 MHz, Toluene- d_8) δ 7.33 – 6.85 (m, 13H), 6.67 – 6.57 (m, 2H), 5.02 (s, 1H), 4.05 (q, $J = 7.1$ Hz, 1H), 1.42 (d, $J = 7.2$ Hz, 3H).^{26b}



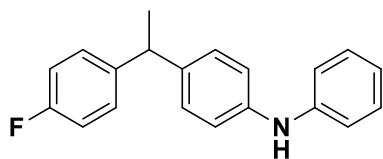
$^1\text{H NMR}$ (400 MHz, Toluene- d_8) δ 7.25 – 7.12 (m, 6H), 7.05 – 7.00 (m, 6H), 6.76 (d, $J = 8.7$ Hz, 2H), 1.57 (s, 6H).



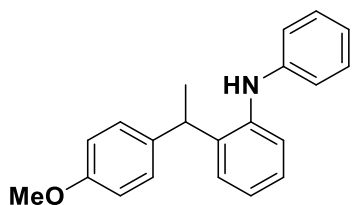
$^1\text{H NMR}$ (400 MHz, Toluene- d_8) δ 7.24 – 7.19 (m, 1H), 7.14 (dd, $J = 8.5, 6.8$ Hz, 1H), 7.09 – 7.03 (m, 5H), 6.83 – 6.74 (m, 7H), 1.56 (s, 6H).³⁸



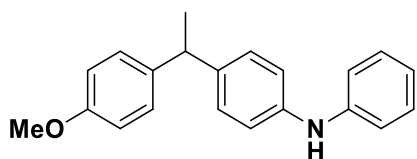
$^1\text{H NMR}$ (400 MHz, Toluene- d_8) δ 7.15-6.70 (18 H), 4.02 (q, $J = 7.2$ Hz, 1H), 1.44 (d, $J = 7.2$ Hz, 3H).³⁷



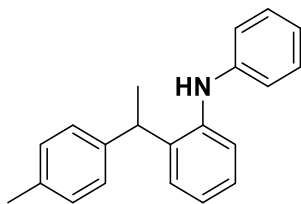
$^1\text{H NMR}$ (400 MHz, Toluene- d_8) δ 7.15-6.70 (18 H), 4.83 (q, $J = 7.2$ Hz, 1H), 1.44 (d, $J = 7.2$ Hz, 3H).³⁷



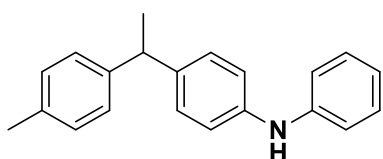
$^1\text{H NMR}$ (400 MHz, Toluene- d_8) δ 7.13-6.67 (18 H), 3.94 (q, $J = 7.3$ Hz, 1H), 1.56 (d, $J = 7.3$ Hz, 3H).



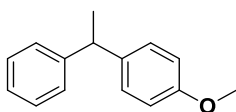
$^1\text{H NMR}$ (400 MHz, Toluene- d_8) δ 7.13-6.67 (18 H),
4.09 (m, 1H), 1.55 (d, $J = 7.2$ Hz, 3H).³⁷



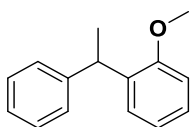
$^1\text{H NMR}$ (400 MHz, Toluene- d_8) δ 7.13-6.68 (18 H),
4.12 (q, $J = 6.8$ Hz, 1H), 1.54 (d, $J = 6.8$ Hz, 3H)



$^1\text{H NMR}$ (400 MHz, Toluene- d_8) δ 7.13-6.68 (18 H),
3.93 (q, $J = 7.2$ Hz, 1H), 1.48 (d, $J = 6.8$ Hz, 3H).³⁷



$^1\text{H NMR}$ (400 MHz, Toluene- d_8) δ 7.27-6.69 (9 H),
3.36 (q, $J = 7.3$ Hz, 1H), 1.52 (d, $J = 7.3$ Hz, 3H).²⁷



$^1\text{H NMR}$ (400 MHz, Toluene- d_8) δ 7.27-6.69 (9 H),
3.95 (q, $J = 7.3$ Hz, 1H), 1.57 (d, $J = 7.2$ Hz, 3H).²⁷

References

1. Nakajima, Y.; Shimada, S. *RSC Adv.* **2015**, *5*, 20603-20616.
2. Oertle, K.; Wetter, H. *Tetrahedron Letters* **1985**, *26*, 5511-5514.
3. Rubin, M.; Schwier, T.; Gevorgyan, V. *J. Org. Chem.* **2002**, *67*, 1936-1940.
4. Fritz-Langhals, E. *Org. Process. Res. Dev.* **2019**, *23*, 2369-2377.
5. McGrath, N. A.; Brichacek, M.; Njardson, J. T. *J. Chem. Ed.* **2010**, *87*, 1348-1349.
6. Some recent examples: *a)* Matsuoka, J.; Terashita, M.; Miyawaki, A.; Tomioka, K.; Yamamoto, Y. *Tetrahedron Letters* **2022**, *89*, 153599; *b)* Chinn, A. J.; Sedillo, K.; Doyle, A. G. *J. Am. Chem. Soc.* **2021**, *143*, 18331-18338; *c)* Takagi, R.; Sakai, Y.; Duong, D. T. *Tetrahedron* **2021**, *85*, 132037.
7. Cheng, X.; Xia, Y.; Wei, H.; Xu, B.; Zhang, C.; Li, Y.; Qian, G.; Zhang, X.; Li, K.; Li, W. *Eur. J. Org. Chem.* **2008**, 1929-1936.
8. Li, L.; Huang, G.; Chen, Z.; Liu, W.; Wang, X.; Chen, Y.; Yang, L.; Li, W.; Li, Y. *Eur. J. Org. Chem.* **2012**, *28*, 5564-5572.
9. Koller, J.; Bergman, R. G. *Chem. Commun.* **2010**, *46*, 4577-4579.
10. Mahdi, T.; Stephan, D. W. *Angew. Chem. Int. Ed.* **2013**, *52*, 12418-12421.
11. Fleige, M.; Mobus, J.; vom Stien, T.; Glorius, F.; Stephan, D. W. *Chem. Commun.* **2016**, *52*, 10830-10833.
12. Yin, Q.; Kemper, S.; Klare, H. F. T.; Oestreich, M. *Chem. Eur. J.* **2016**, *22*, 13840-13844.
13. Rueping, M.; Nachtsheim, B. J.; Scheidt, T. *Org. Lett.* **2006**, *8*, 3717-3719.

14. Li, Y.; Wang, Y.; Xu, D.; Jin, R.; Gu, G.; Guo, H. *Synlett* **2017**, 28, A-D.
15. Peppe, C.; Lang, E. S.; Molinos de Andrade, F.; Borges de Castro, L. *Synlett* **2004**, 10, 1723-1726.
16. Sun, H.; Li, B.; Hua, R.; Yin, Y. *Eur. J. Org. Chem.* **2006**, 18, 4231-4236.
17. Liberman-Martin, A. L.; Bergman, R. G.; Tilley, T. D. *J. Am. Chem. Soc.* **2015**, 137, 5328-5331.
18. Thaddaus, T.; Roth, D.; Greb, L. *Chem. Eur. J.* **2021**, 27, 10422-10427.
19. Roth, D.; Wadepohl, H.; Greb, L. *Angew. Chem. Int. Ed.* **2020**, 59, 20930-20934.
20. Bach, P.; Albright, A.; Laali, K. K. *Eur. J. Org. Chem.* **2009**, 1961-1966.
21. Yang, Z.; Zhong, M.; Ma, X.; Nijesh, K.; De, S.; Parameswaran, P.; Roesky, H. W. *J. Am. Chem. Soc.* **2016**, 138, 2548-2551.
22. Bismuto, A.; Thomas, S. P.; Cowley, M. J. *Angew. Chem. Int. Ed.* **2016**, 55, 15356-15359.
23. Franz, D.; Sirtl, L.; Pothig, A.; Inoue, S. *Z. Anorg. Allg. Chem.* **2016**, 642, 1245-1250.
24. Zhang, G.; Wu, J.; Zeng, H.; Neary, M. C.; Devany, M.; Zheng, S.; Dub, P. A. *ACS Catal.* **2019**, 9, 874-884.
25. Mandal, S.; Verma, P. K.; Geetharani, K. *Chem. Commun.* **2018**, 54, 13690-13693.
26. a) Zhu, W.; Sun, Q.; Wang, Y.; Yuan, D.; Yao, Y. *Org. Lett.* **2018**, 20, 3101-3104; b) Chao, M. R.; Li, W. M.; Zhu, L. L.; Ma, H. H.; Wang, X. B. *Chemical Papers* **2015**, 69, 1004-1011.
27. Sun, H. B.; Li, B.; Hua, R.; Yin, Y. *Eur. J. Org. Chem.* **2006**, 4231-4236.

28. Rueping, M.; Nachtsheim, B. J.; Jeawsuwan, W. *Adv. Synth. Catal.* **2006**, *348*, 1033-1037.
29. Sun, G.; Sun, H.; Wang, Z.; Zhou, M. M. *Synlett* **2008**, *7*, 1096-1100.
30. Matsumo, S.; Oseki, T.; Akazome, M.; Otani, Y. *ACS Omega* **2018**, *3*, 17928-17935.
31. Field, L. D.; Messerle, B. A.; Rehr, M.; Soler, L. P.; Hambley, T. W. *Organometallics* **2003**, *22*, 2387-2395.
32. Vasilikogiannaki, E.; Titilas, I.; Gryparis, C.; Louka, A.; Lykakis, I. N.; Stratakis, M. *Tetrahedron* **2014**, *70*, 6106-6113.
33. Wackerly, J. W.; Dunne, J. F. *J. Chem. Educ.* **2017**, *94*, 1790-1793.
34. Sen, A.; Lai, T.; Thomas, R. R. *J. Orgmet. Chem.* **1988**, *358*, 567-588.
35. Liu, J.; Wu, C.; Hu, T.; Yang, W.; Xie, Y.; Shi, Y.; Liu, Q.; Shao, Y.; Zhang, F. *J. Org. Chem.* **2022**, *87*, 3442-3452.
36. Khalimon, A. Y.; Farha, P.; Kuzmina, L. G.; Nikonov, G. I. *Chem. Commun.* **2012**, *48*, 455-457.
37. Garon, C. N.; McIsaac, D. I.; Vogels, C. M.; Decken, A.; Williams, I. D.; Kleeberg, C.; Marder, T. B.; Westcott, S. A. *Dalton Trans.* **2009**, 1624-1631.
38. Wang, S.; Force, G.; Guilot, R.; Carpentier, J. F.; Sarazin, Y.; Bour, C.; Gandon, V.; Leboef, D. *ACS Catal.* **2020**, *10*, 10794-10802.

Chapter 4

4 Mechanistic Study of Lewis Acid Catalysis with Bis(catecholato)germanes

4.1 Introduction

The understanding of a reaction mechanism, the sequence of elementary steps by which a chemical reaction occurs, is crucial for the development of the chemistry of the reaction. Specifically, the knowledge of the mechanism can be utilized to design more efficient reactions, limit side reactivity, and improve product selectivity. In catalysis, the reaction mechanism can lead the development of more efficient catalysts.

4.1.1 Methods for the Elucidation of Reaction Mechanisms

The analysis of a reaction mechanism requires a series of different experiments, the results of which can be used to hypothesize a reaction mechanism. The analysis of the rate law of a reaction provides insight into how the concentrations of reactants affect the reaction rate. The examination of how the electronic and steric properties of different substrates influence the reaction outcome provide valuable mechanistic information. If the reaction proceeds quicker with electron rich or electron-deficient substrates, it can provide insight into the types of intermediates formed during the reaction. If sterically bulky substrates are difficult to react, a steric clash in the formation of an intermediate can be implied. If certain functional groups on a substrate shut down the desired reactivity, the functional groups could lead to side reactions and potentially poison the catalyst. Isotopic labelling is another method commonly used in mechanistic studies. The isotopic labelling of a specific atom in a reactant, for example deuterium labelling of a single hydrogen in a molecule, can provide information of where the labelled atom is incorporated into the final product. Analysis of the difference in rate between a labelled reactant and an unlabeled reactant through Kinetic Isotope Effect (KIE) experiments, allows an assessment of whether or not a given bond involving the labelled atom is involved in or before the rate-determining step.¹ Mechanisms can also be studied computationally; the calculation of the geometries and energies of various different

intermediates and transition states along the reaction coordinate allows an assessment of the kinetics and thermodynamics of a reaction. In this study, Variable Time Normalization Analysis (VTNA), and a Hammett plot will be used to study the rate law and the influence of substituents with different electronic properties, respectively, on the oligomerization of α -methylstyrene. The information gained will then be used to propose a reaction mechanism for this transformation.

4.1.1.1 Rate Law and VTNA

The experimental determination of the rate law for a reaction gives valuable information on how the concentration of each reactant affects the reaction rate. For the reaction $A + B \rightarrow C$, the reaction rate, v , is given by the equation:

$$(1) \quad v = k[A]^\alpha[B]^\beta$$

Where k is the reaction rate constant, $[A]$ and $[B]$ are the concentrations of the reagents, and α and β are the reactant orders for A and B, respectively. The overall reaction order is the sum of α and β . Reactant orders are usually integers but can be fractions or negative values. If the order of a reactant is zero, the rate of the reaction is unaffected by changes in the reactant concentration. If the order of a reactant is positive, increasing the concentration will increase the rate of the reaction.

One method to determine the rate law is through the use of Variable Time Normalization Analysis (VTNA).² This method allows for a visual comparison of a reaction at different reactant concentrations to determine the order of a reactant. In a VTNA plot, the concentration of product is plotted against a time normalized equation, where $[A]$ is the concentration of a reactant and α is the rate order for the reaction:

$$(2) \quad \int_{t=0}^{t=n} [A]^\alpha dt = \sum_{i=1}^n \left(\frac{[A]_i - [A]_{i-1}}{2} \right)^\alpha (t_i - t_{i-1})$$

The time normalized equation (1) normalizes the time between data points by the average concentration of these points. By monitoring the same reaction with different concentrations for $[A]$, the reaction order α can be varied until the lines of the plot overlap which provides a visual method for the determination of the order in reactant.

4.1.1.2 Hammett Plots

A common method to determine the electronic effects of a substituent on a reagent in a given reaction is through a Hammett plot.³ The Hammett equation defines the relationship between reaction rates of substrates with different substituents, commonly aromatic rings with different substituents in the *para* position. The Hammett equation is as follows:

$$(3) \quad \log \frac{k}{k_0} = \sigma \rho$$

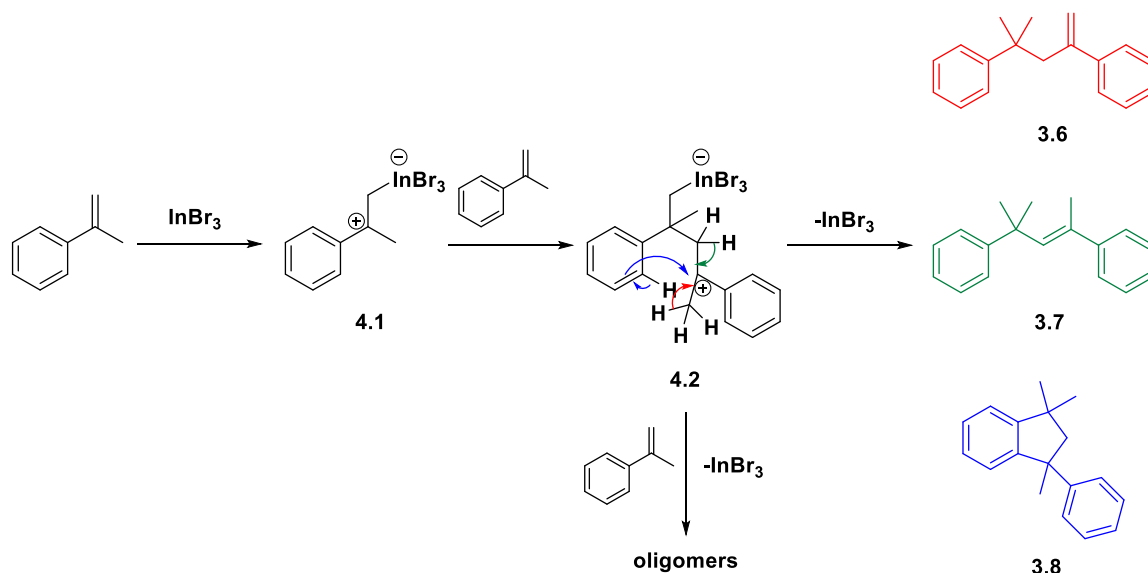
The substituent constant, σ , is a constant for a given substituent on an aromatic ring in either the *para* or *meta* positions. σ values are negative for electron-donating substituents, positive for electron-withdrawing substituents, and 0 for hydrogen. A Hammett plot is generated by plotting $\log k/k_0$ against σ values. The reaction constant, ρ , is represented by the slope of the Hammett plot and is a measure of the magnitude of the influence the substituents on the reaction. If a negative slope is observed, the reaction is accelerated by electron-donating groups, suggesting a buildup of positive charge in the transition state of the rate-determining step. If a positive slope is observed, the reaction is accelerated by electron-withdrawing groups, suggesting a buildup of negative charge in the transition state of the rate-determining step. A non-linear slope can also be observed in a Hammett plot when the different substituents cause a change in mechanism or a change in the rate-determining step.

4.1.2 Mechanisms of Alkene Oligomerization

The polymerization of alkenes typically proceeds via a chain-growth mechanism. Different types of initiators are used in alkene polymerization: anionic, cationic, and radical, which use nucleophiles, electrophiles and radical initiators, respectively. Cationic polymerizations are typically achieved through the use of Brønsted acids in which a proton acts as the initiating electrophile. However, Lewis acids, which react by accepting a lone pair of electrons, can also be used to achieve cationic polymerization.

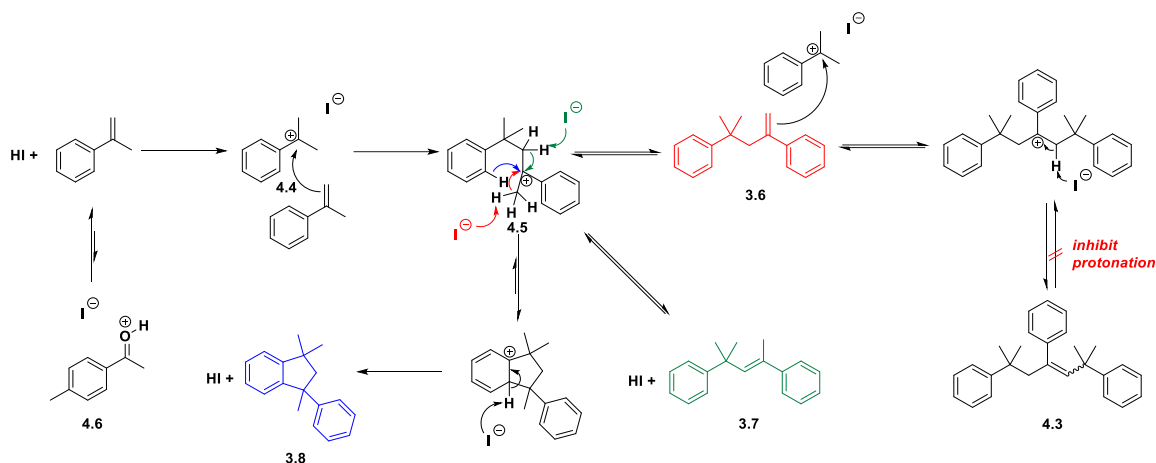
Bis(catecholato)germanes have been shown to be effective catalysts for the oligomerization of α -methylstyrene. To further develop the chemistry of this reaction, a

study of this mechanism was conducted. The only mechanistic study of a Lewis acid catalyzed dimerization of α -methylstyrene is one where the reaction is catalyzed by InBr_3 (Scheme 4.1).⁴ Reaction of α -methylstyrene with 10 mol% of InBr_3 at 0 °C for 2 hours resulted in the selective formation of linear dimer **3.6**. When the reaction was performed at room temperature for 4 hours, cyclic dimer **3.8** was afforded instead. Notably, substitution of the aromatic ring with electron-withdrawing substituents led to the selective formation of derivatives of dimer **3.6** at room temperature, while substitution with electron-donating substituents afforded derivatives of the cyclic dimer **3.8**, suggesting that Friedel-Crafts alkylation is favoured when the aromatic ring is electron-rich. On the basis of the experimental observations, coordination of α -methylstyrene to the Lewis acid was proposed resulting in the carbocationic intermediate **4.1**. Intermediate **4.1** can then add a second equivalent of α -methylstyrene forming intermediate **4.2** which can then give three different isomers depending on the subsequent step. Loss of a proton from either sp^3 -hybridized carbon α to the carbocationic centre, results in the formation of dimer **3.6**, with a disubstituted alkene, or dimer **3.7**, with a trisubstituted alkene. The third isomer is formed by an intramolecular Friedel-Crafts reaction of carbocation **4.2**, resulting in the formation of the cyclic dimer **3.8**.



Scheme 4.1: Proposed mechanism for the dimerization of α -methylstyrene catalyzed by InBr_3 .

The use of various Brønsted acids with methyl *para*-tolyl ketone as an additive has also been used to achieve the oligomerization of α -methylstyrene.⁵ With 20 mol% of HI gas in the presence of methyl *para*-tolyl ketone, the selective formation of dimer **3.8** (61% yield) was observed, with dimers **3.6** and **3.7** observed as minor products (7% **3.6**, 21% **3.7**) (Scheme 4.2). In contrast, in the absence of the ketone, the formation of trimer **4.3** was favoured (68% yield of **4.3**). To explore the reaction further, isolated trimer **4.3** was reacted with HI gas in the absence of ketone and formed dimer **3.8** in 84%. When dimer **3.8** was combined with HI gas and methyl *para*-tolyl ketone, no reaction was observed. Finally, if HI gas and α -methylstyrene were allowed to react for one minute, a mixture of dimers **3.6** and **3.7** as well as trimer **4.3** was observed in 27%, 15%, and 37% yields, respectively. The proposed reaction mechanism is outlined in Scheme 4.2 and shows similar features to the proposed InBr₃-catalyzed mechanism. The addition of an acidic hydrogen from HI to α -methylstyrene results in the formation of carbocation **4.4**. Subsequent addition of a second equivalent of α -methylstyrene results in the formation of carbocationic intermediate **4.5** from which dimers **3.6**, **3.7** and **3.8** can be formed. Dimer **3.6** can add to another equivalent of α -methylstyrene which leads to trimer **4.3**. Dimers **3.6** and **3.7** and trimer **4.3** are formed first, as evident by their formation within a minute in the absence of methyl *para*-tolyl ketone. If the reaction is allowed to proceed over a longer period of time, selective formation of **3.8** is observed as the thermodynamic product. Given that reaction of trimer **4.3** and HI gas gives dimer **3.8**, the reaction is reversible. When methyl *para*-tolyl ketone is present, an equilibrium exists with HI gas favouring the protonated ketone **4.6**. As a weaker acid, **4.6** cannot protonate trimer **4.3**, preventing the equilibrium shift to the thermodynamically favoured product, **3.8**. Comparing to the InBr₃ mechanism (Scheme 4.1), replacing the InBr₃ in intermediate **4.2** with a hydrogen would yield the same carbocation intermediate as the HI gas mechanism, **4.5** (Scheme 4.2).



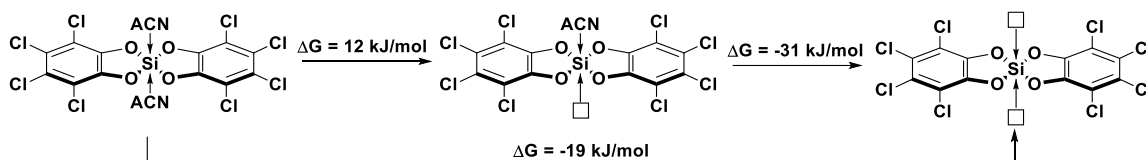
Scheme 4.2: Proposed mechanism for the oligomerization of α -methylstyrene catalyzed by HI gas with the use of methyl *para*-tolyl ketone as an additive.

4.1.3 Mechanistic Studies of Bis(catecholato)silanes as Lewis Acid Catalysts

While a variety of applications have been found for the use of bis(catecholato)silane and -germane Lewis acids as catalysts, limited studies on the mechanism of catalysis have been performed. Bis(perfluorocatecholato)silane, $\text{Si}(\text{cat}^{\text{F}})_2$, catalyzes the hydrosilylation of aldehydes.⁶ The mechanism of the catalysis was also considered. While a stable complex with an aldehyde coordinating to $\text{Si}(\text{cat}^{\text{F}})_2$ was not observed in a stoichiometric reaction, the use of the strongly coordinating *N,N'*-diisopropylbenzamide resulted in coordination of the carbonyl oxygen to the silicon centre; the complex was identified by ^1H NMR spectroscopy as well as X-ray crystallography. Furthermore, no changes in the ^1H NMR spectrum of HSiEt_3 in the presence of $\text{Si}(\text{cat}^{\text{F}})_2$ were observed suggesting that coordination of the aldehyde initiates the reaction rather than coordination of the silane. The aldehyde substrate scope revealed that electron-withdrawing groups on benzaldehydes were required to achieve high conversions while the silane substrate scope tolerated sterically bulky substituents and both electron-withdrawing and electron-donating substituents. Understandably, the silane scope is broad as it is not involved in the critical step in the mechanism. The requirement of electron-withdrawing groups on the aldehydes shows it is involved in the critical step of reaction, consistent with an aldehyde activation mechanism. Furthermore, the electron-withdrawing groups moderate

the donor ability of the aldehyde allowing the reaction to proceed and the final product to eliminate from $\text{Si}(\text{cat}^{\text{F}})_2$.

The number of bis(catecholato)silanes and -germanes catalysts was expanded by Greb *et al.* in the past 5 years to include $\text{Si}(\text{cat}^{\text{Cl}})_2(\text{ACN})_2$,⁷ $\text{Si}(\text{cat}^{\text{Br}})_2(\text{ACN})_2$,⁸ $\text{Si}(\text{cat}^{\text{CF}_3})_2(\text{sulfolane})_2$,⁹ and $\text{Ge}(\text{cat}^{\text{Cl}})_2(\text{ACN})_2$.¹⁰ While a variety of different catalytic reactions were demonstrated, research directed towards understanding the mechanism was minimal, with limited substrate scopes and no experimental mechanistic work. However, computations of the energetics of ACN donor dissociation from $\text{Si}(\text{cat}^{\text{Cl}})_2(\text{ACN})_2$ was performed at the PW6B95-D3(BJ)/def2-TZVPP level of theory (Scheme 4.3).⁸ The calculations showed that the dissociation of the first equivalent of ACN is endergonic while the dissociation of the second equivalent, and the overall dissociation of both ACN donors, is exergonic, suggesting that donor-free $\text{Si}(\text{cat}^{\text{Cl}})_2$ would be accessible during a reaction.



Scheme 4.3: Calculated energetics of ACN dissociation from $\text{Si}(\text{cat}^{\text{Cl}})_2(\text{ACN})_2$.

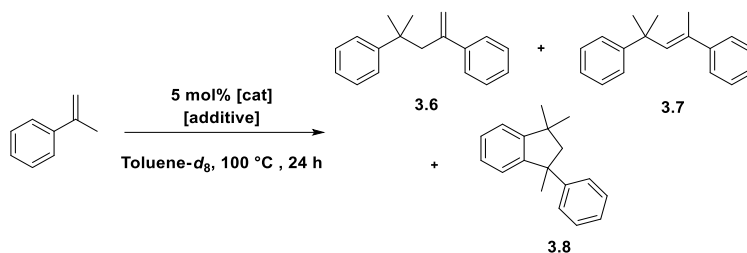
4.1.4 Project Goal

The understanding of reaction mechanisms is often key in the development of the chemistry. The goal of this project was to elucidate the mechanism of catalysis of bis(catecholato)germanes. The mechanism of hydrosilylation of aldehydes was previously studied with $\text{Si}(\text{cat}^{\text{F}})_2$ as a catalyst. Since similar observations in substrate scope were observed with the corresponding germanes, specifically that electron-deficient aldehydes were necessary for high conversions, we propose the bis(catecholato)germanes also activate the aldehyde through coordination allowing subsequent addition of the H-Si bond across the carbonyl moiety. The hydroboration of alkynes and Friedel-Crafts alkylation using alkenes was also shown to be catalyzed by bis(catecholato)germanes. While a small substrate scope revealed some key mechanistic

observations, further investigation expanding the substrate scope should be investigated prior to detailed mechanistic studies. The mechanism of oligomerization of styrene and α -methylstyrene has not been investigated for group 14 bis(catecholato)- Lewis acids. In the oligomerization of α -methylstyrene, high selectivity was observed under certain conditions, notably with the use of donor additives. The substrate scope revealed no reactivity for non-aryl alkenes. Finally, understanding the mechanism of alkene oligomerization may help us understand why hydrosilylation and hydroboration of alkenes was unachievable using the bis(catecholato)germane catalysts. As such, the focus of this chapter was on the reactions with alkene substrates, specifically the oligomerization of styrene and α -methylstyrene. To understand the mechanism of this reaction, a rate law analysis, a Hammett plot, and computational calculations were performed and are discussed herein.

The oligomerization of α -methylstyrene using bis(catecholato)germanes as catalysts, formed several products: **3.6**, **3.7**, **3.8**, and **3.19** (Table 4.1). The conversion of α -methylstyrene and the selectivity of the reaction depends on the catalyst and additives used. Specifically, while the choice of halogen on the catechol substituents plays a minimal role in conversion and selectivity (Table 4.1, Entries 1 and 4, 3 and 5), the choice of donor had a substantial influence on both reactivity and selectivity (Table 4.1, compare Entries 1 and 4 and 5). Catalysts with THF ligands give lower conversions and form a mixture of products (Table 4.1, Entries 1 and 4), while the use of catalysts with bound ACN ligands selectively form the cyclic dimer **3.8** over the linear dimers **3.6** and **3.7** (Table 4.1, Entries 3 and 5). Furthermore, the addition of diethyl ether as an additive altered the selectivity, favouring the formation of linear dimers **3.6** and **3.7** while maintaining high conversions (Table 4.1, compare Entries 6-7 to Entry 5). These observations are key to the formulation of a proposed mechanism. Finally, while reactions in toluene afforded only dimers (**3.6**, **3.7** and **3.8**), reactions in CD_2Cl_2 at room temperature resulted in the formation of a cyclic trimer (**3.19**).

Table 4.1: Summary of key reactions on the catalytic oligomerization of α -methylstyrene.



Entries	Catalyst	Additive	Conversion (%)	Ratio of Products		
				3.6	3.7	3.8
1	$\text{Ge}(\text{cat}^{\text{Br}})_2(\text{THF})_2$	-	92	34	38	20
2	$\text{Ge}(\text{cat}^{\text{Br}})_2(\text{Et}_2\text{O})_2$	-	98	8	18	72
3	$\text{Ge}(\text{cat}^{\text{Br}})_2(\text{ACN})_2$	-	99	0	0	9
4	$\text{Ge}(\text{cat}^{\text{Cl}})_2(\text{THF})_2$	-	94	17	25	8
5	$\text{Ge}(\text{cat}^{\text{Cl}})_2(\text{ACN})_2$	-	99	0	0	99
6	$\text{Ge}(\text{cat}^{\text{Cl}})_2(\text{ACN})_2$	1 eq. Et_2O	82	81	1	0
7	$\text{Ge}(\text{cat}^{\text{Cl}})_2(\text{ACN})_2$	0.5 eq. Et_2O	96	91	3	2
8	$\text{Ge}(\text{cat}^{\text{Cl}})_2(\text{ACN})_2$	1 eq. $\text{Me}_3\text{Si-O-SiMe}_3$	98	18	36	48

4.2 Results and Discussion

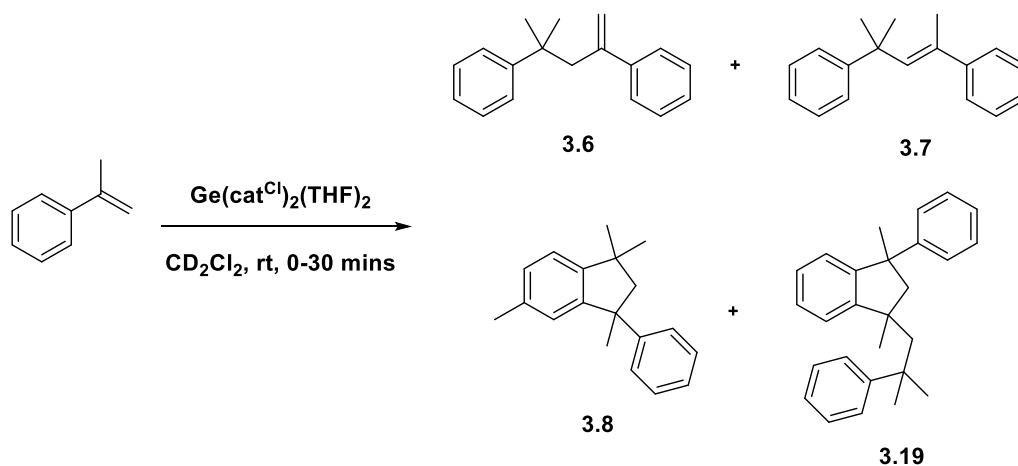
4.2.1 Experimental Studies

4.2.1.1 Rate Studies

A VTNA of the oligomerization of α -methylstyrene was performed using $\text{Ge}(\text{cat}^{\text{Cl}})_2(\text{THF})_2$ as the catalyst, as the reaction proceeds slower with the bound THF ligands on the catalyst allowing for easier monitoring of the reaction by NMR compared to using $\text{Ge}(\text{cat}^{\text{Cl}})_2(\text{ACN})_2$ as the catalyst. CD_2Cl_2 was chosen as the NMR solvent for the VTNA study as the reaction proceeds quickly at room temperature. A solution of α -

methylstyrene in CD_2Cl_2 was added directly to an NMR tube containing a catalytic amount of $\text{Ge}(\text{cat}^{\text{Cl}})_2(\text{THF})_2$ and mesitylene as an internal standard in CD_2Cl_2 (Scheme 4.4). The reaction was monitored over 30 minutes by ^1H NMR spectroscopy.

To analyze the order in styrene, the total concentration of oligomerization products formed (**3.6**, **3.7**, **3.8**, **3.19**) was plotted against $\Sigma[\text{styrene}]^\alpha \Delta t$, where α is the reaction order for styrene (Figure 4.1). The order in styrene was altered between 1-2 and the values are plotted when the starting concentration of styrene is 0.14 M and 0.27 M. Notably, when the reactant order is 1.5, the best overlap between the two concentrations is observed suggesting an order of 1.5 for styrene. The formation of dimers, **3.6**, **3.7**, and **3.8**, and trimer **3.19**, when using CD_2Cl_2 as a solvent is the likely cause of the fractional reactant order.



Scheme 4.4: The reaction conditions used for the VTNA rate study

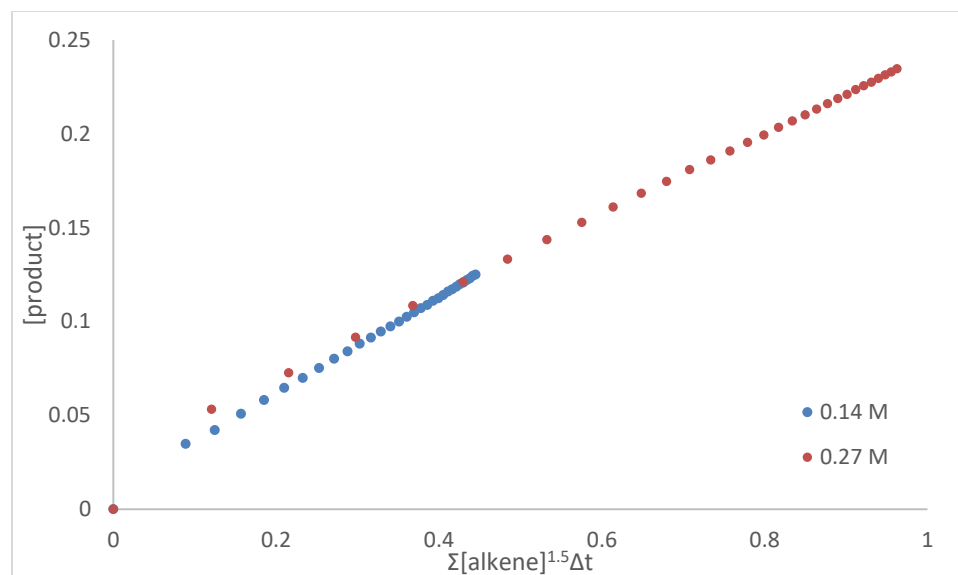
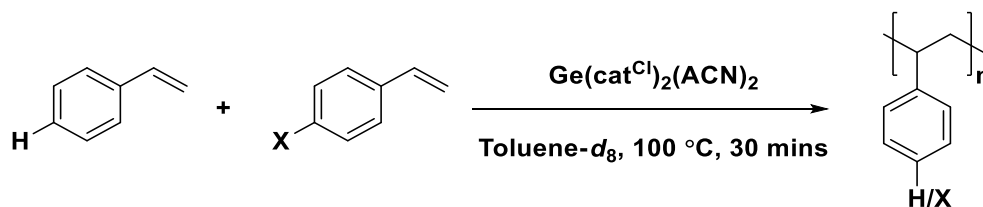


Figure 4.1: VTNA plots for the oligomerization of α -methylstyrene. The order of α -methylstyrene is 1.5.

4.2.1.2 Hammett Plot

To study the mechanism of alkene oligomerization further, a Hammett analysis was performed using *para*-substituted styrene derivatives. The *para*-substituted styrenes were chosen as several derivatives were commercially available in contrast to the *para*-substituted α -methylstyrene derivatives. Styrene was reacted with an equal amount of various *para*-substituted styrene using $\text{Ge}(\text{cat}^{\text{Cl}})_2(\text{ACN})_2$ as the catalyst (Scheme 4.5). After reacting for 30 minutes, a ^1H NMR spectrum was recorded. The consumption of the styrene and *para*-substituted styrenes were determined by integration relative to a mesitylene internal standard. The results are shown in Figure 4.2.



Scheme 4.5: The reaction between styrene and *para*-substituted styrenes used to generate the Hammett plot.

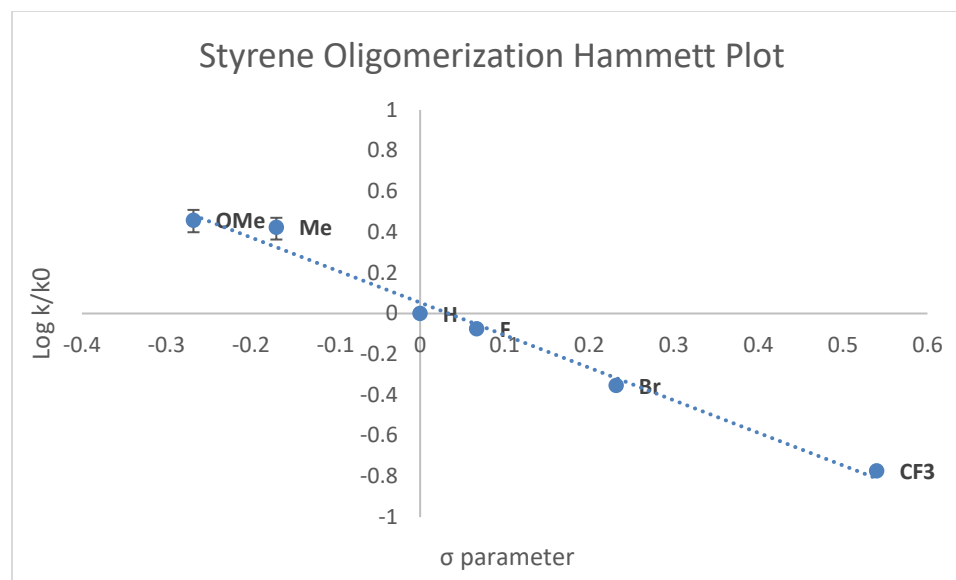


Figure 4.2: Hammett plot for the oligomerization of various *para*-substituted styrene derivatives. The points are averages of at least two runs.

The Hammett plot revealed a good linear correlation with an R^2 value of 0.9853. The rate of reaction for styrenes with electron-withdrawing substituents was less than that for electron-rich styrenes resulting in a negative slope. Together, the results are consistent with the build up of positive charge in the transition state of the rate-determining step. The magnitude of the reaction constant, 1.60, shows that the reaction is quite sensitive to the electronic nature of the substituents in the *para* position.

4.2.1.3 Measuring Product Formation Over Time

Using different donor ligands on the bis(catecholato)germane framework, the selectivity of the dimers could be tuned. While the halogenated bis(catecholato)germanes with THF and diethyl ether donor ligands formed a mixture of the three dimers, using $\text{Ge}(\text{cat}^{\text{Br}})_2(\text{ACN})_2$ or the perchlorocatecholato derivative as the catalyst, the selective formation of the cyclic dimer **3.8** was observed (Table 4.1, Entries 1-5). Monitoring the reaction by ^1H NMR spectroscopy, using $\text{Ge}(\text{cat}^{\text{Br}})_2(\text{ACN})_2$ as the catalyst, confirmed that the formation of **3.6** occurs first and is consecutively consumed to make either **3.7** or **3.8** (Figure 4.3).¹¹ Dimer **3.7** is converted into dimer **3.8** over time; **3.7** is the thermodynamic sink of the reaction.

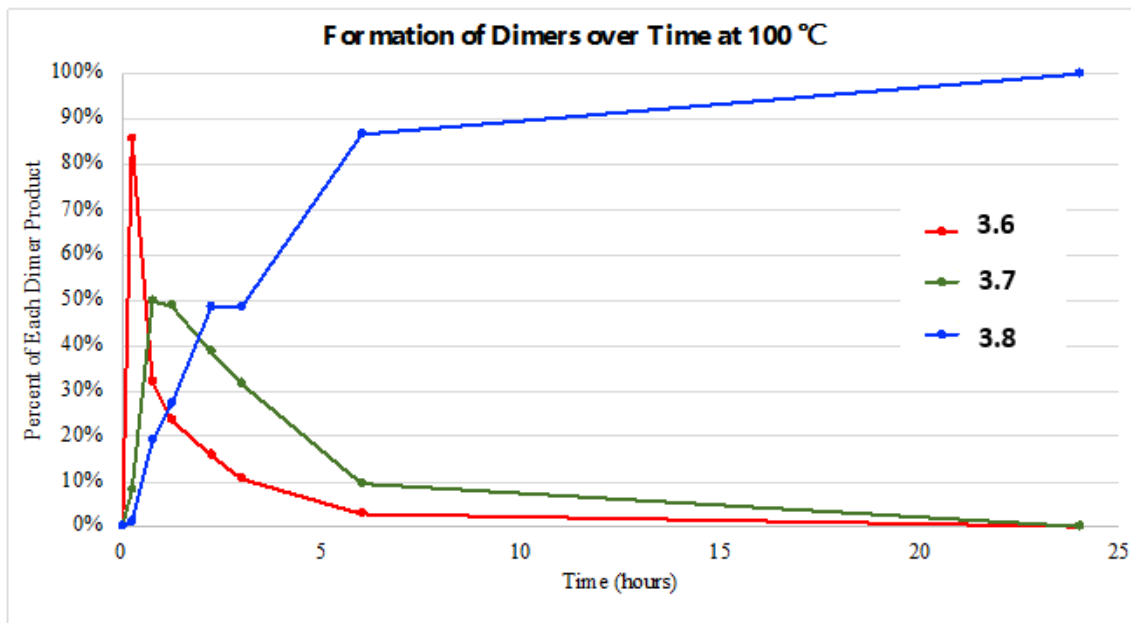


Figure 4.3: Dimers **3.6** (red trace), **3.7** (green trace), and **3.8** (blue trace) formed in reactions with α -methylstyrene and $\text{Ge}(\text{cat}^{\text{Br}})_2(\text{ACN})_2$ over a period of 24 hours at 100 °C.

The experimental studies on the mechanism yielded key pieces of information that will be considered in the proposed mechanism. The VTNA study showed the rate is highly dependent on the concentration of α -methylstyrene. The Hammett plot showed an increase in rate when electron-donating substituents are in the *para*-position of styrene. Furthermore, the negative slope is consistent with the buildup of positive charge in the rate-determining step. Finally, monitoring the formation of dimer products shows the rapid formation of **3.6** which is consumed to form dimers **3.7** and **3.8**.

4.2.2 Computational Calculations

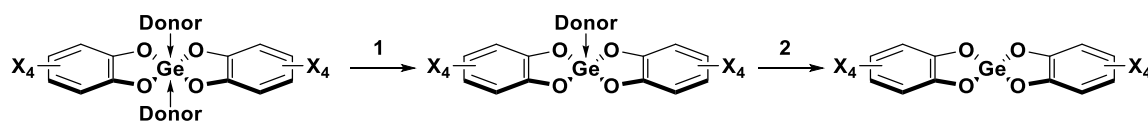
To further understand the reactivity of bis(catecholato)germanes, the energetics of the bis(catecholato)germane core in various states of ligation were calculated using density functional theory at the BP86 D3(BJ)/def2-SVP//PBEh-3c/def2-mSVP level of theory.¹² Geometry optimizations were performed at the PBEh-3c/def2-mSVP level of theory, chosen because it is a computationally inexpensive method that provides accurate geometries; however, the method is not effective at calculating accurate enthalpy and

Gibbs free energy values.^{11g} As such, the optimized geometries were then utilized in a frequency calculation at BP86 D3(BJ)/def2-SVP level of theory, a method and basis set more suitable for generating reliable enthalpy and Gibbs free energy values.^{11h}

4.2.2.1 Weak Donor Dissociation from Bis(catecholato)germanes

The thermodynamics of the stepwise dissociation of the donor ligand from the $\text{Ge}(\text{cat}^{\text{Br}})_2$ core were calculated. The results are presented in Table 4.2. Notably, the dissociation of both the first and second equivalent of a weak donor (THF or ACN) are endergonic (Table 4.2 Entries 1,2). Higher Gibbs free energy values were observed for THF in comparison to ACN, which is consistent with the higher donor ability of THF (Donor number for ACN = 14.1; THF = 20.0).¹³ The analogous Gibbs free energy calculations were reported for bis(perchlorocatecholato)silane and ACN (Table 4.2, Entry 3).⁷ While each subsequent donor dissociation for the bis(perbromocatecholato)germane was endergonic, the dissociation of the first equivalent of acetonitrile from bis(perchlorocatecholato)silane is endergonic but the dissociation of the second equivalent is exergonic. Notably the overall reaction from the bis-ligated $\text{Si}(\text{cat}^{\text{Cl}})_2(\text{ACN})_2$ to the free $\text{Si}(\text{cat}^{\text{Cl}})_2$ is exergonic. The greater stability of hypercoordinate germanium compounds relative to silicon is the likely explanation of the observed differences.

Table 4.2 Calculation of Gibbs free energy of the association of ACN and THF to $\text{Ge}(\text{cat}^{\text{Br}})_2$.



Entry	Element	X	Donor	ΔG Reaction 1 (kJ/mol) ^a	ΔG Reaction 2 (kJ/mol) ^a
1	Ge	Br	ACN	+29.57	+4.40
2	Ge	Br	THF	+89.97	+42.45
3	Si ⁷	Cl	ACN	+12	-31

^a) = BP86 D3(BJ)/def2-SVP//PBEh-3c/def2-mSVP

4.2.2.2 Energetics of the Coordination of Substrate to $\text{Ge}(\text{cat}^{\text{Br}})_2$

The thermodynamics of the coordination of styrene to $\text{Ge}(\text{cat}^{\text{Br}})_2(\text{ACN})_x$ species were calculated, and the results are given in Table 4.3. While the dissociation of one equivalent of acetonitrile from $\text{Ge}(\text{cat}^{\text{Br}})_2(\text{ACN})_2$ was endergonic, coordination of the alkene to the mono-ligated intermediate was, overall, an exergonic process (Figure 4.4). Notably, the relative energies of the cis- and trans-oriented $\text{Ge}(\text{cat}^{\text{Br}})_2(\text{ACN})(\text{styrene})$ complexes were computed and the trans isomer was found to be of lower energy. Coordination of styrene to the donor-free $\text{Ge}(\text{cat}^{\text{Br}})_2$ core is exergonic; however, dissociation of both acetonitrile ligands before styrene coordination is energetically less favourable compared to dissociation of one acetonitrile donor (Figure 4.4). The heptacoordinated species $\text{Ge}(\text{cat}^{\text{Br}})_2(\text{ACN})_2(\text{styrene})$, could not be located as a minimum on the energy surface. As such, the likely pathway to styrene coordination is the dissociation of one ACN donor from $\text{Ge}(\text{cat}^{\text{Br}})_2(\text{ACN})_2$ before the trans coordination of styrene.

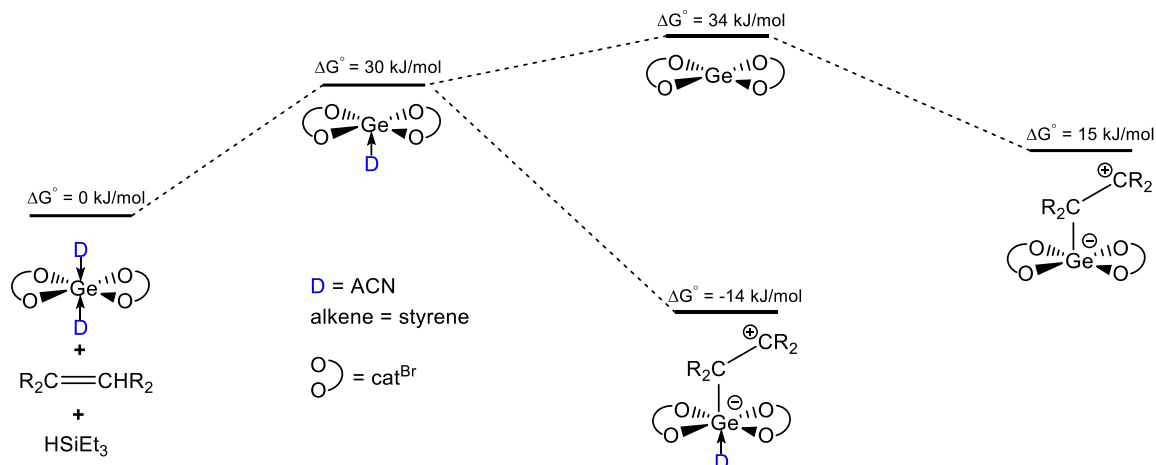


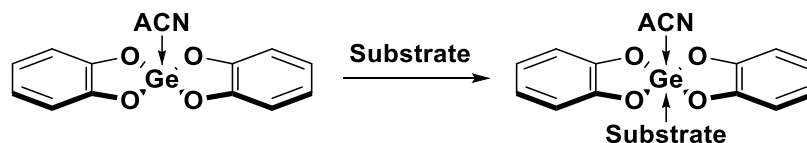
Figure 4.4: Energetics of the coordination of styrene to $\text{Ge}(\text{cat}^{\text{Br}})_2(\text{ACN})_x$ ($x = 0-2$).

With $\text{Ge}(\text{cat}^{\text{Br}})_2(\text{ACN})(\text{styrene})$, with the styrene and acetonitrile in a trans-orientation, calculated to be the lowest energy species along the reaction path, the energetics of the analogous intermediates of an aldehydic, alkenyl, and alkynyl substrate were also calculated (Table 4.3). The coordination of all three substrates, an aldehyde, an alkene, and an alkyne (Table 4.3, Entries 2-4), is energetically more favourable than the re-coordination of a dissociated ACN donor (Table 4.3, Entry 1). Notably, ΔG for the coordination of styrene, p-tolualdehyde, and phenylacetylene to $\text{Ge}(\text{cat}^{\text{Br}})_2(\text{ACN})$ only differ by 1 kJ/mol (Table 4.3, Entries 2-4). Calculation of the $\text{Ge}(\text{cat}^{\text{Br}})_2(\text{ACN})(\text{H})$ intermediate formed from breaking of the H-Si bond of triethylsilane, revealed this pathway to be unfavourable (Table 4.3, Entry 5). Even calculating the SiEt_3^+ cation with the dissociated ACN stabilizing the reactive silylium cation, resulted in an intermediate that is +208 kJ/mol higher in energy and still energetically unfavourable. As such, the coordination of the unsaturated alkenes, alkynes, and aldehydes is preferred over H-Si bond activation.

The DFT calculations provided useful insight into the function of the bis(catecholato)germanes as catalysts. The calculated energetics of the donor dissociation and substrate coordination show the active catalyst species is likely the mono-donor species, $\text{Ge}(\text{cat}^{\text{X}})_2(\text{ACN})$. Furthermore, the coordination of the alkene substrate to the proposed active catalyst species is favoured. While less favoured, the subsequent

recoordination of donor ligand is also an endergonic reaction and should be considered when donor additives are used.

Table 4.3: Calculated Gibbs free energies for the coordination of various substrates to $\text{Ge}(\text{cat}^{\text{Br}})_2(\text{ACN})$.



Entry	Substrate	Gibbs Free Energy (kJ/mol) ^a
1	ACN	-30
2	Styrene	-44
3	Phenylacetylene	-44
4	<i>p</i> -tolualdehyde	-45
5	HSiEt_3	+208

^a) = BP86 D3(BJ)/def2-SVP//PBEh-3c/def2-mSVP

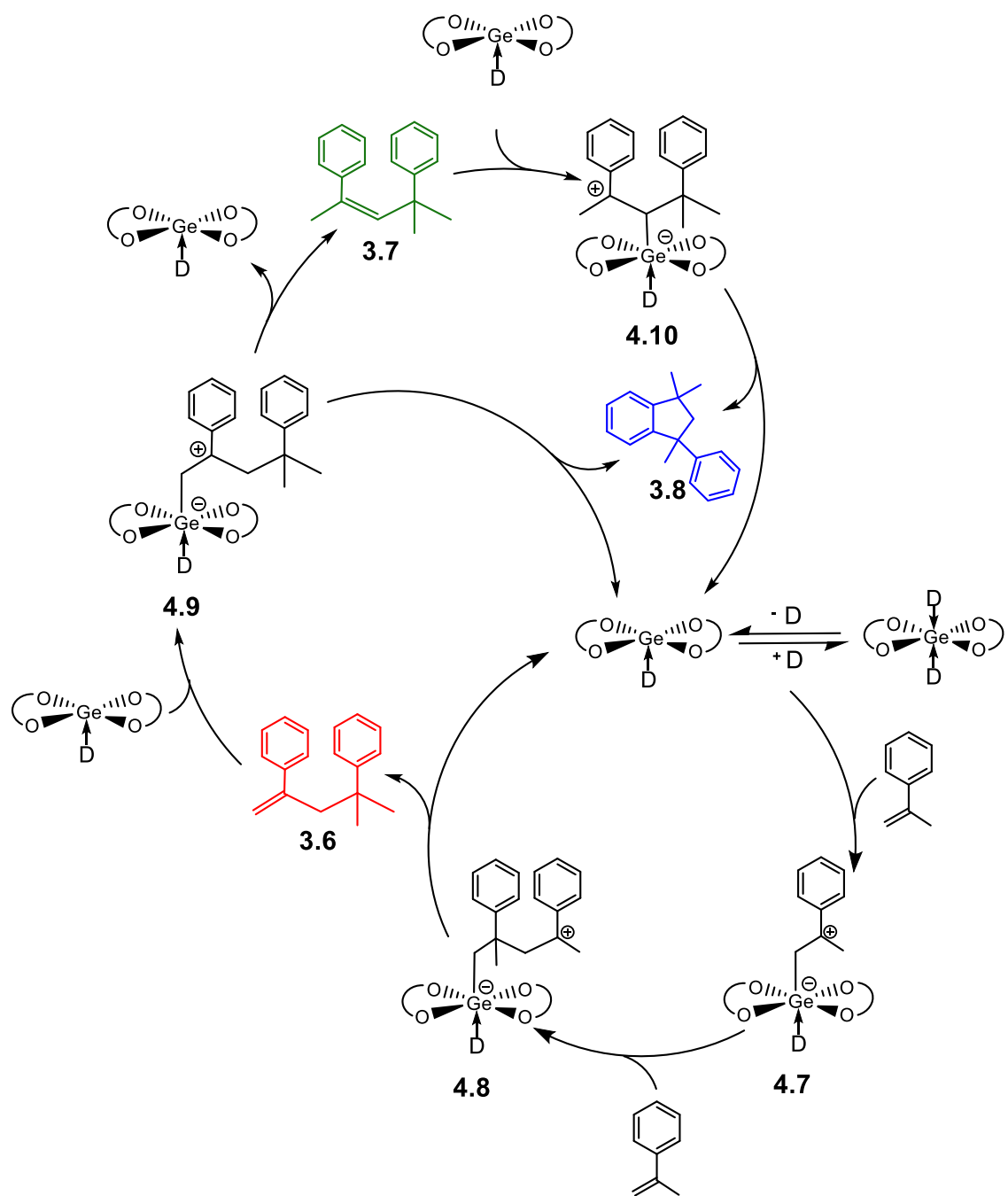
4.2.3 Proposed Mechanism for the Catalytic Oligomerization of α -methylstyrene by Bis(catecholato)germanes

Using the findings described herein, the following mechanism for the dimerization of α -methylstyrene is proposed (Scheme 4.6). The pre-catalyst $\text{Ge}(\text{cat})_2(\text{donor})_2$ and the active catalyst species, and $\text{Ge}(\text{cat})_2(\text{donor})$ are in equilibrium with one another, the position of which is governed by the strength of the donor ligand (Table 4.2). The active catalyst, $\text{Ge}(\text{cat})_2(\text{donor})$, coordinates an equivalent of α -methylstyrene to form intermediate **4.7** (Figure 4.4). The formation of intermediate **4.7** results in the formation of a cationic centre on the α -methylstyrene, which aligns with the buildup of positive charge as suggested by the Hammett plot. Intermediate **4.7** can then add another equivalent of alkene to form **4.8** before releasing the kinetically favoured dimer **3.6** and reforming the active catalyst. Reoordination of **3.6** to the active catalyst can give isomer **3.7** through intermediate **4.9**. While the added steric bulk of α -methylstyrene disfavours further oligomerization, both dimers **3.6** and **3.7** can

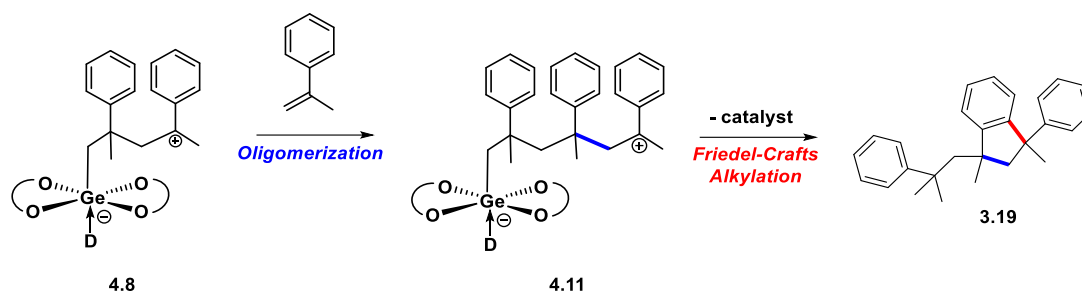
recoordinate, forming intermediates **4.9** and **4.10**, respectively, and facilitate cyclization to form the thermodynamic product **3.8** and recycling the active catalyst. The donor strength of the ACN, THF and Et₂O ligands influences both the pre-catalyst/active catalyst equilibrium and the Lewis acidity of the active catalyst, Ge(cat^X)₂(donor). The VTNA showed a reactant order of 1.5 for the styrene. As such, the rate determining step is likely the addition of the first equivalent of α -methylstyrene to intermediate **4.7**. The fractional reactant order is likely due to the consumption of dimer **3.6** to form the subsequent dimer species.

As shown by the complete conversion to cyclic dimer **3.8**, the acetonitrile derivatives are the most reactive catalysts, which is consistent with the FIA values and the relative energies of the donor-free, mono-ligated and bis-ligated complexes (Figure 4.4). Introducing donor additives to the reaction introduces a competitive pathway in which the active catalyst can coordinate either α -methylstyrene, dimer **3.6**, or the additive. The selectivity for dimer **3.6** obtained upon the addition of ethyl ether suggests that coordination of α -methylstyrene competes well with the added ether; however, coordination of dimer **3.6** is no longer competitive (Table 4.1, Entries 6-7). When using the weaker donors, hexamethyldisiloxane, the coordination of **3.6** is competitive resulting in the mixture of products (Table 4.1, Entry 8). This competitive donor pathway allows for the selectivity of the reaction to be tuned by both the donor strength and concentration of the additives.

Performing the reaction in dichloromethane, the formation of trimer **3.19** was observed (Scheme 4.7). Trimer **3.19** is likely formed by coordination of the styrene derivative to the active catalyst, forming intermediate **4.7**, followed by addition of a second equivalent of α -methylstyrene, forming intermediate **4.8** and addition of a third equivalent of α -methylstyrene then takes place forming intermediate **4.11** (Scheme 4.7). Subsequent Friedel-Crafts alkylation gives the observed cyclic trimer **3.19**. Since, no linear trimer species was observed, it is hypothesized that the Friedel-Crafts alkylation step occurs quite rapidly, preventing further polymeric growth. The influence of donor additives on the reactions performed in DCM need to be investigated further.



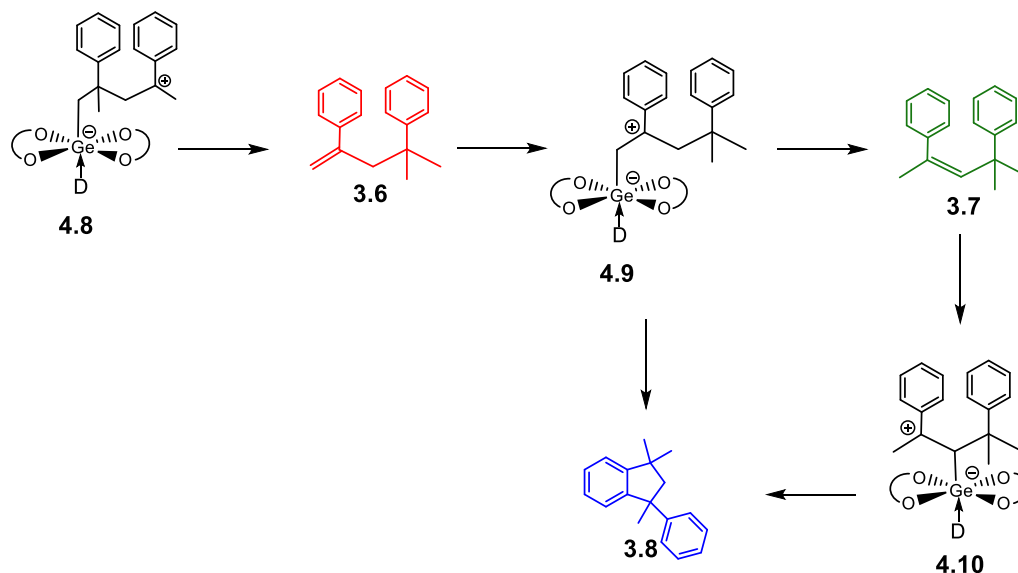
Scheme 4.6: Proposed mechanism for the oligomerization of α -methylstyrene in toluene



Scheme 4.7: Proposed formation of trimer **3.19** by trimerization and subsequent Friedel-Crafts alkylation.

4.3 Comparison to InBr_3 - and HI-Catalyzed Oligomerization of α -methylstyrene

The mechanistic study presented herein illustrates some differences to the InBr_3 - and HI-catalyzed oligomerization mechanisms of α -methylstyrene.^{4,5} In the InBr_3 -catalyzed dimerization of α -methylstyrene, coordination of α -methylstyrene to the catalyst and subsequent addition of another equivalent of α -methylstyrene, gives intermediate **4.2** from which all three dimers **3.6**, **3.7**, and **3.8**, are derived (Scheme 4.1). Similarly, the mechanism of dimerization of α -methylstyrene catalyzed by HI gas has an analogous cationic intermediate that forms **3.6**, **3.7**, and **3.8** directly (Scheme 4.2). In the proposed mechanism for bis(catecholato)germane-catalyzed α -methylstyrene oligomerization, three different carbocationic intermediates are present. Intermediate **4.8**, formed during the initial α -methylstyrene dimerization, is analogous to intermediate **4.2** in the InBr_3 mechanism, which was proposed to lead to dimers **3.6**, **3.7**, or **3.8**. However, based on the rapid formation of **3.6** and subsequent conversion to **3.7** and **3.8** (Figure 4.3), it is proposed that intermediate **4.8** exclusively gives dimer **3.6** and dimer **3.6** then recoordinates to the catalyst to form intermediate **4.9**. Intermediate **4.9** can then form either dimer **3.7** or **3.8**. Reoordination of **3.7** to the catalyst results in a new carbocation intermediate **4.10** which can also undergo a Friedel-Crafts cyclization to form **3.8**. This mechanism is consistent with the mechanism for Brønsted acid HI gas-catalyzed oligomerization as the intermediate in that mechanism, **4.5**, is the same as intermediates **4.8**, **4.9**, and **4.10**, with a proton instead of a Lewis acid (Scheme 4.2 and Scheme 4.8).



Scheme 4.8: Selected portion of the mechanism for the oligomerization of α -methylstyrene by bis(catecholato)germanes highlighting intermediates **4.8**, **4.9**, and **4.10**.

The use of donor additives with the bis(catecholato)germanes to control the selective formation of either dimer **3.6** or **3.8** is similar to the use of methylketones with HI gas. The methylketone establishes an equilibrium between the protonated ketone and the active HI catalyst which both slows down the reaction and inhibits the protonation of trimer **4.3**. We propose that the addition of donor additive to bis(catecholato)germanes results in a similar equilibrium where added ether can coordinate to the mono-donor active catalyst species reforming a bis-donor precatalyst with ether instead of acetonitrile, a process which is competitive with the recoordination of dimer **3.6**. We also propose that the added donors could coordinate to the carbocationic intermediates, **4.7**, **4.8**, **4.9**, and **4.10**, altering the equilibria present.

4.4 Conclusion

Herein, the mechanism of catalysis by bis(catecholato)germanes in the oligomerization of styrenes has been examined. Calculations provide evidence that bis(catecholato)germanes with a single donor molecule ligated is likely the active catalyst. VTNA confirms a dependence on the concentration of alkene in the reaction, with a reactant order of 1.5 for α -methylstyrene, and the Hammett plot confirmed a build-up of positive charge in or

before the rate-determining step. As such the rate determining step was determined to be the addition of the first equivalent of alkene. Monitoring the reaction over time showed the instantaneous formation of dimer **3.6** which is subsequently converted to dimer **3.7** and dimer **3.8**. These experiments lead to a proposed mechanism featuring three carbocation intermediates which accommodate the initial dimerization of **3.6** and the subsequent conversion to **3.7** and **3.8**. This mechanism of Lewis acid catalysis for the oligomerization of α -methylstyrene, improves on the mechanism reported for InBr_3 Lewis acids, in which only a single carbocation intermediate was proposed and is consistent with observations seen in HI gas Brønsted acid catalyzed oligomerization of α -methylstyrene. This mechanism provides the foundation for all future mechanistic studies with the bis(catecholato)germanes, revealing the importance of donor ligand association and dissociation as well as substrate coordination on the reaction which determined the product selectivity of the different dimers. As such, exploring the use of different ligated donors or donor additives to fine tune the selectivity should be explored. While an alkene coordination mechanism was preferred over a silane activation mechanism, future computational studies should explore the reaction of either triethylsilane or an equivalent of α -methylstyrene to intermediate **4.7** to provide further insight into why hydrosilylation of alkenes did not work with the bis(catecholato)germanes as catalysts.

4.5 Experimental

4.5.1 General Experimental

All reactions were conducted under a nitrogen atmosphere using an MBraun Labmaster 130 glovebox. Solvents and reagents were purified by standard methods. NMR data were obtained on a 600 MHz INOVA, 600 MHz Bruker Avance or a 400 MHz Bruker Avance III NMR spectrometer. The standards used were as follows: CH_2Cl_2 (5.32 ppm), toluene- d_7 (2.09 ppm) relative to TMS for ^1H NMR spectra; J values are reported in Hertz.

4.5.2 Hammett Plot

A solution of styrene (0.1 mmol), substituted styrene (0.1 mmol), and mesitylene (0.022 mmol) dissolved in 0.5 mL of toluene- d_8 was added to solid $\text{Ge}(\text{cat}^{\text{Cl}})_2(\text{ACN})_2$

(0.01 mmol) and the reaction was transferred to an NMR tube. The NMR tube was sealed with Parafilm[®] and electrical tape and heated to 100 °C for 30 minutes and then ¹H NMR spectra were recorded at room temperature. The experiments were run in duplicate to $\pm 5\%$ conversion. The integrations of the signals assigned to one of the vinylic hydrogens of the styrene and the styrene derivatives were measured and converted to k_X/k_H values which were plotted against the Hammett parameter for each substituent.

4.5.3 Visual Kinetic Analysis

For each experiment, a suspension of $\text{Ge}(\text{cat}^{\text{Cl}})_2(\text{ACN})_2$ (0.01 mmol) in 0.5 mL of CD_2Cl_2 was transferred to an NMR tube with a Teflon cap. After lock and shimming, 0.25 mL of a solution containing α -methylstyrene was added and a ¹H NMR spectrum was taken every 1-2 minutes for 30 minutes. The total concentration of products formed (**3.6**, **3.7**, **3.8**, **3.19**) was monitored. The concentrations used for each run are presented in Table 4.4.

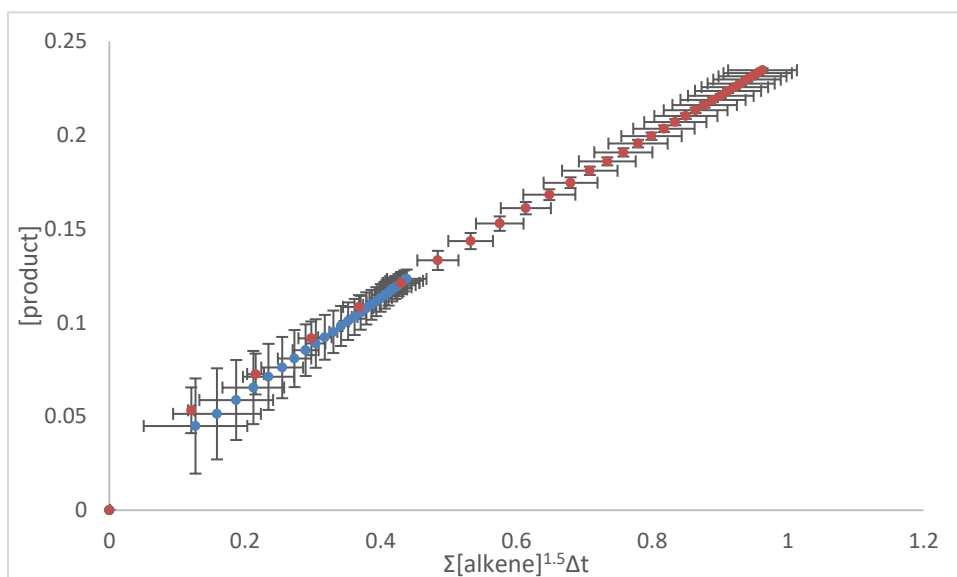


Figure 4.5: VTNA plot of α -methylstyrene oligomerization with a reactant order of 1.5 showing error bars.

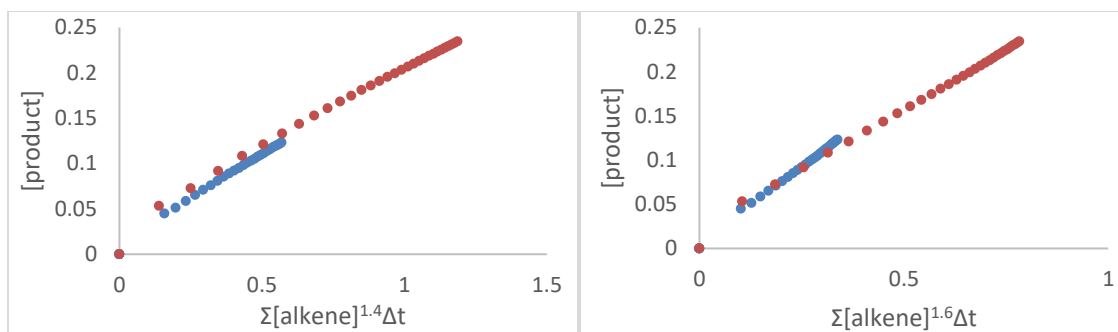


Figure 4.6: VTNA plots of α -methylstyrene oligomerization with reactant orders of 1.4 and 1.6.

Table 4.4: Concentrations used for the VTNA rate study

$[\alpha\text{-methylstyrene}]$	$[\text{catalyst}]$
0.14 M	0.006 M
0.27 M	0.006 M

4.5.4 Computational Details

All calculations have been performed with ORCA 4.1.2 and ORCA 4.2. Geometry optimizations were performed with PBEh-3c/def2-mSVP as implemented in ORCA, using grid5 settings. All calculated geometries have been confirmed as energetic minima on the potential energy surface by analytical calculation of harmonic frequencies at the PBEh-3c level. In case of negative frequencies $>10\text{ cm}^{-1}$, the geometries were reoptimized with grid6, TightOPT and VeryTightSCF settings. For the fluoride ion affinities, the optimized geometries were then used to calculate the single point energies at B3LYP D3(BJ)/def2-TZVPP level of theory using the RIJCOSX approximation and def2/J as the auxiliary basis set. For the reaction coordinate calculations, the optimized geometries were used to calculate the thermodynamic values at BP86 D3(BJ)/def2-SVP level of theory using the RIJCOSX approximation and def2/J as the auxiliary basis set.

References

1. Wiberg, K. B. *Chem. Rev.* **1955**, *4*, 713-743.
2. Burés, J. *Angew. Chem. Int. Ed.* **2016**, *55*, 16084-16087.
3. Hammett, L. P. *J. Am. Chem. Soc.* **1937**, *59*, 96-103.
4. Peppe, C.; Lang, S.; Molinos de Andrade, F.; Borges de Castro, L. *Synlett* **2004**, *10*, 1723-1726.
5. Matsumo, S.; Oseki, T.; Akazome, M.; Otani, Y. *ACS Omega* **2018**, *3*, 17928-17935.
6. Liberman-Martin, A. L.; Bergman, R. G.; Tilley, T. D. *J. Am. Chem. Soc.* **2015**, *137*, 5328-5331.
7. Maskey, R.; Schädler, M.; Legler, C.; Greb, L. *Angew. Chem. Int. Ed.* **2018**, *57*, 1717-1720.
8. Hartmann, D.; Schädler, M.; Greb, L. *Chem. Sci.* **2019**, *10*, 7379-7388.
9. Thaddäus, T.; Roth, D.; Greb, L. *Chem. Eur. J.* **2021**, *27*, 10422-10427.
10. Roth, D.; Wadepohl, H.; Greb, L. *Angew. Chem. Int. Ed.* **2020**, *59*, 20930-20934.
11. Discussed in Chapter 3
12. a) Becke, A. D. *J. Chem. Phys.* **1993**, *98*, 5648-5652; b) Grimme, S.; Antony, J.; Ehrlich, S.; Krieg, H. *J. Chem. Phys.* **2010**, *132*, 154104; c) Grimme, S.; Ehrlich, S.; Goerigk, L. *J. Comput. Chem.* **2011**, *32*, 1456-1465; d) Johnson, E. R.; Becke, A. D. *J. Chem. Phys.* **2005**, *123*, 024101; e) Becke, A. D.; Johnson, E. R. *J. Chem. Phys.* **2005**, *122*, 154101; f) Schafer, A.; Huber, C.; Ahlrichs, R. *J. Chem. Phys.* **1994**, *100*, 5829-

5835; g) Grimme, S.; Brandenburg, J. G.; Bannwarth, C.; Hansen, A. *J. Chem. Phys.* **2015**, *143*, 054107; h) Cavasin, A. T.; Hillisch, A.; Uellendahl, F.; Schneckener, S.; Göller, A. H. *J. Chem. Inf. Model.* **2018**, *58*, 1005–1020.

13. Gutmann, V. *Coord. Chem. Rev.* **1976**, *18*, 225-255.

Chapter 5

5 Bis(catecholato)germanes as Potential Frustrated Lewis Pair Components

5.1 Introduction

Lewis acids and Lewis bases, compounds which can accept an electron pair and donate an electron pair respectively, react with one another to form a Lewis adduct. Typically, the equilibrium for the reaction lies far to the right (Figure 5.1). Hindering the formation of a Lewis adduct by introducing bulky groups onto both the Lewis acid and the Lewis base affects the equilibrium, shifting it to the left in favour of the uncomplexed Lewis acid and base. Using bulky substituents on the Lewis acid and base to synthesize what are now known as frustrated Lewis pairs (FLPs) can facilitate reactions and bond activations cooperatively which cannot be achieved using stable Lewis acid-base pairs.¹

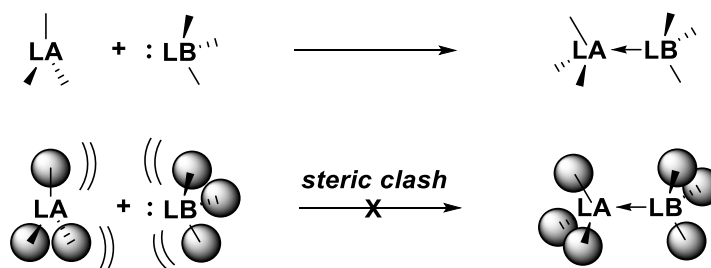


Figure 5.1: The basic premise behind frustrated Lewis pair chemistry

5.1.1 The Design of Frustrated Lewis Pairs

Stephan and coworkers reported the first FLP: the intramolecular boron/phosphorus FLP **1.11** which takes advantage of two different strategies to inhibit Lewis acid-base adduct formation (Chart 5.1).² First, the Lewis acidic boron and Lewis basic phosphorus centres are linked together by a rigid fluorinated aryl bridge (geometrical constraint), preventing an intramolecular interaction between the two centres. Second, the mesityl groups on the phosphine and the pentafluoranyl groups on the borane provide sufficient steric bulk to inhibit intermolecular Lewis acid-base formation (steric constraint). While geometric constraint and steric bulk can be used,

Stephan and coworkers also found that P^tBu_3 and $B(C_6F_5)_3$ could be used to create an intermolecular FLP which utilizes steric bulk alone to generate an FLP.³ Geminal FLP's, in which the Lewis acid and base are located geminal to one another, e.g. LA-CH₂-LB, illustrate the benefit of adding geometrical constraint to the FLP design. In a geminal FLP, to make a Lewis adduct, a three-membered ring would have to be formed, and the strain of the small ring hinders Lewis acid-base-adduct formation. The small ring geometric constraint allows the use of less bulky substituents on at least one component of the pair. For example, whereas the Si/P geminal FLP **5.1** has bulky ^tBu substituents on the phosphine base, the silicon Lewis acid features only halide substituents.⁴

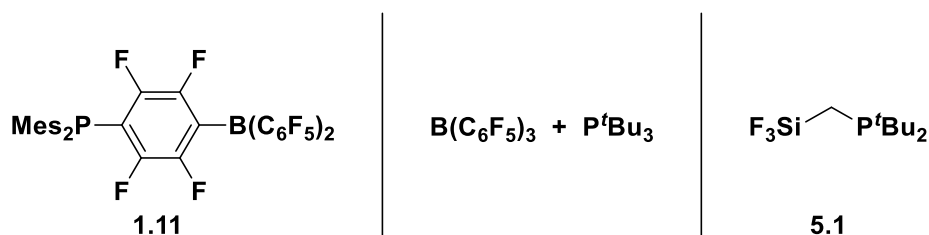


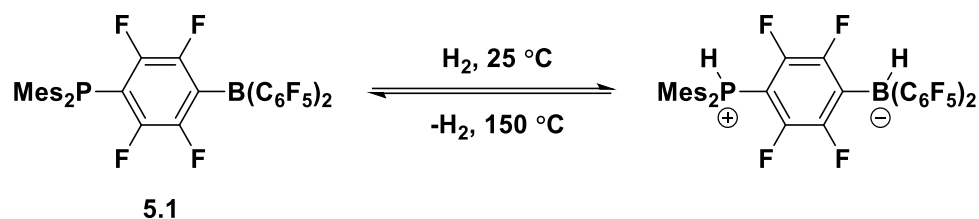
Chart 5.1: FLP's **1.11**, P^tBu_3 and $B(C_6F_5)_3$, and **5.1**.

In the design of frustrated Lewis pairs for catalysis, it is critical that the FLP be able to transfer an activated small molecule onto a substrate. The choice of acid and base not only affects the Lewis acid-base adduct equilibrium, but also affects later steps in the catalytic cycle. For example, N-heterocyclic carbenes (NHC) are strong Lewis bases and can facilitate the activation of dihydrogen when used as part of an FLP.⁵ However, the affinity of NHCs for the hydride prevents transfer of the hydride to a substrate preventing carbenes from being used as FLP catalysts.

5.1.2 Reactivity of Frustrated Lewis Pairs

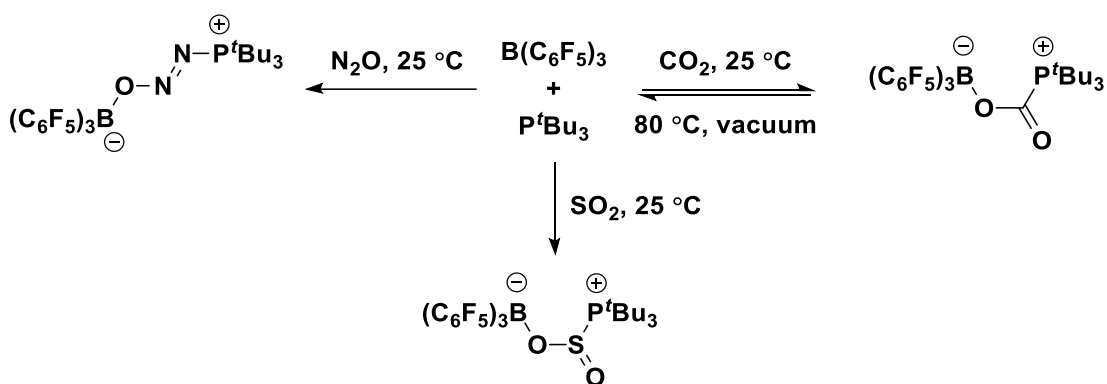
Frustrated Lewis pairs have been used to activate a variety of small molecules. The phenylene-bridged **1.11** can reversibly activate dihydrogen forming **1.12** (Scheme 5.1).² Alongside the report by Power in 2005,⁶ in which dihydrogen activation was achieved by a digermene, these reports presented the first examples of dihydrogen activation by main group elements, an activation that was previously thought to be exclusive to transition metal chemistry and has contributed towards a renaissance in main

group chemistry. Since the initial FLP report, dihydrogen activation has been observed by numerous inter- and intramolecular FLPs.^{1a,b}



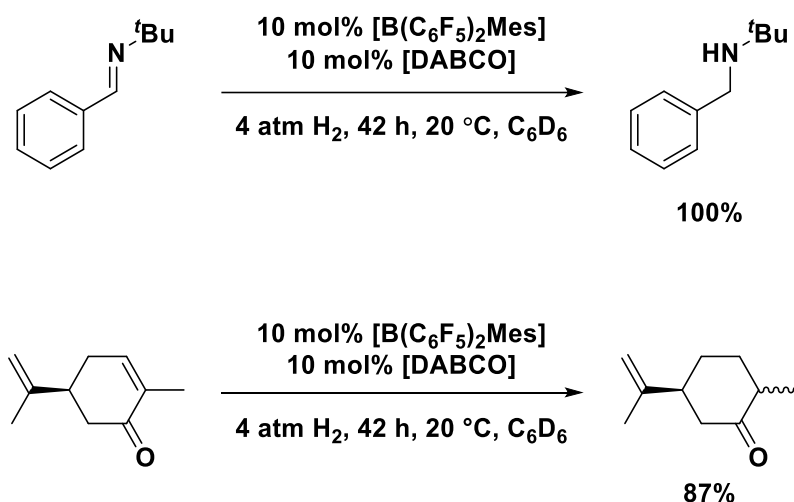
Scheme 5.1: Reversible activation of dihydrogen by FLP **1.11**.

With the impact of main group dihydrogen activation by FLPs, the activation of other small molecules has been explored. For example, FLPs have also been used to activate numerous main group oxides such as CO₂, CO, N₂O, NO, and SO₂. The activation of these main group oxides demonstrates the versatility of FLP chemistry and the potential for the development of various catalytic applications. The activation of CO₂,⁷ N₂O,⁸ and SO₂⁹ has been achieved using P^tBu₃ and B(C₆F₅)₃ under mild conditions (Scheme 5.2). While all three activations proceed at room temperature, the reaction with CO₂ was found to be reversible at higher temperatures and reduced pressure. Reversible activations are indicators of potential use in catalysis where substrate binding and subsequent product release are required. Nonetheless, there are several ongoing challenges in the development of FLPs for catalysis such as the efficient and selective reduction of CO₂ to a C₁ building block.



Scheme 5.2: Activation of various main group oxides by B(C₆F₅)₃ and P^tBu₃.

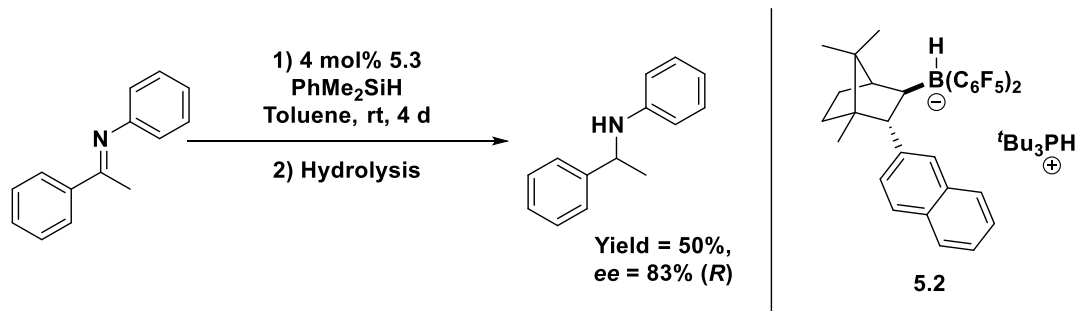
The ability of FLPs to activate small molecules has led to numerous catalytic applications. Notably, FLPs are prominent main group hydrogenation catalysts facilitating the hydrogenation of multiple unsaturated substrates including imines, carbonyl compounds, and alkenes.^{1a,b} For example, using the bulky $B(C_6F_5)_2(Mes)$ Lewis acid with either quinuclidine or 1,4-diazabicyclo[2.2.2]octane (DABCO) as the Lewis base, the hydrogenation of imines and enamines was achieved under mild conditions with 4 atm of H_2 (Scheme 5.3).¹⁰ Furthermore, the selective hydrogenation of the cyclic alkenyl moiety of carvone was achieved; a challenging, selective transformation for conventional palladium and platinum catalysts illustrating an example where the FLP catalyst provides a distinct advantage over transition metal catalysts.¹¹



Scheme 5.3: An example of catalytic hydrogenation of an imine and alkene using $B(C_6F_5)_2Mes$ and DABCO.¹⁰

FLP's have also been shown to catalyze other reactions such as hydrosilylation,¹² hydroamination¹³ and intramolecular cyclizations.¹⁴ For example, the activation of the Si-H bond of dimethylphenylsilane can be achieved using $B(C_6F_5)_3$ and P^tBu_3 in dichloromethane, and the reaction can be incorporated into a catalytic cycle (Scheme 5.4).¹⁵ More specifically, the hydrosilylation of imines can be catalyzed by FLPs to obtain amines, after hydrolysis of the silylamine. Although the use of $B(C_6F_5)_3$ as a Lewis acid catalyst gave higher yields in the hydrosilylation of imines than the use of $B(C_6F_5)_2Mes$ and P^tBu_3 , the FLP catalyst resulted in higher enantioselectivity. The enantioselectivity in

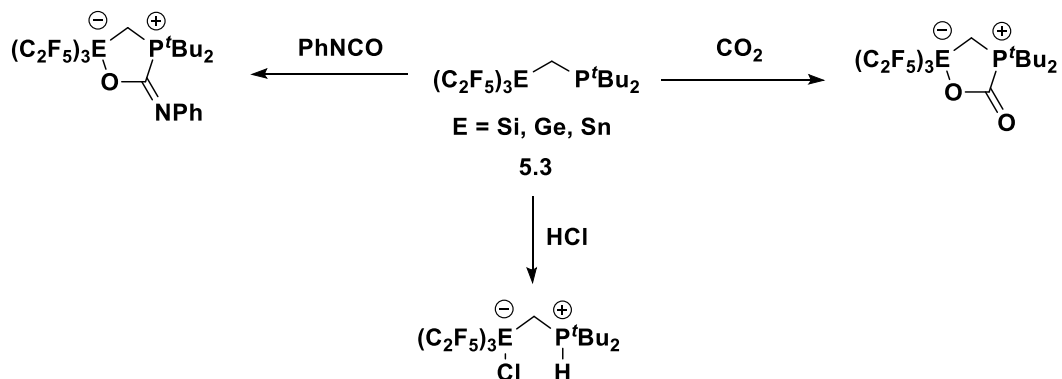
the hydrosilylation of imines was further explored with **5.2**, an FLP with a chiral borane Lewis acid, which resulted in even greater *ee* values than those obtained using $B(C_6F_5)_3$ and P^tBu_3 .



Scheme 5.4: Catalytic hydrosilylation of imines achieved using FLP **5.2**.

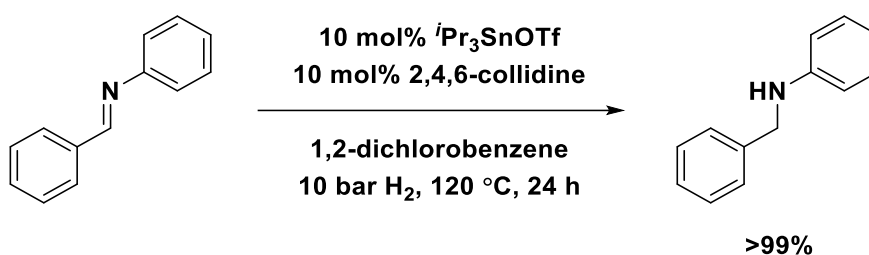
5.1.3 Group 14 Frustrated Lewis Pairs

The use of group 14 based Lewis acids in frustrated Lewis pair chemistry is underexplored compared to the plethora of examples using group 13 elements. One FLP strategy that has worked well for group 14 Lewis acids is the utilization of group 14 Lewis acids as part of geminal FLPs. One example of a group 14 geminal FLP features a methylene bridged *tert*-butyl phosphine Lewis base and a neutral group 14 Lewis acid with fluorinated ethyl substituents **5.3**.¹⁶ Notably, several small molecule activations were achieved including the activation of CO₂ and phenyl isocyanate (Scheme 5.5).



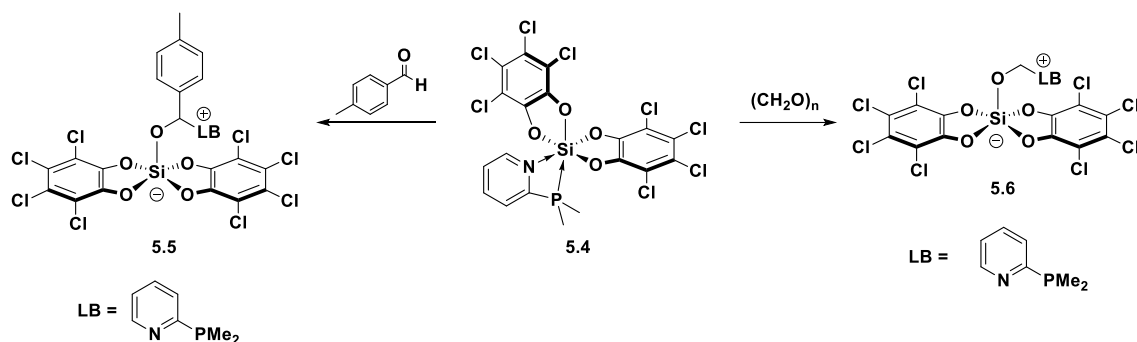
Scheme 5.5: Activation of small molecules using geminal FLP's using group 14 Lewis acid centres.

Another strategy typically used in group 14 FLP chemistry is the use of cationic group 14 Lewis acids as part of an intermolecular FLP. The use of both silylium Lewis acids¹⁷ or the trialkylstannylum Lewis acid, $i\text{Pr}_3\text{SnOTf}$, have been reported.¹⁸ $i\text{Pr}_3\text{SnOTf}$ combined with the nitrogen Lewis bases, DABCO, 2,6-lutidine (lut) and collidine, were tested for FLP reactivity. Notably, the activation of dihydrogen was observed by ^1H NMR spectroscopy. $i\text{Pr}_3\text{SnOTf}$ in combination with various bulky bases were also used as a FLP catalyst in the hydrogenation of a series of imines, ketones and aldehydes (Scheme 5.6).¹⁷



Scheme 5.6: Catalytic hydrogenation of an imine using a Sn/N FLP.

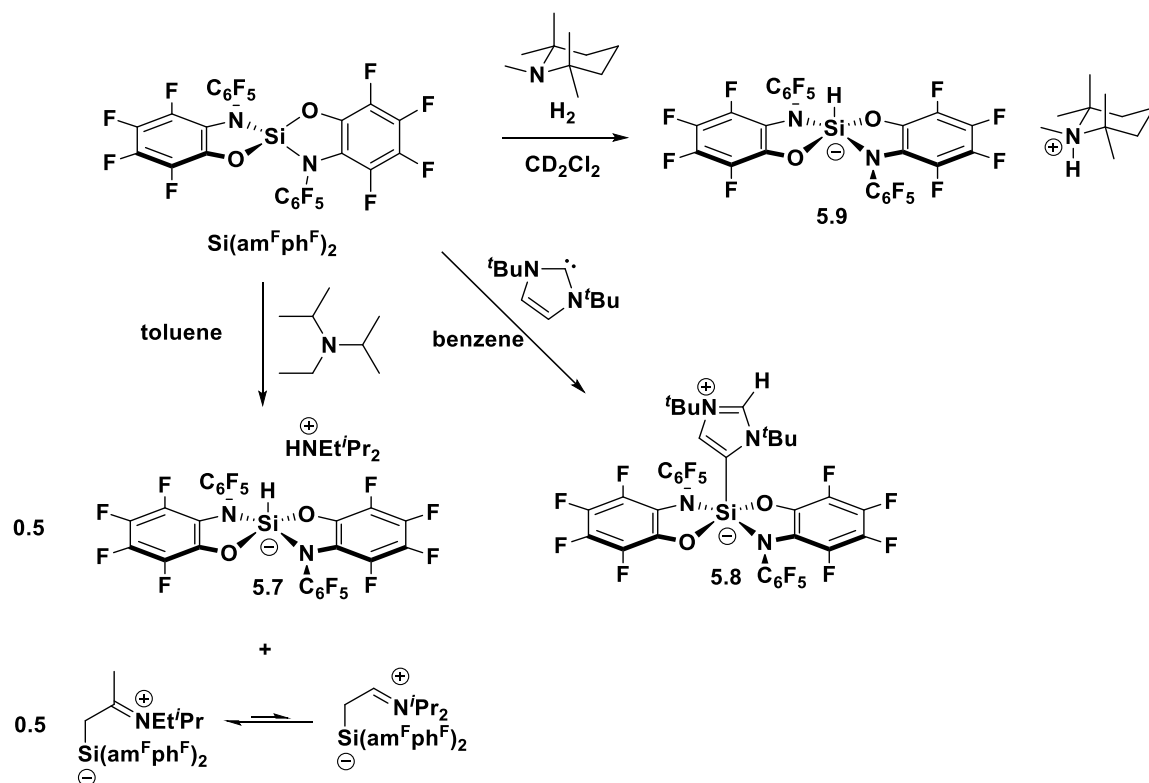
The use of bis(catecholato)silanes as the Lewis acid component in frustrated Lewis pairs has recently been reported.¹⁹ Due to the ability of the bis(catecholato)silanes to bind two Lewis bases (abbreviated as $\text{Si}(\text{cat}^X)_2(\text{donor})_2$), the use of bidentate N,N and N,P ligands as the donors was explored. For example, FLP **5.4** can be synthesized easily by exchange of the sulfolane ligands of $\text{Si}(\text{cat}^{\text{Cl}})_2(\text{sulfolane})_2$ with one equivalent of the N,P bidentate Lewis base (Scheme 5.7). While minimal steric bulk is present on the bidentate Lewis base, binding both Lewis basic sites leads to a strained 4-membered ring, and thus, invokes a geometrically-constrained frustrated Lewis pair. The reactivity of FLP **5.4** is showcased in the activation of *p*-tolualdehyde and paraformaldehyde yielding zwitterions **5.5**, and **5.6**.¹⁹ Furthermore, FLP **5.4** can be used as a catalyst in the dehydrocoupling of dimethylamine borane.¹⁹



Scheme 5.7: Bis(catecholato)silanes in combination with bidentate Lewis bases as FLP's.

Expanding on the bis(catecholato) scaffold, Greb and coworkers recently reported the incorporation of *ortho*-aminophenol substituents (which will be abbreviated as $\text{am}^{\text{X}}\text{ph}^{\text{X}}$, where X denotes the substituents on the aminophenol) instead of catechol substituents for silicon Lewis acids, as illustrated in the Lewis acid $\text{Si}(\text{am}^{\text{F}}\text{ph}^{\text{F}})_2$ (Scheme 5.8).²⁰ There are two advantages to using the aminophenol ligands. First, the nitrogen centres can be substituted with an additional aryl ring providing more steric bulk around the Lewis acid centre. Secondly, unlike the bis(catecholato)silanes, $\text{Si}(\text{am}^{\text{F}}\text{ph}^{\text{F}})_2$ exists without a weakly bound donor ligand. Evidently, the lone pair on the nitrogen of the aminophenol ligand can stabilize the Lewis acidic silicon centre sufficiently. The cleavage of dihydrogen was attempted using $\text{Si}(\text{am}^{\text{F}}\text{ph}^{\text{F}})_2$ and a series of Lewis bases. When P^tBu_3 , tetramethylpiperidine (tmp), or di-*tert*-butylpyridine ($\text{py}^{t\text{Bu}2}$) were used as bulky Lewis bases, no hydrogen activation was observed. Using *N,N'*-diisopropyl-*N*'-ethylamine (DIPEA) as the Lewis base, the formation of half an equivalent of the hydrosilicate complex **5.7** was observed without exposure to dihydrogen. Instead, dehydrogenation of DIPEA occurs breaking the C-H bond of one of the alkyl substituents forming a Si-H bond and a Si-C bond. The NHC, 1,3-di-*tert*-butyl-1,3-imidazol-2-ylidene (*ItBu*), also reacted with $\text{Si}(\text{am}^{\text{F}}\text{ph}^{\text{F}})_2$ in the absence of dihydrogen forming the abnormal NHC adduct **5.8**. Finally, dihydrogen cleavage was achieved using 1,2,2,6,6-pentamethylpiperidine (pmp) and $\text{Si}(\text{am}^{\text{F}}\text{ph}^{\text{F}})_2$. In equimolar amounts of Lewis acid and base, the reaction required an elevated temperature of 115 °C and long reaction times (2 days) to give a 45% yield of **5.9** and only a 64% yield after 8 days. Increasing the amount of pmp to 100 eq. the reaction proceeded at room temperature, although only a yield of 13% was achieved after 20 hours. Increasing the temperature slightly, to 40 °C, a yield of

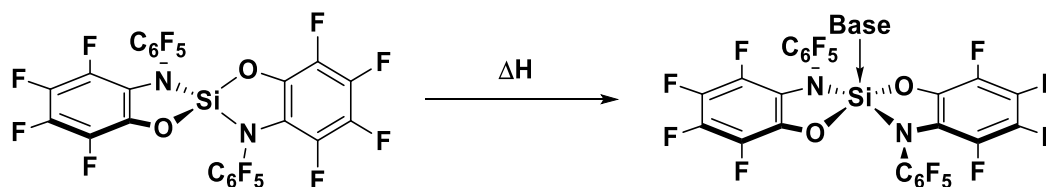
71% was obtained after 7 days. Thus, the first activation of H₂ by a tetrahedral silicon compound was achieved.



Scheme 5.8: Reactivity of $\text{Si}(\text{am}^{\text{Fph}^{\text{F}}})_2$ with various bulky bases.

To further understand the energetics of the hydrogen activation, the Gibbs free energy values of the intermediates involved in Lewis acid-base adduct formation were analyzed using DFT calculations (Table 5.1). Notably, the formation of the Lewis adducts between $\text{Si}(\text{am}^{\text{Fph}^{\text{F}}})_2$ and P^tBu_3 , tmp, DIPEA, and I^tBu were found to be exergonic (Table 5.1, Entries 1-4). For $\text{py}^{t\text{Bu}2}$, an optimized geometry for the Lewis adduct could not be located. The only Lewis base that had an endergonic Lewis adduct formation was pmp, which is also the only Lewis base tested that achieved FLP dihydrogen activation with $\text{Si}(\text{am}^{\text{Fph}^{\text{F}}})_2$ (Table 5.1, Entry 5).

Table 5.1: Calculated Gibbs free energies of formation for Lewis acid-base adduct formation.



Entry	Lewis Base	ΔG (kJ/mol) ^a
1	P ^t Bu ₃	-20.7
2	tmp	-31.5
3	DIPEA	-6.5
4	<i>t</i> Bu	-42.7
5	pmp	3.8

^a) = DLPNO-CCSD(T)/aug-cc-pVQZ//PBE0-D3(BJ)/def2-TZVPP

5.1.4 Project Goal

One of the common methods to generate an FLP is to introduce a bulky base to a bulky Lewis acid *in situ*. Sufficient steric bulk is required either to completely prevent Lewis acid-base adduct formation or to allow a weak hemilabile interaction between the Lewis acid and base. The use of sterically encumbered monodentate Lewis bases, such as bulky amines or phosphines, with bis(catecholato)germanes has not been explored. The goal of this project was to explore the synthesis of frustrated Lewis pairs composed of bis(catecholato)germanes and monodentate bulky Lewis bases and to explore the activation of small molecules and the use of these FLPs as catalysts. The structure and relative energies of the Lewis acid-base pairs were explored computationally to assess the strength of the interaction and the reactivity of the complexes.

5.2 Results and Discussion

To gather insight on the steric bulk required to generate a frustrated Lewis pair using bis(catecholato)germanes as the Lewis acid component, the interaction between

bis(catecholato)germanes and a variety of bulky bases was examined in the absence of any substrate.

5.2.1 Synthesis of Lewis Acid-Base Adducts

The Baines group has shown that the pyridine ligands of $\text{Ge}(\text{dtbc})_2(\text{py})_2$ can be exchanged with other amines such as triethylamine.²¹ When $\text{Ge}(\text{dtbc})_2(\text{py})_2$ is stirred in an excess of triethylamine and then the volatiles are removed, the desired $\text{Ge}(\text{dtbc})_2(\text{NEt}_3)_2$ is obtained. The ligand exchange strategy was applied with the bulkier Lewis base, 2,6-lutidine (lut). To explore this as a potential synthetic route, $\text{Ge}(\text{dtbc})_2(\text{py})_2$ was dissolved in 250 eq. of 2,6-lutidine and allowed to stir overnight (Scheme 5.9). Vacuum distillation of the reaction mixture to remove volatiles yielded a brown powder. The ^1H NMR spectrum of the brown powder revealed that the signals from the 3,5-di-*tert*-butyl catecholato fragment of $\text{Ge}(\text{dtbc})_2(\text{py})_2$ (1.18, 1.40, 6.50, and 6.78 ppm) had disappeared and new signals at 1.22, 1.37, 6.56, and 6.66 were present and assigned to the 3,5-di-*tert*-butyl catecholato fragment of the product. Furthermore, the signals from the pyridine moiety of $\text{Ge}(\text{dtbc})_2(\text{py})_2$ were no longer present. Signals at 7.75, 7.14 and a signal at 2.58 ppm were observed and assigned to the 2,6-lutidine fragment. Integration of the ^1H signals revealed a 1:1 ratio between the catecholato and lutidine fragments. Notably, these signals are shifted from those of free 2,6-lutidine (Figure 5.2). To further identify the product, ESI-MS was performed. A cluster of signals consistent with the formula $\text{C}_{42}\text{H}_{61}\text{GeN}_2\text{O}_5$ was observed at m/z 743.3836 corresponding to the exact mass of $\text{Ge}(\text{dtbc})_2(\text{lut})_2 + \text{H}_3\text{O}^+$. No signals were observed corresponding to $\text{Ge}(\text{dtbc})_2(\text{lut})$ or $\text{Ge}(\text{dtbc})_2(\text{lut})_2$ with either a H^+ or a Na^+ . The mass spectrum result suggests the incorporation of water into the structure.



Scheme 5.9: Reaction of $\text{Ge}(\text{dtbc})_2(\text{py})_2$ with excess 2,6-lutidine.

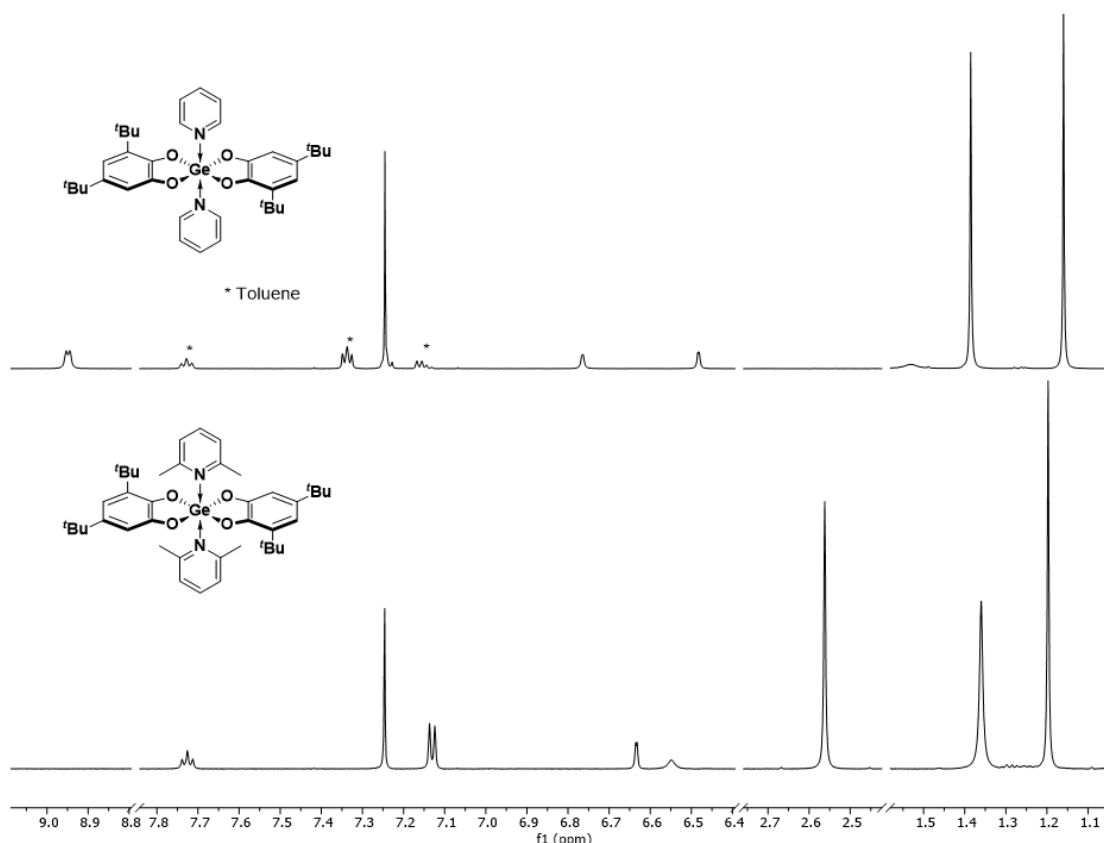


Figure 5.2: ¹H NMR spectra stack (600 MHz) of Ge(dtbc)₂(py)₂ and Ge(dtbc)₂(lut)₂ in CDCl₃.

Attempts to grow single crystals suitable for X-ray crystallography resulted in a clear, colourless crystal that was, surprisingly, identified as Ge(dtbc)₂(py)₂. Based on the lack of any signals in the ¹H NMR spectrum of the product corresponding to the pyridine adduct, the signals observed corresponding to lutidine and the small number of crystals formed, it is proposed that Ge(dtbc)₂(py)₂ is a minor component in the product mixture; however, the pyridine adduct preferentially crystallized. Evidently, Ge(dtbc)₂(py)₂ is present even after ligand exchange reaction with a substantial excess of 2,6-lutidine (250 eq.). Nevertheless, the ¹H NMR spectrum of Ge(dtbc)₂(lut)₂ provides strong evidence that a Lewis adduct is formed. Since pyridine has similar basicity to 2,6-lutidine which may explain the presence of Ge(dtbc)₂(py)₂ in the mixture, the starting material was changed to the THF-ligated complexes because THF is less basic (Donor Number, DN = 20) than the bulky base that is to be installed (For comparison: pyridine, DN = 33.1).

The reactions of bis(catecholato)germanes, $\text{Ge}(\text{dtbc})_2(\text{THF})_2$, $\text{Ge}(\text{cat}^{\text{Cl}})_2(\text{THF})_2$, and $\text{Ge}(\text{cat}^{\text{Br}})_2(\text{THF})_2$, with 2,6-lutidine, 2,6-di-*tert*-butylpyridine, and tri-*tert*-butylphosphine were explored. Due to the insolubility of the halogenated bis(catecholato)germanes, the experiments involving $\text{Ge}(\text{cat}^{\text{Cl}})_2(\text{THF})_2$, or $\text{Ge}(\text{cat}^{\text{Br}})_2(\text{THF})_2$ with either 2,6-lutidine or 2,6-di-*tert*-butylpyridine resulted in white insoluble powders which could not be characterized using solution-based methods such as NMR spectroscopy and ESI-MS.

The reaction of $\text{Ge}(\text{dtbc})_2(\text{THF})_2$ and 2,6-lutidine in DCM was performed and the resulting crude mixture was analyzed by ^1H NMR spectroscopy which revealed a mixture of products in solution. The resulting mixture was placed in an NMR tube and layered with hexanes which lead to the formation of several single crystals suitable for X-ray crystallography. The molecular structure of the crystal was determined to be $[\text{H-Lut}][\text{Ge}(\text{dtbc})_2\text{Cl}]$ (Figure 5.3). The most reasonable source of chlorine is either from unreacted $\text{GeCl}_2\cdot\text{diox}$ from the synthesis of $\text{Ge}(\text{dtbc})_2(\text{THF})_2$ or the solvent, dichloromethane. To eliminate dichloromethane as a potential source of chlorine, the reaction was performed in toluene.

The reaction of $\text{Ge}(\text{dtbc})_2(\text{THF})_2$ with one equivalent of lutidine in toluene resulted in a yellowish-green reaction mixture. Removal of the volatiles and crystallization of the off-white solid in hexanes yielded a white precipitate and a green mother liquor. ^1H NMR spectroscopy of the green mother liquor in C_6D_6 revealed broad signals for the lutidine component at 6.47, 5.99, and 2.68 ppm, and signals for the catecholato component at 7.26, 7.06, 1.61, 1.33 ppm in a ratio of 1:2 suggesting the structure: $\text{Ge}(\text{dtbc})_2(\text{Lut})$ (Figure 5.4 and Scheme 5.10). ESI-MS was performed in acetonitrile and revealed a signal in positive ion mode at m/z 662.2891 which is assigned to $\text{Ge}(\text{dtbc})_2(\text{Lut}) + \text{ACN} + \text{H}^+$, in which an equivalent of ACN, used as the carrier solvent, was incorporated into the mass of the fragment. These results are consistent with the formation of a Lewis adduct between $\text{Ge}(\text{dtbc})_2$ and 2,6-lutidine. However, the broadness of the ^1H signals for the lutidine component is indicative of a dynamic process in solution which might suggest lability of the lutidine in $\text{Ge}(\text{dtbc})_2(\text{Lut})$.

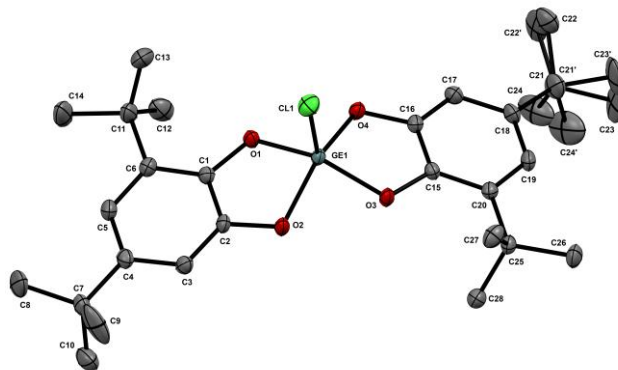


Figure 5.3: Thermal ellipsoid plot of $[\text{Ge}(3,5\text{-dtbc})_2\text{Cl}]^-$ showing naming and numbering scheme. Ellipsoids are at the 50% probability level and hydrogen atoms and cation were omitted for clarity. Selected bond lengths (\AA) and angles ($^\circ$): $\text{Ge1-O1} = 1.8322(12)$, $\text{Ge1-O2} = 1.8585(13)$, $\text{Ge1-O3} = 1.8416(12)$, $\text{Ge1-O4} = 1.8261(13)$, $\text{Ge1-Cl1} = 2.1755(7)$; $\text{O1-Ge1-O3} = 153.96(6)$, $\text{O1-Ge1-O4} = 87.37(6)$, $\text{O1-Ge1-Cl1} = 101.95(5)$.

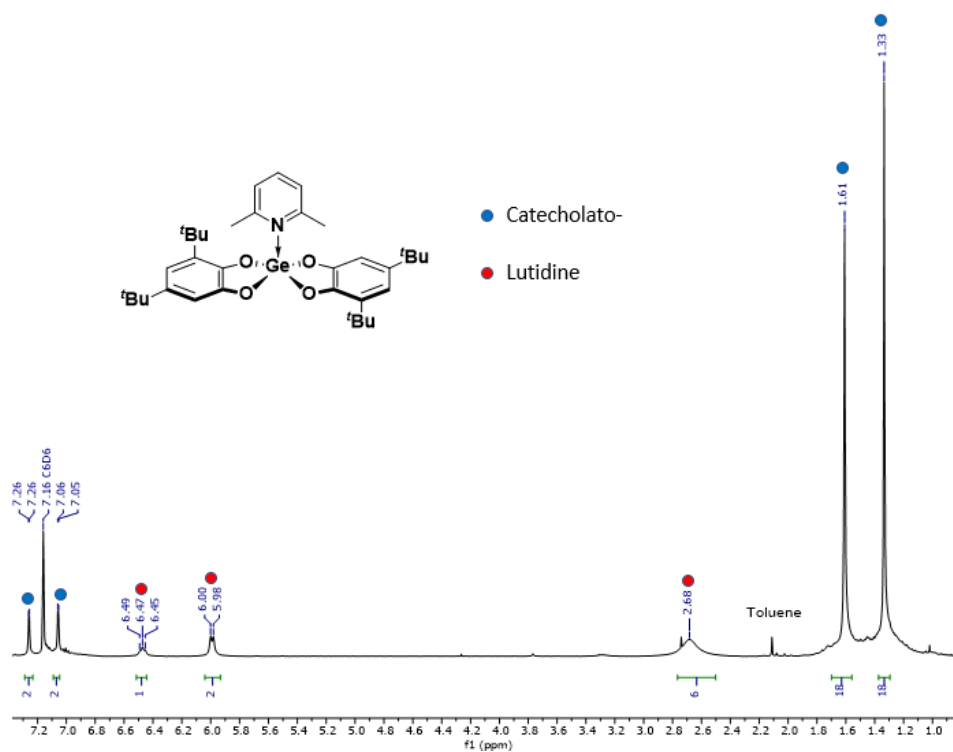
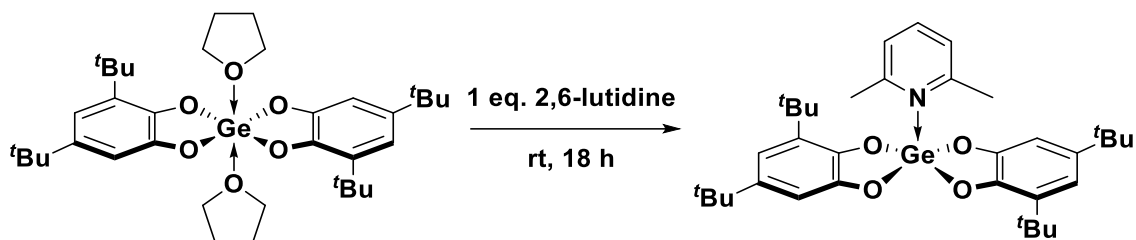
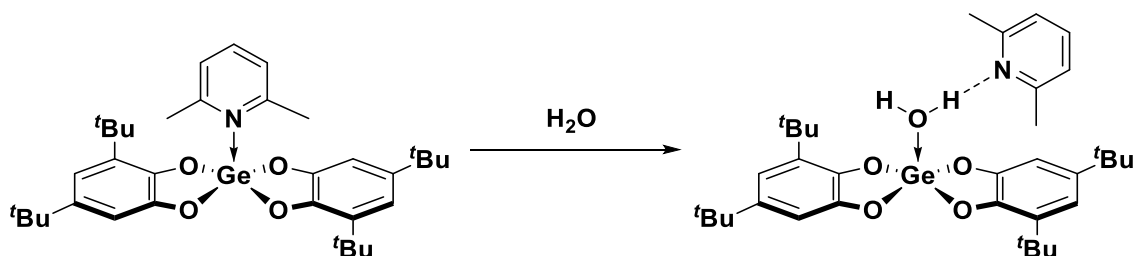


Figure 5.4: ^1H NMR (400 MHz, C_6D_6) spectrum of $\text{Ge}(\text{dtbc})_2(\text{lut})$



Scheme 5.10: Reaction of $\text{Ge}(\text{dtbc})_2(\text{THF})_2$ with 2,6-lutidine.

Attempts to grow crystals under an inert atmosphere were unsuccessful. However, when an NMR tube of $\text{Ge}(\text{dtbc})_2(\text{lut})$ in C_6D_6 was exposed to air/moisture, crystals suitable for X-ray crystallography were obtained (Figure 5.5). The molecular structure shows the coordination of water to the bis(catecholato)germane core, displacing the lutidine. While no hydrogens from the water molecule were found in the difference map, hydrogen bonding was inferred from the distance between O1-N1 2.610 Å and the bond angles. One of the hydrogens of the water molecule is participating in hydrogen bonding with the nitrogen centre of lutidine. The formation of the water adduct highlights the moisture sensitivity of the $\text{Ge}(\text{dtbc})_2(\text{lut})$ which is in contrast to the water-stable $\text{Ge}(\text{dtbc})_2(\text{py})_2$ derivative (Scheme 5.11). Furthermore, the formation of the water adduct highlights the lability of the Ge-N bond between the $\text{Ge}(\text{dtbc})_2$ and the lutidine fragments which shows potential to achieve the free Lewis acid and base in solution.



Scheme 5.11: Addition of water to $\text{Ge}(\text{dtbc})_2(\text{lut})$.

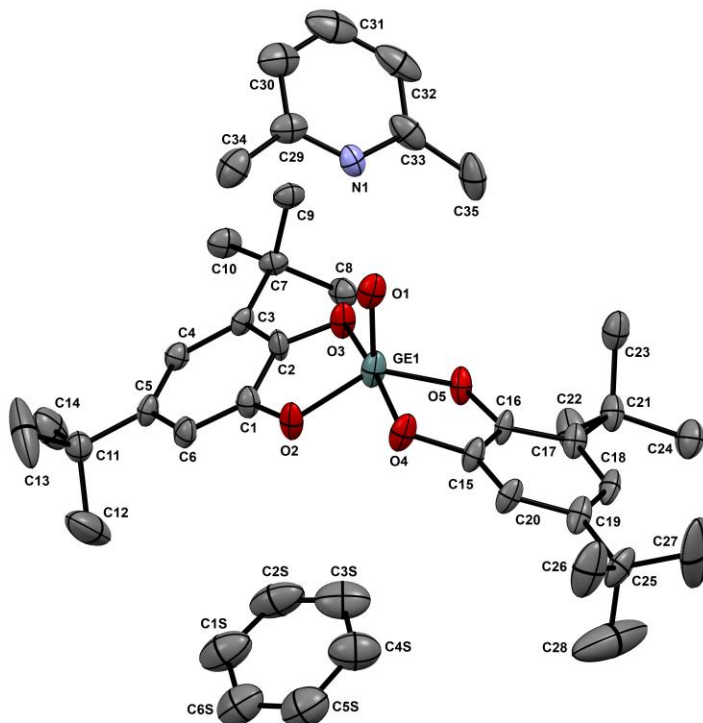
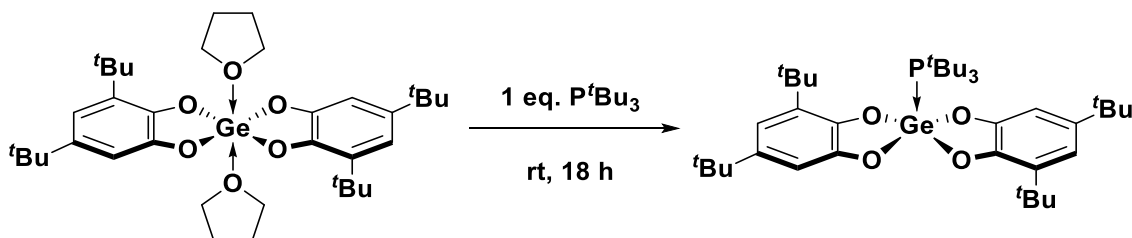


Figure 5.5: Thermal ellipsoid plot of $\text{Ge}(\text{3,5-dtbc})_2\text{OH}_2\text{-lut}$, with a C_6D_6 solvent molecule showing naming and numbering scheme. Ellipsoids are at the 50% probability level and hydrogen atoms were omitted for clarity. Selected bond lengths (Å) and angles ($^\circ$): $\text{Ge1-O1} = 1.788(8)$, $\text{Ge1-O2} = 1.811(7)$, $\text{Ge1-O3} = 1.854(6)$, $\text{Ge1-O4} = 1.871(7)$, $\text{Ge1-O5} = 1.825(7)$; $\text{O2-Ge1-O5} = 129.6(4)$, $\text{O3-Ge1-O4} = 170.1(4)$.

Similar to the reaction with $\text{Ge}(\text{dtbc})_2(\text{THF})_2$ and 2,6-lutidine, the reaction of $\text{Ge}(\text{dtbc})_2(\text{THF})_2$ with one equivalent of P^tBu_3 was attempted in both DCM and toluene (Scheme 5.12). When the reaction was performed in DCM, several signals in the $^{31}\text{P}\{^1\text{H}\}$ NMR spectrum of the reaction mixture were observed consistent with the reported results of the reaction of P^tBu_3 with $\text{Si}(\text{am}^{\text{F}}\text{ph}^{\text{F}})_2$ using DCM as a solvent; decomposition to multiple products was reported.²⁰ Notably, the reaction in toluene was cleaner as evident by $^{31}\text{P}\{^1\text{H}\}$ NMR spectroscopy. Removal of volatiles yielded a white powder. The ^1H NMR spectrum of the white powder revealed a change in the ^1H chemical shifts assigned to the catecholato- and phosphine moieties. The signals at 1.38, 1.66, 7.02 and 7.15 ppm in the ^1H NMR spectrum were assigned to the catecholato ligands while the doublet with a J coupling of 2.1 Hz at 1.22 ppm was assigned to the phosphine. The two components

are present in a 1:1 ratio. $^{31}\text{P}\{^1\text{H}\}$ NMR spectrum of the white powder revealed a signal at 53.0 ppm which is similar in shift to that observed in the reaction of P^tBu_3 with $\text{Si}(\text{am}^F\text{ph}^F)_2$ (56 ppm in CD_2Cl_2).²⁰ Based on the similar chemical shifts of the $^{31}\text{P}\{^1\text{H}\}$ signals to those obtained in the reaction with $\text{Si}(\text{am}^F\text{ph}^F)_2$ the formation of the Lewis adduct $\text{Ge}(\text{dtbc})_2(\text{P}^t\text{Bu}_3)$ is proposed.



Scheme 5.12: Reaction of $\text{Ge}(\text{dtbc})_2(\text{THF})_2$ with tri-*tert*-butylphosphine.

The halogenated bis(catecholato)germanes, $\text{Ge}(\text{cat}^{\text{Cl}})_2(\text{THF})_2$ and $\text{Ge}(\text{cat}^{\text{Br}})_2(\text{THF})_2$, were also reacted with P^tBu_3 . One equivalent of P^tBu_3 was added to a suspension of the insoluble $\text{Ge}(\text{cat}^{\text{Cl}})_2(\text{THF})_2$ or $\text{Ge}(\text{cat}^{\text{Br}})_2(\text{THF})_2$ in toluene. As the phosphine was added, dissolution of the suspended $\text{Ge}(\text{cat}^{\text{Cl}})_2(\text{THF})_2$ or $\text{Ge}(\text{cat}^{\text{Br}})_2(\text{THF})_2$ was observed. After removal of the solvent, a white solid was obtained. The ^1H NMR spectrum of the solid derived from $\text{Ge}(\text{cat}^{\text{Cl}})_2(\text{THF})_2$ revealed a doublet at 1.28 ppm and the $^{31}\text{P}\{^1\text{H}\}$ NMR spectrum showed a single singlet at 62.1 ppm, downfield from free P^tBu_3 at 56.7 ppm. For the brominated derivative, a doublet at 0.79 ppm in the ^1H NMR spectrum and a signal at 53.02 ppm in the $^{31}\text{P}\{^1\text{H}\}$ NMR spectrum was observed. These chemical shifts are consistent with those obtained from the reactions of $\text{Ge}(\text{dtbc})_2$ and $\text{Si}(\text{am}^F\text{ph}^F)_2$ with P^tBu_3 .²⁰

Similar to the reactions of $\text{Ge}(\text{dtbc})_2(\text{THF})_2$ and the reported reaction with $\text{Si}(\text{am}^F\text{ph}^F)_2$ with P^tBu_3 in DCM,²⁰ the reactions between either $\text{Ge}(\text{cat}^{\text{Cl}})_2(\text{THF})_2$ or $\text{Ge}(\text{cat}^{\text{Br}})_2(\text{THF})_2$ with P^tBu_3 in DCM resulted in multiple signals in the $^{31}\text{P}\{^1\text{H}\}$ NMR spectrum. Single crystals were obtained from the crude reaction mixture derived from $\text{Ge}(\text{cat}^{\text{Cl}})_2(\text{THF})_2$ and P^tBu_3 in DCM, by layering hexanes on the crude product mixture in an NMR tube. The molecular structure of the crystals revealed the formation of $[\text{Cl-P}^t\text{Bu}_3]_2[\text{Ge}(\text{cat}^{\text{Cl}})_2\text{Cl}_2]$ (Figure 5.6). The most plausible source for the additional chlorine

atoms is the solvent, DCM, or potentially, unreacted $\text{GeCl}_2 \cdot \text{diox}$ from the synthesis of $\text{Ge}(\text{cat}^{\text{Cl}})_2(\text{ACN})_2$. Interestingly, when the bis(catecholato)germanes are reacted with an equivalent of NBu_4Cl ,²² the pentacoordinated $\text{Ge}(\text{cat}^{\text{X}})_2\text{Cl}^-$ complex was formed and not the di-chloride species which indicates that the chloride source is present in significant amounts. Single crystals suitable for X-ray crystallography were also grown from the crude reaction mixture of $\text{Ge}(\text{cat}^{\text{Br}})_2(\text{THF})_2$ and P^tBu_3 in CD_2Cl_2 upon slow exposure to air/moisture. The molecular structure revealed the oxo-bridged dianion $[\text{Ge}(\text{cat}^{\text{Br}})_2\text{-O-Ge}(\text{cat}^{\text{Br}})_2]^{2-}$, with two $[\text{H-P}^t\text{Bu}_3]^+$ counteranions. The formation of the oxo-bridged structure is likely from the addition of water, illustrating the water sensitivity of these Lewis adducts. Once again, these crystal structures illustrate the lability of the bulky donors which demonstrates the potential for these adducts to be used as FLPs.

The reactivity of bis(catecholato)germanes with weakly bound donors with 2,6-lutidine and tri-*tert*-butylphosphine resulted in noticeable changes in the ^1H NMR spectra and, where applicable, the $^{31}\text{P}\{^1\text{H}\}$ NMR spectra of the reaction mixture in comparison to the two starting materials and is consistent with the formation of Lewis adducts. Some FLPs show no sign of adduct formation by NMR spectroscopy, such as the FLP derived from $\text{B}(\text{C}_6\text{F}_5)_3$ with P^tBu_3 .³ The lack of change in the NMR spectra indicates minimal or no interaction between the Lewis acid and base due to steric bulk. However, FLP reactivity can be achieved even when a Lewis adduct is formed. For example, while borane **5.10** exhibits no change in chemical shift when reacted with P^tBu_3 (Table 5.2, Entry 5), when reacted with $\text{P}(\textit{para}\text{-tolyl})_3$, PEt_3 , PBu_3 , or PCy_3 , changes in NMR chemical shifts are observed (Table 5.2, Entries 1-4).²³ However, all five combinations lead to dihydrogen activation. Notably, the most efficient frustrated Lewis pair was not the one with P^tBu_3 , but rather the one with PCy_3 which was able to achieve higher conversion to the corresponding hydride salt in less time. The efficiency of the FLP with **5.10** and PCy_3 is consistent with calculations which show that PCy_3 has the lowest affinity for the borane out of the tested phosphines.²³ As such, even though strong evidence for Lewis adduct formation is present in the reactions of the bis(catecholato)germanes with bulky Lewis bases, these Lewis adducts should be tested for FLP reactivity.

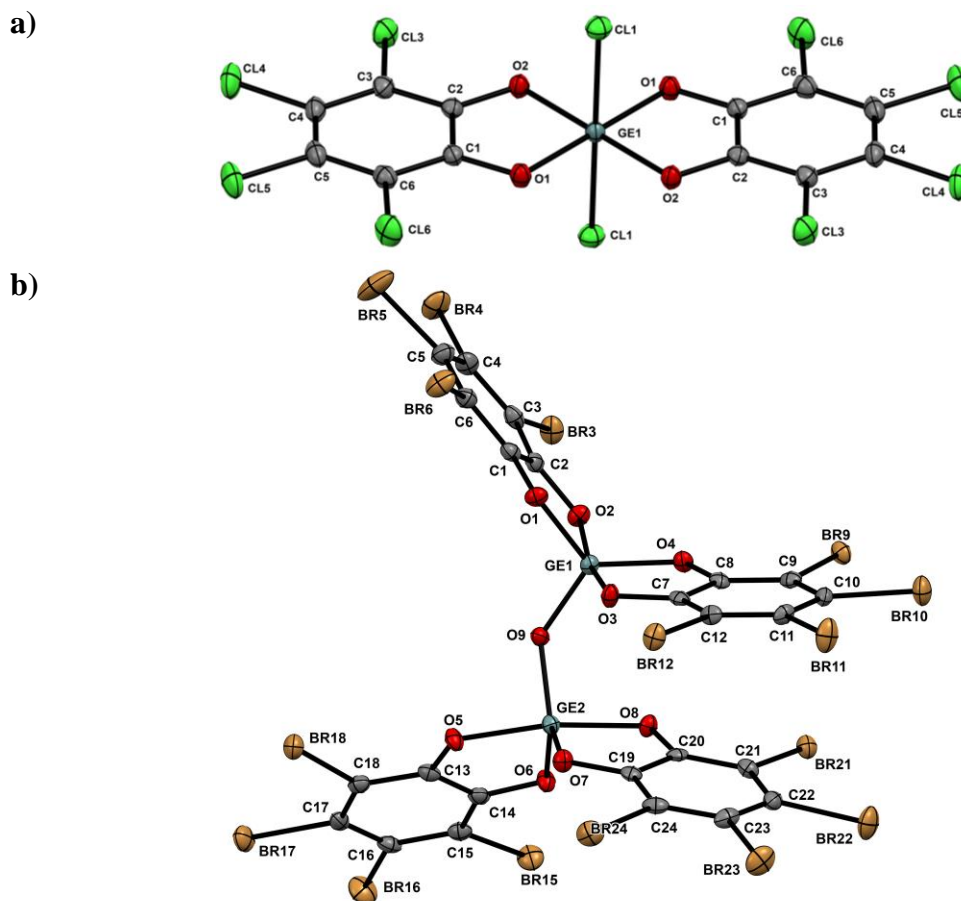
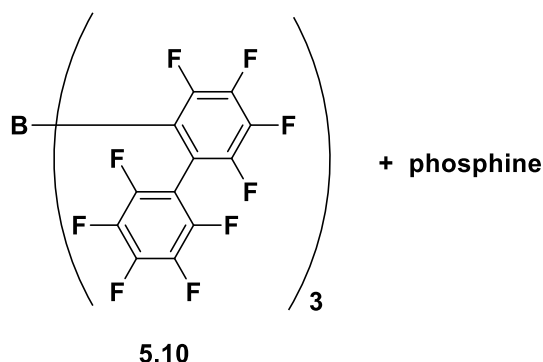


Figure 5.6: a) Thermal ellipsoid plot of $[\text{Ge}(\text{cat}^{\text{Cl}})_2\text{Cl}_2]$ showing naming and numbering scheme. Ellipsoids are at the 50% probability level and the cations and hydrogen atoms were omitted for clarity. Selected bond lengths (\AA) and angles ($^\circ$): $\text{Ge1-O1} = 1.8683(12)$, $\text{Ge1-O2} = 1.8685(11)$, $\text{Ge1-Cl1} = 2.3419(9)$, $\text{O1-Ge1-O2} = 89.11(4)$, $\text{O1-Ge1-Cl1} = 89.15(4)$, $\text{O2-Ge1-Cl1} = 88.85(3)$. b) Thermal ellipsoid plot of $[\text{Ge}(\text{cat}^{\text{Br}})_2\text{-O-Ge}(\text{cat}^{\text{Br}})_2]^{2-}$ showing naming and numbering scheme. Ellipsoids are at the 50% probability level and hydrogen atoms and cation were omitted for clarity. Selected bond lengths (\AA) and angles ($^\circ$): $\text{Ge1-O1} = 1.833(2)$, $\text{Ge1-O2} = 1.888(2)$, $\text{Ge1-O3} = 1.882(2)$, $\text{Ge1-O4} = 1.824(2)$, $\text{Ge1-O9} = 1.750(2)$; $\text{O1-Ge1-O3} = 87.31(10)$, $\text{O2-Ge1-O3} = 167.49(10)$.

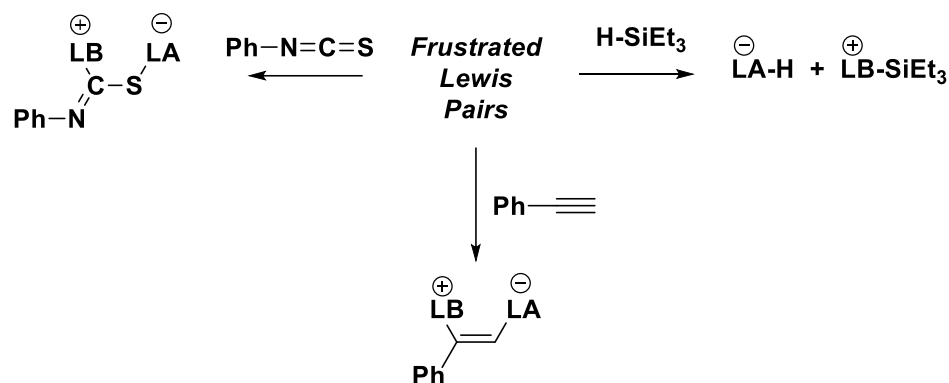
Table 5.2: The change in $^{31}\text{P}\{^1\text{H}\}$ chemical shift of various phosphines when in solution with borane **5.10**.



Entry	Phosphine	$\Delta\delta$ $^{31}\text{P}\{^1\text{H}\}$ (ppm)
1	P(<i>para</i> -tolyl) ₃	+22.1
2	PEt ₃	+57.6
3	PBu ₃	+64.4
4	PCy ₃	+29.8
5	P ^t Bu ₃	+0.0

5.2.2 Attempted Reactivity of FLPs

To test for frustrated Lewis pair-type reactivity from complexes derived from the bis(catecholato)germanes, a variety of different small molecule activations and catalytic reactions were attempted. For example, the activation of isocyanates and isothiocyanates by FLPs generally occurs under mild conditions and yields isolable zwitterions.²⁴ Furthermore, the activation of phenylacetylene has also been reported to yield isolated intermediates.²⁵ The general method to test FLP reactivity is to generate the FLP *in situ* and then add in the substrate of interest. The reactivity of the bis(catecholato)germanes as FLPs was tested using the *in situ* method and also by adding the isolated Lewis acid-base adduct to the reaction mixture containing the substrate (Scheme 5.13).



Scheme 5.13: The reactivity that will be attempted with the bis(catecholato)germane FLPs.

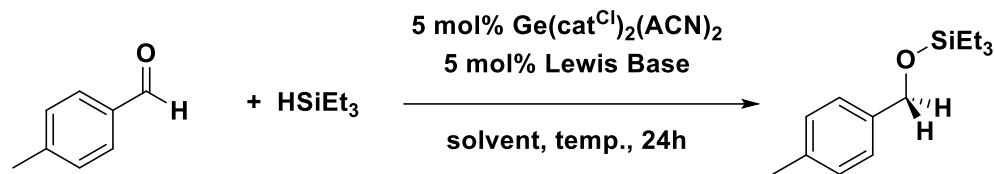
Attempts to activate phenyl isothiocyanate in a solution containing bis(catecholato)germanes with weakly bound THF ligands and one equivalent of tri-*tert*-butylphosphine were performed in CD₂Cl₂ at room temperature. Even though the ¹H and ³¹P{¹H} NMR spectra of the reactions between bis(catecholato)germanes and P^{*t*}Bu₃ showed multiple signals indicative of several products, the test reactions were still conducted in DCM as it is commonly used as the solvent in FLP chemistry. Both the bulky Ge(dtbc)₂(THF)₂ derivative and the Lewis acidic Ge(cat^{Br})₂(THF)₂ derivative were tested as the Lewis acid components. The reaction of Ge(dtbc)₂(THF)₂, P^{*t*}Bu₃ and phenyl isothiocyanate resulted in no visible change to the ¹H signals assigned to the phenyl isothiocyanate moiety by ¹H NMR spectroscopy. Similarly, the reaction of Ge(cat^{Br})₂(THF)₂, P^{*t*}Bu₃ and phenyl isothiocyanate also showed no change in the ¹H NMR signals for phenyl isothiocyanate. Furthermore, the ³¹P{¹H} NMR spectra of the reaction mixtures showed evidence for decomposition as observed in the independent reactions between the bis(catecholato)germanes and P^{*t*}Bu₃.

Since the reaction of bis(catecholato)germanes and Lewis bases in DCM lead to multiple products, the reaction of phenyl isothiocyanate with the combination of either Ge(dtbc)₂(THF)₂ or Ge(cat^{Br})₂(THF)₂ with P^{*t*}Bu₃ in toluene-*d*₈ at 100 °C was attempted. Once again, no reaction with the phenyl isothiocyanate was observed by ¹H NMR spectroscopy after 24 hours, even at the elevated temperature of 100 °C. To test a bulky N-donor Lewis base, the activation of phenyl isothiocyanate with either Ge(dtbc)₂(THF)₂

or $\text{Ge}(\text{cat}^{\text{Br}})_2(\text{THF})_2$ in combination with 2,6-di-*tert*-butylpyridine was probed. Using both sets of conditions, CD_2Cl_2 at rt or toluene-*d*₈ at 100 °C, no reaction was observed.

Phenylacetylene and triethylsilane were also tested for small molecule activation with bis(catecholato)germanes and bulky Lewis bases. $\text{Ge}(\text{dtbc})_2(\text{THF})_2$ or $\text{Ge}(\text{cat}^{\text{Br}})_2(\text{THF})_2$ with either P^tBu_3 or 2,6-di-*tert*-butylpyridine were reacted with phenylacetylene or triethylsilane on a small scale. Similar to the phenyl isothiocyanate reactions, no change in the ^1H NMR signals of phenylacetylene was observed in either CD_2Cl_2 at room temperature or toluene-*d*₈ at 100 °C after 18 hours. The lack of small molecule activation with the bis(catecholato)germanes and either 2,6-lutidine, 2,6-di-*tert*-butylpyridine, or P^tBu_3 is similar to the lack of dihydrogen activation observed with $\text{Si}(\text{am}^{\text{F}}\text{ph}^{\text{F}})_2$ and either P^tBu_3 or 2,6-di-*tert*-butylpyridine.¹⁹

To further probe the reactivity of these compounds, the hydrosilylation of *p*-tolualdehyde with triethylsilane was attempted with catalytic amounts of both $\text{Ge}(\text{cat}^{\text{Cl}})_2(\text{ACN})_2$ and either 2,6-lutidine, 2,6-di-*tert*-butylpyridine, or tri-*tert*-butylphosphine as the Lewis base component (Scheme 5.14). In chapter 3, bis(catecholato) were shown to catalyze the hydrosilylation of *para*-tolualdehyde at room temperature. As such, if the equilibrium, between the Lewis acid-base adduct and the free Lewis acid and base, is such that free Lewis acid is available then hydrosilylation should proceed. The catalytic reactions were performed in CD_2Cl_2 at room temperature and in toluene-*d*₈ at 100 °C for 24 hours. The resulting ^1H NMR spectra revealed no change in the signals attributed to either *para*-tolualdehyde or the triethylsilane suggesting that the formation of a Lewis acid-base adduct inhibits the reaction by preventing coordination of aldehyde to $\text{Ge}(\text{cat}^{\text{Cl}})_2(\text{ACN})_2$. Thus, the Lewis acidic and Lewis basic sites are inaccessible in solution which explains the lack of FLP reactivity observed with the bis(catecholato)germane complexes.



Lewis Base = 2,6-lutidine, 2,6-di-*tert*-butylpyridine, P(^tBu)₃

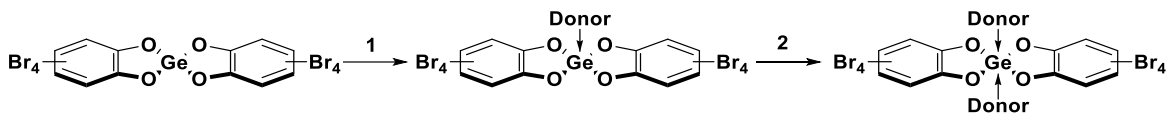
Scheme 5.14: The attempted hydrosilylation of *para*-tolualdehyde with bis(catecholato)germanes and bulky Lewis bases.

5.2.3 Computational Analysis of Lewis Adduct Formation

To gain a deeper understanding of the experimental results for the reactions of bis(catecholato)germanes with 2,6-lutidine or tri-*tert*-butylphosphine, the energetics of ligand association and dissociation were calculated at the BP86 D3(BJ)/def2-SVP//PBEh-3c/def2-mSVP level of theory.²⁶ Geometry optimizations of the Lewis adduct intermediates were performed at the PBEh-3c/def2-mSVP level of theory, chosen because it is a computationally inexpensive method that is useful for geometry calculations; however, calculated thermodynamic values obtained at this level of theory are inaccurate.^{26g} Thus, the optimized geometries were then used in a frequency calculation at the BP86 D3(BJ)/def2-SVP level of theory to obtain enthalpy and Gibbs free energy values.^{26h}

The calculated energetics of complexes between the germanium Lewis acid and 2,6-lutidine, 2,6-di-*tert*-butylpyridine, tri-*tert*-phosphine, pyridine and acetonitrile are presented in Table 5.3. Ge(cat^{Br})₂ was chosen for the calculation as Ge(cat^{Br})₂ is the most Lewis acidic.²² Starting from the ‘naked’ bis(perbromocatecholato)germane, the association of the first donor, via reaction 1, is endergonic for all tested bases (Table 5.3). Notably, the association is most favoured for the coordination of tri-*tert*-butylphosphine (Table 5.3, Entry 1). While ~50 kJ/mol less favoured than tri-*tert*-butylphosphine, the association of 2,6-lutidine and pyridine (Table 5.3, Entries 3-4) are similar in Gibbs free energy values (95-97 kJ/mol). For 2,6-di-*tert*-butylpyridine, an optimized geometry for the Lewis adduct could not be located, presumably due to the increased steric bulk (Table 5.3, Entry 2). Finally, acetonitrile, while energetically favoured is the least favoured of

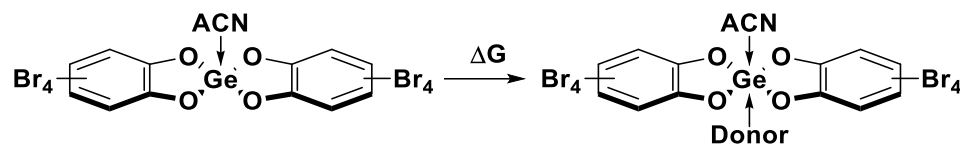
the tested donors (Table 5.3, Entry 5) due to the weaker donor ability of acetonitrile compared to the other bases. The main difference between the bulky bases, pyridine and acetonitrile was observed with the association of the second equivalent of donor (reaction 2). The association of the weaker donor and less bulky acetonitrile is energetically favoured, consistent with the room temperature synthesis of acetonitrile-ligated bis(catecholato)germanes and -silanes. The association of the second equivalent of pyridine is exergonic. Notably, the geometry of bis(perbromocatecholato)germane with two equivalents of either 2,6-lutidine, 2,6-di-*tert*-butylpyridine, and tri-*tert*-butylphosphine, did not converge to the structure with two equivalents of donors coordinated, even after multiple attempts. Instead, as the optimization progressed for 2,6-di-*tert*-butylpyridine and tri-*tert*-butylphosphine, the second equivalent of donor moved away from the germanium core to give what appears to be the mono-donor structure with an equivalent of free donor. An optimized structure was obtained for 2,6-lutidine; however, the structure obtained was not consistent with the coordination of two equivalents of 2,6-lutidine through the nitrogen atoms to the germanium. Instead, the second equivalent of 2,6-lutidine appears to π -stack with one of the catechol rings. Full dissociation of both weak donors of $\text{Ge}(\text{cat}^{\text{Br}})_2(\text{ACN})_2$ to generate the ‘naked’ $\text{Ge}(\text{cat}^{\text{Br}})_2$ is not energetically favoured,²⁷ and thus, the energetics of association of one equivalent of bulky base to the mono-donor adduct, $\text{Ge}(\text{cat}^{\text{Br}})_2(\text{ACN})$, were calculated (Table 5.4). Notably, the association of 2,6-lutidine and pyridine to the mono-ACN adduct have similar ΔG values, within 10 kJ/mol, compared to the association to the donorless $\text{Ge}(\text{cat}^{\text{Br}})_2$ (Table 5.4, Entries 3,4). An optimized geometry could not be located for P^tBu_3 and 2,6-di-*tert*-butylpyridine.

Table 5.3: Energetics of ligand association of various Lewis bases with $\text{Ge}(\text{cat}^{\text{Br}})_2$.

Entry	Donor	ΔG Reaction 1 (kJ/mol) ^a	ΔG Reaction 2 (kJ/mol) ^a
1	P^tBu_3	-143.20	-
2	py^tBu_2	-	-
3	lut	-95.18	-
4	py	-96.62	+65.71
5	ACN	-4.40	-29.57

^a) = BP86 D3(BJ)/def2-SVP//PBEh-3c/def2-mSVP

The formation of Lewis adducts with bis(catecholato)germanes is favourable. The association of at least one bulky base is favourable for all Lewis bases examined. Comparing the calculated energetics of adduct formation, the reaction between $\text{Si}(\text{am}^{\text{F}}\text{ph}^{\text{F}})_2$ and P^tBu_3 has a calculated ΔG of -20.7 kJ/mol,¹⁹ while the reaction between $\text{Ge}(\text{cat}^{\text{Br}})_2$ and P^tBu_3 has a calculated ΔG of -143.2 kJ/mol. The increased steric bulk of the extra aryl group on the nitrogen of $\text{Si}(\text{am}^{\text{F}}\text{ph}^{\text{F}})_2$ evidently makes adduct formation with P^tBu_3 less favoured than with $\text{Ge}(\text{cat}^{\text{Br}})_2$; however, the reaction is still exergonic. The only FLP combination with $\text{Si}(\text{am}^{\text{F}}\text{ph}^{\text{F}})_2$ as the Lewis acid to achieve dihydrogen activation was with pmp, which was also the only Lewis base that had an endergonic change in energy upon Lewis adduct formation (ΔG of +3.8 kJ/mol). The calculated values for the reaction between $\text{Ge}(\text{cat}^{\text{Br}})_2$ and 2,6-lutidine, 2,6-di-*tert*-butylpyridine, tri-*tert*-phosphine, pyridine and acetonitrile, were all exergonic, which is consistent with the lack of reactivity seen with the bis(catecholato)germanes as FLPs.

Table 5.4: Energetics of the association of different Lewis bases to $\text{Ge}(\text{cat}^{\text{Br}})_2(\text{ACN})$ 

Entry	Donor	ΔG (kJ/mol) ^a
1	P^tBu_3	-
2	py^tBu_2	-
3	lut	-94.71
4	py	-105.20
5	ACN	-29.57

^a) = BP86 D3(BJ)/def2-SVP//PBEh-3c/def2-mSVP

5.3 Conclusion

Bis(catecholato)germanes were tested as potential Lewis acid components for FLP chemistry. Reactivity studies with the bis(catecholato)germanes and bulky Lewis bases, 2,6-lutidine and P^tBu_3 , revealed the formation of Lewis adducts. Small molecule activation and catalysis was attempted with bis(catecholato)germane FLPs but were unsuccessful. Computational calculations revealed that the formation of Lewis adducts was energetically favoured even with the use of bulky Lewis bases. Overall, the favoured formation of Lewis adducts with the investigated Lewis bases inhibits the use of bis(catecholato)germanes as Lewis acid components for these specific FLPs. While the bis(catecholato)germanes were not effective in FLPs when using monodentate bulky Lewis bases, the recent reports of bidentate Lewis bases with bis(catecholato)silanes and the use of aminophenol ligands with silicon show there is still potential for bis(catecholato)germane FLPs for further studies in FLP chemistry.

5.4 Experimental

5.4.1 General Experimental

All reactions were conducted under a nitrogen atmosphere using an MBraun Labmaster 130 glovebox. Solvents and reagents were purified by standard methods.¹⁹ NMR data were obtained on a 600 MHz INOVA, 400 MHz INOVA or a 400 MHz Bruker Avance III NMR spectrometer. The standards used were as follows: residual C₆D₅H (7.16 ppm), CHDCl₂ (5.32 ppm), toluene-d₇ (2.09 ppm) relative to TMS for ¹H NMR spectra; CDCl₃ (77.16 ppm) for ¹³C NMR spectra; J values are reported in Hertz.

5.4.2 Ligand Exchange Reactions from Ge(dtbc)₂(py)₂

The reaction followed a similar procedure as described for the synthesis of Ge(dtbc)₂(NEt₃)₂.²¹ To Ge(dtbc)₂(py)₂ (0.25g, 0.37 mmol) was added 2,6-lutidine (11 mL, 93.08 mmol). The white solid suspended in a light brown solution was allowed to stir neat overnight before drying in vacuo while heating.

Ge(dtbc)₂(Lut)₂: 68% Yield; ¹H NMR (400 MHz, CDCl₃): δ 7.75 (t, 2H), 7.14 (d, 4H), 6.65 (d, 2H), 6.56 (br, 2H), 2.58 (s, 12H), 1.37 (s, 18H), 1.21 (s, 18H); ESI-MS (positive ion mode): *m/z* calcd for Ge(dtbc)₂(Lut)₂ + H₃O⁺ 743.3836; found C₄₂H₆₁GeN₂O₅ 743.3823.

5.4.3 Ligand Exchange Reactions from Bis(catecholato)germanes with weak donors

To a solution of either Ge(dtbc)₂(THF)₂, Ge(cat^{Cl})₂(THF)₂, or Ge(cat^{Br})₂(THF)₂ (0.12 mmol) in 5 mL of toluene was added one equivalent of either 2,6-lutidine, or tri-*tert*-butylphosphine (0.12 mmol). The reaction was allowed to stir overnight before the volatiles were removed in vacuo.

Ge(dtbc)₂(Lut): 38% Yield; ¹H NMR (400 MHz, C₆D₆): δ 7.26 (d, *J* = 2.2 Hz, 2H), 7.06 (d, *J* = 2.3 Hz, 2H), 6.47 (t, *J* = 7.7 Hz, 1H), 5.99 (d, *J* = 7.9 Hz, 2H), 2.36 (br, 6H), 1.61

(s, 18H), 1.33 (s, 18H); ^{13}C NMR (101 MHz, C_6D_6)³: δ 148.1, 143.5, 141.4, 133.7, 123.8, 113.5, 108.6, 35.1, 34.7, 32.1, 30.1; ESI-MS (positive ion mode): m/z calcd for $\text{Ge}(\text{dtbc})_2(\text{Lut}) + \text{ACN} + \text{H}^+$ 662.2891; found 662.3240

$\text{Ge}(\text{dtbc})_2(\text{PrBu}_3)$: 54% Yield; ^1H NMR (400 MHz, C_6D_6): δ 7.15 (d, $J = 2.1$ Hz, 2H), 7.02 (d, $J = 2.2$ Hz, 2H) 1.66 (s, 18 H), 1.38 (s, 18 H), 1.21 (d, $J = 13.6$ Hz, 27 H); $^{31}\text{P}\{^1\text{H}\}$ NMR (162 MHz, C_6D_6): δ 53.2;

$\text{Ge}(\text{cat}^{\text{Cl}})_2(\text{PrBu}_3)_2$: 96% Yield; ^1H NMR (400 MHz, C_6D_6): δ 1.27 (d, $J = 9.7$ Hz, 27H); $^{31}\text{P}\{^1\text{H}\}$ NMR (162 MHz, Solvent): δ 62.1;

$\text{Ge}(\text{cat}^{\text{Br}})_2(\text{PrBu}_3)_2$: 78% Yield; ^1H NMR (400 MHz, C_6D_6): δ 0.79 (d, $J = 15.4$ Hz, 27 H); $^{31}\text{P}\{^1\text{H}\}$ NMR (162 MHz, C_6D_6): δ 53.0;

5.4.4 Reactivity studies with Bis(catecholato)germanes and Bulky Bases

To a solution of either $\text{Ge}(\text{dtbc})_2(\text{base})_2$, where base = 2,6-lutidine, 2,6-di-*tert*-butylpyridine, or tri-*tert*-butylphosphine, or $\text{Ge}(\text{dtbc})_2(\text{THF})_2$ plus an equivalent of bulky base in either CD_2Cl_2 or toluene- d_8 was added an equivalent of substrate. The reaction was monitored by NMR spectroscopy.

5.4.5 Catalytic Activity of $\text{Ge}(\text{cat}^{\text{X}})_2$ and Bulky Bases in the hydrosilylation of *p*-tolualdehyde

A solution containing *p*-tolualdehyde (0.2 mmol), triethylsilane (0.2 mmol) and mesitylene (0.022 mmol) in 0.5 mL of either CD_2Cl_2 or toluene- d_8 was added to a mixture of bis(catecholato)germane (0.01 mmol) and either 2,6-lutidine, 2,6-di-*tert*-butylpyridine, or tri-*tert*-butylphosphine (0.01 mmol) and transferred to an NMR tube and allowed to react for 24 hours. Control experiments without catalyst were performed in parallel. Conversion of substrates to products was determined by integration against mesitylene (C_9H_{12}) as an internal standard. No conversion was observed.

³ Signal for the 2,6-lutidine methyl was not observed in the ^{13}C NMR spectra

5.4.6 Computational Details

All calculations have been performed with ORCA 4.1.2 and ORCA 4.2. Geometry optimizations were performed with PBEh-3c/def2-mSVP as implemented in ORCA, using grid5 settings. All calculated geometries have been confirmed as energetic minima on the potential energy surface by analytical calculation of harmonic frequencies at the PBEh-3c level. In case of negative frequencies $>10\text{ cm}^{-1}$, the geometries were reoptimized with grid6, TightOPT and VeryTightSCF settings. For the fluoride ion affinities, the optimized geometries were then used to calculate the single point energies at B3LYP D3(BJ)/def2-TZVPP level of theory using the RIJCOSX approximation and def2/J as the auxiliary basis set. For the reaction coordinate calculations, the optimized geometries were used to calculate the thermodynamic values at BP86 D3(BJ)/def2-SVP level of theory using the RIJCOSX approximation and def2/J as the auxiliary basis set.

5.4.7 X-Ray Crystallography Details

The samples were mounted on a Mitegen polyimide micromount with a small amount of Paratone N oil. All X-ray measurements were made on a Bruker Kappa Axis Apex2 diffractometer at a temperature of 110 K. The unit cell dimensions were determined from a symmetry-constrained fit of 9916 reflections with $5.46^\circ < 2\theta < 63.72^\circ$. The data collection strategy was a number of ω and φ scans which collected data up to 67.682° (2θ). The frame integration was performed using SAINT.²⁸ The resulting raw data were scaled and absorption corrected using a multi-scan averaging of symmetry equivalent data using SADABS.²⁹

The structures were solved by using a dual space methodology using the SHELXT program.³⁰ All non-hydrogen atoms were obtained from the initial solution. The hydrogen atoms were introduced at idealized positions and were allowed to ride on the parent atom. The structural models were fit to the data using full matrix least-squares based on F^2 . The calculated structure factors included corrections for anomalous dispersion from the usual tabulation. The structures were refined using the SHELXL program from the SHELX suite of crystallographic software.³¹ Graphic plots were produced using the Mercury program suite.³²

References

1. a) Lam, J.; Szkop, K. M.; Mosaferi, E.; Stephan, D. W. *Chem. Soc. Rev.* **2019**, *48*, 3592–3612; b) Stephan, D. W. *J. Am. Chem. Soc.* **2021**, *143*, 20002–20014; c) Stephan, D. W. *Org. Biomol. Chem.* **2008**, *6*, 1535–1539; d) Fontaine, F. G.; Stephan, D. W. *Phil. Trans. R. Soc. A.* **2017**, *375*, 201770004; e) Li, N.; Zhang, W. X. *Chin. J. Chem.* **2020**, *38*, 1360–1370; f) Stephan, D. W. *Chem* **2020**, *6*, 1520-1526; g) Stephan, D. W. *J. Am. Chem. Soc.* **2015**, *137*, 10018–10032; h) Stephan, D. W.; Erker, G. *Chem. Sci.* **2014**, *5*, 2625-2641; i) Pal, R.; Ghara, M.; Chattaraj, P. K. *Catalysts* **2022**, *12*, 201; j) Jupp, A. R.; Stephan, D. W. *Trends Chem.* **2019**, *1*, 35-48.
2. Welch, G. C.; Juan, R. R. S.; Masuda, J. D.; Stephan, D. W. *Science* **2006**, *314*, 1124–1126.
3. Welch, G. C.; Stephan, D. W. *J. Am. Chem. Soc.* **2007**, *129*, 1880–1881.
4. Kinder, T. A.; Bloymeyer, S.; Franke, M.; Depenbrock, F.; Neumann, B.; Stammeler, H. G.; Mitzel, N. W. *Eur. J. Inorg. Chem.* **2019**, 3933-3939.
5. Kolychev, E. L.; Bannenberg, T.; Freytag, M.; Daniliuc, C. G.; Jones, P. G.; Tamm, M. *Chem. Eur. J.* **2012**, *18*, 16938-16946.
6. Spikes, G. H.; Fettingner, J. C.; Power, P. P. *J. Am. Chem. Soc.* **2005**, *127*, 12232–12233.
7. Mömning, C. M.; Otten, E.; Kehr, G.; Fröhlich, R.; Grimme, S.; Stephan, D. W. Erker, G. *Angew. Chem. Int. Ed.* **2009**, *48*, 6643 –6646.
8. Otten, E.; Neu, R. C.; Stephan, D. W. *J. Am. Chem. Soc.* **2009**, *131*, 9918-9919.
9. Sajid, M.; Klose, A.; Birkmann, B.; Liang, L. Y.; Schirmer, B.; Wiegand, T.; Eckert, H.; Lough, A. J.; Fröhlich, R.; Daniliuc, C. G.; Grimme, S.; Stephan, D. W.; Kehr, G.; Erker, G. *Chem. Sci.* **2013**, *4*, 213-219.

10. Erös, G.; Mehdi, H.; Pápai, I.; Rokob, T. A.; Király, P.; Tárkányi, G.; Soós, T. *Angew. Chem. Int. Ed.* **2010**, *49*, 6559-6563.
11. Barrero, A. F.; Alvarez-Manzaneda, E. J.; Chahboun, R.; Meneses, R. *Synlett* **1999**, 1663–1666.
12. Tamke, S.; Daniliuc, C. G.; Paradies, J. *Org. Biomol. Chem.* **2014**, *12*, 9139-9144.
13. Mahdi, T.; Stephan, D. W. *Angew. Chem. Int. Ed.* **2013**, *52*, 12418-12421.
14. a) Melen, R. L.; Hansmann, M. M.; Lough, A. J.; Hashmi, S. K.; Stephan, D. W. *Chemistry* **2013**, *19*, 11928-11938; b) Wlikins, L. C.; Wieneke, P.; Newman, P. D.; Kariuki, B. M.; Rominger, F.; Hashmi, A. S. K.; Hansmann, M. M.; Melen, R. L. *Organometallics* **2015**, *34*, 5298-5309.
15. Chen, D.; Leich, V.; Pan, F.; Klankermayer, J. *Chem. Eur. J.* **2012**, *18*, 5184-5187.
16. a) Waerder, B.; Pieper, M.; Körte, L. A.; Kinder, T. A.; Mix, A.; Neumann, B.; Stammler, H. G.; Mitzel, N. W. *Angew. Chem. Int. Ed.* **2015**, *54*, 13416–13419; b) Kinder, T. A.; Pior, R.; Blomeyer, S.; Neumann, B.; Stammler, H. G.; Mitzel, N. W. *Chem. Eur. J.* **2019**, *25*, 5899–5903; c) Holtkamp, P.; Friedrich, F.; Stratmann, E.; Mix, A.; Neumann, B.; Stammler, H. G.; Mitzel, N. W. *Angew. Chem. Int. Ed.* **2019**, *58*, 5114–5118.
17. a) Reißmann, M.; Shafer, A.; Jung, S.; Muller, T. *Organochemicals* **2013**, *32*, 6736-6744; b) Herrington, T. J.; Ward, B. J.; Doyle, L. R.; McDermott, J.; White, A. J. P.; Hunt, P. A.; Ashley, A. E. *Chem. Commun.* **2014**, *50*, 12753-12756.
18. Scott, D. J.; Phillips, N. A.; Sapsford, J. S.; Deacy, A. C.; Fuchter, M. J., Ashley, A. E. *Angew. Chem. Int. Ed.* **2016**, *55*, 14738–14742.
19. Hartmann, D.; Braner, S.; Greb, L. *Chem. Commun.* **2021**, *57*, 8572-8578.

20. Thorwart, T.; Hartmann, D.; Greb, L. *Chem. Eur. J.* **2022**, e202202273.
21. Glavinović, M., Krause, M., Yang, L., McLeod, J. A., Liu, L., Baines, K. M., Friščić, T., Lumb, J. P. *Sci. Adv.* **2017**, *3*, e1700149.
22. Discussed in Chapter 2
23. Travis, A. L.; Binding, S. C.; Zaher, H.; Arnold, T. A. Q.; Buffet, J. C.; O'Hare, D. *Dalton Trans.* **2013**, *42*, 2431-2437.
24. Szykiewicz, N.; Ordyszewska, A.; Chojnacki, J.; Grubba, R. *Inorg. Chem.* **2021**, *60*, 3794-3806.
25. Jiang, C.; Blacque, O.; Berke, H. *Organometallics* **2010**, *29*, 125-133.
26. a) Becke, A. D. *J. Chem. Phys.* **1993**, *98*, 5648-5652; b) Grimme, S.; Antony, J.; Ehrlich, S.; Krieg, H. *J. Chem. Phys.* **2010**, *132*, 154104; c) Grimme, S.; Ehrlich, S.; Goerigk, L. *J. Comput. Chem.* **2011**, *32*, 1456-1465; d) Johnson, E. R.; Becke, A. D. *J. Chem. Phys.* **2005**, *123*, 024101; e) Becke, A. D.; Johnson, E. R. *J. Chem. Phys.* **2005**, *122*, 154101; f) Schafer, A.; Huber, C.; Ahlrichs, R. *J. Chem. Phys.* **1994**, *100*, 5829-5835; g) Grimme, S.; Brandenburg, J. G.; Bannwarth, C.; Hansen, A. *J. Chem. Phys.* **2015**, *143*, 054107; h) Cavasin, A. T.; Hillisch, A.; Uellendahl, F.; Schneckener, S.; Göller, A. H. *J. Chem. Inf. Model.* **2018**, *58*, 1005–1020.
27. Discussed in Chapter 4
28. Bruker-AXS, SAINT version 2013.8, 2013, Bruker-AXS, Madison, WI 53711, USA.
29. Bruker-AXS, SADABS version 2012.1, 2012, Bruker-AXS, Madison, WI 53711, USA.
30. Sheldrick, G. M. *Acta Cryst* **2015**, *A71*, 3-8.
31. Sheldrick, G. M. *Acta Cryst* **2015**, *C71*, 3-8.

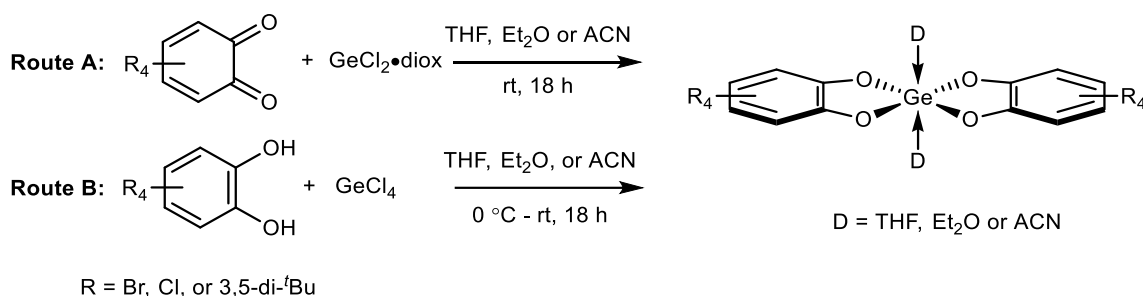
32. Macrae, C. F.; Bruno, I. J.; Chisholm, J. A.; Edington, P. R.; McCabe, P.; Pidcock, P.; Rodriguez-Monge, L.; Taylor, R.; van de Streek, J.; Wood, P. A. *J. Appl. Cryst.* **2008**, *41*, 466-470.

Chapter 6

6 Conclusions and Future Work

6.1 Summary

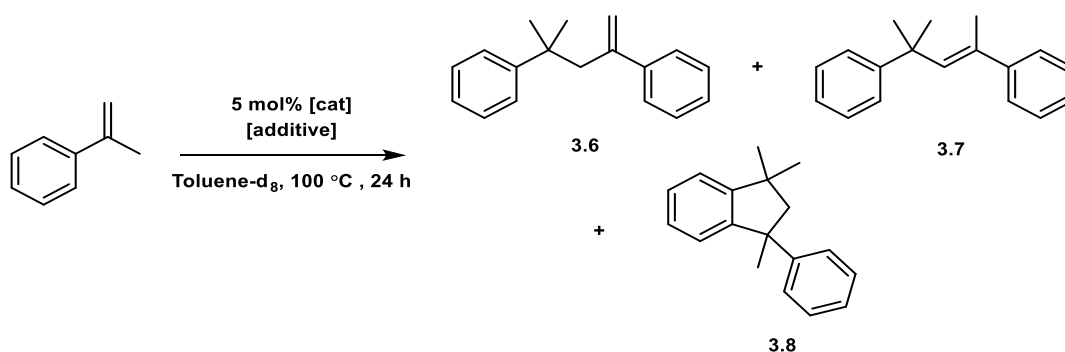
The synthesis of multiple bis(catecholato)germanes with a variety of catecholato ligands and different donor ligands was successful. Two synthetic pathways are possible: a substitution route using GeCl_4 and a substituted catechol or a redox pathway using $\text{GeCl}_2 \cdot \text{dioxane}$ and a substituted quinone (Scheme 6.1). The Lewis acidity of the bis(catecholato)germanes were assessed by the Gutmann-Beckett method and FIA calculations. The Gutmann-Beckett method showed that the halogenated bis(catecholato)germane derivatives were highly Lewis acidic. Furthermore, the choice of the halogen substituent (Cl vs. Br) had less of an influence on the Lewis acidity than the choice of the bound donor ligands (THF vs. ACN). FIA calculations confirmed the high Lewis acidity of the halogenated bis(catecholato)germanes both with one equivalent of bound donor ligand or donorless.



Scheme 6.1: Synthesis of bis(catecholato)germanes

With a series of highly Lewis acidic bis(catecholato)germanes in hand, their use as Lewis acid catalysts was demonstrated in several reactions. The hydrosilylation of aldehydes was achieved. Notably, the use of electron-deficient aldehydes greatly improved conversions compared to the conversions achieved using electron-rich aldehydes. $\text{Ge}(\text{cat}^{\text{Cl}})_2(\text{ACN})_2$ is the most efficient catalyst among the bis(catecholato)germanes as judged using conversion and product selectivity, and ease of

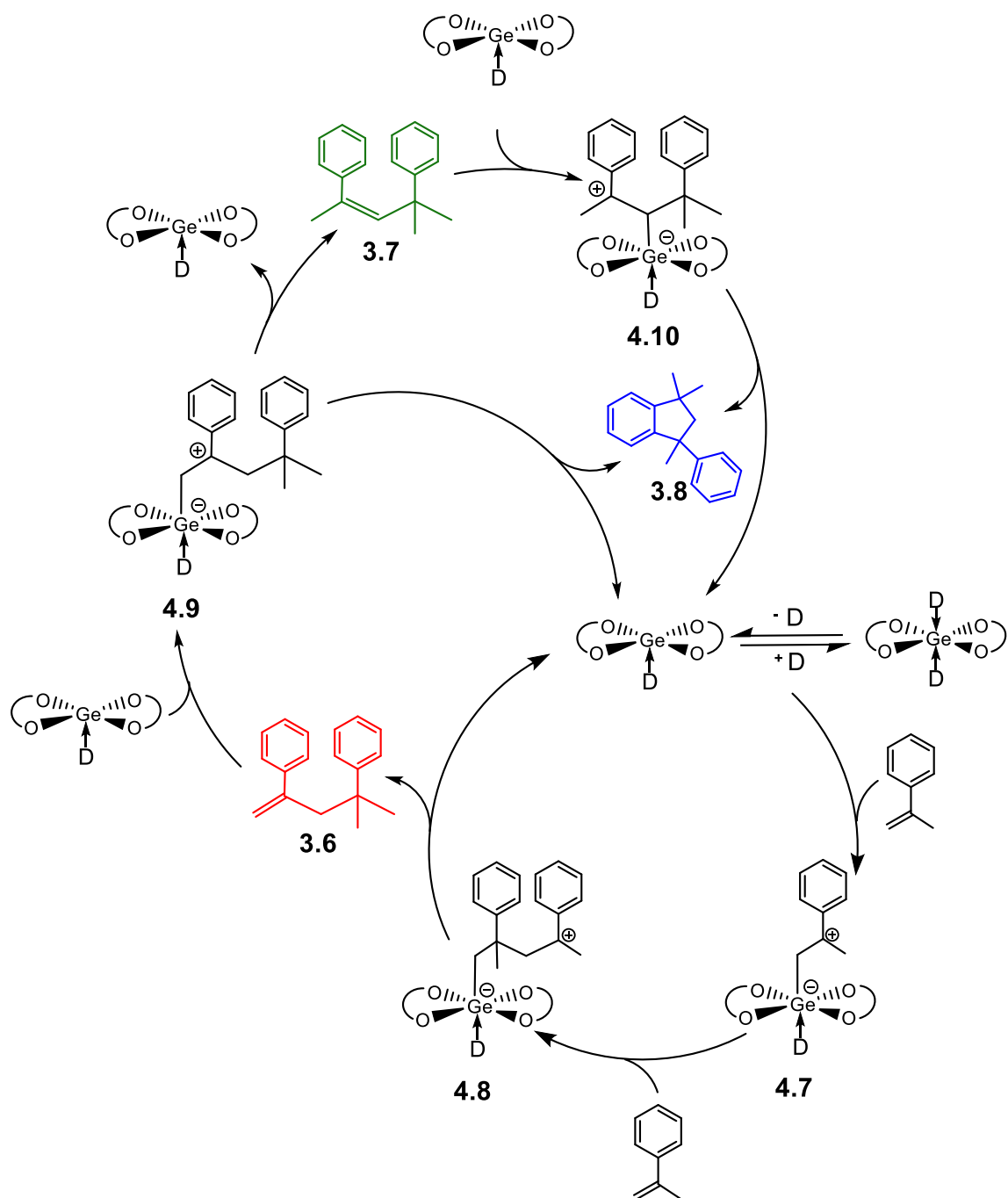
synthesis. The hydroboration of phenylacetylene and the Friedel-Crafts alkylation of diphenylamine with styrene, was also achieved. However, conversions for these reactions are not as high as those achieved in the hydrosilylation of aldehydes, even after prolonged periods of reaction. Attempts to hydrosilylate and hydroborate alkenes were unsuccessful. Styrene and α -methylstyrene were successfully oligomerized using $\text{Ge}(\text{cat}^{\text{Cl}})_2(\text{ACN})_2$. For α -methylstyrene, the formation of three dimers (or a 4th trimer product when DCM was used as the solvent) was observed in different ratios depending on the catalyst and the additive used in the reaction (Scheme 6.2). Selective formation of dimer **3.8** was obtained by using $\text{Ge}(\text{cat}^{\text{Cl}})_2(\text{ACN})_2$ without an additive, while the use of diethyl ether as an additive selectively gave rise to dimer **3.6**. The bis(catecholato)germanes are the first main group Lewis acids to give tunable selectivity in this manner.



Scheme 6.2: Dimerization of α -methylstyrene catalyzed by $\text{Ge}(\text{cat}^{\text{Cl}})_2(\text{ACN})_2$

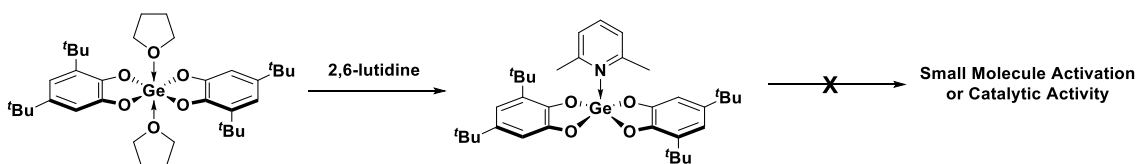
Given the success of bis(catecholato)germanes as Lewis acid catalysts, an in-depth look into the mechanism of the oligomerization of α -methylstyrene was undertaken. Variable time normalization rate law studies showed a reactant order of 1.5 for α -methylstyrene. A Hammett analysis revealed an increased reaction rate for electron-rich styrenes. The reaction constant was 1.60. DFT calculations revealed that a monodonor ligated bis(catecholato)germane species, $\text{Ge}(\text{cat}^{\text{X}})_2(\text{donor})$, is the active catalyst. In conjunction with the observed rapid conversion of α -methylstyrene to dimer **3.6** and subsequent consumption of **3.6** to form **3.7** and **3.8**, a mechanism was proposed (Scheme 6.3). Compared to other mechanisms by main group catalysts, the mechanism proposed for the bis(catecholato)germanes features three different intermediates, **4.8**, **4.9**, and **4.10**

which accounts for the rapid formation of **3.6** and subsequent consumption of **3.6** to form **3.7** and **3.8**.



Scheme 6.3: Proposed mechanism for the oligomerization of α -methylstyrene catalyzed by bis(catecholato)germanes.

The use of bis(catecholato)germanes as the Lewis acid component in a FLP was examined. Reaction of the bis(catecholato)germanes with 2,6-lutidine or tri-*tert*-butylphosphine resulted in a noticeable shift in the ^1H NMR signals and, in the case of P^tBu_3 , the $^{31}\text{P}\{^1\text{H}\}$ NMR spectra, suggesting the formation of Lewis adducts. While crystals of the adducts suitable for X-ray crystallography were not obtained, several crystals of various different water and chlorine adducts were obtained. Although the formation of a Lewis adduct was strongly suggested, the formation of water and chloride adducts suggested the equilibrium did not lie fully to the Lewis adduct. However, attempted reactions of the bis(catecholato)germanes with the bulky bases to achieve small molecule activation or catalysis were not successful (Scheme 6.4). DFT calculations on the thermodynamics of the reactions between the bis(catecholato)germanes and the bulky bases revealed the formation of a Lewis adduct is favourable. As such, the bis(catecholato)germanes were determined to be not suitable as a FLP candidate with the bases used in this study.



Scheme 6.4: The formation of Lewis adducts which inhibits FLP reactivity.

6.2 Conclusion

This thesis expanded on the underexplored field of bis(catecholato)germanes, providing two synthetic routes which can be used to synthesize a variety of derivatives, showcasing several catalytic applications, highlighting the level of tuneability the bis(catecholato)germane scaffold provides and providing a mechanistic understanding of how bis(catecholato)germanes function as catalysts. The potential of bis(catecholato)germanes as catalysts is being recognized, as demonstrated with the recent report on the water-ligated parent catechol derivative, $\text{Ge}(\text{cat})_2(\text{H}_2\text{O})_2$ which showcases the green synthesis of the catalysts and catalytic activity using water as a solvent.¹ The availability and cheaper price of germanium in combination with the ease

of synthesis and water-tolerability, make bis(catecholato)germanes viable potential alternatives to expensive transition metal catalysts.

6.3 Future Work

While a variety of bis(catecholato)germanes were synthesized, expanding the number of derivatives and assessing their Lewis acidity and catalytic activity would provide a greater understanding of the tunability of the bis(catecholato)- framework. Greb *et al.* showed the increased Lewis acidity of $\text{Si}(\text{cat}^{\text{CF}_3})_2(\text{sulfolane})_2$, compared to the halogenated derivatives, which also resulted in different reactivity.² For example when catalyzing the reaction of *para*-tolualdehyde with triethylsilane, the perhalogenated bis(catecholato)silanes and -germanes catalysts form the silylether product while $\text{Si}(\text{cat}^{\text{CF}_3})_2(\text{sulfolane})_2$ forms a dibenzyl ether product. As such, a similar synthesis of the germanium derivative, $\text{Ge}(\text{cat}^{\text{CF}_3})_2(\text{donor})_2$ may result in increased Lewis acidity and potentially new reactivity for the germanium catalyst in comparison to the derivatives explored to date (Chart 6.1). Furthermore, Greb *et al.* showcased the use of the aminophenol ligand instead of a catechol ligand in the synthesis of $\text{Si}(\text{am}^{\text{F}}\text{ph}^{\text{F}})_2$.³ While $\text{Si}(\text{am}^{\text{F}}\text{ph}^{\text{F}})_2$ was not tested as a Lewis acid catalyst, the synthesis and catalytic activity of $\text{Ge}(\text{am}^{\text{F}}\text{ph}^{\text{F}})_2$ would be interesting to explore and compare to the bis(catecholato)germanes. While the silicon derivatives have been studied extensively, the use of bis(catecholato)stannanes is relatively unexplored. A complete investigation on the bis(catecholato)stannanes would provide a valuable comparison to the silicon and germanium counterparts.

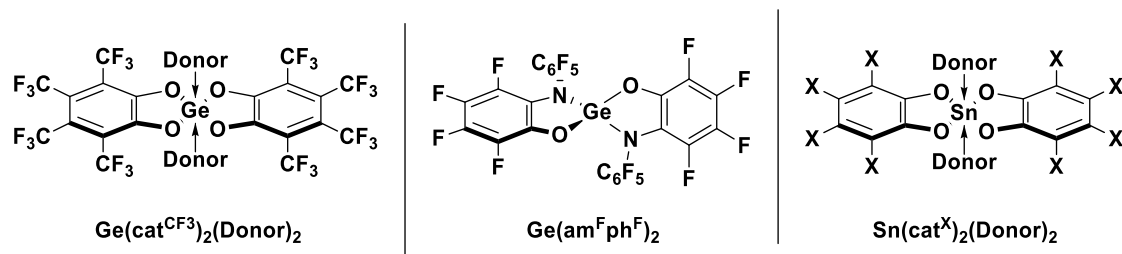
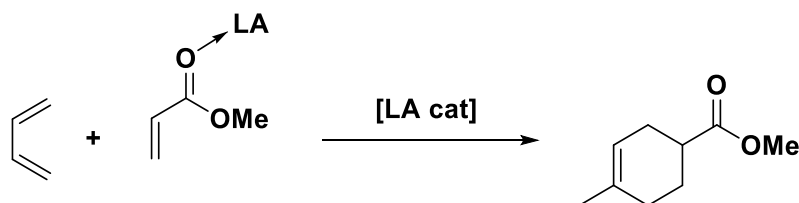


Chart 6.1: Proposed synthetic targets.

An area that the bis(catecholato)germanes show promise for is that of green chemistry. The mechanochemical ball mill synthesis of $\text{Ge}(\text{dtbc})_2(\text{py})_2$ provides

precedence that a similar solvent free synthesis of bis(catecholato)germanes with weak donor ligands could be achieved and should be explored.⁴ Furthermore, the use of $\text{Ge}(\text{cat}^{\text{Cl}})_2(\text{H}_2\text{O})_4$ as a Lewis acid catalyst has been reported; however, only two reactions have been examined.⁵ Recently, the use of water-ligated complex, $\text{Ge}(\text{cat})_2(\text{H}_2\text{O})_2$, has been shown to be an effective catalyst in Friedel-Crafts alkylations between benzaldehyde and indole with water as the solvent.¹ In line with green chemistry principles, exploration into the catalytic activity of the water-ligated species would provide insight into a green catalytic alternative which would not require an organic solvent for synthesis.

The catalytic applications of the bis(catecholato)germanes can be expanded to other reactions. Reactions other Lewis acids are known to catalyze could be explored, such as Diels-Alder reactions, carbonyl-ene reactions, and Mukaiyama aldol condensations to name a few.⁶ For example, the use of methyl acrylate, as the dienophile, can coordinate to a Lewis acid to increase reactivity (Scheme 6.5).⁷ Furthermore, while the catalytic hydrosilylation of alkenes was unsuccessful using the bis(catecholato)germanes presented in this thesis, the need for alternative catalysts for this reaction is critical to the polysiloxane industry. As such further exploration into tuning the bis(catecholato)germane scaffold, such as altering the substituents on the catechol ring to CF_3 groups and increasing Lewis acidity, in an effort to catalyze the hydrosilylation of alkenes is warranted.



Scheme 6.5: A Lewis acid catalyzed Diels-Alder reaction illustrating the Lewis acid coordination with methyl acrylate.

DFT calculations were critical in this study for the elucidation of the mechanism of catalysis by the bis(catecholato)germanes and to understand the energetics of Lewis adduct formation with bulky bases. However, only the energies of the postulated

intermediates were calculated. The transition states along the reaction pathway should also be calculated to understand the energy barriers involved. Furthermore, calculations of all species involved in the proposed mechanism of the dimerization of α -methylstyrene should be performed. These calculations would provide insight into the competitive coordination of the donor additives, which is proposed to slow the reaction leading to selective product formation and may be used to find potential candidates for an optimal additive.

FLPs with $\text{Si}(\text{cat}^{\text{Cl}})_2(\text{sulfolane})_2$ ⁸ and $\text{Si}(\text{am}^{\text{F}}\text{ph}^{\text{F}})_2$ ³ have been reported recently.⁹ Notably, the use of bidentate donors with $\text{Si}(\text{cat}^{\text{Cl}})_2(\text{sulfolane})_2$ was necessary to achieve the activation of small molecules. As such, the use of bidentate donor ligands with bis(catecholato)germanes should be explored as a viable strategy to achieve the activation of small molecules through the use of an FLP (Chart 6.2).

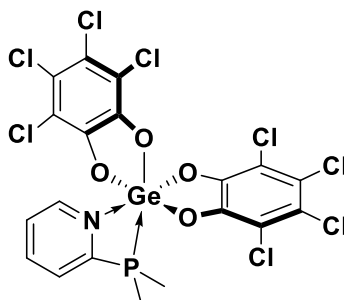


Chart 6.2: Proposed FLP involving bis(catecholato)germanes and a bidentate Lewis base.

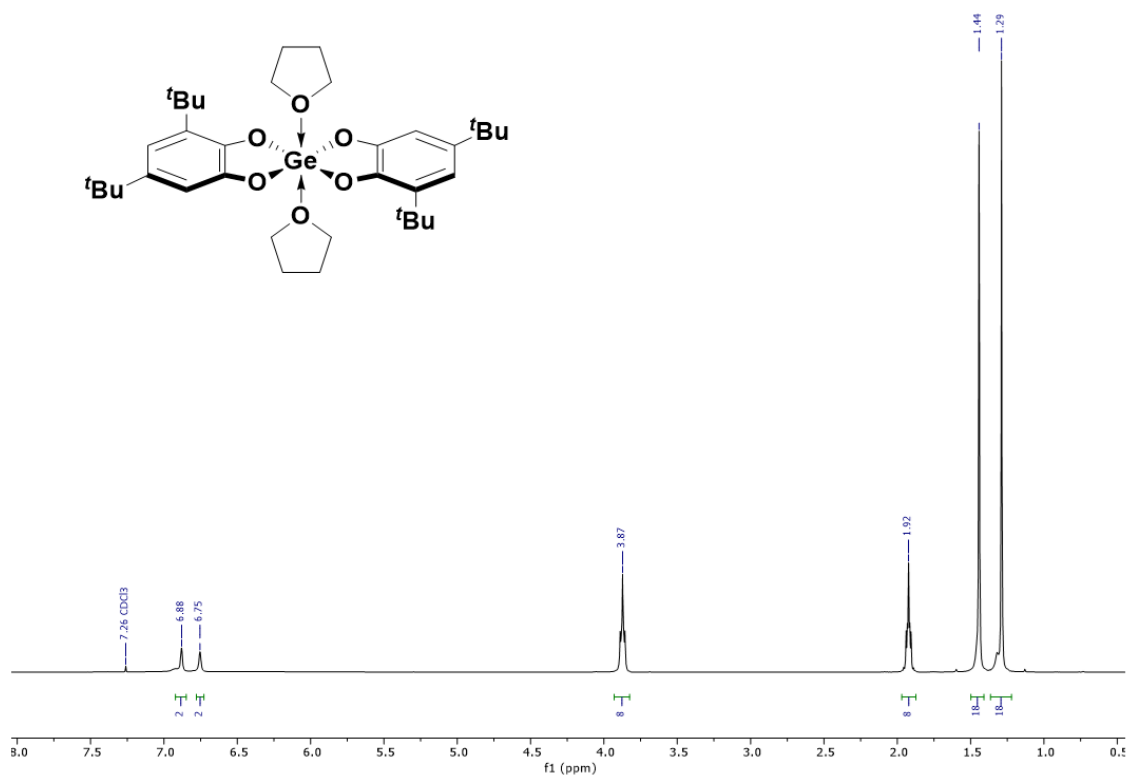
Overall, the future of bis(catecholato)germanes is bright. This work presented an in-depth analysis on the synthesis and use of bis(catecholato)germanes as Lewis acid catalysts, which is but a stepping stone in advancing the field of germanium Lewis acid chemistry. With the principles of green chemistry in mind and the high Lewis acidity and catalytic activity, the bis(catecholato)germanes have to potential to be viable alternative catalysts. The ability to tune various parts of these catalysts allow for a plethora of different potential catalysts to be targeted synthetically, and the use of additives enhancing products selectivity and altering reaction equilibria, provide the handles to achieve various catalytic applications.

References

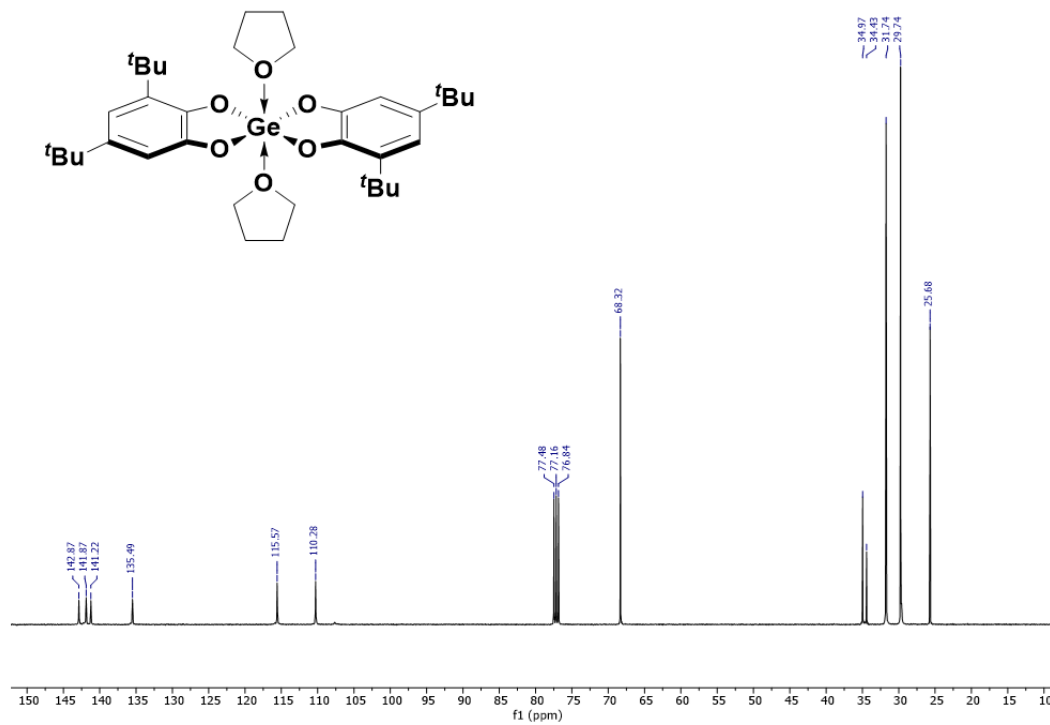
1. Basu, D.; Nayek, H. P. *Dalton Trans.* **2022**, *51*, 10587-10594.
2. Thorwart, T.; Roth, D.; Greb, L. *Chem. Eur. J.* **2021**, *27*, 10422-10427.
3. Thorwart, T.; Hartmann, D.; Greb, L. *Chem. Eur. J.* **2022**, e202202273.
4. Glavinović, M., Krause, M., Yang, L., McLeod, J. A., Liu, L., Baines, K. M., Friščić, T., Lumb, J. P. *Sci. Adv.* **2017**, *3*, e1700149-1-e1700149-8.
5. Roth, D.; Wadepohl, H.; Greb, L. *Angew. Chem. Int. Ed.* **2020**, *59*, 20930-20934
6. Corma, A.; Garcia, H. *Chem. Rev.* **2003**, *103*, 4307-4366.
7. Vermeeran, P.; Tiezza, M. D.; van Dongen, M.; Fernandez, I.; Bickelhaupt, F. M.; Hamlin, T. A. *Chem. Eur. J.* **2021**, *27*, 10610-10620.
8. Hartmann, D.; Braner, S.; Greb, L. *Chem. Commun.* **2021**, *57*, 8572-8578.
9. Thorwart, T.; Hartmann, D.; Greb, L. *Chem. Eur. J.* **2022**, e202202273.

Appendices

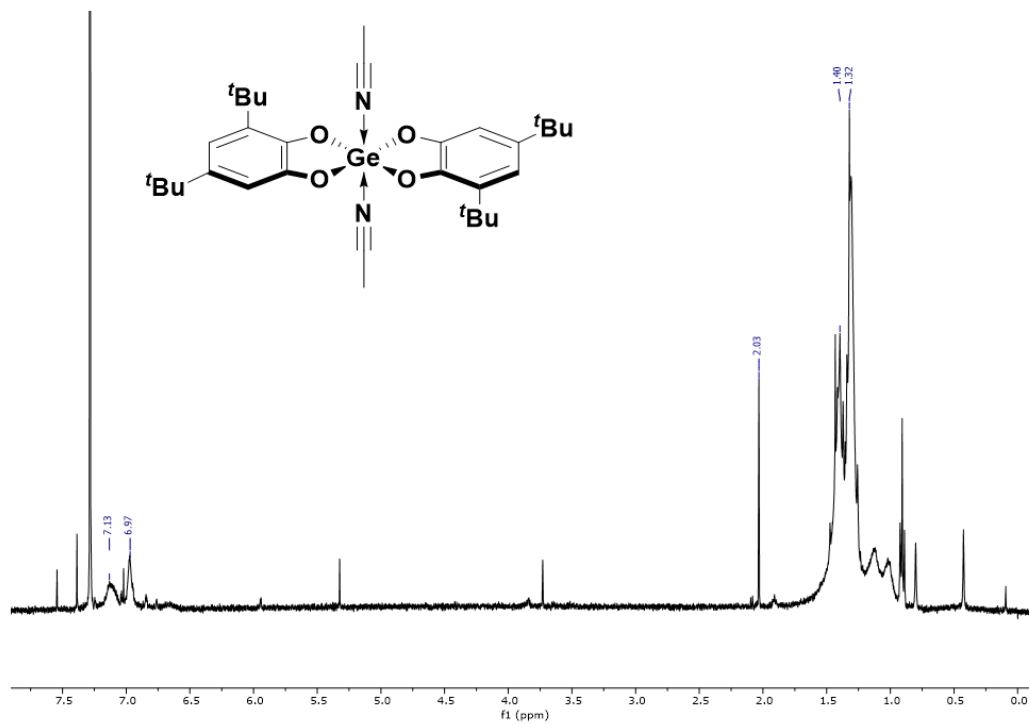
NMR spectra of synthesized compounds.



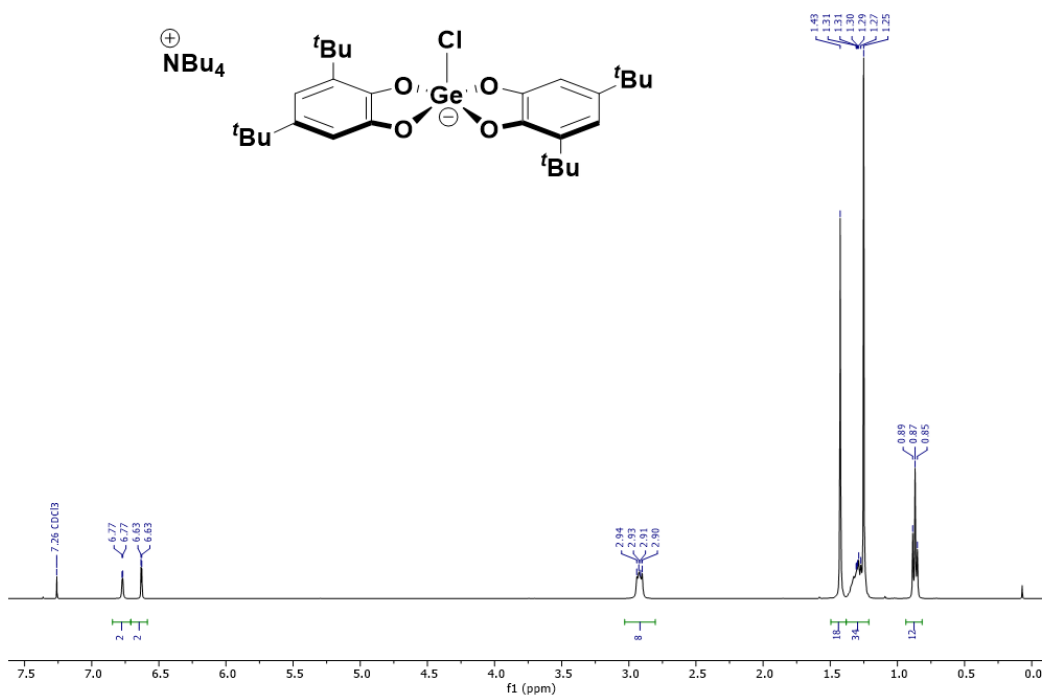
Appendix A: ^1H NMR (CDCl_3 , 400 MHz) spectrum of $\text{Ge}(\text{dtbc})_2(\text{THF})_2$.



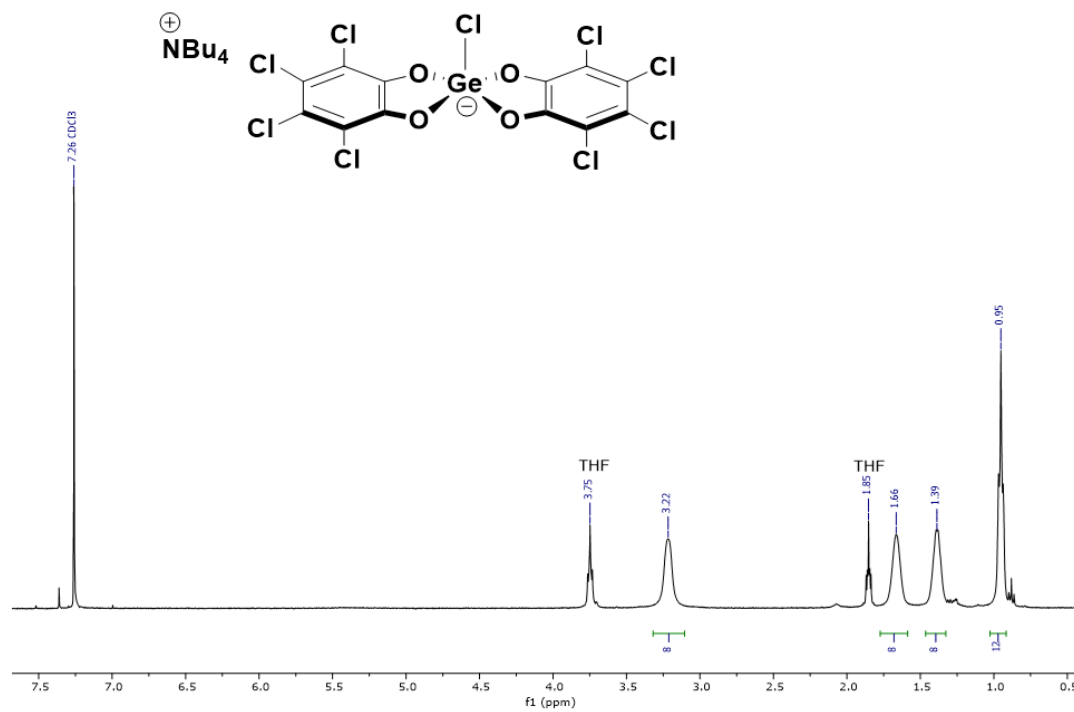
Appendix B: $^{13}\text{C}\{^1\text{H}\}$ NMR (CDCl_3 , 101 MHz) spectrum of $\text{Ge}(\text{dtbc})_2(\text{THF})_2$.



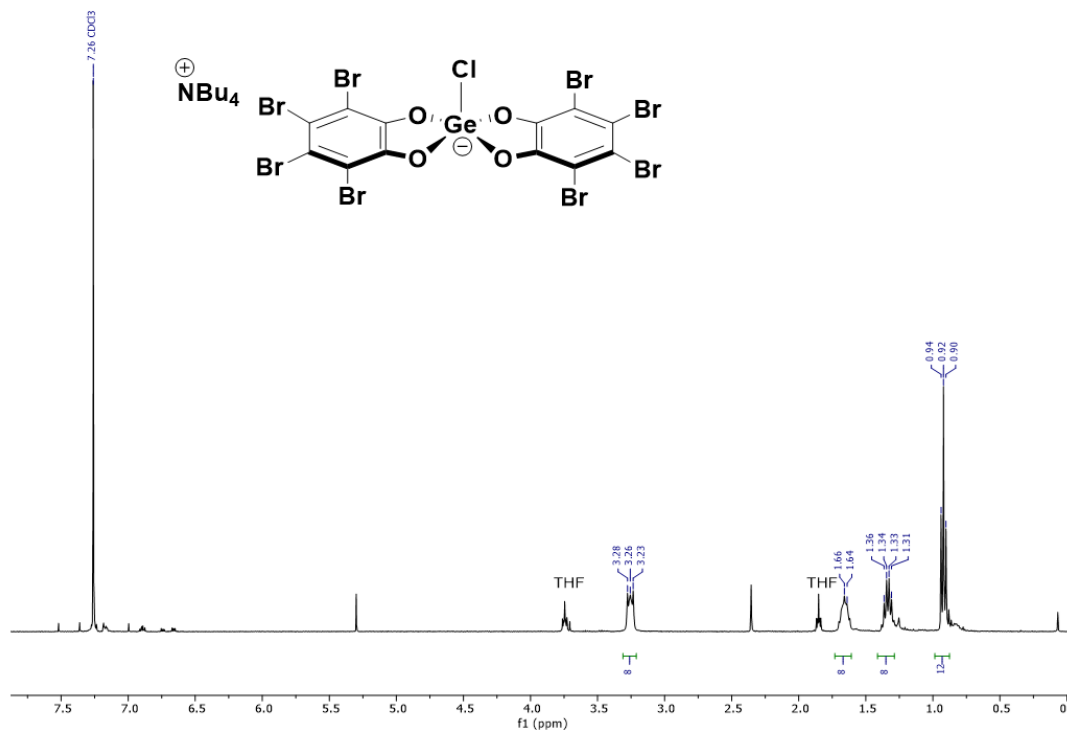
Appendix C: ^1H NMR (CDCl_3 , 400 MHz) spectrum of $\text{Ge}(\text{dtbc})_2(\text{ACN})_2$.



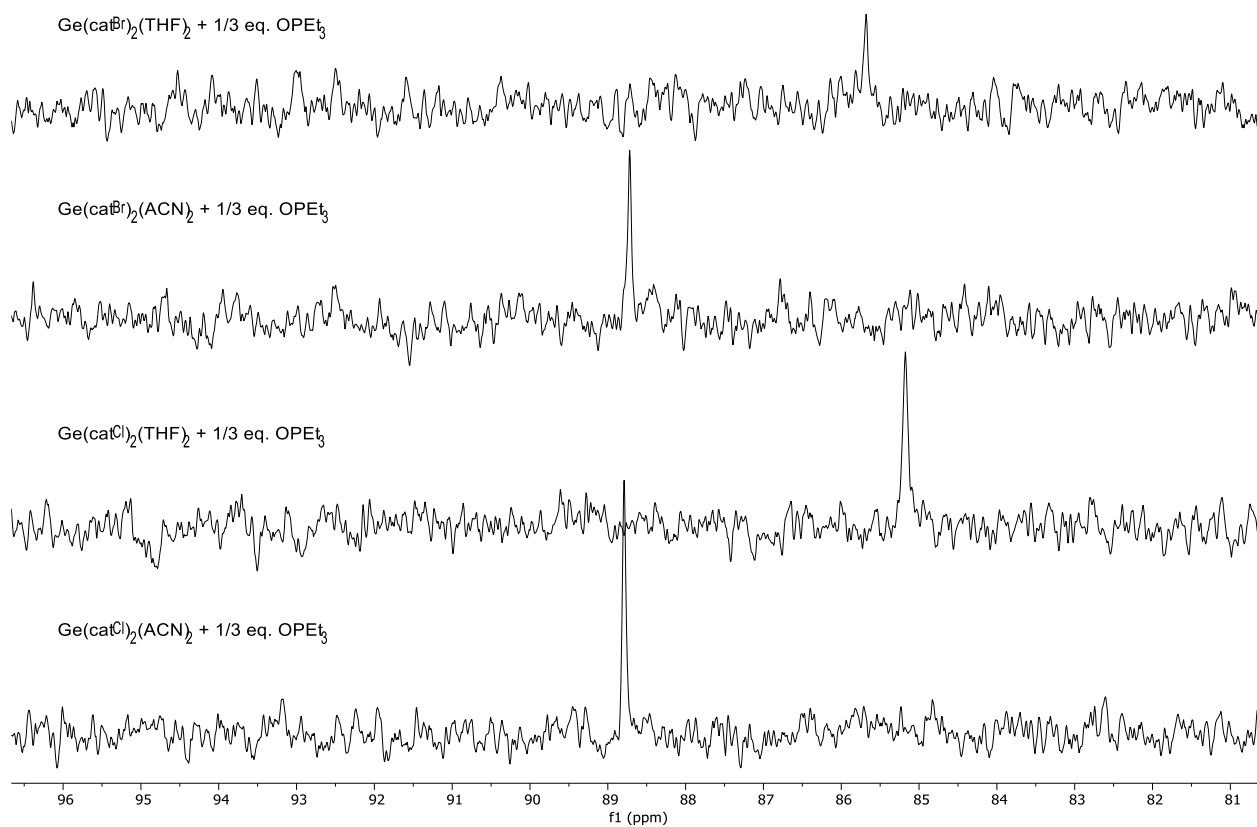
Appendix D: ^1H NMR (CDCl₃, 400 MHz) spectrum of [NBu₄][Ge(dtbc)₂Cl].



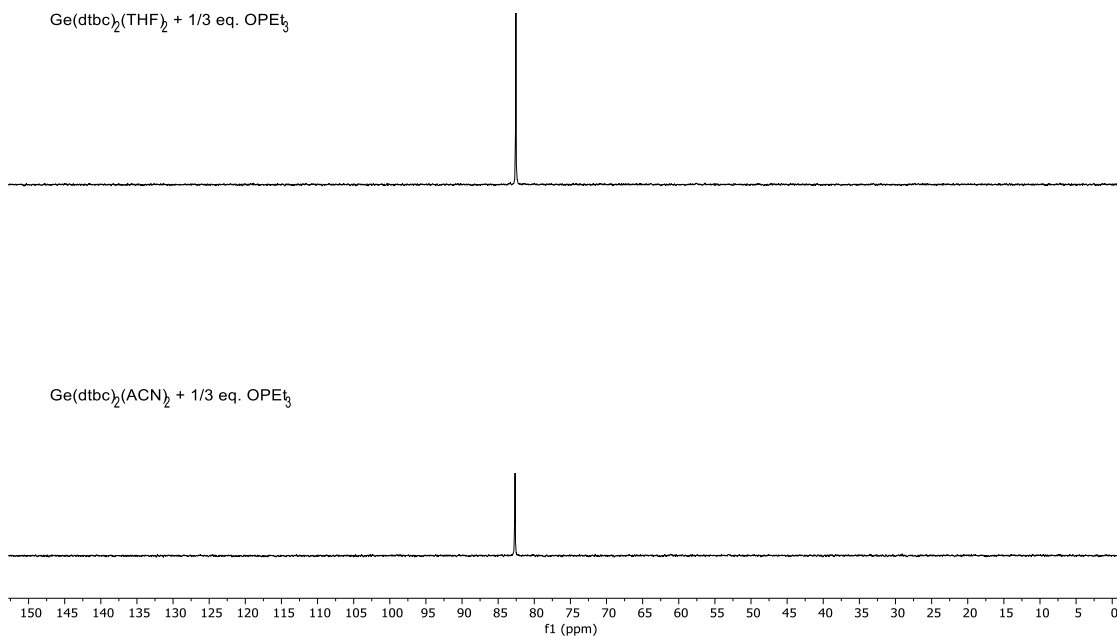
Appendix E: ^1H NMR (CDCl₃, 400 MHz) spectrum of [NBu₄][Ge(catCl)₂Cl].



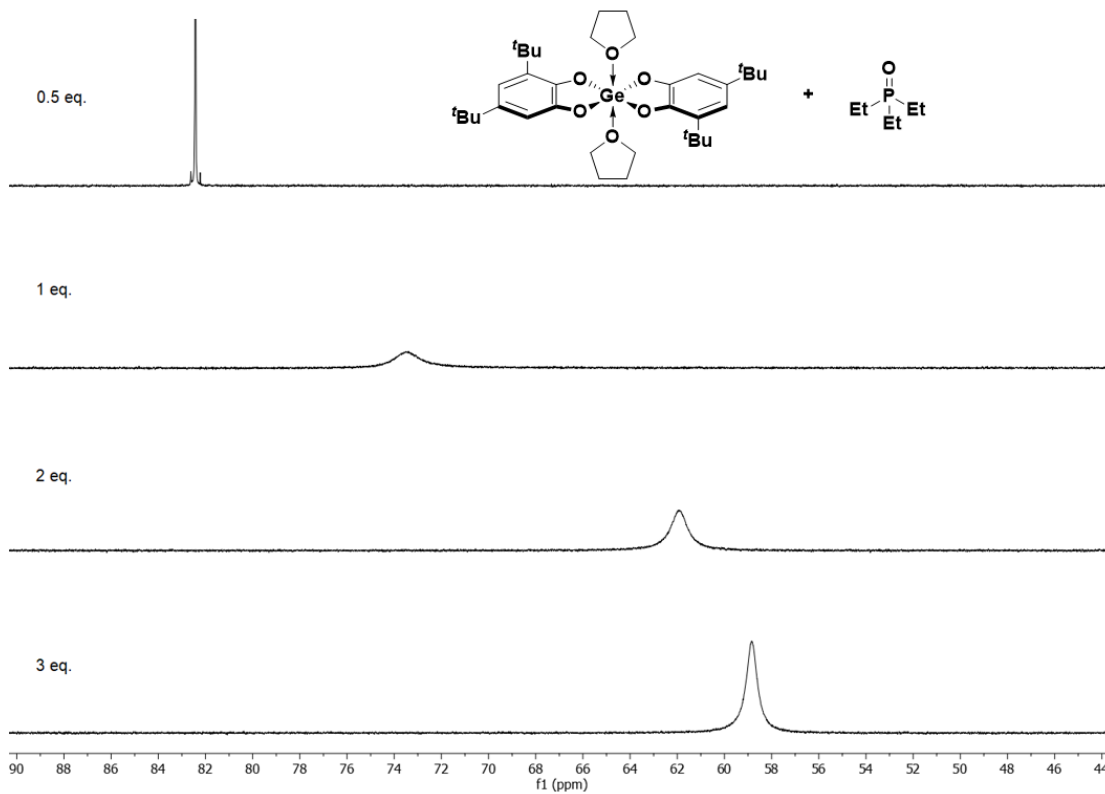
Appendix F: ^1H NMR (CDCl_3 , 400 MHz) spectrum of $[\text{NBu}_4][\text{Ge}(\text{cat}^{\text{Br}})_2\text{Cl}]$.



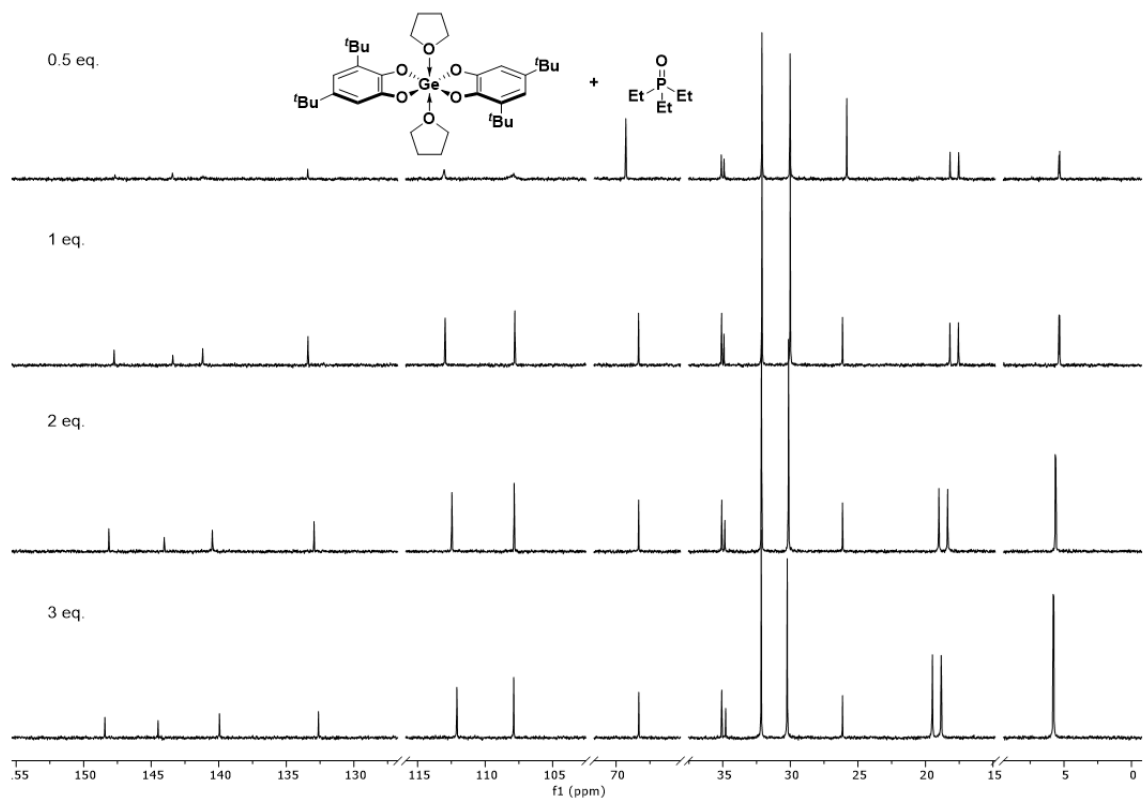
Appendix G: $^{31}\text{P}\{^1\text{H}\}$ NMR (CH_2Cl_2 , 162 MHz) stacked spectrum of the Gutmann-Beckett analysis performed with sub-stoichiometric amounts of triethylphosphine oxide on the halogenated bis(catecholato)germanes.



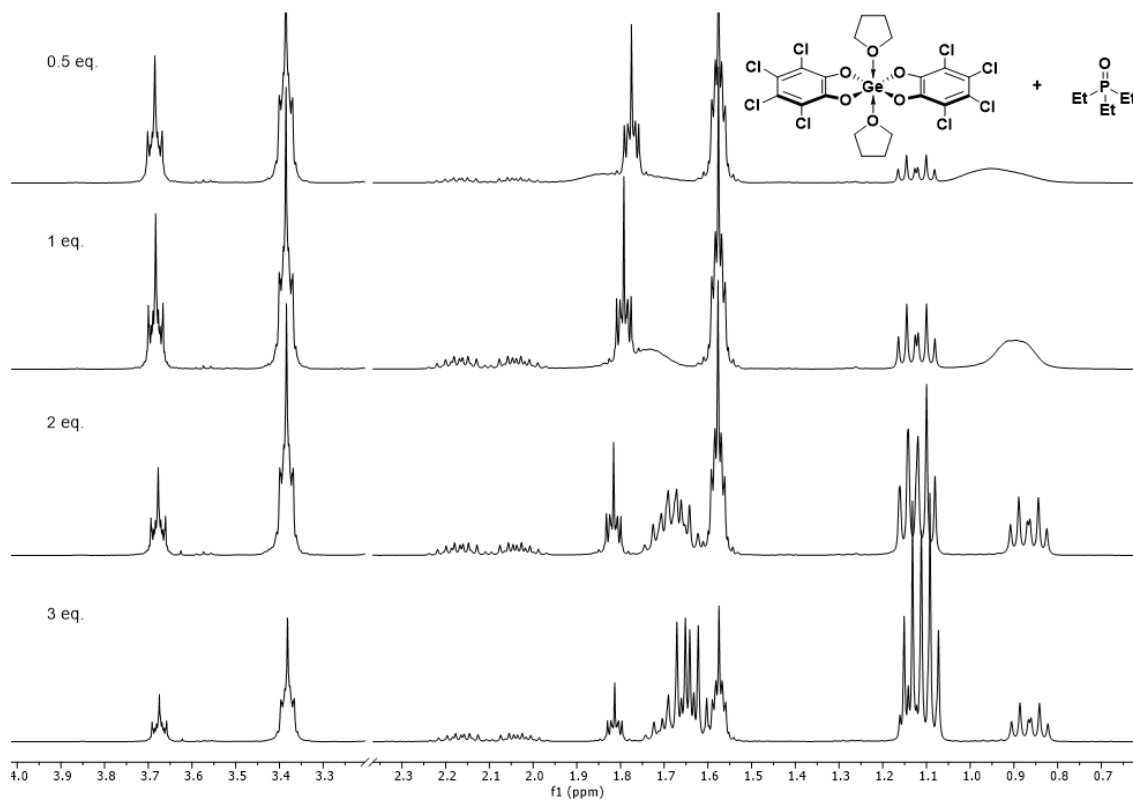
Appendix H: $^{31}\text{P}\{^1\text{H}\}$ NMR (162 MHz, CD_2Cl_2) stacked spectrum of the Gutmann-Beckett analysis performed with sub-stoichiometric amounts of triethylphosphine oxide on the 3,5-di-*tert*-butyl bis(catecholato)germanes. In each case, the signal is assigned to $\text{Ge}(3,5\text{-dtbc})_2(\text{OPEt}_3)$.



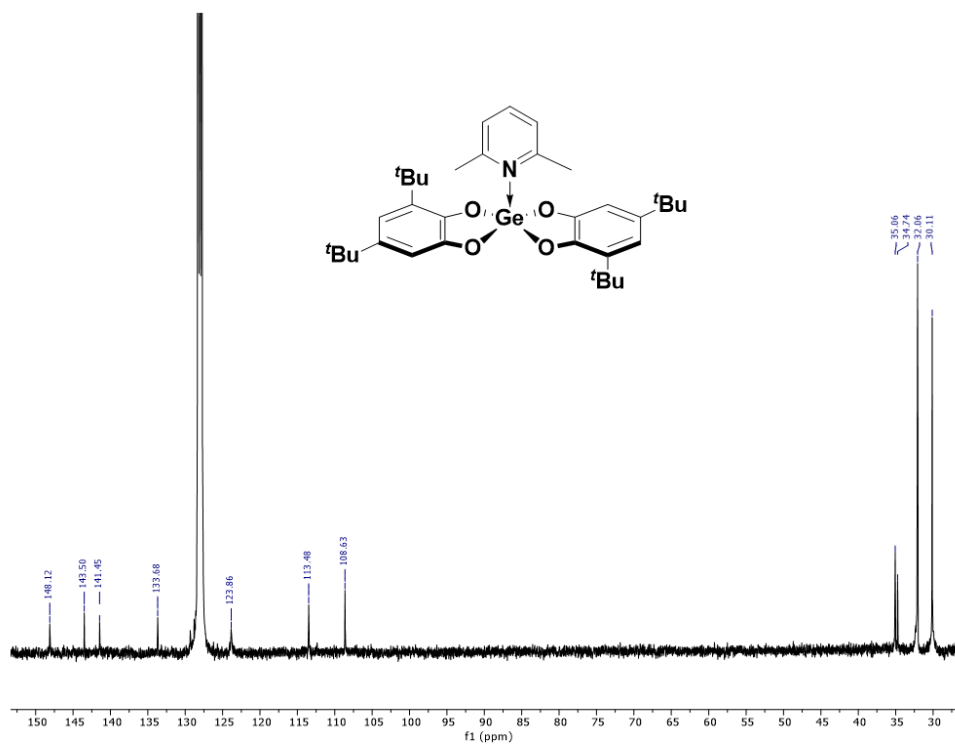
Appendix I: $^{31}\text{P}\{^1\text{H}\}$ NMR (162 MHz in CD_2Cl_2) stacked spectra of $\text{Ge}(\text{3,5-dtbc})_2(\text{THF})_2$ and various equivalents of triethylphosphine oxide



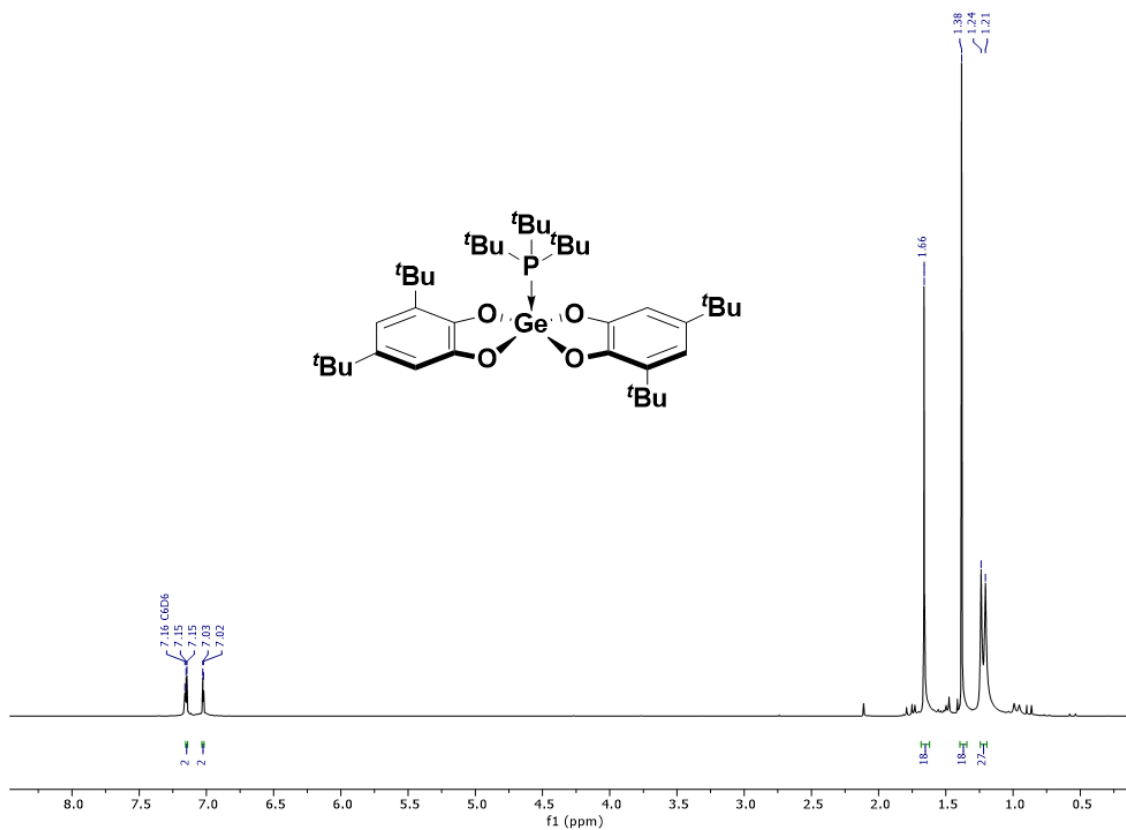
Appendix J: $^{13}\text{C}\{^1\text{H}\}$ NMR (101 MHz in CD_2Cl_2) stacked spectra of $\text{Ge}(\text{3,5-dtbc})_2(\text{THF})_2$ and various equivalents of triethylphosphine oxide



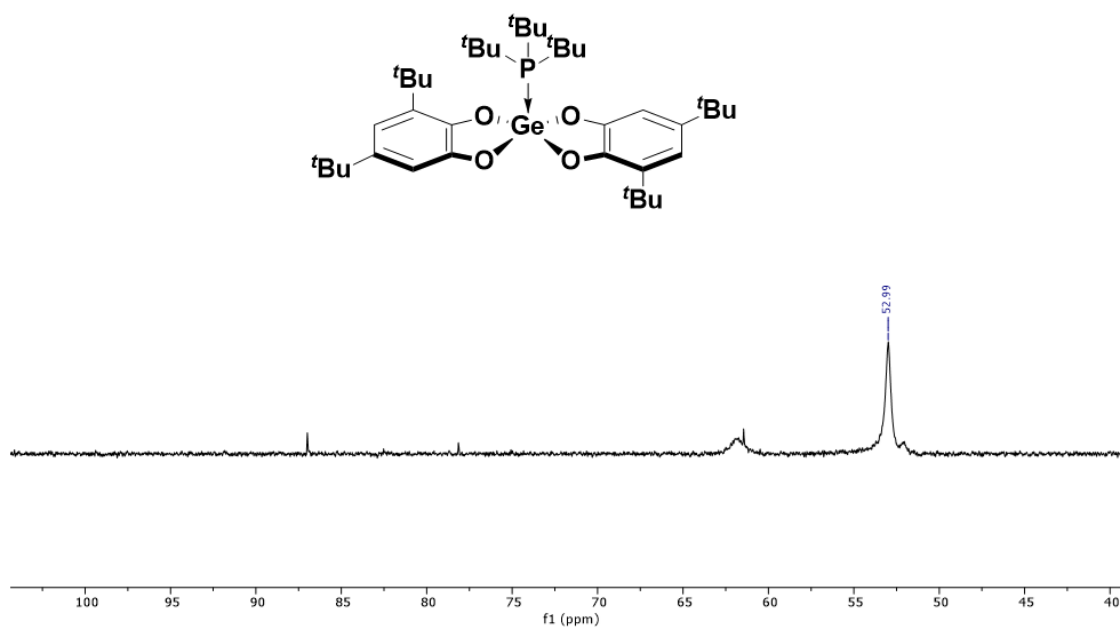
Appendix K: ^1H NMR (400 MHz in CD_2Cl_2) stacked spectra of $\text{Ge}(\text{cat}^{\text{Cl}})_2(\text{THF})_2$ and various equivalents of triethylphosphine oxide



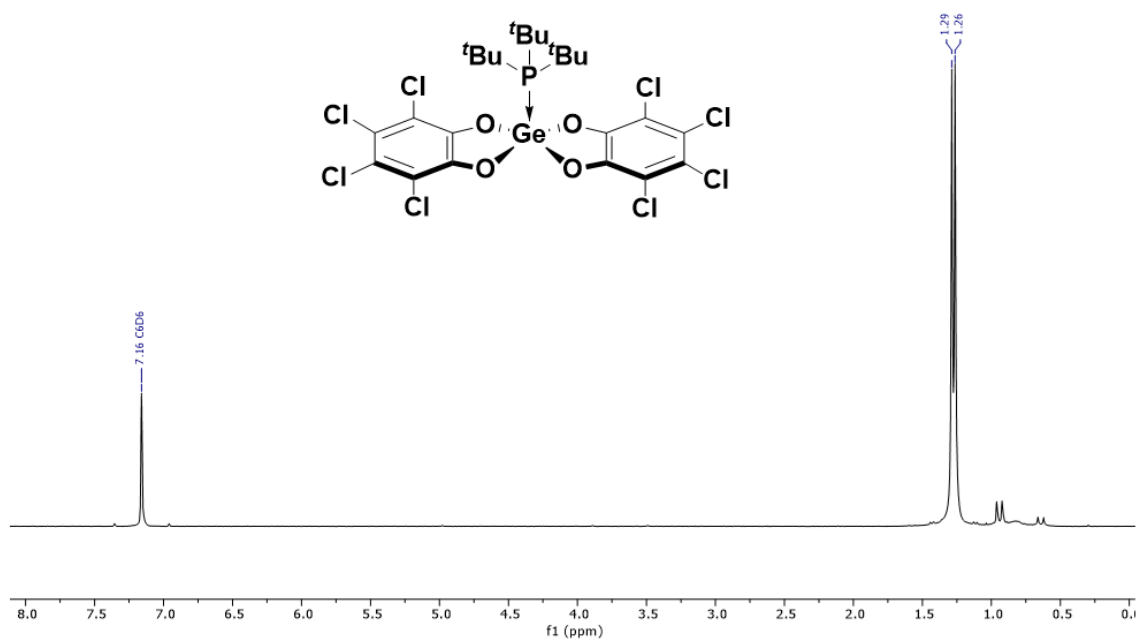
Appendix L: $^{13}\text{C}\{^1\text{H}\}$ NMR (C_6D_6 , 101 MHz) spectrum of $\text{Ge}(\text{dtbc})_2(\text{lut})$.



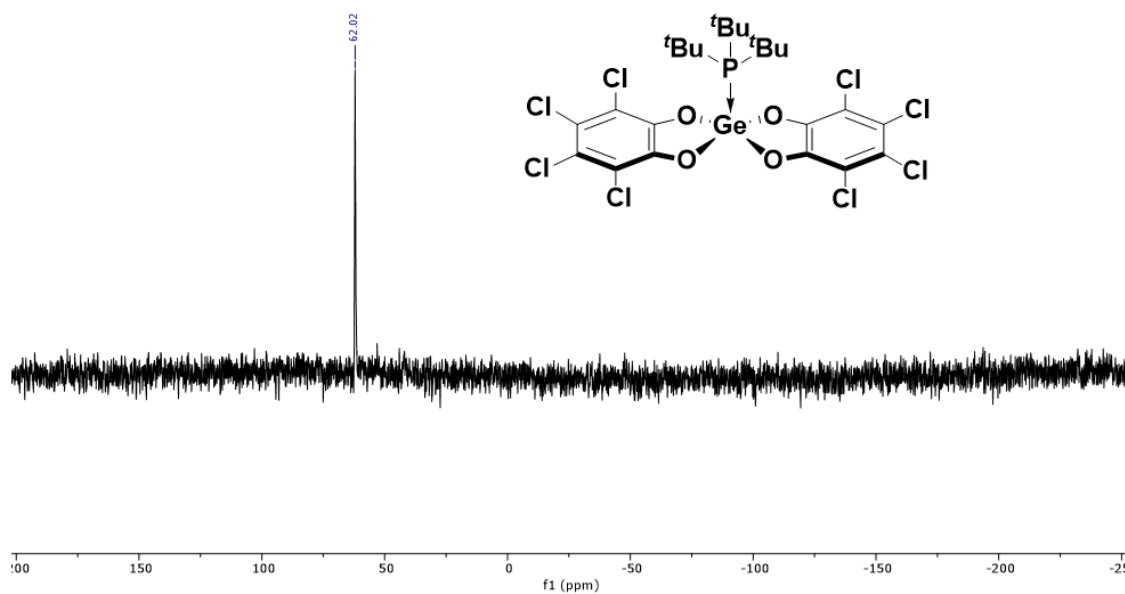
Appendix M: ^1H NMR (C_6D_6 , 400 MHz) spectrum of $\text{Ge}(\text{dtbc})_2(\text{P}^t\text{Bu}_3)$.



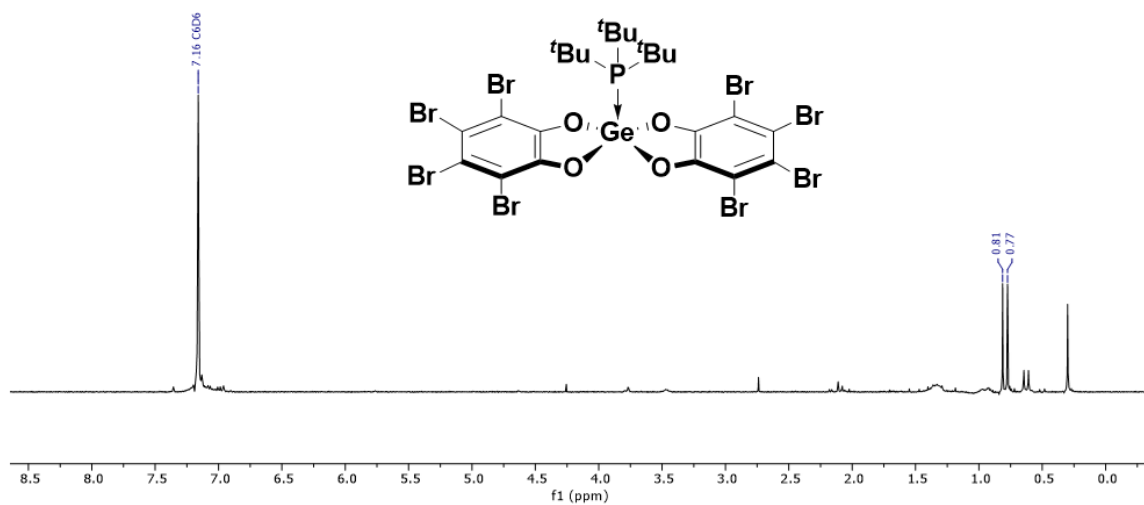
Appendix N: $^{31}\text{P}\{^1\text{H}\}$ NMR (C_6D_6 , 162 MHz) spectrum of $\text{Ge}(\text{dtbc})_2(\text{P}^t\text{Bu}_3)$.



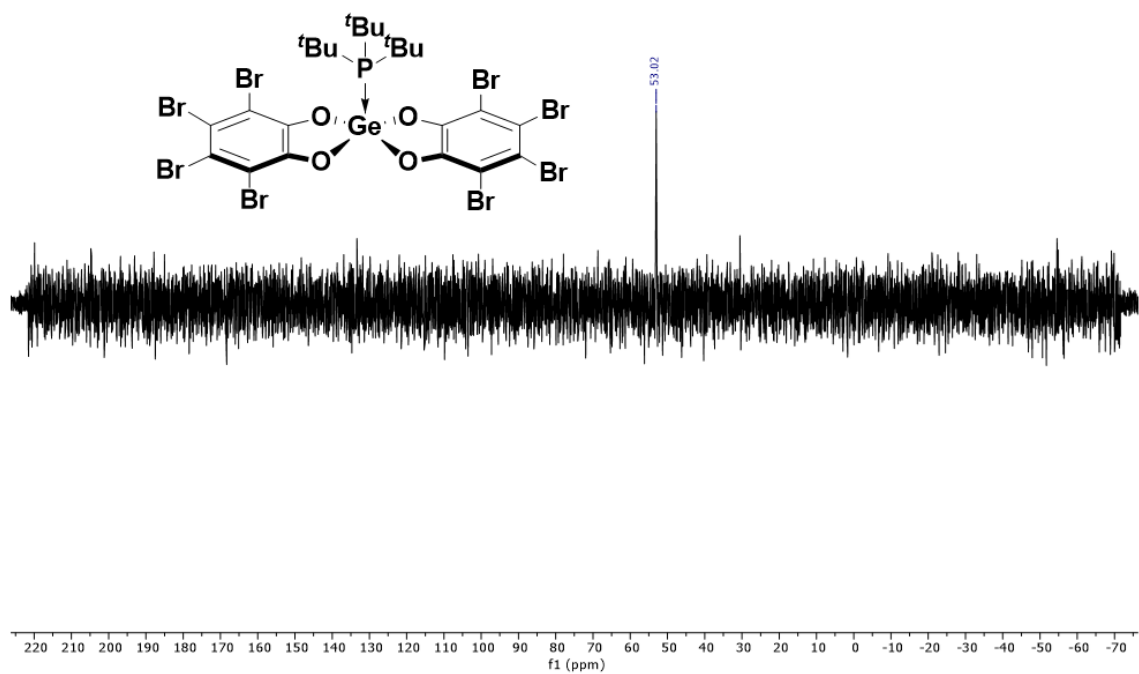
Appendix O: ^1H NMR (C_6D_6 , 400 MHz) spectrum of $\text{Ge}(\text{cat}^{\text{Cl}})_2(\text{P}^t\text{Bu}_3)$.



Appendix P: $^{31}\text{P}\{^1\text{H}\}$ NMR (C_6D_6 , 162 MHz) spectrum of $\text{Ge}(\text{cat}^{\text{Cl}})_2(\text{P}^t\text{Bu}_3)$.



Appendix Q: $^1\text{H NMR}$ (C₆D₆, 400 MHz) spectrum of Ge(cat^{Br})₂(P^tBu)₃.



Appendix R: $^{31}\text{P}\{^1\text{H}\}$ NMR (C₆D₆, 162 MHz) spectrum of Ge(cat^{Cl})₂(P^tBu)₃.

X-Ray Crystallography Details

Appendix S: Summary of Crystal Data for $\text{Ge}(\text{dtbc})_2(\text{THF})_2$, $[\text{NBu}_4][\text{Ge}(\text{cat}^{\text{Br}})_2\text{Cl}]$, and $\text{Ge}(\text{dtbc})_2(\text{OPEt}_3)_2$.

Formula	$\text{C}_{36}\text{H}_{56}\text{GeO}_6$	$\text{C}_{28}\text{H}_{36}\text{Br}_8\text{ClGeNO}_4$	$\text{C}_{40}\text{H}_{70}\text{GeO}_6\text{P}_2$
CCDC	2090115	2090116	2090117
Formula Weight (g/mol)	657.39	1197.90	781.49
Crystal Dimensions (mm)	$0.294 \times 0.153 \times 0.043$	$0.354 \times 0.340 \times 0.144$	$0.373 \times 0.229 \times 0.167$
Crystal Colour and Habit	colourless plate	colourless prism	colourless prism
Crystal System	monoclinic	triclinic	triclinic
Space Group	$P 2_1/c$	$P -1$	$P -1$
Temperature, K	110	223	110
$a, \text{\AA}$	7.091(2)	9.864(5)	8.012(3)
$b, \text{\AA}$	18.355(5)	11.942(6)	9.945(4)
$c, \text{\AA}$	12.889(5)	16.473(7)	14.528(6)
$\alpha, ^\circ$	90	84.984(10)	109.138(11)
$\beta, ^\circ$	94.130(14)	88.202(8)	92.133(9)
$\gamma, ^\circ$	90	73.534(13)	95.396(13)
$V, \text{\AA}^3$	1673.2(9)	1853.6(16)	1085.9(8)
Number of reflections to determine final unit cell	9916	9198	9440
Min and Max 2θ for cell determination, $^\circ$	5.46, 63.72	4.76, 60.9	6.04, 74.58
Z	2	2	1
$F(000)$	704	1144	420
ρ (g/cm ³)	1.305	2.146	1.195
$\lambda, \text{\AA}$, (MoK α)	0.71073	0.71073	0.71073
μ , (cm ⁻¹)	0.959	9.554	0.819
Diffractometer Type	Bruker Kappa Axis Apex2	Bruker Kappa Axis Apex2	Bruker Kappa Axis Apex2
Scan Type(s)	phi and omega scans	phi and omega scans	phi and omega scans
Max 2θ for data collection, $^\circ$	67.682	61.112	84.336
Measured fraction of data	0.999	0.999	0.998

Number of reflections measured	56754	112781	125120
Unique reflections measured	6714	11316	15267
R_{merge}	0.0652	0.0456	0.0385
Number of reflections included in refinement	6714	11316	15267
Cut off Threshold Expression	I > 2sigma(I)	I > 2sigma(I)	I > 2sigma(I)
Structure refined using	full matrix least-squares using F ²	full matrix least-squares using F ²	full matrix least-squares using F ²
Weighting Scheme	w=1/[sigma ² (Fo ²)+(0.0458P) ² +1.9778P] where P=(Fo ² +2Fc ²)/3	w=1/[sigma ² (Fo ²)+(0.0219P) ² +1.5099P] where P=(Fo ² +2Fc ²)/3	w=1/[sigma ² (Fo ²)+(0.0399P) ² +0.0621P] where P=(Fo ² +2Fc ²)/3
Number of parameters in least-squares	202	392	232
R₁	0.0487	0.0275	0.0269
wR₂	0.1103	0.0518	0.0700
R₁ (all data)	0.0718	0.0462	0.0362
wR₂ (all data)	0.1195	0.0571	0.0733
GOF	1.045	1.033	1.045
Maximum shift/error	0.000	0.002	0.001
Min & Max peak heights on final DF Map (e⁻/Å³)	-0.678, 2.679	-0.928, 0.941	-0.323, 0.687

Where:

$$R_1 = \sum (|F_o| - |F_c|) / \sum F_o$$

$$wR_2 = [\sum w (F_o^2 - F_c^2)^2 / \sum w F_o^4]^{1/2}$$

$$GOF = [\sum w (F_o^2 - F_c^2)^2 / (\text{No. of reflns.} - \text{No. of params.})]^{1/2}$$

Appendix T: Summary of Crystal Data for [H-lut][Ge(dtbc)₂Cl], Ge(dtbc)₂(H₂O)—lut, 2[Cl-P^tBu₃][Ge(cat^{Cl})₂Cl₂], Ge(cat^{Br})₂-O- Ge(cat^{Br})₂.

Formula	C ₃₅ H ₅₀ ClGeNO ₄	C ₄₁ H ₅₇ GeNO ₅	C ₄₀ H _{62.70} Cl _{18.70} GeO _{5.30} P ₂	C ₅₀ H ₆₀ Br ₁₆ Cl ₄ Ge ₂ O ₉ P ₂
Formula Weight (g/mol)	656.80	716.46	1425.84	2432.46
Crystal Dimensions mm)	0.344 × 0.130 × 0.082	0.355 × 0.308 × 0.098	0.269 × 0.229 × 0.164	0.227 × 0.120 × 0.117
Crystal Colour and Habit	colourless prism	colourless plate	colourless prism	colourless prism
Crystal System	monoclinic	tetragonal	monoclinic	monoclinic
Space Group	P 2 ₁ /c	I 4 ₁ /a	P 2 ₁ /n	P 2 ₁ /c
Temperature, K	110	110	110	110
a, Å	10.187(2)	18.223(6)	12.120(4)	17.226(7)
b, Å	11.949(3)	18.223	20.154(8)	19.954(9)
c, Å	32.214(6)	59.78(2)	12.462(4)	21.109(10)
a, °	90	90	90	90
b, °	98.339(7)	90	90.660(10)	90.49(2)
g, °	90	90	90	90
V, Å ³	3879.8(15)	19854(16)	3043.8(19)	7255(6)
Number of reflections to determine final unit cell	9305	9996	9845	9988
Min and Max 2q for cell determination, °	5.28, 55.1	5.04, 35.6	5.14, 59.58	4.94, 48.52
Z	4	16	2	4
F(000)	1392	6112	1450	4616
r (g/cm)	1.124	0.959	1.556	2.227
l, Å, (MoKa)	0.71073	0.71073	0.71073	0.71073
m, (cm ⁻¹)	0.891	0.650	1.416	9.879
Diffractometer Type	Bruker Kappa Axis Apex2	Bruker Kappa Axis Apex2	Bruker Kappa Axis Apex2	Bruker Kappa Axis Apex2
Scan Type(s)	phi and omega scans	phi and omega scans	phi and omega scans	phi and omega scans
Max 2q for data collection, °	57.524	36.054	66.328	49.486
Measured fraction of data	0.999	0.996	0.999	0.998

Number of reflections measured	159113	91105	179625	12383
Unique reflections measured	10039	3418	11613	12383
R_{merge}	0.0869	0.1099	0.0539	0.1071
Number of reflections included in refinement	10039	3418	11613	12383
Cut off Threshold Expression	I > 2sigma(I)	I > 2sigma(I)	I > 2sigma(I)	I > 2sigma(I)
Structure refined using	full matrix least-squares using F ²	full matrix least-squares using F ²	full matrix least-squares using F ²	full matrix least-squares using F ²
Weighting Scheme	$w=1/[\sigma^2(F_o^2) + (0.0296P)^2 + 3.5745P]$ where $P=(F_o^2+2F_c^2)/3$	$w=1/[\sigma^2(F_o^2) + (0.0481P)^2 + 252.2379P]$ where $P=(F_o^2+2F_c^2)/3$	$w=1/[\sigma^2(F_o^2) + (0.0386P)^2 + 1.9221P]$ where $P=(F_o^2+2F_c^2)/3$	$w=1/[\sigma^2(F_o^2) + (0.0185P)^2 + 5.1223P]$ where $P=(F_o^2+2F_c^2)/3$
Number of parameters in least-squares	418	434	388	774
R₁	0.0367	0.0823	0.0334	0.0259
wR₂	0.0810	0.1894	0.0791	0.0459
R₁ (all data)	0.0507	0.0931	0.0482	0.0388
wR₂ (all data)	0.0866	0.1966	0.0859	0.0487
GOF	1.031	1.172	1.025	1.066
Maximum shift/error	0.004	0.001	0.002	0.002
Min & Max peak heights on final DF Map (e/Å³)	-0.465, 0.388	-0.353, 0.474	-0.863, 0.770	-0.595, 0.703

A.3 Computational Data

Appendix U: The anchor point data used in the determination of FIA values

Species	kJ	Reaction 2
Me ₃ Si ⁺	-1071911.3	
Me ₃ SiF	-1334866.1	952.5
F ⁻	-262002.2	

Appendix V: Calculated data for the determination of the FIA values of the bis(catecholato)germane complexes.

Complex	Energy B3LYP D3(BJ) /def2-TZVPP		Thermal Correction PBEh-3c/def2-SVP		Electronic + Thermal	LA + Me ₃ SiY	Me ₃ Si+ + LA-F-	Rxn 1	FIA
	Hartree	kJ	Hartree	kJ	kJ	kJ	kJ	kJ	kJ
Ge(dtbc) ₂	-3468.81	-9107359.86	0.68	1786.28	-9105573.59	-10442012.13	-10441492.90	519.23	433.27
Ge(dtbc) ₂ F ⁻	-3568.82	-9369935.50	0.68	1790.98	-9368144.52				
Ge(cat) ₂	-2839.93	-7456226.40	0.20	512.82	-7455713.58	-8792152.12	-8791616.04	536.09	416.41
Ge(cat) ₂ F ⁻	-2939.93	-7718785.07	0.20	517.42	-7718267.65				
Ge(cat ^F) ₂	-3633.85	-9540669.19	0.14	358.27	-9540310.91	-10876749.46	-10876299.32	450.13	502.37
Ge(cat ^F) ₂ F ⁻	-3733.89	-9803317.32	0.14	366.38	-9802950.94				
Ge(cat ^{Cl}) ₂	-6516.41	-17108838.56	0.13	332.76	-17108505.81	-18444944.35	-18444499.64	444.71	507.79
Ge(cat ^{Cl}) ₂ F ⁻	-6616.45	-17371493.29	0.13	342.03	-17371151.25				
Ge(cat ^{Br}) ₂	-23427.46	-61508778.69	0.12	323.92	-61508454.77	-62844893.31	-62844453.36	439.95	512.55
Ge(cat ^{Br}) ₂ F ⁻	-23527.50	-61771438.50	0.13	333.53	-61771104.97				
Ge(dtbc) ₂ (ACN)	-3601.55	-9455868.55	0.73	1921.77	-9453946.79	-10790385.33	-10789861.82	523.51	428.99
Ge(dtbc) ₂ (ACN)F ⁻	-3701.56	-9718446.16	0.74	1932.73	-9716513.44				
Ge(cat) ₂ (ACN)	-2972.66	-7804736.55	0.25	650.58	-7804085.97	-9140524.51	-9139991.90	532.61	419.89
Ge(cat) ₂	-3072.67	-8067300.44	0.25	656.92	-8066643.52				

(ACN)F ⁻									
Ge(cat ^F) ₂ (ACN)	-3766.60	-9889208.71	0.19	498.59	-9888710.11	-11225148.66	-11224680.20	468.45	484.05
Ge(cat ^F) ₂ (ACN)F ⁻	-3866.63	-10151835.34	0.19	503.52	-10151331.82				
Ge(cat ^{Cl}) ₂ (ACN)	-6649.16	-17457379.49	0.18	471.04	-17456908.46	-18793347.00	-18792886.60	460.39	492.11
Ge(cat ^{Cl}) ₂ (ACN)F ⁻	-6749.20	-17720020.17	0.18	481.95	-17719538.22				
Ge(cat ^{Br}) ₂ (ACN)	-23560.21	-61857320.91	0.18	464.82	-61856856.09	-63193294.64	-63192841.94	452.70	499.80
Ge(cat ^{Br}) ₂ (ACN)F ⁻	-23660.25	-62119966.98	0.18	473.43	-62119493.55				
Ge(cat ^{Br}) ₂ (THF)	-23659.90	-62119064.95	0.25	662.72	-62118402.23	-63454840.77	-63454382.12	458.65	493.85
Ge(cat ^{Br}) ₂ (THF)F ⁻	-23759.94	-62381704.69	0.26	670.95	-62381033.74				
Ge(cat ^{Br}) ₂ (Et ₂ O)	-23661.11	-62122236.86	0.27	721.08	-62121515.77	-63457954.31	-63457500.02	454.29	498.21
Ge(cat ^{Br}) ₂ (Et ₂ O)F ⁻	-23761.14	-62384881.02	0.28	729.39	-62384151.64				

Appendix W: Calculated data for the determination of the GEI values of the bis(catecholato)germane complexes.

Complex	HOMO	LUMO	Chemical Potential (μ)	Chemical Hardness (η)	GEI Values (ω)
Ge(cat) ₂	-6.369	-0.8745	-3.62175	5.4945	1.194
Ge(dtbc) ₂	-6.0017	-0.6984	-3.35005	5.3033	1.058
Ge(cat ^F) ₂	-7.1595	-2.0776	-4.61855	5.0819	2.099
Ge(cat ^{Cl}) ₂	-6.9335	-1.8747	-4.4041	5.0588	1.917
Ge(cat ^{Br}) ₂	-6.8631	-1.9912	-4.42715	4.8719	2.012
Ge(cat) ₂ (ACN)	-5.4311	-1.4356	-3.43335	3.9955	1.475
Ge(dtbc) ₂ (ACN)	-5.1478	-1.4195	-3.28365	3.7283	1.446
Ge(cat ^F) ₂ (ACN)	-6.1888	-2.154	-4.1714	4.0348	2.156
Ge(cat ^{Cl}) ₂ (ACN)	-6.1275	-2.1738	-4.15065	3.9537	2.179
Ge(cat ^{Br}) ₂ (ACN)	-6.1242	-2.1942	-4.1592	3.93	2.201
Ge(cat ^{Br}) ₂ (Ether)	-6.3495	-1.6325	-3.991	4.717	1.688
Ge(cat ^{Br}) ₂ (THF)	-6.4024	-1.6202	-4.0113	4.7822	1.682

Appendix X: Calculated energetics of ligand dissociation and substrate activation with $\text{Ge}(\text{cat}^{\text{Br}})_2$.

Complex	Enthalpy (hartree)	Enthalpy (kJ/mol)	Gibbs (hartree)	Gibbs (kJ/mol)
$\text{Ge}(\text{cat}^{\text{Br}})_2(\text{ACN})_2$	-23692.90088	-62205711.27	-23692.99072	-62205947.13
$\text{Ge}(\text{cat}^{\text{Br}})_2(\text{ACN})$	-23560.25869	-61857459.2	-23560.34328	-61857681.27
$\text{Ge}(\text{cat}^{\text{Br}})_2(\text{THF})_2$	-23892.05995	-62728603.39	-23892.15298	-62728847.65
$\text{Ge}(\text{cat}^{\text{Br}})_2(\text{THF})$	-23659.83407	-62118894.35	-23659.92072	-62119121.85
$\text{Ge}(\text{cat}^{\text{Br}})_2$	-23427.62475	-61509228.78	-23427.70542	-61509440.58
ACN	-132.6064582	-348158.2559	-132.6361785	-348236.2865
THF	-232.1676769	-609556.2356	-232.1991325	-609638.8223
Styrene	-309.302937	-812074.8612	-309.3421922	-812177.9256
$\text{Ge}(\text{cat}^{\text{Br}})_2(\text{Styrene})$	-23736.96198	-62321393.68	-23737.0548	-62321637.37
<i>Cis</i> - $\text{Ge}(\text{cat}^{\text{Br}})_2(\text{Styrene})(\text{ACN})$	-23869.59659	-62669625.85	-23869.69422	-62669882.18
<i>Trans</i> - $\text{Ge}(\text{cat}^{\text{Br}})_2(\text{Styrene})(\text{ACN})$	-23869.60727	-62669653.89	-23869.70222	-62669903.19
Phenylacetylene	-308.0730972	-808845.9166	-308.1092989	-808940.9643
<i>Trans</i> - $\text{Ge}(\text{cat}^{\text{Br}})_2(\text{PhCCH})(\text{ACN})$	-23868.37636	-62666422.13	-23868.4692	-62666665.87
<i>Para</i> -tolualdehyde	-384.4930966	-1009486.625	-384.5336354	-1009593.06
<i>Trans</i> - $\text{Ge}(\text{cat}^{\text{Br}})_2(\textit{para}$ -tolualdehyde)(ACN)	-23812.15959	-62518825.01	-23812.24953	-62519061.14
HSiEt_3	-527.3560081	-1384573.199	-527.3986291	-1384685.101

SiEt_3^+	-526.494541	-1382311.417	-526.5342082	-1382415.564
$\text{ACN}^--\text{SiEt}_3^+$	-659.1825821	-1730683.869	-659.2302814	-1730809.104
$\text{Ge}(\text{cat}^{\text{Br}})_2\text{H}^-$	-23428.35791	-61511153.7	-23428.43766	-61511363.07
$\text{Ge}(\text{cat}^{\text{Br}})_2(\text{ACN})\text{H}^-$	-23560.9817	-61859357.45	-23561.06848	-61859585.28
$\text{Ge}(\text{cat}^{\text{Br}})_2(\text{H})(\text{SiEt}_3)$	-23955.0062	-62893868.79	-23955.1002	-62894115.58

Appendix Y: Calculated energetics of ligand dissociation association of tested Lewis bases with $\text{Ge}(\text{cat}^{\text{Br}})_2$.

Complex	Enthalpy (hartree)	Enthalpy (kJ/mol)	Gibbs (hartree)	Gibbs (kJ/mol)
$\text{Ge}(\text{cat}^{\text{Br}})_2(\text{ACN})_2$	-23692.90088	-62205711.27	-23692.99072	-62205947.13
$\text{Ge}(\text{cat}^{\text{Br}})_2(\text{ACN})$	-23560.25869	-61857459.2	-23560.34328	-61857681.27
$\text{Ge}(\text{cat}^{\text{Br}})_2$	-23427.62475	-61509228.78	-23427.70542	-61509440.58
ACN	-132.6064582	-348158.2559	-132.6361785	-348236.2865
P^tBu_3	-814.136556	-2137515.528	-814.1917204	-2137660.362
$\text{Ge}(\text{cat}^{\text{Br}})_2(\text{P}^t\text{Bu}_3)$	-24241.84702	-63646969.34	-24241.95168	-63647244.15
lut	-326.5576669	-857377.1544	-326.5969476	-857480.2858
$\text{Ge}(\text{cat}^{\text{Br}})_2(\text{lut})$	-23754.24825	-62366778.79	-23754.33862	-62367016.05
<i>trans</i> - $\text{Ge}(\text{cat}^{\text{Br}})_2(\text{ACN})(\text{lut})$	-23886.9763	-62715256.27	-23886.88237	-62715009.65
py	-248.0242169	-651187.5814	-248.0574503	-651274.8358
$\text{Ge}(\text{cat}^{\text{Br}})_2(\text{py})$	-23675.71252	-62160583.24	-23675.79967	-62160812.04
$\text{Ge}(\text{cat}^{\text{Br}})_2(\text{py})_2$	-23923.73103	-62811755.83	-23923.83209	-62812021.16
<i>trans</i> - $\text{Ge}(\text{cat}^{\text{Br}})_2(\text{ACN})(\text{py})$	-23808.35064	-62508824.61	-23808.4408	-62509061.31

Curriculum Vitae

Name:	Andrew Henry
Post-secondary Education and Degrees:	<p>The University of Western Ontario London, Ontario, Canada 2011-2015 B.Sc. Chemistry Thesis Project: Wisner Group</p> <p>The University of Western Ontario London, Ontario, Canada Fall 2015-Winter 2018 M.Sc. Chemistry Baines Group</p> <p>The University of Western Ontario London, Ontario, Canada Summer 2018 – Fall 2022 Ph.D. Chemistry Baines Group</p>
Honours and Awards:	Lipson Baines Award Winner 2021
Related Work Experience	Teaching Assistant The University of Western Ontario 2015-2022
Publications	<p>“The Addition of a Cyclopropyl Alkyne to an Asymmetrically-Substituted Disilene: A Mechanistic Study” Henry, A. T.; Bourque, J. L.; Vacirca, I.; Scheschkewitz, D.; Baines, K. M.; <i>Organometallics</i>, 2019, 38, 1622-1626.</p> <p>“Selective dimerization of α-methylstyrene by tunable bis(catecholato)germane Lewis acid catalysts” Henry, A. T.; Cosby, T. P. L.; Baines, K. M.; <i>Dalton Trans.</i>, 2021, 50, 15906-15913.</p> <p>“Facile reduction of Phosphine Oxides and <i>H</i>-Phosphonates by Ditetrelenes” Belcina, M. B.; Farhadpour, B.; Tashkandi, N.; <u>Henry, A.</u>; Bourque, J. L.; <i>Can. J. Chem. Accepted Article</i>. 2021</p>

“The Lewis Acidity of Germanium(II) Crown Ether Cations”
McOnie, S. L.; Henry, A. T.; Baines, K. M.; *Eur. J. Chem., Manuscript in Preparation. 2022*

Presentations

CSC 2016 – Poster Session – Halifax - June 7, 2016 – “Exploring the Reactivity of 1,2,3-Azaditetraene Ring Systems.” Henry, A. T.; Baines, K. M.;

IDW 2016 – Poster Session – Hamilton - November 12, 2016 – “Mechanistic Study of an Asymmetric Disilene” Henry, A. T.; Baines, K. M.;

CSC 2017 – Poster Session – Toronto - May 30, 2017 – “Mechanistic Study of the Cycloaddition Addition of an Alkyne to an Asymmetric Disilene” Henry A.T., Baines K.M.;

IDW 2017 – Poster Session – Toronto - November 4, 2017 – “Addition of Alkynes to a NHC-Stabilized Silylene: A Mechanistic Study” Henry, A. T.; Baines, K. M.; Inoue, S.;

CSC 2018 – Poster Session – Edmonton – May 30, 2018 – “The Addition of Alkynes to Low-Valent Silicon Compounds: A Mechanistic Study” Henry, A. T.; Baines, K. M.; Inoue, S.; Scheschkewitz, D.;

CSC 2019 – Poster Session – Quebec City – June 4, 2019 – “Germanium Catechol Complexes: Synthesis and Assessment of their Lewis Acidity and Catalytic Activity” Henry, A. T.; Baines, K. M.;

GIDW 2020 - Poster Session – Online – July 9, 2020 – “Germanium Catechol Complexes: Synthesis and Assessment as Lewis Acids and Catalysts” Henry, A. T.; Baines, K. M.;

ISOS 2021 – Poster Session – Online – July 5, 2021 – “Germanium Catechol Complexes: Lewis Acid Catalytic Activity and FLP Reactivity” Henry, A. T.; Baines, K. M.;

CCCE 2021 – Poster Session – Online – August 18, 2021 – “Germanium Catechol Complexes: Synthesis and Assessment of their Lewis Acidity, Catalytic Activity and FLP Reactivity” Henry, A. T.; Cosby, T. P. L.; Baines, K. M.;

CCCE 2022 – Oral Presentation – Calgary – June 14, 2022 –
“Germanium Catechol Complexes: Synthesis and Assessment of
their Lewis Acidity, Catalytic Activity” Henry, A. T.; Cosby, T. P.
L.; Baines, K. M.;